



**School of Pharmacy and Pharmaceutical Science,
School of Optometry and Vision Sciences
Cardiff University**

**NOVEL DRUG THERAPY FOR MITOCHONDRIAL
OPTIC NEUROPATHY**

Carmine Varricchio

Supervisor: **Prof Andrea Brancale**

Supervisor: **Dr Charles Heard**

Supervisor: **Dr Malgorzata Rozanowska**

Supervisor: **Prof Marcela Votruba**

Acknowledgements

First, I would like to express my sincere gratitude to my supervisors: Dr Charles Heard, Prof Andrea Brancale, Prof Marcela Votruba, Dr Malgorzata Rozanowska, for continual feedback on all aspects of experimental design and execution, for their dedicated and seemingly tireless efforts in moulding me into a research scientist. I would like to thank Prof. Andrew Westwell for insightful comments and encouragements during the PhD. My gratitude goes to Life Science Research Network Wales for sponsoring my PhD and giving me the opportunity for being involved in such a great project.

It has been undoubtedly challenging to work in such an interdisciplinary project, but it also gave me the opportunity to meet and work with culturally and scientifically different people. The time I spent in the laboratory would not have been so pleasant without many of past and present members of team groups, so a special thanks to my colleagues/friends: Roberto Manganaro, Dr Gilda Giacotti, Birgit Zonics, Dr Gaia Pasqualetto, Dr Martin Schepelmann., Dr Marcella Bassetto, Dr. Salvo Ferla, Dr Cinzia Bordoni, Dr Giulio Nannetti, Kestutis Satkus, Dr. Irina Erchova, Dr. Kathy Beirne, Sharon Seto. I would like to thank the Biohazard Team and all the guys from Wednesday Football, for cheering me up when everything seemed to be going wrong in the lab, and to take my mind off work.

I would like to thank my mum and dad for their love and support, thank you for letting me find my own way, without judging or questioning me, but always believing in me. Finally, I would like to thank Laura.... I can see you in all my achievements, I would be lost without you here.

Abstract

Mitochondrial optic neuropathies (MON) represent an important cause of chronic visual impairment, affecting at least 1 in 10,000 individuals in the United Kingdom. Despite the efforts of recent years, the treatment options remain limited, with only a few drug candidates and therapeutic approaches, either approved or in development. Recently, Idebenone has been investigated as drug therapy in the treatment of Leber's hereditary optic neuropathy (LHON), a rare genetic MON, although evidence for the efficacy of Idebenone is limited in the literature. Cytoplasmic NAD(P)H:quinone oxidoreductase 1 (NQO1) and mitochondrial complex III were recently identified as the major enzymes involved in Idebenone activity. Based on this mode of action, computer-aided techniques were employed to identify potential Idebenone-related small molecules which are capable of interacting selectively with both enzymes. A series of quinone compounds were selected and evaluated in *in vitro* assays, and one of them was found to rescue the effects of LHON in cell models at a low μM concentration. Based on these observations, 50 derivatives were rationally designed and synthesised in order to enhance activity, and investigate the structure-activity relationship (SAR) and mode of action of this quinone family. Of these, 7 compounds showed improved activity compared to the original hit in the nM range, and these were further evaluated in a range of biological assays. The culmination of this study was the identification a novel naphthoquinone compound 2-((4-fluoro-3-(trifluoromethyl)phenyl)amino)-3-(methylthio)naphthalene-1,3,-dione (**92**) which demonstrated significantly greater potency in the *ex-vivo* assays, in addition to lower cytotoxicity, compared to Idebenone. Although further studies are needed to further elucidate the mechanism of action, this new compound has potential for being taken *forward* into pre-clinical development.

TABLE OF CONTENTS

List of Figures	IX
List of Tables.....	XII
List of Schemes	XIII
Abbreviation and Acronyms	XV
Chapter 1: Introduction	1
1.1 Mitochondria	2
1.1.1 Mitochondria structure	2
1.1.2 Mitochondria dynamics: fusion and fission.....	3
1.1.3 Oxidative phosphorylation	4
1.1.3 Mitochondrial genetics	8
1.1.4 ROS production and damage to mitochondria	10
1.2 Mitochondrial optic neuropathies.....	12
1.2.1 Leber’s hereditary optic neuropathy.....	14
1.2.2 Compounds under clinical investigation	16
1.3 Idebenone	18
1.3.1 Different mechanisms of action.....	19
1.3.2 NQO1 pathway	20
1.3.4 Current status: idebenone pros and cons	22
1.4 Research question.....	26
Chapter 2 Computational studies.....	37
2.1 Computer-aided drug design	28
2.1.1 NQO1 enzyme as a target.....	29
2.1.3 Complex III (Ubiquinol-cytochrome <i>c</i> oxidoreductase)	30
2.1.4 Homology model and study of quinol binding site	33
2.1.5 Virtual screening of commercial compounds.....	36
2.1.6 Quinone compounds	38
2.1.7 DFT theory and prediction of standard reduction potential	40
2.1.8 Conclusion.....	47
Chapter 3 Optimisation of biochemical and biological assays using Idebenone.....	49
3.1 Biological evaluations	50
3.1.2 Overview of the enzymatic assays optimised and used in the study.....	51
3.1.2.1 NQO1 activity in the presence of a quinone.....	51

3.2 Selection of cell lines	57
3.2 Development, optimization and validation of cell-based assays	58
Chapter 4 Biological evaluation of compounds selected from virtual screening	74
4.1 Hit identification	75
4.1.1 Results enzymatic assays of virtual screening compounds	76
4.1.2 Results cell based -assay of virtual screening compounds	84
4.1.3 Conclusion: biological results obtained using compounds indicated from virtual screening	87
Chapter 5 Synthesis of novel 1,4-naphthoquinone	89
5.1.1 Design and synthesis of idebenone naphthoquinone analog (28).....	91
5.1.2 Design and synthesis of 2-chloro-3-amino-1,4-naphthoquinones analogs.....	92
5.1.3 Design and synthesis of 3-anilino-2-chloronaphthalene-1,4-dione analogs of..	93
5.1.4 Design and synthesis of 2-fluoro-3-((3(trifluoromethyl)phenyl) amino) naphthalene-1,4-dione (38)	96
5.1.5 Design and synthesis of 2-((3-(trifluoromethyl) phenyl) amino)-3-((trifluoromethyl)thio) naphthalene-1,4-dione (39).....	97
5.1.6 Design and synthesis of 3-anilino-2-methoxynaphthalene-1,4-dione analog (82-85)	98
5.1.8 Design and synthesis of 3-anilino-2-thionaphthalene-1,4-dione (37) analogs	99
5.1.9 Design and synthesis of analogs of 3-((3-(trifluoromethyl) phenyl) amino)-3-((trifluoromethyl)thio) naphthalene-1,4-dione (39)	100
5.1.10 Scaffold-hopping approach.....	100
5.2 Conclusion.....	105
Chapter 6 Biological evaluation of designed and synthesized compounds	109
6.1 Hit-to-Lead workflow	110
6.1.1 Results and discussion: ATP rescue and cytotoxicity SAR-1	111
6.1.2 Results and discussion: ATP rescue and cytotoxicity SAR-2	114
6.1.3 Results and discussion ATP rescue and cytotoxicity SAR-3	119
6.1.5 Conclusion ATP rescue assay and cytotoxicity assay	122
6.1.6 Results and discussion Pro-oxidant activity	125
6.1.7 Quinone reduction in cells.....	128
6.1.8 Seahorse bioenergetics analysis.....	129
6.1.9 Dose-response curve ATP rescue and cytotoxicity	132
6.2 Upregulation of the NQO1 Expression and ATP results	134
6.3 Discussion Ex-vivo studies of compounds 37 and 92.....	137
6.4 Conclusion: biological results obtained using synthesized compounds	139

Chapter 7 Conclusion and Future perspectives	141
7.1 Conclusion.....	142
7.2 Future perspective	144
Chapter 8 Methods and Materials.....	145
8.1 Statistic analysis	146
8.2 Mitochondrial isolation	146
8.3 Determination of protein concentration-bicinchonic acid assay (BCA)	147
8.4 Investigation of interactions of quinone compounds with NQO1.....	148
8.5 Investigation of interactions of quinone compounds with Complex I	148
8.6 Investigation of interactions of quinone compounds with Complex II.....	149
8.7 Investigation of interactions of novel compounds with cytochrome c and Complex III in presence of NQO1	149
8.8 Culturing of Cells.....	150
8.9 Thawing and Freezing of Cells	150
8.10 Treatment of Cells Compound	150
8.11 Determination of ATP level	151
8.11.1 Rescue of ATP level in HepG2	151
8.11.2 Rescue of ATP level SH-SY5Y.....	151
8.11.3 Rescue of ATP level SH-SY5Y after lipoic Acid treatment	151
8.12 Determination of cell viability assessed by MTT	152
8.12.1 Cytotoxicity assay HepG2 assessed by MTT	152
8.12.2 Cytotoxicity assay SH-SY5Y assessed by MTT	152
8.12.3 Determination of cell viability assessed by ATP quantification.....	153
8.14 Seahorse assay.....	153
8.16 Determination of H ₂ O ₂ level by the ROS-Glo™ H ₂ O ₂	154
8.17 Determination of quinone reduction by WST-1.....	155
8.17.1 Quinone reduction in SH-SY5Y cell line	155
8.17.2 Quinone reduction in HepG2 cell line.....	155
8.18 Western blot	156
8.19 Induce NQO1 lipoic acid in SH-SY5Y	157
Chapter 9 Experimental section	158
9.1 COMPUTATIONAL METHODS	159
9.1.2 General information.....	159
9.1.3 Protein preparation	159
9.1.4 Pharmacophore	159

9.1.6 Molecular Docking	160
9.1.10 Prediction of standard reduction potential.....	160
9.2 SYNTHESIS	161
9.2.1 General Information	161
9.2.2 Thin Layer Chromatography	161
9.2.3 Column Chromatography	161
9.2.4 NMR Spectroscopy.....	161
9.2.5 UPLC-MS analysis	162
9.3 Chemistry: general procedure and compound characterization	163
References	199

List of Figures

<i>Figure 1 The mitochondrion</i> ⁵	3
<i>Figure 2 Mitochondria dynamics</i>	4
<i>Figure 3 Mitochondrial electron transport chain</i>	5
<i>Figure 4 CI₂/CIII/CIV₂ supercomplex</i>	8
<i>Figure 5 Proteins encoded for ETC components</i>	9
<i>Figure 6 ROS damage to mitochondria and possible consequences</i>	11
<i>Figure 7 Schematic diagram of the retina</i> ¹¹	13
<i>Figure 8 Compounds under clinical investigation and their mitochondrial targets</i>	18
<i>Figure 9 Comparison of the two quinones CoQ10 and Idebenone</i>	19
<i>Figure 10 Interaction between Idebenone and complex I Idebenone (in green) can bind two different binding site of complex I.</i>	20
<i>Figure 11 Ping-pong mechanism.</i>	21
<i>Figure 12 NQO1 pathway</i>	22
<i>Figure 13 Idebenone metabolism and its metabolites</i>	24
<i>Figure Figure 14 NQO1 crystal structure and binding site</i>	30
<i>Figure 15 Ribbon presentation of the complex III</i>	31
<i>Figure 16 Schematic illustration of the Q-cycle model</i>	32
<i>Figure 17 Homology model of human subunit bc1 (blue) with the bovine complex III template (red)</i>	34
<i>Figure 18 Qo binding site, with highlighted in green the residues that make contacts with UHDBT (yellow)</i>	35
<i>Figure 19 Qo Chemical structures of bc1 inhibitors</i>	36
<i>Figure 20 Virtual screening workflow and selected commercial compounds.</i>	38
<i>Figure 21 Quinone compounds which possess diverse bioactivities</i>	39
<i>Figure 22 Bio-activation of quinones by NQO1</i>	40
<i>Figure 23 Representations of Menadione orbitals elaborated with Gaussian 98</i>	42
<i>Figure 24 Predicted binding mode for the compound 19</i>	47
<i>Figure 25 Experimental workflow and selective criteria to screen the identified compounds</i> 50	
<i>Figure 26 UV/VIS spectral analysis of NADH oxidation by NQO1 in presence of idebenone.</i>	52
<i>Figure 27 Michaelis-Menten plot depict oxidation of NADH by NQO1 in presence of Idebenone or CoQ₁</i>	53
<i>Figure 28 UV/VIS spectral analysis of DCPIP reduction by Complex in presence of CoQ₁</i> ..	54

<i>Figure 29 Michaelis -Menten plot depicts the reduction of DCPIP by Complex I in presence of Idebenone or CoQ₁</i>	55
<i>Figure 30 Michaelis -Menten plot depicts the reduction of DCPIP by Complex I in the presence of Idebenone and CoQ₁</i>	55
<i>Figure 31 UV/VIS spectral analysis of DCPIP reduction by Complex II in presence of CoQ₁</i>	56
<i>Figure 32 Michaelis -Menten plot depicts the reduction of DCPIP by Complex II in presence of idebenone or CoQ₁</i>	57
<i>Figure 33 Images of HepG2 cell line</i>	59
<i>Figure 34 Images of SH-SY5Y cell line</i>	59
<i>Figure 35 Influence of glucose on Rotenone toxicity</i>	60
<i>Figure 36 ATP rescue dose response curve for Idebenone</i>	61
<i>Figure 37 Influence of NQO1 and complex III inhibitors in the idebenone activity</i>	62
<i>Figure 38 The comparison of ATP rescue activity of idebenone in HepG2 cell line and SH-SY5Y</i>	63
<i>Figure 39 Seahorse assay</i>	64
<i>Figure 40 Influence of Rotenone on Oxygen consumption rate and OCR rescue by idebenone</i>	65
<i>Figure 41 Rescue of mitoATP production by idebenone</i>	66
<i>Figure 42 Idebenone reduction in SH-SY5Y and HepG2 cell line</i>	67
<i>Figure 43 Schematic representation of naphthoquinones cytotoxicity</i>	68
<i>Figure 44 The idebenone cytotoxicity on HepG2 and SH-SY5Y</i>	69
<i>Figure 45 Cell viability of SHSY-5Y cells exposed to idebenone and various concentrations of NAC for 24h</i>	70
<i>Figure 46 The ROS-Glo™ H₂O₂ Assay workflow</i>	71
<i>Figure 47 Quantification of ROS using CellROX® Green Reagent</i>	71
<i>Figure 48 Quantification of H₂O₂ using ROS-Glo™ H₂O₂</i>	72
<i>Figure 49 Experimental workflow used to select the hit compound</i>	75
<i>Figure 50 Results of the NQO1 assay</i>	76
<i>Figure 51 Comparison between 14 and 13 in the NQO1 assay</i>	77
<i>Figure 52 Cyclic reaction of NADH- re-oxidation</i>	78
<i>Figure 53 Effect of oxygen on the re-oxidation reaction</i>	79
<i>Figure 54 Results of the Complex I and Complex II assay</i>	80
<i>Figure 55 Comparison between idebenone and 28 in the complex I and complex II assay</i>	81
<i>Figure 56 Results obtained for the NQO1-complex III assay by selected naphthoquinones</i> ..	82

<i>Figure 57 Results obtained for the NQO1-complex III assay in presence of Antimycin A or Dicoumarol</i>	83
<i>Figure 58 Change in absorbance spectrum of 92 according to the amount of reducing agent (NABH₄) added</i>	84
<i>Figure 59 Efficacy of ATP rescue in the presence of rotenone by quinones at 5 μM.</i>	85
<i>Figure 60 Efficacy of ATP rescue in presence of rotenone by quinones at 1 μM</i>	85
<i>Figure 61 Cytotoxicity of quinones selected from virtual screening on HepG2 and SH-5YSY</i>	87
<i>Figure 62 Summarize of 19 bioactivity.</i>	88
<i>Figure 63 General strategy for identifying 19 analogs, showing 2-amino-1,4-naphthoquinone scaffold and four regions for diversification</i>	90
<i>Figure 64 UPLC chromatograms of compound 37 in reduced and oxidized forms.</i>	104
<i>Figure 65 Experimental workflow used to screen the synthesized compounds</i>	110
<i>Figure 66 Schematic representation of SAR-1 scaffold modification strategy</i>	111
<i>Figure 67 Efficacy of ATP rescue in presence of rotenone by naphthoquinones 14,47,55,56,39</i>	112
<i>Figure 68 Efficacy of ATP rescue in presence of rotenone by naphthoquinones synthesized (SAR-1)</i>	113
<i>Figure 69 Cytotoxicity of naphthoquinones synthesized (SAR-1) on HepG2 and SH-5YSY.</i> 114	
<i>Figure 70 schematic representation of SAR-2 scaffold modifications made</i>	115
<i>Figure 71 Efficacy of ATP rescue in presence of rotenone by synthesized naphthoquinones (SAR-2) at 5 μM</i>	115
<i>Figure 72 Efficacy of ATP rescue in presence of rotenone by synthesized naphthoquinones (SAR-2) at 1 μM</i>	116
<i>Figure 73 NQO1 activity of compounds 70,75,76,78.</i>	117
<i>Figure 74 Cytotoxicity of naphthoquinones synthesized (SAR-2) on HepG2s</i>	118
<i>Figure 75 Schematic representation of redox potential changes in ETC and hypothesized redox effect of different naphthoquinones. n</i>	119
<i>Figure 77 Efficacy of ATP rescue in presence of rotenone and cytotoxicity of naphthoquinones 37,70,76</i>	120
<i>Figure 78 Efficacy of ATP rescue in presence of rotenone and cytotoxicity of synthesized naphthoquinones (SAR-3)</i>	121
<i>Figure 79 Efficacy of ATP rescue in presence of rotenone and cytotoxicity of synthesized naphthoquinones (SAR-4) 1</i>	122
<i>Figure 80 correlation between ATP rescue activity and cytotoxicity of studied naphthoquinones.</i> 124	

<i>Figure 81 Efficacy of ATP rescue in presence of rotenone and cytotoxicity of selected naphthoquinones.</i>	123
<i>Figure 82 Chemical structures of compounds showing significant ATP rescue activity at 100nM.</i>	125
<i>Figure 83 Evaluation of intracellular ROS induce by naphthoquinones.</i>	126
<i>Figure 84 Evaluation of intracellular H₂O₂ induces by naphthoquinones in HepG2 and SH-SY cells.</i>	127
<i>Figure 85 WST-1 reduction in presence of hydroquinone as electron donator in HepG2 cell line in presence of absence of Dicoumarol.</i>	128
<i>Figure 86 WST-1 reduction in presence of hydroquinone as electron donator in SH-SY5Y cell line.</i>	129
<i>Figure 87 Comparison between the mitoATP production rate and GlycoATP production after quinone injection. es</i>	130
<i>Figure 88 Total ATP production rate of naphthoquinones in presence of Rotenone.</i>	131
<i>Figure 89 OCR rescue by 78,104 and idebenone in complex I impairment.</i>	132
<i>Figure 90 Dose response curve and EC50 values for idebenone, 37 and 92.</i>	133
<i>Figure 91 Dose response curve for idebenone, 37 and 92 in SH-SY5Y and HepG2.</i>	133
<i>Figure 92 Efficacy of ATP rescue in presence of rotenone by debenone,37 and 92 at a concentration of 10 μM and the influence of inhibitors</i>	134
<i>Figure 93 Chemical Structures of NQO1 inducers.</i>	135
<i>Figure 94 Protein expression of NQO1 induced by lipoic Acid.</i>	136
<i>Figure 95 ATP rescue activity by idebenone and naphthoquinone after inducing NQO1</i>	137
<i>Figure 96 NQO1 expression in retina layer</i>	138
<i>Figure 97 Treatment of retinal explants with selected naphthoquinones (37, 92).</i>	138
<i>Figure 98 Figure 97 Treatment of retinal explants with selected naphthoquinones (37, 92).</i>	140

List of Tables

<i>Table 1 Standard reduction potential for some mammalian oxidation systems</i>	42
<i>Table 2 Predicted reduction potential of quinone compounds</i>	45
<i>Table 3 Predicted reduction potential of designed quinone compounds</i>	46
<i>Table 4 Summarize of naphthoquinones bioactivity.</i>	88
<i>Table 5 Chemical structure details of synthetized compounds 42-59.</i>	93
<i>Table 6 Optimization Buchwald-Hartwig coupling</i>	94

<i>Table 7 Reagents and reagent condition synthesis compounds 61-77</i>	95
<i>Table 8 chemical structure details of synthesized compound 37, 79-80</i>	96
<i>Table 9 Chemical structure details of synthesized compound 82-86</i>	98
<i>Table 10 Chemical structure details of synthesized compound 88-93</i>	99
<i>Table 11 Chemical structure details of synthesised compounds 96-99</i>	100
<i>Table 12 Overview chemical structure synthesized compounds</i>	109

List of Scheme

<i>Scheme 1 Schematic representation of semiquinones formation in presence of oxygen</i>	48
<i>Scheme 2 WST-1 reduction in presence of hydroquinone as electron donator</i>	68
<i>S Scheme 3 Schematic reaction for idebenone analog 28</i>	91
<i>Scheme 4 Mechanism of the Menisci reaction</i>	92
<i>Scheme 5 Schematic reaction for the synthesis of 2-chloro -3-amino-1,4-naphthoquinones..</i>	92
<i>Scheme 6 Schematic synthesis of 2-hydroxy-3-(phenylamino) naphthalene-1,4-dione</i>	93
<i>Scheme 7 Synthetic route for compounds 70-77</i>	94
<i>Scheme 8 Synthesis of compound 78</i>	95
<i>Scheme 9 Synthesis of compound 37, 79-80</i>	95
<i>Scheme 10 Mechanism of nucleophilic attack using CeCl₃ as catalyst</i>	96
<i>Scheme 11 Synthesis of compound 38</i>	97
<i>Scheme 12 Synthesis of compound 39</i>	97
<i>Scheme 13 Mechanism of trifluoromethylthiolation of quinone 39</i>	98
<i>Scheme 14 Synthesis of compound 82-86</i>	98
<i>Scheme 15 Synthesis of compounds 91-93</i>	99
<i>Scheme 16 Synthesis of compound 95</i>	99
<i>Scheme 17 Synthesis of compounds 98-99</i>	100
<i>Schema 18 Synthesis of compound 103</i>	101
<i>Scheme 19 Mechanism of oxidative chlorination of 5 aminoquinolin-8-ol</i>	101
<i>Scheme 20 Synthesis of compounds 104-105</i>	102
<i>Scheme 21 Mechanism of oxidative conversion of 106 to 107</i>	102
<i>Schema 22 Synthesis of compound 109</i>	103
<i>Scheme 23 Synthesis of compound 113</i>	103
<i>Scheme 24 Mechanism of nucleophile addition</i>	103
<i>Scheme 25 Schematic representation of hydroquinone synthesis</i>	104

Abbreviation and Acronyms

A Adenine

AcOEt Ethyl acetate

ADME Absorption, distribution, metabolism, and excretion

ADOA Autosomal-Dominant Optic Atrophy

Ala Alanine

AMP Cyclic adenosine monophosphate

APS Ammonium persulfate

APS Ammonium persulfate

ARE antioxidant response element

Arg Arginine

ARs Aromatic rings

Asp Aspartate

ATP Adenosine triphosphate

AVV Adeno-associated virus

BCA Bicinchonic acid assay

BSA Bovine serum albumin

C Cytosine

CI Complex I

CII Complex II

CIII Complex III

CIV Complex IV

CoQ₁₀ Coenzyme Q10 (Ubiquinone)

CoA Coenzyme A

CPCM Conductor-like Polarizable Continuum Model

CuA Bimetalliccopper center

CYP 450 Cytochromes P450

Cytc Cytochrome c

DCA Dichloroacetate

DCM Dichloromethane

DCPIP dichlorophenol indophenol

DFT Density functional theory

DHLA Dihydrolipoic acid

DIPEA N-Diisopropylethylamine
DMD Duchenne Muscular Dystrophy
DMF Dimethylformamide
DMSO Dimethylsulfoxide
DNA Deoxyribonucleic acid
DRP1 Dynamin-related protein 1
EDG Electron donating group
EDTA Ethylenediaminetetraacetic acid
EMA European Medicines Agency
ETC electron transport chain
EWG Electron withdrawing groups
FA Friedreich's ataxia
FBS Fetal bovine serum
FDA US Food and Drug Administration
FADH Flavin adenine dinucleotide
FMN Flavin mononucleotide
G Guanine
G3PDH Glycerol-3-phosphate dehydrogenase
Glu Glutamate
Gly Glycine
GSH Glutathione
GSSG Glutathione disulphide
HBAs Hydrogen bond acceptors
HBDs Hydrogen bond donors
HEPES (4-(2-hydroxyethyl)-1-piperazineethanesulfonic acid)
His Histidine
HOMO Highest occupied molecular orbital
Hs Hydrophobic areas
Ile Isoleucine
ITC Isothermal Titration Calorimetry technique
LA Lipoic acid
Leu Leucine
LHON Leber's hereditary optic neuropathy
LUMO Lowest unoccupied molecular orbital

Lys Lysine
Met Methionine
MOE Molecular operating environment
MON Mitochondrial optic neuropathies
MS Mass spectrometry
MTT 3-(4,5-Dimethylthiazol-2-yl)-2,5-diphenyltetrazolium bromide)
NAC *N*-acetyl cysteine
NADH Nicotinamide adenine dinucleotide
NCE New chemical entity
ND4 NADH dehydrogenase 4
NMR Nuclear magnetic resonance
NQO1 cytoplasmic NAD(P)H: quinone oxidoreductase 1
Nrf1 Nuclear factor erythroid-derived 2 related factor 1
Nrf2 Nuclear factor erythroid-derived 2 related factor 2
OCR Oxygen consumption rate
OPA1 Optic atrophy 1
OXPHOS oxidative phosphorylation
PGC-1 α peroxisome proliferator-activated receptor-gamma coactivator 1 alpha
Phe Phenylalanine
PLIFs Protein-Ligand Interaction Fingerprints
Pro Proline
Qi site Quinone reduction binding site
Qo site Quinol oxidation binding site
RBPMS RNA-binding protein with multiple splicing
Rf Retention factor
RGC Retinal ganglion cells
RNA Ribonucleic acids
ROS Reactive oxygen species
Rt Retention time
SAR Structure-activity relationship
SDS Sodium dodecyl sulfate
SOD₁ Superoxide dismutase-1
SOD₂ Superoxide dismutase-2

SOD₃ Superoxide dismutase-3

T Thymine

TEMED Tetramethylethylenediamine

TFFA Trifluoroacetic anhydride

THF Tetrahydrofuran

TLC Thin-layer chromatography

Trp Tryptophan

UPLC Ultra performance liquid chromatography

UQ Ubiquinone

UQH₂ Ubiquinol

WST-1 4-[3-(4-Iodophenyl)-2-(4-nitrophenyl)-2H-5-tetrazolio]-1,3-benzene Disulfonate

XVOLs Exclusion volumes

CHAPTER 1: INTRODUCTION

1.1 Mitochondria

Mitochondria are intracellular organelles, present in the cytoplasm of eukaryotic cells, whose primary function is to support aerobic respiration and produce the energy necessary for all cellular functions¹. If cells do not have enough energy, they cannot function properly: mitochondria play a key role in their life and death, especially for cells with high energy demand. Each organelle has a double membrane structure, which is the house of the numerous mitochondrial functions such as ATP (adenosine triphosphate) production, calcium handling and the formation of iron sulfur clusters¹.

Mitochondria show important similarities with prokaryotes, suggesting that they were gradually assimilated by primitive glycolytic eubacteria in symbiotic relationships. The original hypothesis for this was proposed by Margulis in 1971 who suggested the origin of mitochondria has its roots in the increase of atmospheric oxygen concentrations, which led to the symbiotic relationship between a eubacterium and a primitive eukaryotic cell to take advantage of O₂ high level². This theory is supported by the presence of a single circular DNA inside mitochondria, which has the same size and structure of bacterial DNA³.

1.1.1 Mitochondria structure

Mitochondria are organised in different compartments: intermembrane space, intracristal space and matrix (Figure. 1)⁴. These compartments are different from phospholipidic bilayer membranes for their composition and function. The outer membrane defines the shape of mitochondria and allows the movement of molecules, through a variety of channels, to the intermembrane space; it is permeable for molecules up to 5000 kDa and contains proteins responsible for mitochondrial fission⁴.

The inner membrane is relatively impermeable except for specific active transport channels, necessary for establishing an electrochemical gradient across this barrier and for ATP production⁴. This membrane is organised in numerous invaginations called cristae, which increase the surface area, improving the capacity to produce ATP.

The inner membrane is also the place for most enzymatic reactions, which occur in the mitochondria and the electron transport chain.¹ The mitochondrial matrix compartment contains the mitochondrial DNA, and it is the site of multiple metabolic pathways such as the citric acid cycle and the oxidation of fatty acid⁴.

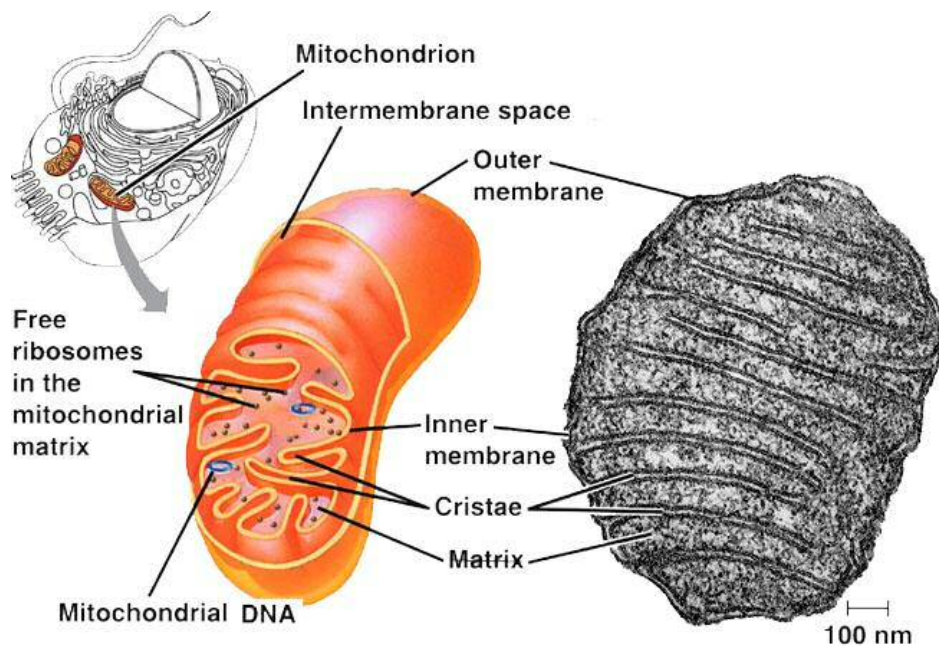


Figure 1 The mitochondrion⁵

1.1.2 Mitochondria dynamics: fusion and fission

Mitochondria are not static organelles, but they are constantly remodelling through repetitive fission and fusion events⁶. This dynamism facilitates the transport of mitochondria into daughter cells during the mitosis, the removal of damaged mitochondria, and communication and sharing of content among organelles. Fusion and fission are carefully regulated by a series of specific proteins. Fusion guarantees the organelle integrity and facilitates the exchange of mitochondrial DNA. It is mediated by the mitofusin proteins, which involve three nuclear encoded proteins: OPA1, mitofusin 1, and mitofusin 2. OPA1 regulates the fusion of the inner mitochondrial membrane, whereas the mitofusins are necessary for fusing the outer membrane⁶. Mutant forms of these proteins result in mitochondrial fragmentation and general mitochondrial dysfunctions⁷. The fission is a crucial mechanism ensuring an equilibrated distribution of mitochondria DNA between the daughter cells during mitosis. It is regulated by DRP1 (dynamin-related protein 1), which assembles into rings around a future site of scission and promote the division as shown in the (Figure. 2)⁷.

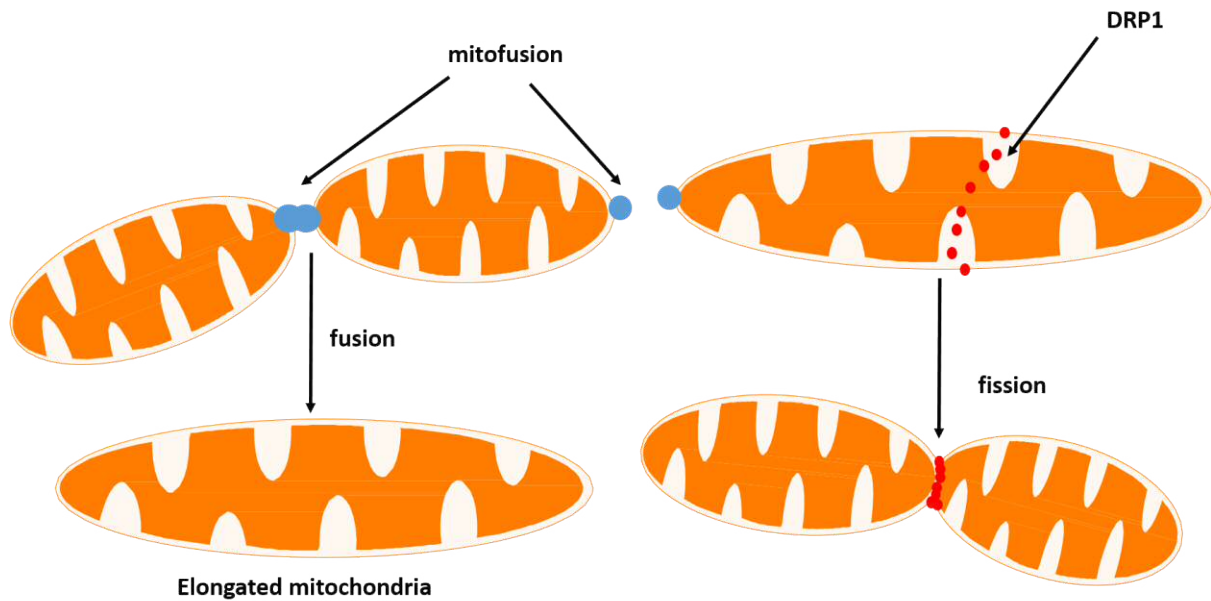


Figure 2 Mitochondria dynamics. Mitochondrial fusion of both outer and inner mitochondrial membranes facilitated by Mfn1/Mfn2 and Opa1 respectively. Drp1 induced fission resulting in mitochondria with preserved essential component.

1.1.3 Oxidative phosphorylation

The major function of mitochondria is the production of the majority of the cellular ATP by oxidative phosphorylation (OXPHOS)⁸. OXPHOS is a metabolic process, with which all nutritionally derived substances are metabolised in molecules rich of energy, which are used as a source of energy like ATP or as electron carrier (NADH, FADH)⁸.

The OXPHOS is the final stage of mitochondria respiration, a long process that begins with pyruvate generated from glucose during the glycolysis. The pyruvate is transported across the double mitochondrial membrane into the matrix where it is converted into acetyl CoA by pyruvate dehydrogenase⁴. Successively, the acetyl CoA enters the citric acid cycle (Krebs cycle), a series of chemical reactions, which generates energy through the metabolism of the acetyl CoA producing ATP, CO₂ and reduced electron carriers: NADH and FADH₂, ATP and CO₂⁹. These molecules are high energy compounds and important reducing agents used in the electron transport chain (ETC) to drive the production of the majority of ATP.

The ETC is at the heart of this metabolic pathway, and it is a complicated cascade mechanism relying on a series of redox reactions between reducing and oxidising species⁸. The ETC consists of four major multiprotein complexes called NADH: CoQ reductase (complex I),

succinate: CoQ reductase (complex II), ubiquinol: cytochrome *c* reductase (complex III) and cytochrome *c* oxidase (complex IV)¹⁰ (Figure. 3). This series of protein complexes work in steps catalysing the reaction between an electron acceptor and donor and a flow of electrons, which creates an electron proton gradient between the matrix and the intermembrane space. The ATP synthase (complex V) utilises this proton gradient to produce ATP from ADP and phosphate group.

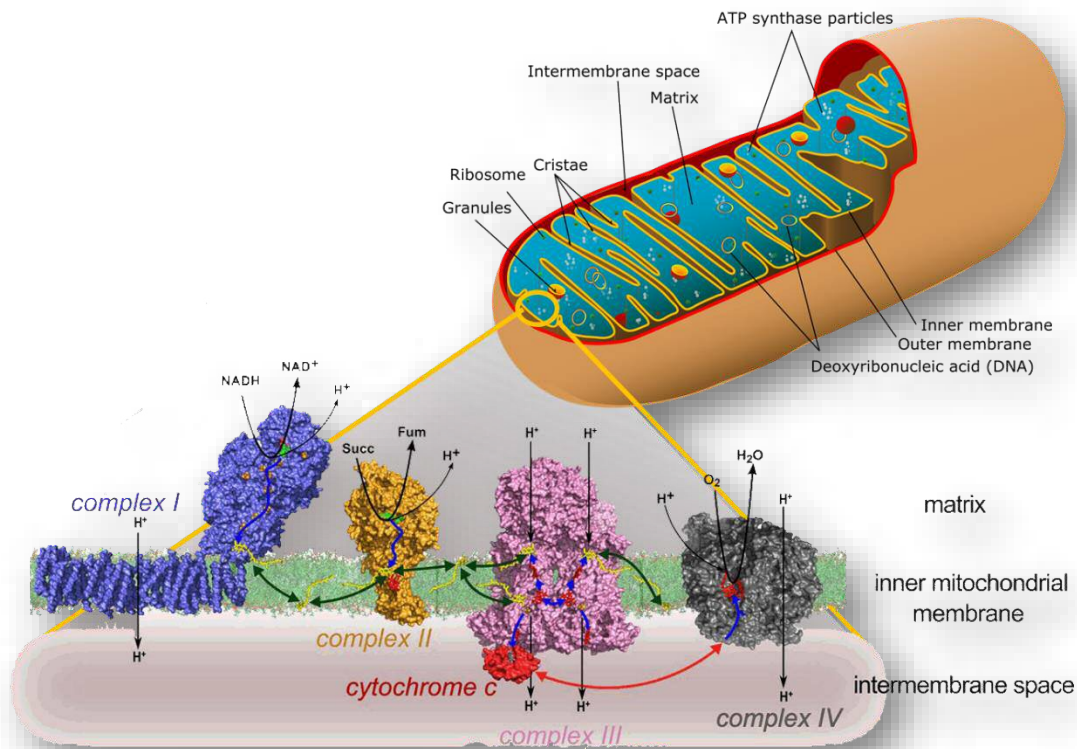


Figure 3 Mitochondrial electron transport chain.¹¹The electron transport chain consists of series of electron transporters (called complexes) embedded in the inner mitochondrial membrane, that shuttle electrons from reduced substrates (NADH, FADH) to molecular oxygen. During the electron transfer, protons are pumped from the mitochondrial matrix to the intermembrane space, in order to generate a proton gradient

It was widely accepted that individual complexes diffuse freely in the membrane, and ubiquinone and cytochrome *c* work as electron carriers moving efficiently between them. This organisation of the mitochondrial respiratory complexes is commonly called “fluid state”¹². In the fluid state model, the first step of this long chain reaction is the oxidation of NADH catalysed by complex I. Complex I consist of 38 subunits, 7 of which are encoded by mtDNA¹⁰. The complex can be divided into three modules (N, Q and P) each has different functions. The first reaction occurs in module N, in which NADH is oxidised, and two electrons are donated

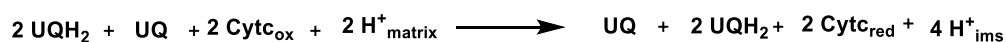
to flavin mononucleotide (FMN). The electrons are then transferred via a series of Fe–S clusters to ubiquinone, located in the ubiquinone reduction site in the Q module. The proton translocation module (P module) contains the three subunits, ND2, ND4 and ND5, which it is thought to be involved in the proton-pumping activity. During electron transport its 4 protons are pumped into the intermembrane space. The overall reaction is shown in equation



The second step involves the complex II, which is the only complex entirely encoded by the nuclear genome and consists of 4 subunits. Complex II is a direct enzymatic component of the Krebs cycle, catalysing the oxidation of succinate to fumarate, generating FADH₂. The resulting reduced flavoprotein is then oxidised to FAD⁺ by ubiquinone. During this process, no protons are transferred into intermembrane space, but a high energy molecule is produced such as ubiquinol



Once ubiquinone is reduced to its hydroquinone form, it is able to pass electrons to complex III (cytochrome bc₁ complex), which catalyses the reduction of cytochrome c (cyt c). Complex III is made up of 11 subunits, encoded by nuclear DNA, except for one subunit (apocytochrome *b*, that is encoded by the mitochondrial genome. The ubiquinol molecule produced previously in the complex I and II are oxidised back by this complex III transferring an electron to a molecule of cytochrome c and at the same time releasing 4 protons into inner membrane space.

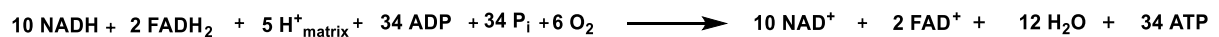


Complex IV concludes this flow of reactions using electrons and hydrogen ions to reduce molecular oxygen into water. It is made up of 13 subunits, of which three (subunits I – III) are encoded by mtDNA. The electron from Cytochrome c is initially transferred to a bimetallic copper center, CuA, which is the entry point for the electrons in the complex, successively these electrons are transferred to a series of haem centre and then to another bimetallic copper center CuB, where water a molecule of oxygen is bound. The complete reduction of oxygen to water requires 2 protons and 2 electrons. This reaction increases the electron proton gradient transferring other 4 protons to the inner membrane space:



Complex V is able to utilise the proton electrochemical gradient, generated by three of the four complexes, to phosphorylate ADP to ATP. It consists of two functional domains: F₁, situated in the mitochondrial matrix, and F_o, located in the inner mitochondrial membrane. F₁ is composed of three copies of each of subunits α and β , assembled in a ring and one each of subunits γ , δ and ϵ , that form a central stalk, which supports the ring. The F_o is composed of hydrophobic c-subunits, assembled in a rotatable ring. The two subunits work together to synthesise ATP from ADP. The proton gradient establishes a proton-motive force H⁺ ions move through F_o back to the mitochondrial matrix. The proton-motive force causes the rotation of the ring in F_o along with subunits γ , δ and ϵ in F₁. This rotary movement releases energy that is used by F₁ to drive the formation of ATP, in a process called “rotary catalysis”.

In summary, the result of this complicated mechanism is the transfer of ten protons through the inner membrane for each NADH that enters, resulting in the production of three ATP molecules.



The solid-state model does not change the mechanism behind the fluid state model neither the final result, but nowadays there is strong evidence showing that respiratory enzymes exist in a stable complex composed of varying ratios of different complexes associating with each other to form supercomplexes^{13,14,15,16}. With the sophisticated advent technique such as super-resolution light microscopy and electron, cryotomography has been possible described different structure of these macromolecular assemblies. In mitochondria from mammalian tissues, has revealed supercomplexes of varying stoichiometry including CI/CIII₂/CIV, CI/CIII₂, and CIII₂/CIV, these complexes are stabilized in these macrostructures by cardiolipin, which is present in high amounts in the inner mitochondrial membrane presumably filling the spaces between the complex and facilitating the diffusion of the electron carries. Researchers were able to study a high-resolution structural model of the mammalian respirasome, isolated from porcine heart mitochondria determined at 5.4 Å resolution¹⁷. In the architecture of the supercomplex, the majority of CI surrounds a CIII dimer and CIV, like a pincer, that contains all complexes necessary to pass electrons from NADH to O₂, and consequently produce ATP (Figure. 4). This model can be mostly considered as representative of all the mammalian structures studied in these last years, but it is not exclusively, there are other supercomplex structures, which lacks CIV entirely or CIV surrounds the CI, and finally combination in which

CIII is completely dissociated by the other complex¹⁵. The supercomplexes and their role in oxidative phosphorylation are still unclear, and only the "tip of the iceberg" has been studied. In the last few years, evidence of the architecture of mammalian supercomplex has been accumulated, continuing advances in the high resolution imaging and biochemical techniques can provide more information how supercomplexes assemble and function, facilitating the understanding of different mitochondrial diseases¹³.

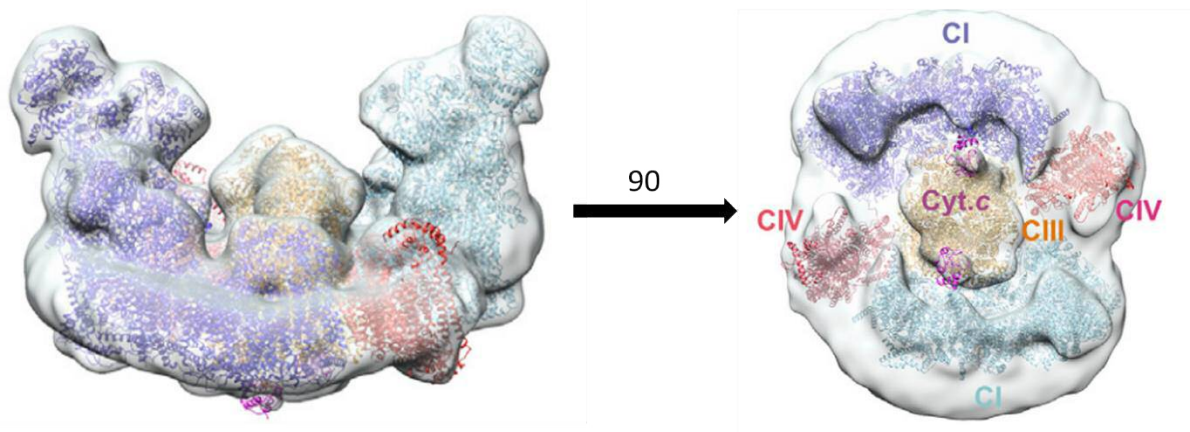


Figure 4 CI₂/CIII/CIV₂ supercomplex¹⁷ Structural models of CI, CIII, and CIV complex

1.1.3 Mitochondrial genetics

Mitochondria are the only organelles with their own genetic material and the ability to produce their ribonucleic acids (RNAs) and proteins. Differently, from nuclear DNA, mitochondrial DNA is a multicopy, circular DNA molecule 16,569 bp long³. This genome is necessary but not sufficient to support all the functions of mitochondria¹⁸. In the course of evolution, mitochondria gradually lost much of their original autonomy, and now they strictly depend on nDNA, which encodes numerous factors needed for mtDNA transcription, translation and replication.²

Mitochondrial DNA contains 37 genes, which encode for 13 essential polypeptides which assemble the complexes I, III, IV, and V, and the RNA machinery (2 rRNAs and 22 tRNAs) for their translation within the organelle. The nuclear DNA encodes for the remaining proteins of OXPHOS, in particular, the complex II and the other proteins necessary for the correct function and maintenance of mitochondria (Figure. 5).

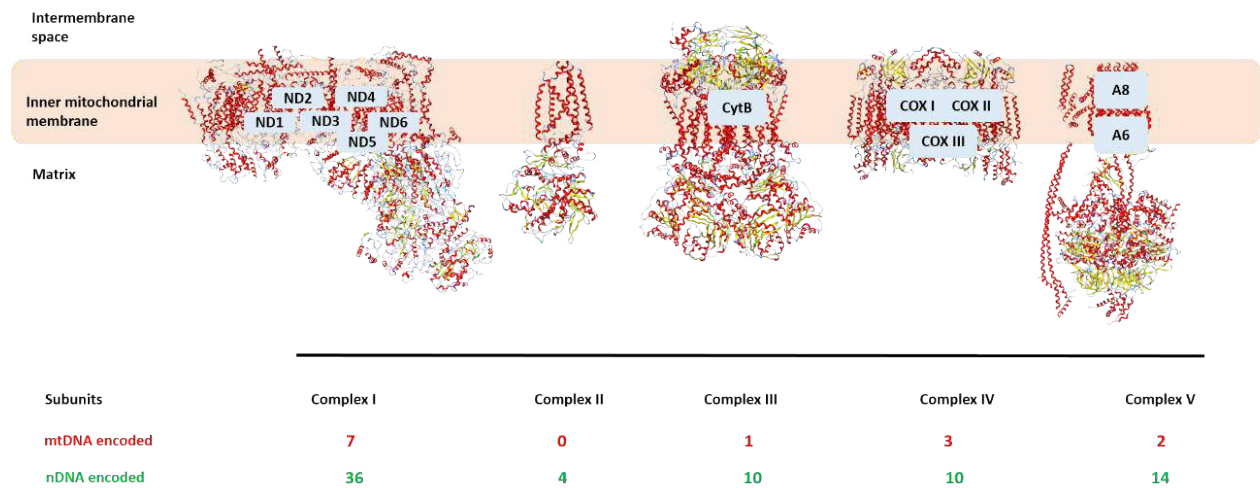


Figure 5 Proteins encoded for ETC components. Schematic representation of electron transport chain proteins and mtDNA- and nDNA-encoded components of the ETC

Each cell contains thousands of mitochondria and multiple copies of the mitochondrial genome. The presence of co-existence of two or more distinct mtDNA variants in the same cell is called heteroplasmy and its due to the high rate of mutations accumulated during the mitochondrial dynamics event¹⁹. The high rate of mutations in mitochondria could be caused by different factors, such as a lower fidelity of replication of mitochondrial DNA polymerase γ , the lack of effective repair mechanisms, and chronic exposure of mtDNA to ROS, which are normally produced during the oxidative phosphorylation²⁰.

This accumulation of mutations could cause defects in mitochondrial DNA and consequently might result in a full-blown mitochondrial disease when it reaches a particular level¹⁹. In fact, although mutations can accumulate in cells, the pathogenic mutation might need to reach high levels before showing deleterious effect. Below this critical point the mitochondria, which do not present the mutations, can compensate for the mutated one. Above it, the cells do not have enough ATP to function properly, and consequently show a deficient phenotype.

Over the last few years, mitochondrial DNA has become not only an important target for medicinal chemists, but it is also a very powerful tool used for tracking the ancestry of many species including humans. mtDNA is inherited through the maternal lineage and shows a high rate of mutations (more than nuclear DNA), which are highly conserved and unique from person to person²¹. These factors make mitochondrial DNA an ancestral map for different species in the world. This assumption even if it is still valid and that maternal inheritance remains absolutely dominant, a recently study found that occasional paternal transmission

events can occur in particular stress condition providing an alternative approach to study the mitochondrial inherited diseases²².

1.1.4 ROS production and damage to mitochondria

Mitochondria are considered the major source of ROS produced in cells. The term ROS defines different reactive chemical species containing oxygen, which, as natural by-products of the normal metabolism of oxygen, have essential roles in cell signalling and homeostasis^{23,24}. The level of ROS produced by mitochondria can be influenced by numerous cellular stimuli, but a basal level of ROS are produced during normal OXPHOS. Complex I and Complex III are the major sources of mitochondrial ROS²³, which are released in the on both sides of the inner membrane, making these complexes necessary for the regulation of cell signalling. Although, nowadays a normal level of ROS is considered necessary for correct cellular function, the accumulation of ROS can lead to oxidative stress, in which the cell is vulnerable to damage²⁴. In fact, ROS are reactive species that can react with the side chains of lipids in the various membranes of the cell, especially mitochondrial membranes, generating lipid-peroxidation and cell lysis. ROS also inflict oxidative damage on mtDNA, resulting in mutations that lead to defective electron transport chain components²⁴ (Figure. 6). Fortunately, mitochondria have different defence mechanisms, such as enzymes and physiological antioxidants, which promptly eliminate normal levels of ROS from cells. Superoxide O_2^- is the major species produced by mitochondria and it is usually converted to H_2O_2 by SOD₁ (Superoxide dismutase-1) in the intermembrane space and cytosol, SOD₂ (Superoxide dismutase-2) in the matrix and SOD₃ (Superoxide dismutase-3) in the extracellular space²⁵. Successively, different Catalases convert H_2O_2 to H_2O and O_2 , regulation the ROS level. When the balance between ROS/antioxidants is lost, this situation leads to detrimental consequences not only to the cellular environment but to whole organs.²⁴ In the case of ROS accumulation, the radical species can generate lipid radical "stealing" electrons from fatty acid chains of phospholipid²⁶. The lipid peroxy radical is then generated by addition of O_2 to the lipid radical, it also, in turn, can steal an electron from a proximate fatty acid chain resulting in further production of lipid peroxide and lipid radical in a continues vicious cycles²⁶. The liperoxidation of the fatty acids influences membrane stability and fluidity and consequently, the life of the cell. Several

physiological antioxidant compounds are able to quench this reaction such as glutathione, CoQ₁₀ and vitamin E²⁷.

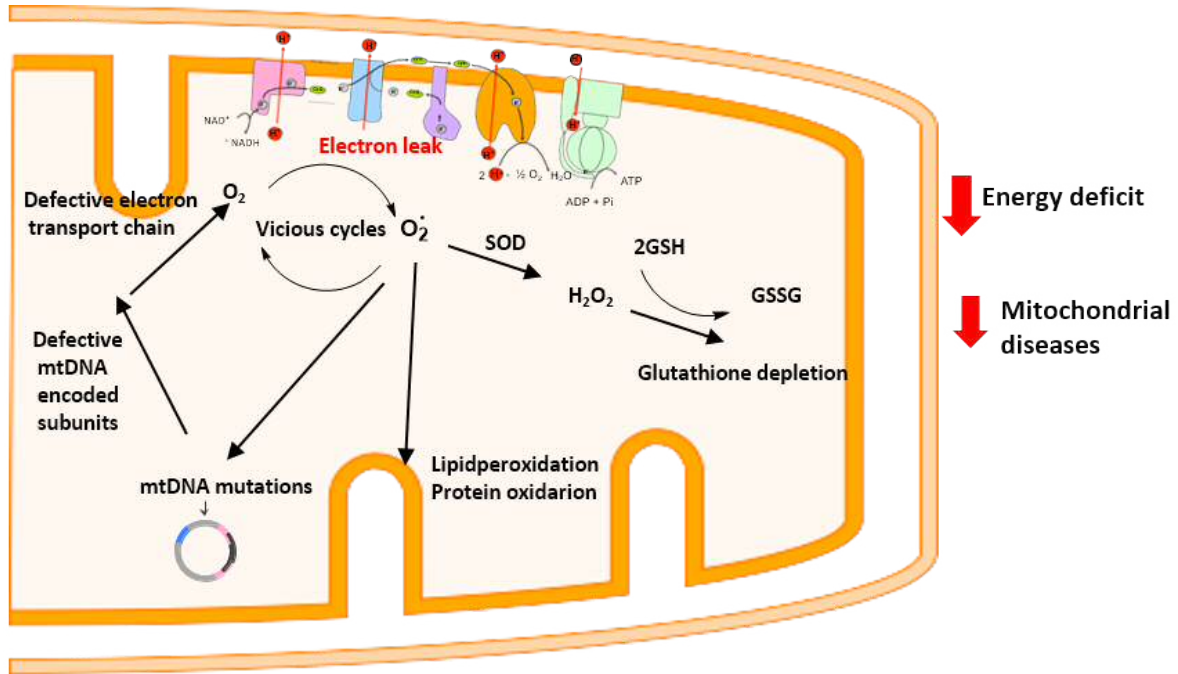


Figure 6 ROS damage to mitochondria and possible consequences. High level of ROS can lead to oxidative damage to mitochondrial proteins, DNA and membranes (fatty acid oxidation). The $O_2^{\cdot -}$ within the mitochondrial matrix, can be in part converted in H_2O_2 by Superoxide dismutase (SOD), which, in turn, is degraded by GSH peroxidase (GPx) to water. The glutathione peroxidases depend on glutathione for the reduction. The high level of ROS can lead to a depletion of glutathione, a fundamental physiological antioxidant. thereby contributing to a vicious cycle of accumulating mitochondrial damage.

1.2 Mitochondrial optic neuropathies

In recent years, an increasing number of studies have shown evidence of mitochondrial involvement in a variety of diseases.^{28,29} Mitochondrial dysfunctions are frequently the cause of a range of diseases, most notably in the heart and in the central nervous system,^{30,31} additionally they can also lead to neuro-ophthalmologic symptoms and signs.³² The visual impairment due to mitochondrial dysfunctions is one of the most significant causes of optic neuropathies.³² This situation becomes even more significant considering that mitochondrial optic neuropathies affect at least 1 in 10,000 individuals,³² and treatment options that lead to an appreciable amelioration of the condition are not available. The difficulty in finding an appropriate cure lies in the heterogeneous nature of these diseases. The causes and pathogenic mechanisms behind them can be very different and, as a consequence, the symptoms can be as different as the pathogenic pathway involved.³³ The most common mitochondrial optic neuropathies are genetic, but they can also be caused by side effects of drugs, toxins, infections and nutritional deficiency of antioxidants.

By convention, mitochondrial optic neuropathies are defined as a group of diseases characterised by the primary sensitivity to mitochondrial dysfunction of retinal ganglion cells (RGCs) and their axons forming the optic nerve (Figure.7). These cells play a crucial role in the correct functionality of the retina. They receive visual information from photoreceptors and send out this information in the form of the action potential to the thalamus, hypothalamus and midbrain.³⁴ The prelaminar region of these cells is normally non myelinated, and the propagation of the action potential is correlated with a high-energy demand in order to transmit the signal. The energy required is produced only by the ganglion cells through mitochondrial oxidative phosphorylation.³⁴ For this reason, these cells have a high presence of mitochondria, probably more than any other neurons in the brain, and they are frequently involved in mitochondrial dysfunction diseases.³⁵ When RGCs do not have enough energy, they cannot function properly, and this condition evolves into a degenerative process, which eventually leads to complete optic atrophy and blindness.

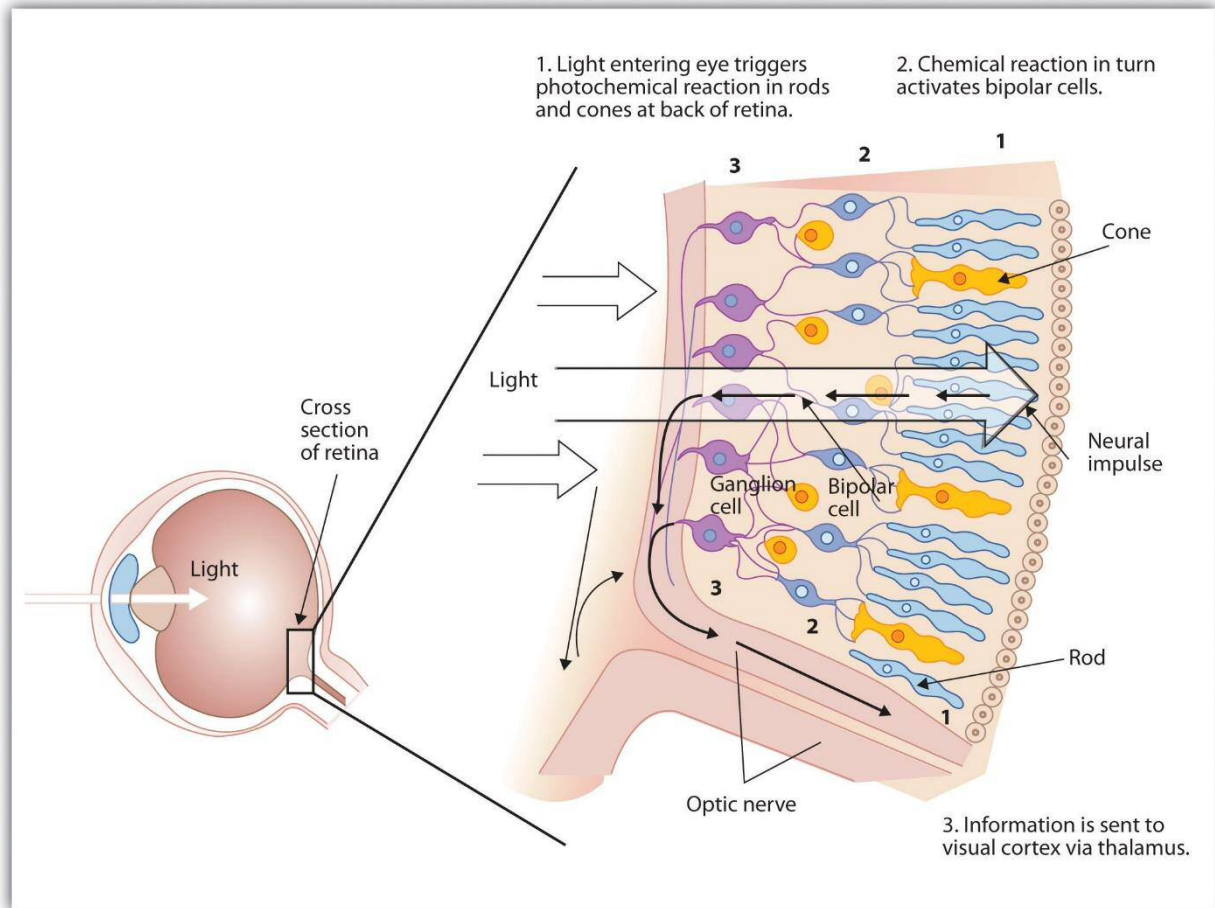


Figure 7 Schematic diagram of the retina¹¹

Optic neuropathies involve inherited (primary mitochondrial diseases) or acquired impairments of the mitochondrial function (secondary mitochondrial diseases). Inherited optic neuropathies are characterised by mutations associated with either primary mitochondrial DNA (mtDNA) mutations or defects in DNA, which code for mitochondrial proteins.²⁸ Secondary mitochondrial diseases are a result of the accumulation of mitochondrial damage due to other diseases such as Parkinson's or Alzheimer's diseases. Two representative primary mitochondrial diseases are Leber Hereditary Optic Neuropathy (LHON) and Autosomal-Dominant Optic Atrophy (ADOA), which are both characterised by the preferential loss of retinal ganglion cells.³⁶ LHON is the most common primary mtDNA disease, with one statistic showing it affects 1 in 31 000 persons in the North East of England.³⁷ This condition is characterized by three mitochondrial DNA (mtDNA) point mutations, m.3460 G>A, m.11778 G>A and m.14484 T>C, which all involve genes encoding subunits of the complex I of the mitochondrial respiratory chain.³² People affected by this disease do not suffer from any clinically evident peripheral neuropathy; the condition is usually painless, and the first

symptoms appear at 15-30 years of age, but the progression is in most cases rapid, and acute bilateral visual impairment occurs in few months.³⁸

Unlike LHON, the majority of patients with DOA show mutations within the OPA1 gene, which is a gene present in nuclear DNA, encoding for a mitochondrial inner membrane protein.³⁹ This disease represents a group of inherited mitochondrial optic neuropathies, which are caused by mutations in the nuclear genome involving the structure and functionality of the respiratory chain. In particular, most mutations in patients with DOA affect the synthesis of the OPA protein, which regulates the fusion process of mitochondria.³⁹ This condition generally appears in younger patients and leads to a progressive onset of visual failure in early childhood. There are similarities between DOA and LHON, as both conditions are bilateral optic neuropathies, involve RGCs, and are thought to present an excessive production of reactive oxygen species (ROS). These reactive species are a by-product of normal cellular respiration,²³ but they can generate an inflammatory state, in which the area involved is associated with cellular damage.²⁴

Not surprisingly, the combination of these factors makes optical mitochondrial diseases difficult to diagnose and manage, and represents a challenging goal for current researchers in the field.

1.2.1 Leber's hereditary optic neuropathy

LHON was firstly described in the nineteenth century by the ophthalmologist Theodor Leber 1840-1917, who noticed few of his patients were related by the same anomaly, that seemed to be heritable, indicating that a genetic basis for the disease⁴⁰. As mentioned in Chapter 1.2, three primary mitochondrial DNA mutations are involved in the development of the diseases. The first mutation identified was found in the gene that codes for NADH dehydrogenase 4 (ND4). This point mutation involves an alteration in a single base pair at position 11778, in particular, a guanine (G) is substituted for an adenine (A). This mutation leads to a change in the primary structure of the ND4 protein⁴⁰. The ND4 is an important subunit in the Complex I core proteins, it is required to catalyse NADH dehydrogenation and electron transfer to ubiquinone⁴¹. Among all the mutation, the ND4 account for about 70% of all LHON cases worldwide. The remaining cases are largely related to mutation polypeptide subunits of ubiquinone ND1 and ND6⁴². Also,

these mutations are due to an alteration in a single base pair, ND1 is caused by a Guanine to Adenine substitution at position 346, while ND6 is caused by a replacement of thymine (T) for a cytosine (C) at point 14484. These two subunits have a similar function, and they are apparently involved in attaching the hydrophilic part of the enzyme to the inner membrane⁴³. All these mutations lead to a block of electron flow at the first step of the chain, with deleterious consequence in the ATP production. This lack of ATP ultimately leads to cellular apoptosis. Retinal ganglion cells are particularly susceptible to the decrease of ATP caused by loss of proper mitochondrial activity. RGCs are responsible for the communication between the eye and the brain, taking visual information from photoreceptors and sending to the brain through the optic nerve⁴⁴. The propagation of these signals down their axons demands a large amount of energy more than other cells, which is mostly the reason for the almost selective visual loss rather than other symptoms⁴⁴. Although there are cases, in which there have been other manifestations reported beside the vision loss, such as Cardiac arrhythmias, peripheral neuropathies, dystonia. These phenotypes have been called “LHON plus syndromes” and have been linked to other mtDNA point mutations that affect OXPHOS complex I activity⁴⁵.

LHON usually arises during the adolescence to young adult, and interesting not all individuals who inherit these primary mtDNA mutations develop optic neuropathy and loss of vision, only approximately 50% of the males and approximately 10% of the females carrying these mutations manifest visual symptoms. Typically, the disorder had slow and constant progress to the point of severe optic atrophy and permanent impairment of visual activity. To date, a definitive cure is still not available and many of the therapies currently being developed focus on vision management and slowing the progression of the disorder, with a few promising drugs under clinical investigation³⁷.

1.2.2 Compounds under clinical investigation

For several years, researchers have synthesised small molecules with the aim of treating mitochondrial diseases, but most of the available treatments for mitochondrial disorders are limited to dietary supplements, and currently, there are no US Food and Drug Administration (FDA)-approved drugs for the effective treatment of primary mitochondrial disease.⁴⁶ This is due in part to the heterogeneity of these diseases, which involves simultaneously different factors, and in part to the difficulties of targeting mitochondria. Treatment options are therefore limited to symptomatic therapies and to delaying the progression of the disease.⁴⁷

The most common prescription medicine for mitochondrial disease patients is a high dose of a variety of vitamins and co-factors, called a “mitochondrial cocktail”: coenzyme Q₁₀ and vitamin E are always present in these cocktails, along with folic acid, L-carnitine, and creatine, vitamin B2 and B1. The therapy is very expensive and ineffective in most cases, showing limited clinical efficacy, and the long-term benefits of such treatment remain unproven.^{48,49}

However, a few new small molecules are now under clinical investigation, claiming to improve mitochondrial function.⁴⁶ These compounds have very different chemical structures and functions, but they can be grouped into families according to their target and pharmacological activity (Figure. 8):

- compounds that increase the rate of OXPHOS, increasing ATP production and recovering the energy deficits associated with mitochondrial dysfunction;
- antioxidants that maintain the normal homeostasis within the mitochondria, reducing ROS levels;
- compounds that influence mitochondrial biogenesis, the process by which cells increase the number of mitochondria;
- molecules that can be utilised by mitochondria as a supplement to produce ATP (fatty acids and analogs).

L-carnitine is a ubiquitous amino acid that plays a critical role in the transport of long chain fatty acids across the inner mitochondrial membrane. Fatty acids are transported via carnitine into mitochondria. These fatty acids are subsequently oxidised to acetyl CoA, which enters the Krebs cycle to generate ATP. It is an FDA approved compound and is used to treat a range of metabolic diseases as supplementing substrate due to its role in increasing the ATP production⁵⁰. Another nutritional supplement used in the treatment of LHON is the DCA

(dichloroacetate). DCA increases the mitochondrial respiration inhibiting the pyruvate dehydrogenase kinase, an enzyme which catalyses the inactivation of the pyruvate. The amount of pyruvate imported into the mitochondria increase and consequently the level of reduced cofactors available for the oxidative phosphorylation⁵¹. The benefit of using these nutritional supplements as an alternative fuel for the mitochondria remains limited and unclear^{48,49}.

AICAR, Bezafibrate and Rapamycin are some examples of a larger class of compounds, that functions as activators of mitochondrial biogenesis⁵². The drugs can increase the mass and number of mitochondria in the cells, and therefore the level of ATP. The mitochondrial biogenesis is regulated by the transcriptional activator PGC-1 α . The activation of PGC-1 α is triggered by different factors such as the decrease of ATP and NADH and it is controlled by peroxisome proliferator-activated receptors and AMP-activated protein kinase⁵². Bezafibrate and other mitochondrial biogenesis activators can activate this protein, and consequently the mitochondrial biogenesis. The use of these drugs in the treatment of mitochondrial optic neuropathies has not been clinically proved so far⁵².

Ubiquinone is a physiological fat soluble molecule present in all eukaryotic species. It is a fundamental component of the electron transport chain, and it participates in aerobic cellular respiration as electron carrier, transporting electrons from complex I and II to complex III⁵³. Another important function of this compound is its ability to work as antioxidant, reducing the concentration of ROS and free radicals.⁵⁴ For these peculiar qualities, it has been used as a food supplement in patients with respiratory chain deficiencies, in the hope to improve the efficiency of electron transferring and ATP rescuing and to reduce the oxidative stress. Early in vitro studies showed that ubiquinone in its reduced state could reduce the lipid peroxidation of mitochondrial membranes. However, more recent studies showed that supplementing CoQ₁₀ in patients, were ineffective mostly due to its poor bioavailability⁵⁵. Recently, in order to improve the pharmacokinetics property of ubiquinone a series of quinone analogs were synthesised and tested such as MitoQ, EPI-743 and idebenone⁵⁶. These novel quinones can increase ATP production, directly interacting with the electron transport and/or act as antioxidant reducing the level of ROS. Among them, idebenone seems to be one of the most promising, having shown in the last few years encouraging results for the treatment of LHON, Duchenne Muscular Dystrophy (DMD) and Friedreich's ataxia (FA)^{57,58,59}.

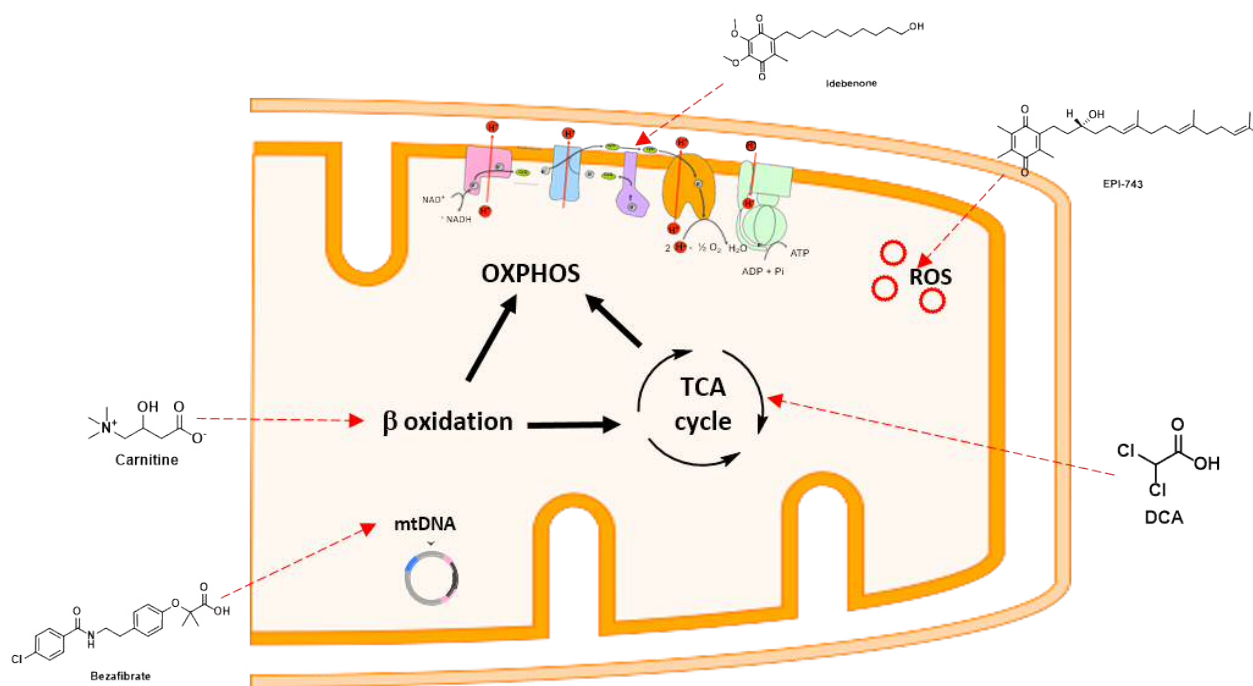


Figure 8 Compounds under clinical investigation and their mitochondrial targets

1.3 Idebenone

In the last few years, idebenone has been prominent in the area as a promising drug for the treatment of different mitochondrial diseases; however its history is older. Idebenone was selected from a medicinal chemistry program conducted in the 1980s by Takeda Pharmaceuticals as a possible cure for Alzheimer's disease, but showed a limited success.⁶⁰ Idebenone was considered as an analog of physiological ubiquinone CoQ₁₀, and it was believed to emulate the same physiological mechanism of ubiquinone.⁶¹ But even if idebenone shows structural similarities with natural CoQ₁₀, sharing its quinone moiety and lipophilic tail, different targets and mechanisms of action have recently been suggested.⁵⁵ Ubiquinone is lipophilic molecule (logD 19.12), with a long isoprenoid tail and a hydrophilic quinone head. These two features give to this compound a unique ability to move inside cellular membranes and work as electron donor and acceptor. However, CoQ₁₀ has significant limitations due to its high lipophilicity in terms of low absorption and bioavailability.⁵⁵

Idebenone was first synthesised in order to improve ubiquinone characteristics, whilst retaining its pharmacological activity.⁵⁵ For this reason, idebenone possesses the same benzoquinone core of ubiquinone, but with a shorter, less lipophilic side chain: instead of ten repeats of

isoprenoid elements, idebenone has a saturated ten carbons tail with a terminal hydroxyl group⁵⁵ (Figure. 9)

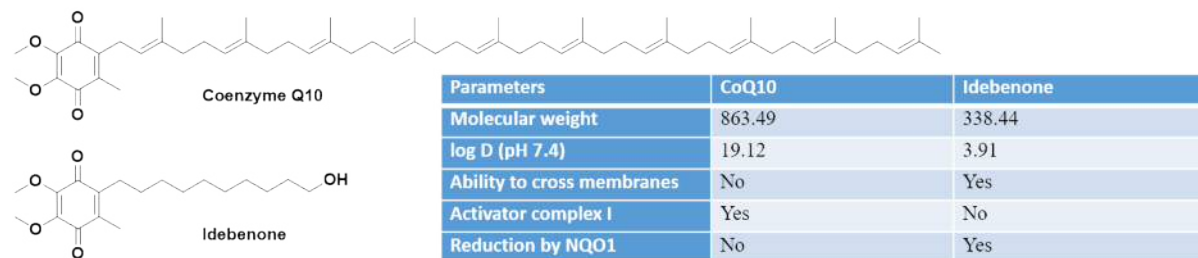


Figure 9 Comparison of the two quinones CoQ₁₀ and idebenone

1.3.1 Different mechanisms of action

As ubiquinone works as an electron carrier, transporting electrons from complex I and II to complex III, it was anticipated that idebenone would work in the same way. However, recent evidence suggests a major difference between these two compounds: idebenone is not a suitable substrate for complex I; on the contrary, recent studies demonstrated that a concentration of idebenone above 10 μM is enough to inhibit this enzyme.⁶¹

The inhibitory activity of idebenone is likely due to a slow release of reduced idebenone from the CoQ₁₀ binding site within complex I, thus blocking the physiological reduction of CoQ₁₀.⁶² Moreover, idebenone can stimulate oxygen radical generation by complex I, binding a second quinone-binding site within complex I. Idebenone is likely able to occupy the hydrophilic NADH binding site and is then reduced by Flavin mononucleotide (FMN) to an unstable semiquinone that generates superoxide.⁶³ On the other hand, extremely hydrophobic compounds like CoQ₁₀ are incapable of interacting with this non-physiological hydrophilic binding site.⁶²

Mitochondrial complex I inhibition, combined with superoxide generation, may lead to idebenone being toxic at certain doses rather than a promising drug for the treatment of mitochondrial diseases. Nevertheless, idebenone has proven effective in recovering ATP in cells even under conditions of dysfunctional complex I.⁶⁴ From this evidence it becomes clear that there is an alternative pathway in which idebenone can show its beneficial therapeutic effects.

Haefeli *et al.* have recently identified this additional idebenone-dependent metabolic pathway, by which idebenone can transfer electrons from the cytosol directly to complex III: idebenone is efficiently reduced by the cytoplasmic enzyme NADH-quinone oxidoreductase 1 (NQO1), and in its reduced form it is able to donate electrons to complex III or to work as antioxidant to reduce the oxidative stress⁶⁴ (Figure. 10).

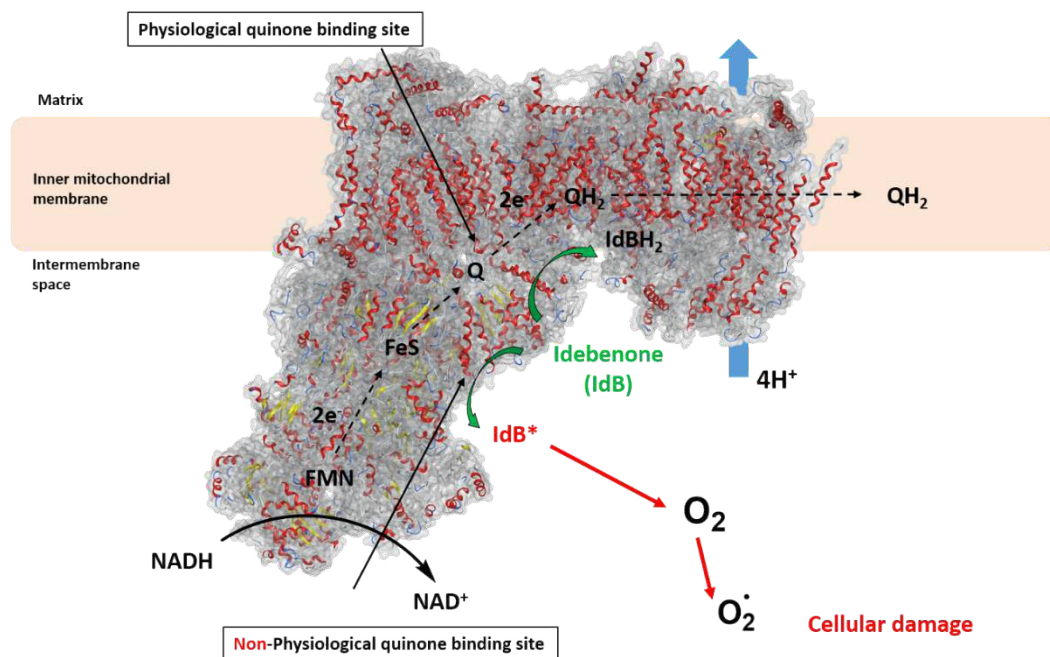


Figure 10 Interaction between idebenone and complex I Idebenone (in green) can bind two different binding site of complex I. In the physiological quinone binding site idebenone competes with ubiquinone, acting as an inhibitor, in the non-physiological quinone binding site Idebenone is reduced to a semi-quinone, which can generate ROS

1.3.2 NQO1 pathway

NAD(P)H: Quinone oxidoreductase 1 (NQO1) is an obligatory two-electron donor flavoenzyme which catalyses the direct reduction of quinones to hydroquinones, avoiding the formation of semiquinones. This enzyme works through a ‘ping-pong’ mechanism: NAD(P)H occupies its binding site and transfers electrons to FAD, the resulting NAD(P)⁺ leaves the site to be replaced by the quinone substrate, and consequently FADH donates electrons to the

quinone, converting it into hydroquinone, which leaves the binding pocket to restart the catalytic cycle⁶⁵ (Figure. 11).

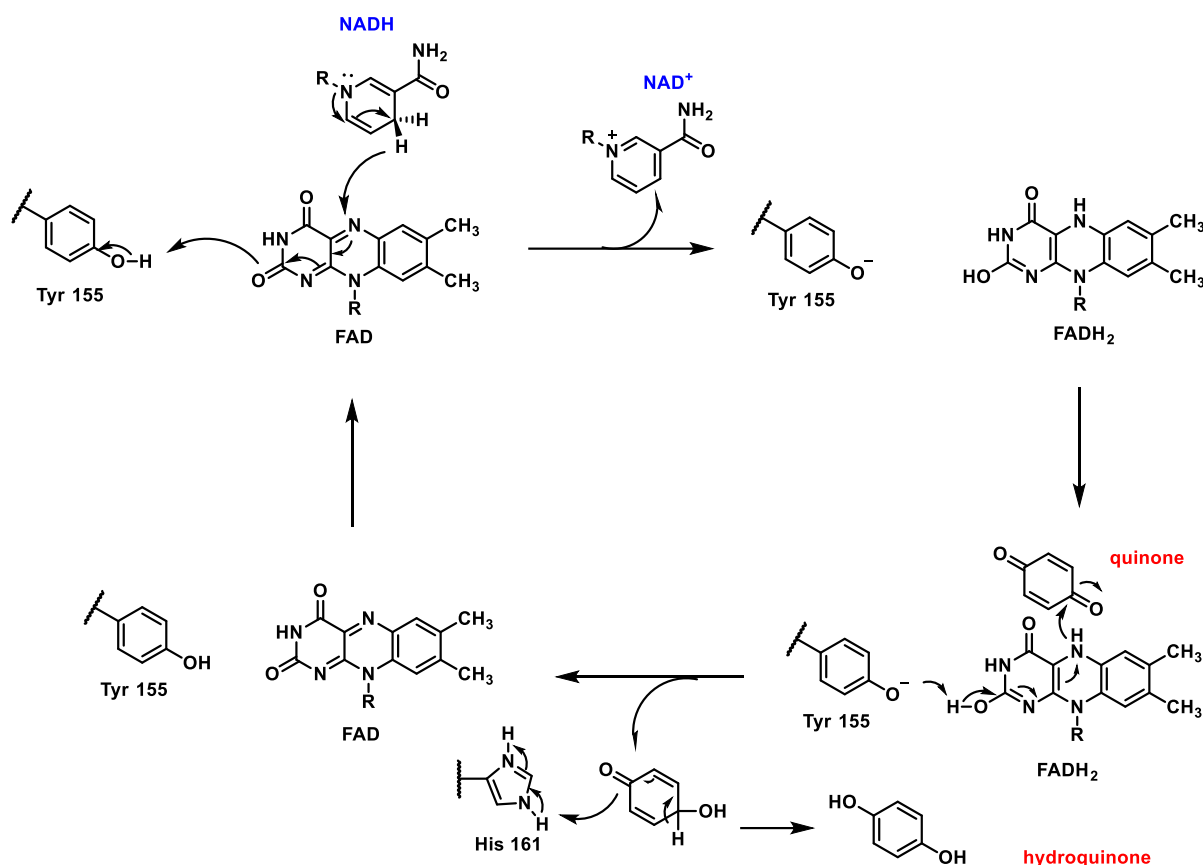


Figure 11 Ping-pong mechanism. NADH and quinone share the same binding site; initially, FAD is reduced by NADH, successively NAD is replaced by quinone, which undergoes a two electron reduction regenerating FAD

NQO1 is a cytosolic enzyme expressed in different tissues, particularly present in the liver for its detoxification activity, but also expressed in other tissues, including the brain, mainly in astrocytes⁶⁶. Its expression is regulated by the antioxidant response element (ARE) both in basal and during oxidative stress conditions, and the nuclear transcription factors Nrf1 (nuclear factor erythroid-derived 2 related factor 1) and Nrf2 (nuclear factor erythroid-derived 2 related factor 2) are known to mediate this induction⁶⁷. This family of transcriptional proteins that binds to ARE leads to the induction of many cytoprotective and antioxidant genes⁶⁷. Once activated, NQO1 shows his detoxification activity introducing functional groups into xenobiotics, as quinones, metabolised into their less reactive and less toxic hydroquinones forms. It is believed that idebenone itself is metabolized/activated by NQO1: once idebenone is reduced by this enzyme, it becomes sufficiently hydrophilic to traverse the cytosol, but also

lipophilic to cross the mitochondrial membrane and interact with complex III, re-establishing the correct electron flow in the mitochondrial electron chain (Figure. 12).⁶²

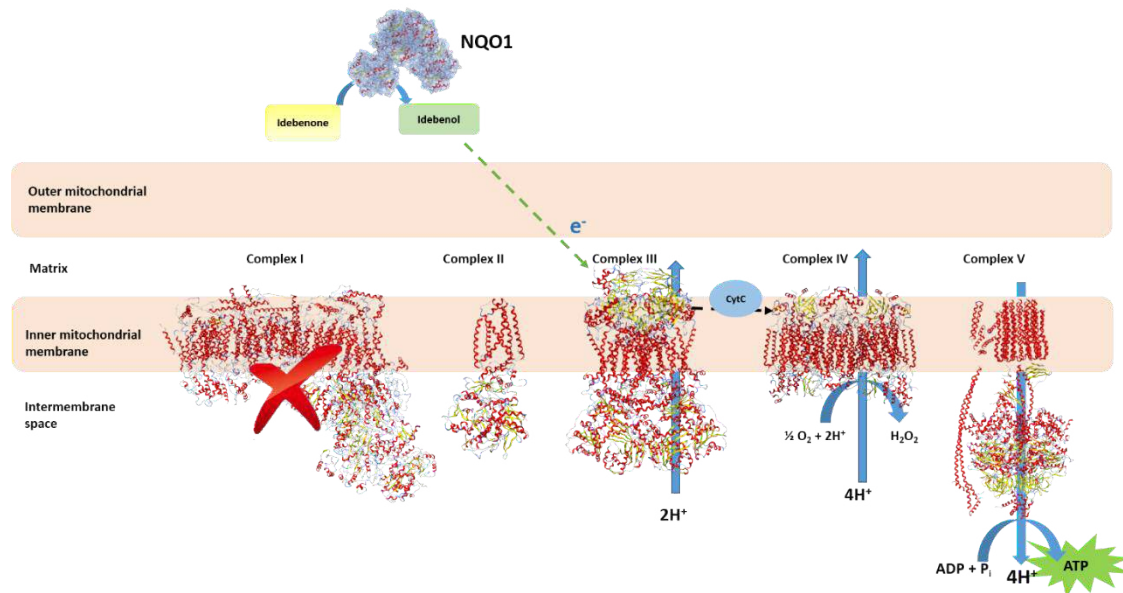


Figure 12 NQO1 pathway. In the postulated mechanism of action, idebenone is reduced into Idebenol (the active form) by NQO1 in the cytoplasm, and then successively it can mediate electron transfer to complex III in the mitochondrial inner membrane, reactivating the electron flow.

1.3.4 Current status: idebenone pros and cons

Several studies provide convincing evidence of the efficacy of oral idebenone 900 mg/day for promoting vision recovery in patients with LHON - in these studies, idebenone is very well tolerated and safe. Consequently, idebenone was recently approved for the treatment of LHON by the EMA⁶⁸ (European Medicines Agency), but under "exceptional circumstances", with the requirement for continued evaluation of its clinical benefits. Indeed, the evidence for idebenone's efficacy is limited, and it failed to demonstrate the superiority over placebo in the primary randomised, double-blind, placebo-controlled study⁶⁸. The beneficial effects associated with idebenone have not been reliably determined in the studies conducted so far, with some patients completely failing to respond to the therapy. More recently, Yu-Wai-Man et al (2018) tested idebenone in LHON fibroblast cells, derived from 4 patients and

characterised by the m.11778G>A mutation. In this study, idebenone showed only a partial recovery, with a slight ATP rescue only in one cell line.³²

On the other hand, various papers report the negative effects of idebenone, which involve different targets and pathways. Recently, the accumulative deleterious effect of idebenone was highlighted – this is due to oxidative stress in healthy wild type mice, with an adverse impact on RGC dendrite morphology and visual function, confirming the increase of NQO1 enzyme in response to this oxidative environment.⁶⁹

This adverse effect could be due to the impairment of complex I, or to superoxide generation due to the interaction between idebenone and the hydrophilic binding site within complex I.^{61,63} Moreover, idebenone could promote the opening of the permeability transition pore complex,⁷⁰ and furthermore, it has been shown that idebenone can inhibit the activity of a calcium-activated chloride channel and induce apoptosis in cells⁷¹. This evidence causes concern among researchers: could idebenone be considered safe for administration to patients long term or at high doses?

Another problem associated with idebenone is its low bioavailability.⁷² In fact, idebenone undergoes an extensive first-pass metabolism in the liver, so that less than 1% of the compound reaches the blood-stream, as it is rapidly metabolised through oxidation and sidechain shortening into its inactive metabolites QS10, QS8, QS6, QS4⁴¹ (Figure. 13). Even if it is reported that a concentration of idebenone above 10 nM is cytoprotective against complex I inhibition in RGC cell lines *in vitro*, due to this strong first pass metabolism, idebenone needs to be administered at a high dose to achieve pharmacological efficacy.⁷³

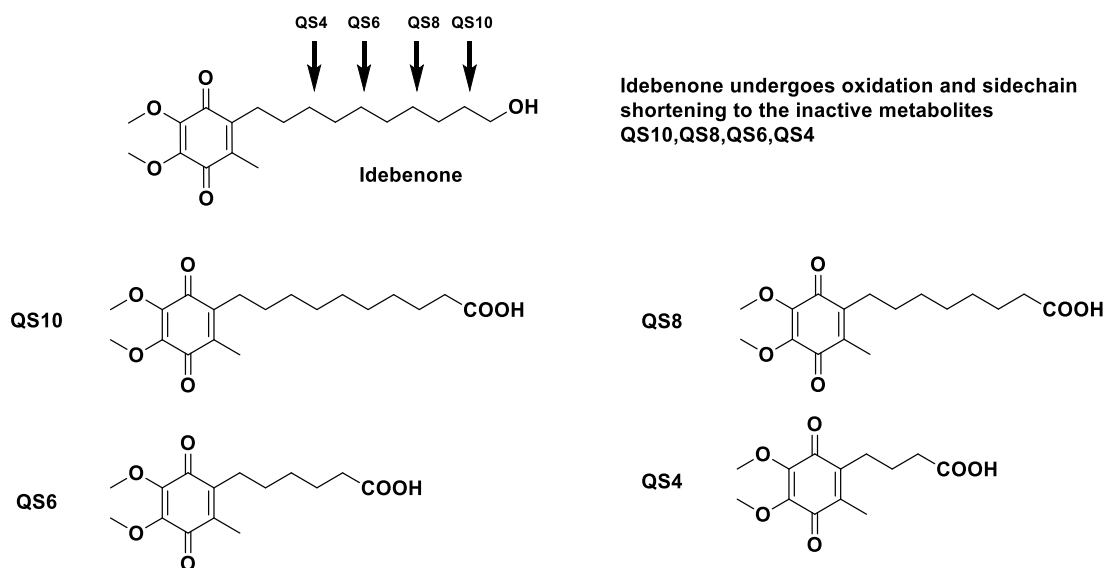


Figure 13 Idebenone metabolism and its metabolites

Such factors indicate that a non-systemic route of delivery would be more efficacious and safer than a systemic delivery. Overall, the lack of an effective alternative drug for the treatment of mitochondrial optic neuropathies diseases, combined with some promising results obtained in early clinical trials, should not prevent the search for better agents.

1.4 Emerging gene therapy treatment modalities for Leber's hereditary optic neuropathy

In the last years, alternative treatments have been investigated for mitochondrial optic neuropathies, such as gene therapy⁷⁴. In gene therapy, a defective gene is replaced by the normal wild type gene. In the treatment of LHON diseases, the unmated ND4 is transferred into the cells of patients. Once this gene is encoded, a function ND4 subunits will be incorporated in the cells, replacing the mutant ND4. In the last years, several efforts have focused on delivery to deliver the gene to the mitochondria, but due to the difficulty to penetrate the relatively impermeable intermembrane, an alternative approach, called Allotopic gene expression has been used. In this approach a different⁷⁵ Adeno-associated virus (AAV) vector has been used to deliver the gene to the cell nucleus, the corresponding protein is functionalized with mitochondrial targeting sequence, which allows the protein to accumulate into mitochondria⁷⁵. A limitation in this approach is that not all mitochondrial proteins can be transported in the mitochondria. Although the intensively studies in the last year, their results are still inconsistent, with some patients exhibited significant improvements in visual acuity,

whereas no significant changes were found in the others patients⁷⁶. In 2018 GenSight Biologics, a biopharma company focused on gene therapies for retinal neurodegenerative diseases, has carried out a clinical trial on LHON gene therapy with positive results in phase III⁷⁷. Successful gene therapies have the potential to treat directly the cause of chronic genetic diseases, with perhaps just one treatment rather than treat its symptoms as many conventional drug therapies, but to date, there are still some ethical and economic issues that need to be addressed. In fact, a major concern in this field, it is the high cost of a gene therapy^{78,79}. In 2015, uniQure developed a gene therapy for lipoprotein lipase deficiency, a genetic disorder that cause acute pancreatitis and diabetes, but unfortunately, although approximately 2 million persons are affected worldwide by this deficiency, only one patient was treated post-market release of the therapy, due to the high cost of the therapy : \$1 million for treatment⁸⁰.

1.4 Research question

Despite the efforts of recent years, there are currently limited treatment options for mitochondrial optic neuropathies, and to date idebenone is the only drug approved for the treatment of LHON, although there is still uncertainty on its clinical benefits. Due to the recently identified shortcomings of idebenone, the development of better treatment options for these diseases are urgently needed. We hypothesise that the lack of idebenone activity is correlated in part with the unspecific NQO1 target and its low bioavailability. Following this, the overarching aim of this PhD thesis was to identify a novel compound that could restore energy production and/or reduce the level of oxidative stress, improving the pharmacological activity of idebenone, and at the same time limiting its negative effects. This main aim was subdivided as follows.

- I. Identification of novel NQO1 and Complex III substrates. Computational techniques have been used to evaluate the binding mode of the compounds in the pocket of the two proteins and the intrinsic physico-chemical properties of these compounds.
- II. Hit optimization. Novel organic compounds have been synthesized in order to investigate the SAR of the NQO1 substrates selected from the virtual screening and identify more biological active compounds
- III. In vitro assessment of the biological activities of the identified substrates. The selected compounds have been tested in specific *in vitro* assays, in order to investigate their ability to enable mitochondrial respiration under the impairment of complex I and their cytotoxicity compared to idebenone.
- IV. The study of the mode of action of the identified substrates. A series of *in vitro* assays has been used to understand the role of NQO1-complex III pathway as drug target and to underline the mechanism for the observed biological activity

CHAPTER 2: COMPUTATIONAL STUDIES

2.1 Computer-aided drug design

Computational drug design has played a key role in the discovery and development of small molecules with therapeutic effects in the last decades.⁸¹ The rapid expansion of computational chemistry lies in the advantage of this approach in terms of time and cost reduction in drug discovery programs, since it allows the rapid generation of structure activity relationship (SAR) data and the obtainment of lead structures that are likely to proceed in subsequent preclinical and clinical stages.⁸¹ Computer-based methods can be divided into two categories: structure-based approaches and ligand-based approaches.⁸² Structure based methods are based on the structure information available for target proteins, while ligand-based methods use only ligand information for predicting the activity of the novel structures depending on their similarity/dissimilarity to known actives.⁸² Both these strategies were taken into consideration to develop this project. In order to modify and optimise the lead compound idebenone, a ligand-based pharmacophore model represented a primary strategy; given the abundance of crystal structure information available for the NQO1 enzyme, this ligand-based approach was combined with a target-based method in order to increase the affinity of idebenone derivative to this enzyme and identify novel suitable substrates. Moreover, the postulated mechanism of action of idebenone posits that it can transfer electrons to complex III after metabolic activation by NQO1. Hence, the potential idebenone derivatives were further evaluated for their capacity to bind the complex III and transfer electrons. But, despite the numerous studies, the specific mechanism that rules the electron transfer between the physiological ubiquinol (UQH₂) and the complex III remains unclear, and so the exact protein conformation^{83,84,83}. The limitation of the available crystal structures makes the drug design more challenging. Nevertheless, several complex III structures crystallised with competitive inhibitors are available, and they can be analysed to interpret where UQH₂ may bind^{85,86,87}.

In this study, a structure-based approach was used to study the complex III protein structure and acquire useful information to focus the synthetic efforts onto those molecules that are most likely to bind the target. In order to identify an agonist of complex III, the physiological compound, ubiquinone, has been used as a starting point to identify the structural elements in the molecules that are responsible for its agonist activity. In this case, clearly, the quinone moiety is responsible for the reversible reduction of the ubiquinone and for the agonist activity. This specific characteristic has been considered in the virtual screening study and the design of novel agonist. Once identified the key structure moiety involved in the biological activity, it

was possible to further modify the molecules to investigate structural features that will enhance the agonistic activity.

2.1.1 NQO1 enzyme as a target

NAD(P)H: quinone oxidoreductase 1 (NQO1, DT-diaphorase) is a cytosolic obligate two-electron reductase, which exists as a homodimeric flavoprotein composed of two closely associated monomers of 273 residues, each containing one molecule of FAD, the fundamental co-factor involved in the reduction mechanism. In each monomer, there are two different domains: a major catalytic (1-220 residues) and a small C-terminal domain (221-273 residues); the catalytic sites are located at the dimer interface.⁸⁸

NQO1 was widely studied during the last years for its important involvement as a target in anti-tumour therapies; therefore, several crystal structures are available for a structure-based approach.^{89,90,91} Crystal structures of protein-ligand complexes are very useful tools to acquire information on protein-ligand binding, and researchers use them to predict the correct orientation in the active site and the corresponding protein-ligand interactions. These data can, in turn, contribute to SAR studies and subsequent structure-based ligand design and optimisation. Faig M *et al*⁸⁸ have determined the crystal structure for the human NQO1 enzyme and the complex of the human enzyme with the substrate Duroquinone by X-ray diffraction to a resolution of respectively 1.4 Å and 2.5 Å. (Protein Data Bank = PDB ID: 1D4A⁸⁸). The comparison between the Apo enzyme and the complex with Duroquinone reveals that the binding site of this quinone compound overlaps with the one of NADPH, in accordance with the ping-pong mechanism of action of this enzyme, in which NADH and Duroquinone share and switch the same binding sites.⁸⁸

Exploration of the protein structure and the interactions of the substrate (Duroquinone) indicated the residue composition of the biologically relevant binding sites: five aromatic residues (Trp-105, Phe-106, Phe-178', Tyr-126', and Tyr-128') that interact with the quinone through hydrophobic contacts, and three additional residues, Tyr-126, Tyr-128 and His-161, which interact through hydrogen bonds.⁹¹ Furthermore, the isoalloxazine of FAD provides most of the contacts within the binding pocket, and plays a crucial role, resulting fundamental for the correct orientation of the quinone compound within the pocket. In fact, in order to ensure the reduction of quinone compounds, these must be stacked parallel to the isoalloxazine ring and make π - π interactions⁹¹ (Figure 14). The distance between the flavin N5 (hydride donor)

to the possible acceptors of the hydride in the quinone is not more than 4.5 Å to O1, 4.1 Å to C1, and 3.55 Å to C2 of the quinones. The 3-D crystal structures of human NQO1 in complex with other substrates (Dicoumarol, EO9 and ARH019; PDB ID: 2F1O⁹¹, 1GG5⁹⁰ and 1H69⁸⁹, respectively) provide additional useful information. From these structures, it appears clear that this enzyme possesses a highly plastic active site, which can accommodate quinone compounds of different sizes, making it possible to design and modify several potential substrates.

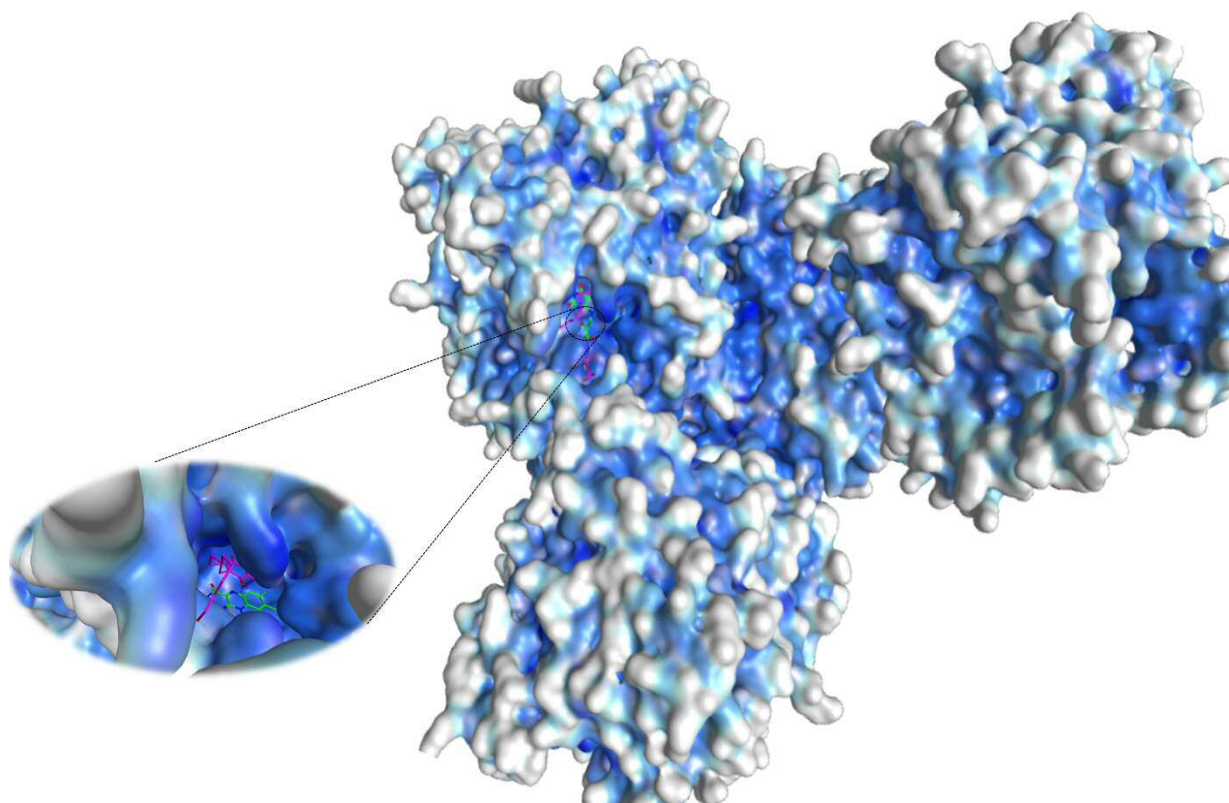


Figure 14 NQO1 crystal structure and binding site. The Figure shows the proposed binding mode of idebenone (purple) with the isoalloxazine of FAD (green) in the NQO1 binding site

2.1.3 Complex III (Ubiquinol-cytochrome *c* oxidoreductase)

Complex III (Ubiquinol-cytochrome *c* oxidoreductase) is a fundamental component of the cellular respiratory chain, it is located in the inner mitochondrial membrane, and it catalyses the electron transfer from a ubiquinol molecule to cytochrome *c* and simultaneously movement of protons across membranes for ATP synthesis. It consists of a homodimeric protein, composed of 11 subunits, of which just one is encoded by mitochondrial DNA, the remaining are encoded in the nucleus (Figure15).⁸³ Nevertheless, only three subunits are essential for the

electron transfer (ET) and proton translocation function: the cytochrome b (cyt b), that contains two b-type hemes (low potential bL and high potential bH heme) and is entirely located in the membrane.

The cytochrome c1 (cyt c1), which has a c-type heme covalently attached to its active domain that is located in the intermembrane space of mitochondria. The c-type heme accepts electrons from Rieske protein and transfers electrons to cytochrome c. The Rieske protein (ISP subunit), which features an integrated 2Fe-2S cluster in its extrinsic domain (ISP-ED), that is on the same side as the cyt c1 subunit and anchored to the membrane by a helix.

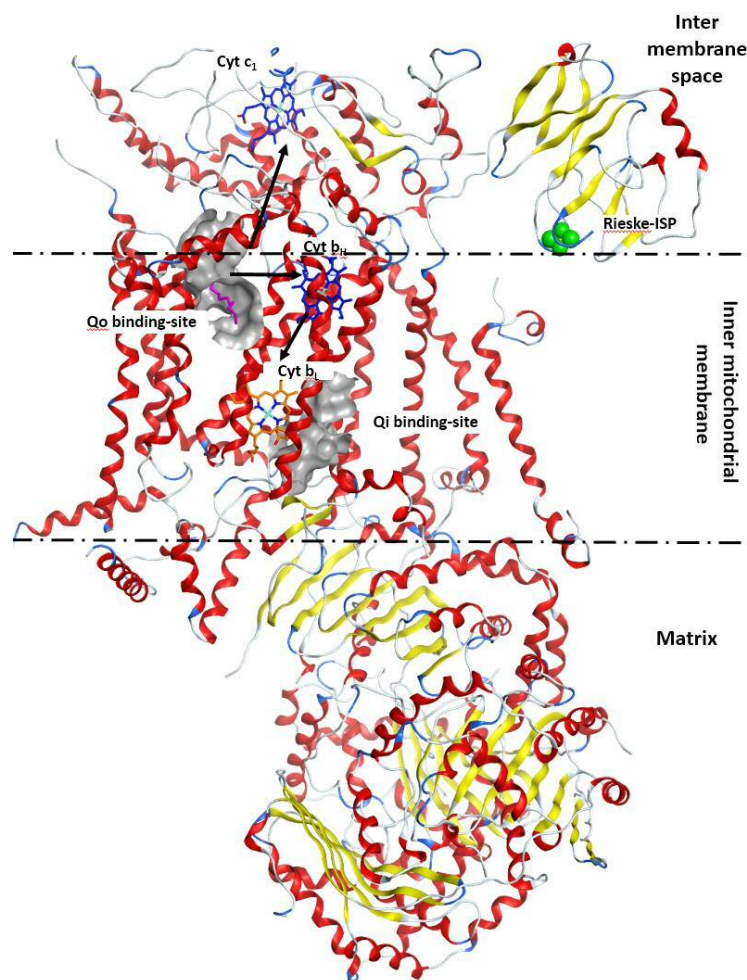


Figure 15 Ribbon presentation of the complex III. Ribbon diagram of the monomeric complex III. the two substrate binding pockets, Qo and Qi, are defined by cavity maps (grey), The Rieske protein (ISP subunit) is highlighted in green

These four redox centers of the bc1 complex work together in the process known as the Q cycle, in which the final result is the transfer of electrons from the ubiquinol to cytochrome c.

This transfer of electrons is not straightforward; indeed it is rather complicated and, it was not yet entirely decoded at the molecular level⁹². The most largely accepted mechanism of electron and proton transfer within the complex III is the Q-cycle hypothesis originally proposed by P. Mitchell.⁹³ This model consists of two separate processes called half-cycle and two separate quinone binding sites: one for quinol oxidation (Q_o site) and the other for quinone reduction (Q_i site).

In the first half-cycle, a ubiquinol molecule binds the Q_o binding-site and transfers the two electrons to the complex. One of these electrons moves to the Rieske center, then to cytochrome c₁ and finally to cytochrome c. It is defined as the high potential pathway. The other electron proceeds through a different pathway (low potential pathway) and moves through the heme groups of cytochrome b and to ubiquinone to form a semiquinone.

In the second half-cycle of the Q cycle, another ubiquinol binds the Q_o bind-site, and the electron follows the same pathways as before, with the reduction of another cytochrome c and the other electron, instead completes the reduction of ubiquinone, from semiquinone to hydroquinone (ubiquinol). In summary, after one Q cycle two cytochrome c molecules are reduced, four protons are pumped into the intermembrane space, and one ubiquinol is oxidised into ubiquinone (Figure 16).

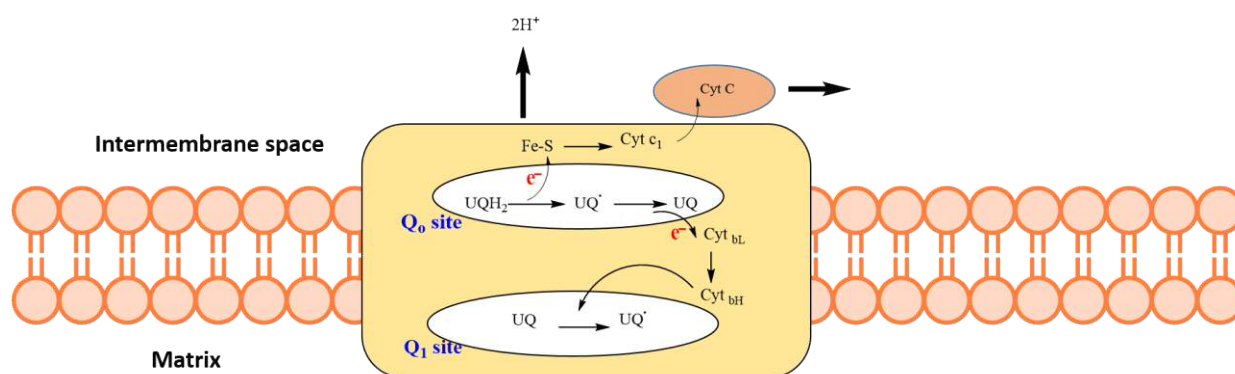


Figure 16 Schematic illustration of the Q-cycle model

Studying the mechanism of ubiquinol oxidation at the Q_o site is a crucial step in the development of novel drugs with the hypothesised mechanism of actions: direct transfer of electrons to complex III, bypassing complex I and II by quinone reduction by NQO1. Unfortunately, to date, there is not a high-resolution crystal structure of cytochrome c, that shows the binding of substrate UQH₂ at Q_o binding. In the absence of x-ray structures of

complex III bound to agonists, antagonists have been used to study the Qo binding site. In this study, different bovine cytochrome bc₁ complex crystal structure (PDB IDs: 1ntz, 1sqv, 1sqq, 1sqz) were used in order to acquire information for SAR studies of novel substrates for complex III.^{83,85,86}

2.1.4 Homology model and study of quinol binding site

Homology modelling is the process by which one or more template proteins with known structures are used as scaffolds to build an unknown protein structure, applying the aminoacids sequence of the interested protein.⁹⁴ This technique allows prediction of the 3D structure of proteins based on experimental data of the 3D structure of homologous reference proteins.⁹⁴ The crystal structure of bovine cytochrome bc₁ (PDB ID: 1ntz) has been used as a template for modelling the human complex III. The original input sequence of the human subunit cytochrome c₁ (cyt c₁) was retrieved from the Swiss-Prot database,⁹⁵ the sequence of the human enzyme was aligned to those of the template (1ntz) in order to identify the amino acid residues that could form the subunit.

The overall sequence identity between bovine cytochrome c and the human is 78.8 %, very high and suitable for creating an acceptable description of the binding site. Most of the residues of the binding site are conserved, with the exception of methionine 190 and 194, replaced by alanine and threonine respectively (Figure 17). The formal validation of the created model was done with MOE.

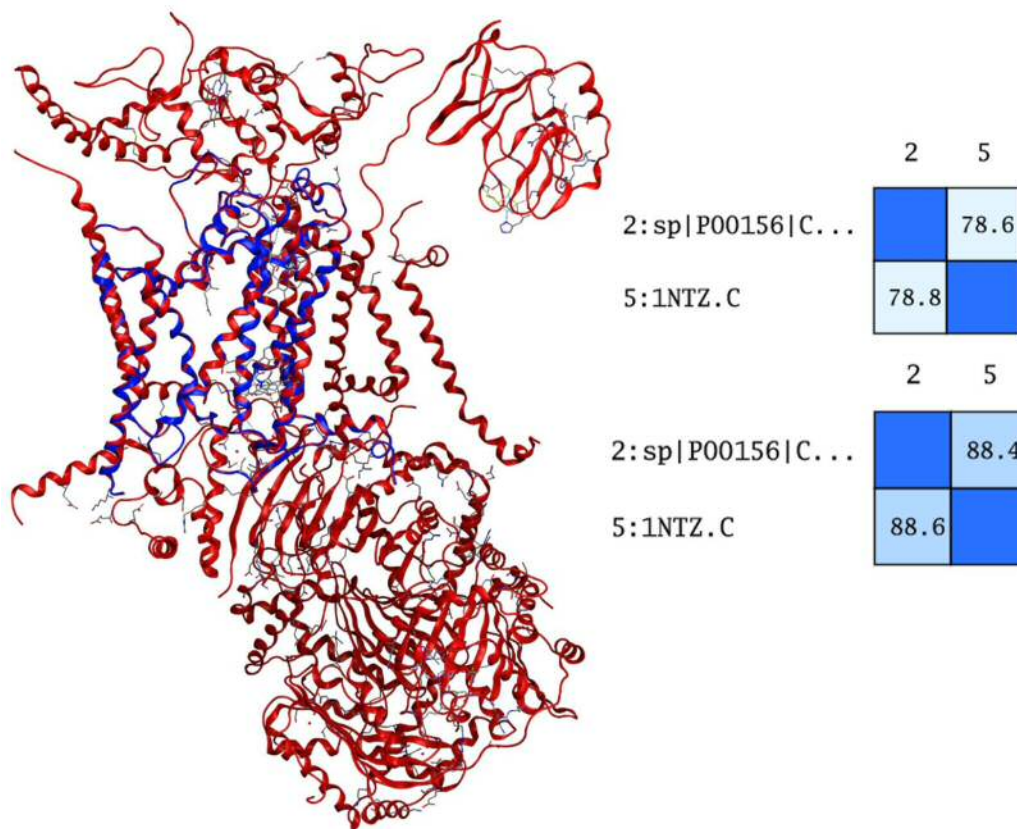


Figure 17 Homology model of human subunit bc1 (blue) with the bovine complex III template (red).

The Qo pocket of the native bovine crystal structure (1ntz) is located on the positive side of the membrane close to the mitochondrial intermembrane space. The Qo pocket is highly hydrophobic with six prominent aromatic residues in addition to a number of aliphatic residues. The exploration of the binding site and the interactions with the different inhibitors NQNO, UHDBT, MAOS show different conformational changes at the Qo site upon inhibitor binding, with only three residue making contacts with all three inhibitors: Ile146, Pro270 and Phe274⁸⁵. Phe274 is located near the entrance of the Qo pocket, and in a position to stabilise inhibitor binding by π - π or van der Waals interactions. Ile146 and Pro270 converge to form a narrow, flat construction into which the hydrophilic quinone portion inserts. Other residues in the Qo pocket that can be interesting in the development of quinone substrates are Tyr128, which can interact through a hydrogen bond with the carboxyl group of quinone, and Phe128, which is located close to the naphthoquinone core and can make noncovalent interactions with aromatic rings (Figure18).

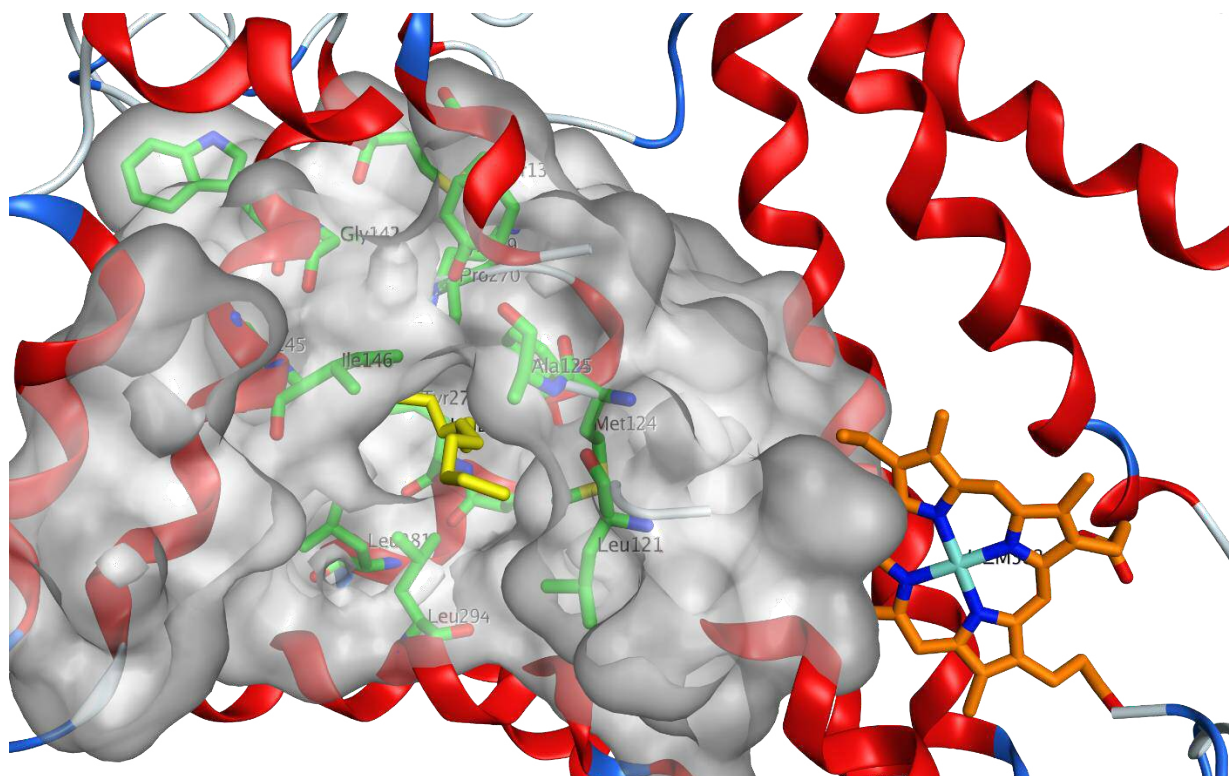


Figure 18 Qo binding site, with highlighted in green the residues that make contacts with UHDBT (yellow)

These three compounds (NQNO, UHDBT, MAOS) show their inhibition, changing the conformation of the extrinsic domain of the ISP⁸⁵ (Figure19). In the postulated mechanism of action, once the first electron moves from Ubiquinol to Rieske center, the position of ISP domain is proximal to the site Qo of the bound ubiquinol, when it donates the electron to cytochrome c, it performs a rotational-translational movement to allow this transfer.⁹⁶ Hence the transfer between donor and acceptor sites, dependent upon the flexibility of the linker region. The inhibitors can immobilise or fix the conformation of the ISP-ED in one of the two positions.⁹⁶

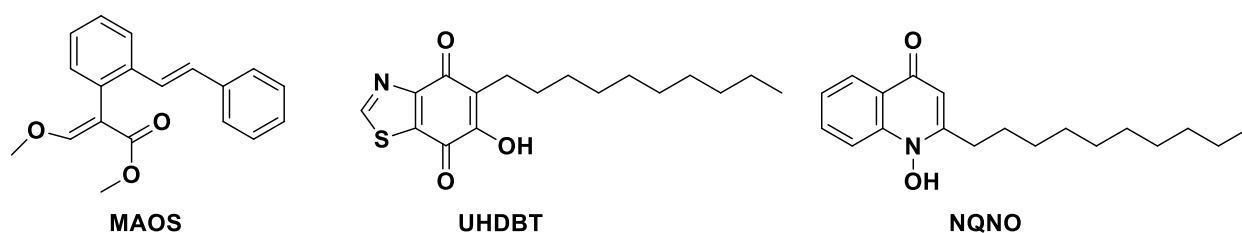


Figure 19 Qo Chemical structures of bc1 inhibitors

2.1.5 Virtual screening of commercial compounds

In order to identify novel analogs of idebenone, which are substrates of both enzymes: NQO1 and complex III, an approach based on a pharmacophore combined with a structure –based method was applied. This search was divided into two steps: first, a selection of some commercial compounds was made on the basis of the pharmacophoric model, while in the second step the most interesting structures were evaluated using a docking-based method.

Pharmacophore modelling is a powerful technique that consists in searching for the 3D-arrangement of the chemical features possessed by a ligand molecule, which is necessary for its interaction with a target receptor in a specific binding site.⁹⁷ These features describe chemical functionalities such as hydrogen bond acceptors (HBAs), hydrogen bond donors (HBDs), hydrophobic areas (Hs), aromatic rings (ARs), positively/negatively ionisable groups (PIs/NIs), and exclusion volumes (XVOLs).

From the crystal structures of NQO1 with different substrates (PDB ID: 2F1O⁹¹, 1GG5⁴⁶ and 1H69⁴⁵, 1D4A⁸⁸) the most important features for binding were identified: an aromatic quinone ring to make a π - π stacking with isoalloxazine of FAD and the presence of two electron acceptors. These features were used to generate a pharmacophoric query (figure 20) using the PLIFs (Protein-Ligand Interaction Fingerprints) tool in MOE 2015.10.⁹⁸ In particular, the π - π stacking between the isoalloxazine of FAD and naphthoquinone core was represented by an “aromatic group feature” (in orange), while the electron acceptor capability of carbonyl groups were considered by a “hydrogen bond acceptor feature” (in blue), and the exclusion volume (black grids) corresponding to space occupied by FAD was also included in the pharmacophoric query. A large data set consisting of commercially available compounds was downloaded from three different vendors (SPECS, ENAMINE and Life Chemicals, ChemDiv) and was screened for structures that match the pharmacophore query generated (Figure 20). As a result of this pharmacophoric search, 2845 compounds were obtained and analysed through visual inspection in order to discard compounds which could not show the desired pharmacological activity *a priori*. In fact, an essential requirement for idebenone and its analogs is the possibility to be reduced: compounds must be reducible in order to interact and pass electrons to the complex III of the electron chain, restoring the ATP production and showing their pharmacological activity.⁹⁹

The compounds filtered on the basis of the visual inspection were further investigated for their binding affinities and mode of interaction with the human NQO1 protein using the GLIDE SP¹⁰⁰ docking algorithm, in a 12 Å radius grid generated from the 2F1O crystal structure. Docking techniques are among the most frequently used in structure-based methods, given their ability to predict the structure of intramolecular complexes formed between substrates and proteins.¹⁰¹ Characterizing this behaviour of small molecules in the binding sites of target proteins makes possible to establish the ability of a ligand to bind to a target protein and promote its activity.

These two processes combined with a second visual inspection led to the identification of 62 compounds, which show a suitable orientation in the binding site and the possibility to be reduced. These 62 compounds were further evaluated for their ability to binding the Qo binding-site of complex III, since these compounds, once they are activated from NQO1, they have to interact with Complex III in order to transfer electrons.

To predict which structures can be a suitable substrate for both enzymes, the compounds were investigated for their affinities to bind complex III using GLIDE SP docking algorithm, in a 12 Å radius grid generated from the 1ntzz crystal structure. The results show that most of the compounds were able to bind complex III. In particular, the majority of compounds with a naphthoquinone ring could occupy the hydrophobic Qo -pocket with a binding mode similar to the idebenone. To explore the biological activity of these compounds, a final selection of 21 compounds was made.

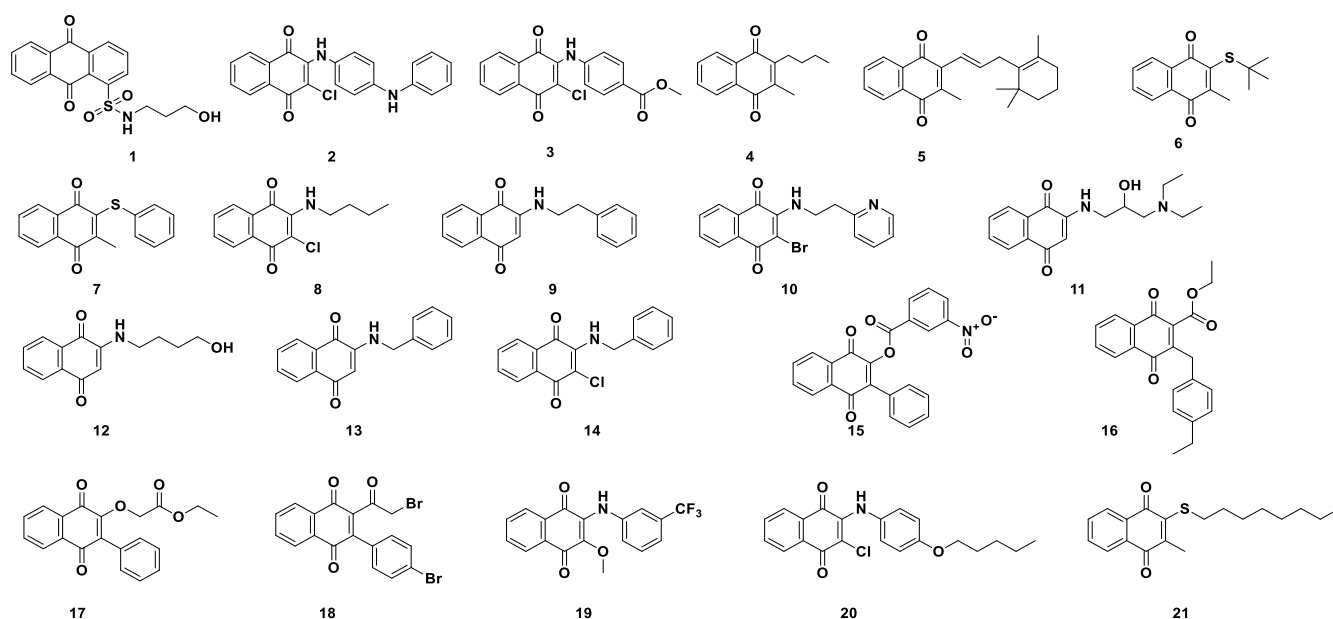
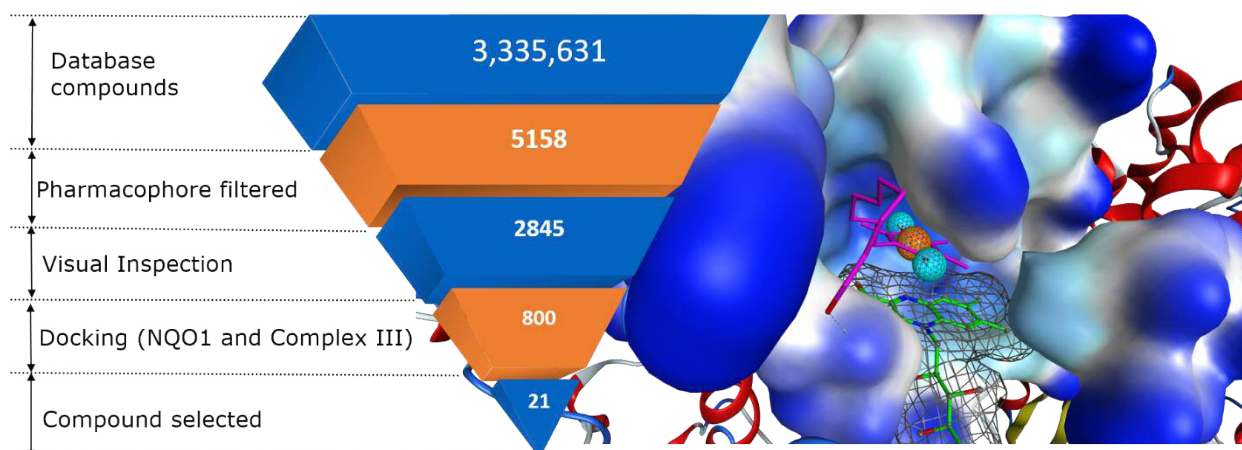


Figure 20 Virtual screening workflow and selected commercial compounds.

2.1.6 Quinone compounds

Quinones are ubiquitous compounds found predominantly in plants, but also in fungi and animals. They are important electron carriers in biological processes such as photosynthesis and cellular respiration, natural pigments and antioxidants, but they also include toxic compounds used as herbicides, fungicides, and they are present in the air as pollutants, including cigarette smoke, which shows a high presence of benzo-semiquinones (Figure 21).¹⁰² These diverse features have captured the attention of scientists on quinones for years, and they are used in a wide variety of applications, such as colourants in the textile industry,¹⁰³ as antioxidants in the cosmetic industry, and in the last few years they have been explored as replacements for metals in flow battery to produce energy.¹⁰⁴

In medicinal chemistry, they represent an interesting class of compounds for their bivalent functions: they can work as electrophiles but also as nucleophilic compounds due to their tendency to donate and accept electrons. This is possible because quinone compounds can exist in three different oxidative states: quinones, semi-quinones and hydroquinones, which correspond to different physicochemical properties. For example, Mitomycin C is a well known antitumor drug, which in its hydroquinone form is a potent electrophilic compound that forms several covalent adducts with the DNA, responsible for its cytotoxic effects.¹⁰⁵ On the contrary, Menadione in its quinone form works as a nucleophilic compound: it was demonstrated to inhibit protein tyrosine phosphatase(s) by dephosphorylating them through a Michael-addition mechanism.¹⁰⁶ In its state of semi-quinone, β -lapachone is a potent antitumor compound due to its ability to increase the presence of ROS through radical reactions.¹⁰⁶ In the same way, other quinone structures can show beneficial effects, with compounds such as vitamin E,¹⁰⁷ Alkannin¹⁰⁷ and Shikonin¹⁰⁷ showing antioxidant and anti-inflammatory effects. An important quinone is physiological CoQ₁₀, which, as described above, is a potent antioxidant and plays a crucial role as an electron carrier in the cellular respiration.¹⁰⁸

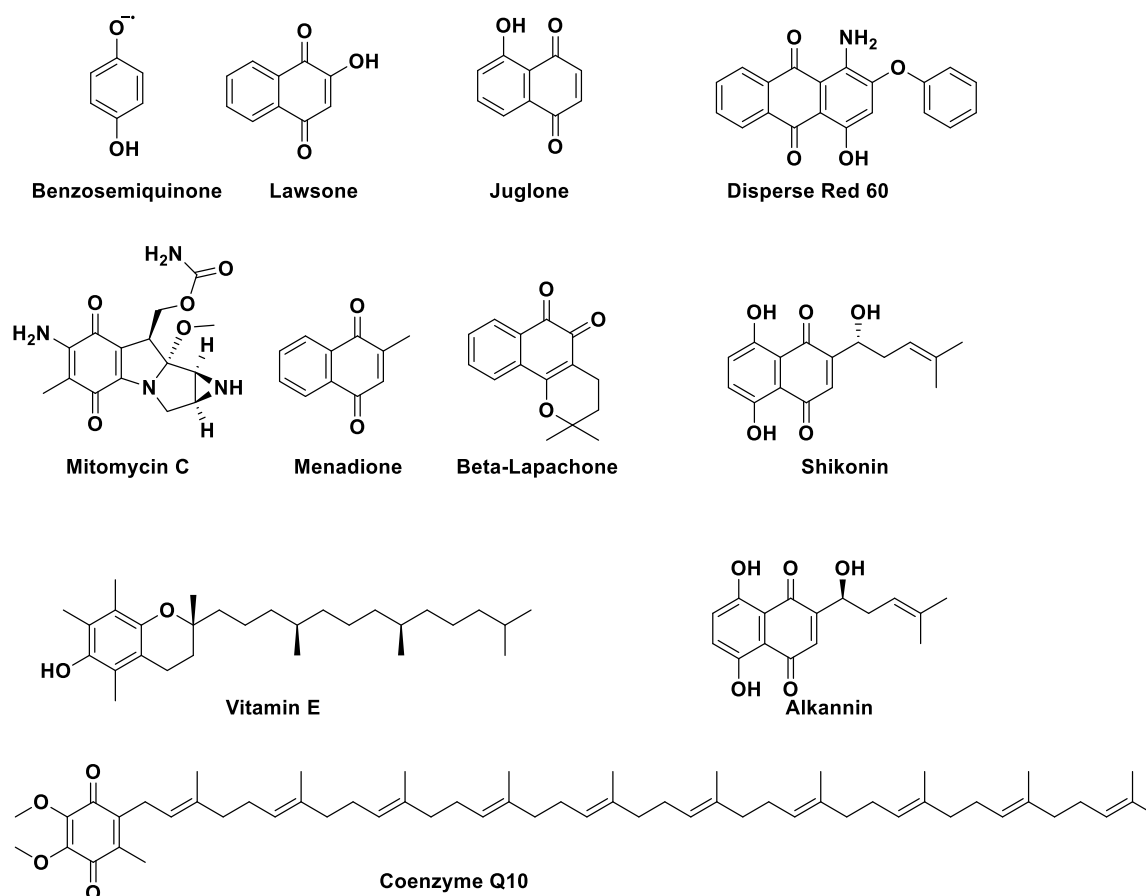


Figure 21 Quinone compounds which possess diverse bioactivities

In vivo, the quinone can be reduced to the semiquinone, a free radical, then to the hydroquinone, by a sequence of two one-electron reductions by cytochrome P450 reductase and other flavoprotein enzymes or can undergo to another metabolic pathway, where the NQO1 reduces quinones directly to hydroquinones¹⁰⁹. In both cases, the final product is a more hydrophilic molecule, which can be conjugated with glucuronic acid and eliminated. Hence, the quinone is present in all three oxidative forms *in vivo*, but most of them exert their activities after reduction.¹⁰⁶ The ability of quinones to participate in electron transfer reactions depend on their stability in reduced form, since the semiquinone is an unstable compound, which can be oxidised to the quinone under normal oxygen levels, producing superoxide radical anions¹¹⁰ (Figure.22). A hydroquinone is less reactive than a semiquinone and may have a greater pharmacological activity than the parent quinone (as the antifungal and antioxidant activities of flavonoids), but it may be unstable and rapidly reconverted into its quinone form with consequent ROS generation.¹¹⁰

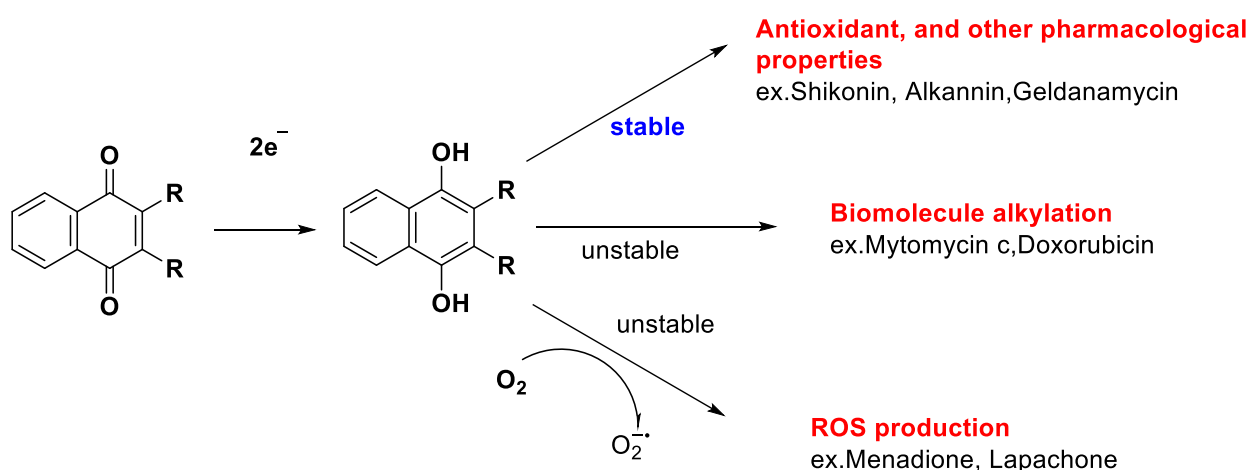


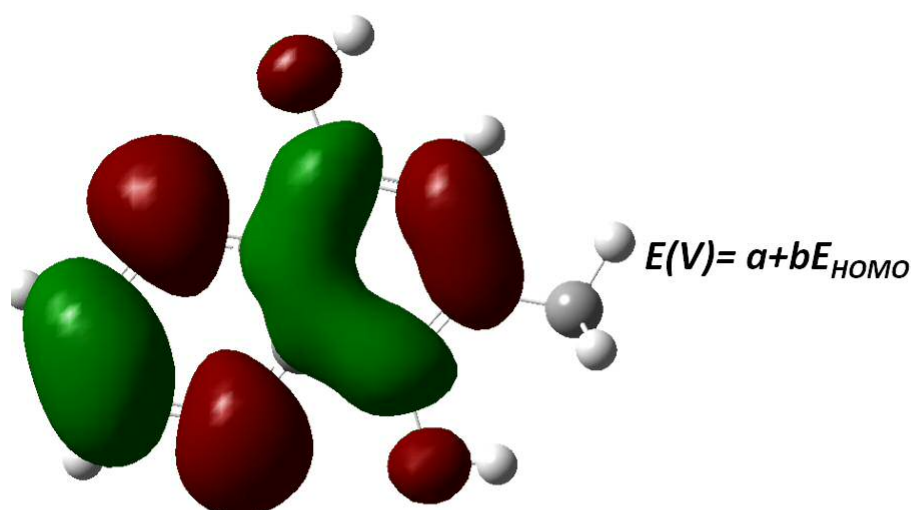
Figure 22 Bio-activation of quinones by NQO1

2.1.7 DFT theory and prediction of standard reduction potential

As stated above, the redox capacity of quinones is potentially their most relevant feature, which influences and modulates their biological activity. Hence, the ability to predict the redox potential of these compounds *a priori* could represent an advantage for this part of the project on quinone compounds. Density functional theory (DFT) is a powerful computational tool to study many electron systems in their ground states, and investigate the structural, magnetic and electronic properties of molecules and in consequence the standard reduction potential.¹¹¹

DFT theory lies on quantum mechanics calculations able to provide approximate solutions to the Schrödinger equation, the fundamental equation of quantum mechanics that describes any given chemical system.¹¹² There are different approaches to solve the Schrödinger equation; nowadays, hybrid DFT is one of the most used theorems to describe complex molecules, which tends to be systematically more accurate in energy predictions in comparison with other functions.¹¹³

To evaluate the standard electrode potential (E°) of a molecule, it is necessary to evaluate what is the energy associated with its ground state, in other words, it is necessary to optimise the geometry of the compound and find a stable structure with a minimum energy. Recent studies provide strong evidence of a correlation between the molecule optimisation using B3LYP calculations and experimental results for molecular properties;^{114,115,116,117} in particular, Rzepa *et al.* and Namazian *et al.* investigated the standard potentials for various quinones using the B3LYP function for their calculation.¹¹⁶ Recently, Namazian's group found a simple correlation between the energies of HOMO (highest occupied molecular orbital) and LUMO (lowest unoccupied molecular orbital) for the reduced and oxidised forms of studied quinones and the electrode potentials (Figure. 23).¹¹⁶ The correlation between the energy of the highest occupied molecular level of the molecule in its reduced form and electrode potential is explained by the fact that molecules in reduced form have gained electrons, so there is a change in the potential of the compound.¹¹⁵



Oxidant	Reductant	N (electrons)	E° volts
acetate	acetaldehyde	2	-0.600
O ₂	O ₂ ^{•-}	1	-0.400
NAD ⁺	NADH	2	-0.320
FAD ⁺	FADH	2	-0.220
2H ⁺	H ₂	2	0.000
Methylene Blue	Leucomethylene blue	2	0.001
CoQ ₁₀	CoQ ₁₀ red	2	0.100
Cytochrome c ₁ , Fe ³⁺	Cytochrome c ₁ , Fe ²⁺	1	0.250
benzoquinone	hydrobenzoquinone	2	0.700
1/2 O ₂ + 2H ⁺	H ₂ O	2	0.800

Figure 23 Representations of Menadione orbitals elaborated with Gaussian 98 and Table 3 Standard reduction potential for some mammalian oxidation systems Figure 23 shows a graphical representation of orbitals of Menadione and the equation, which describes the correlation between electrode potential and energy associated to HOMO orbitals, The constants a and b in the equations are -2.115 and -12.845, respectively. Table 1 shows the redox potential of some physiologically important redox systems in mammals.

In order to predict the reduction potential of new analogs of idebenone, a similar approach to Namazian was applied. The GAUSSIAN 98¹¹⁸ package was employed for all calculations. The quinone compound structures were optimised using B3LYP with 6-311+G- (d, p) basis set. The effect of solvation of water was applied to have a value closer to the one that would be

found in cells, and this effect was investigated using a polarized continuum model (PCM) in the optimisation calculation.¹¹¹

This procedure was used to evaluate the effect of the reduction potential of the new analogs in their activity, with the possibility to identify a correlation between these two values. Table 2 summarises the prediction of reduction potential obtained for the different compounds. Firstly, the LUMO energy level of quinones, having the known redox potential (22-27), were calculated and compared to the results reported by Namazian et al. (2012) Successively, a series of reasonable structural modifications of the quinone-core was performed with the aim to validate the predictions.

Compounds	Homo red	Lumo red	E° <i>Gaussian</i>	E° (exp)
 22	-0.2195	-0.02328	0.700	0.700
 23	-0.20422	-0.04798	0.508	0.470
 24	-0.22148	-0.03350	0.730	0.712
 25	-0.21443	-0.2051	0.639	0.644
 26	-0.20846	-0.04908	0.562	0.547
 27	-0.20997	-0.01930	0.582	0.590
 28	-0.20058	-0.04789	0.461	Not available
 29	-0.20942	-0.05352	0.575	Not available
 30	-0.20350	-0.05312	0.499	Not available
 31	-0.19735	-0.04512	0.420	Not available
 32	-0.19626	-0.04684	0.410	Not available
 33	-0.20061	-0.04792	0.461	Not available
 34	-0.20062	-0.04798	0.461	Not available
 35	-0.20226	-0.07805	0.483	Not available

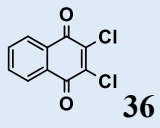
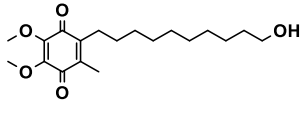
 36	-0.21527	-0.05623	0.650	Not available
 Idebenone	-0.21132	-0.01332	0.600	Not available

Table 4 Predicted reduction potential of quinone compounds. The table shows the calculated HOMO and LUMO orbital energies for the reduced form and the corresponding calculated electrode potentials. The known experimental electrode potentials are taken from Namazian works¹¹³. The energies are in atomic units, Hartree (1 Hartree = 2625.49975 kJ/mol)

Table 2 shows two distinct trends for the effect of nature and position of the substituents studied on the quinone core. Quinone compounds with electron-donating groups (methoxy, methylamino group) show a lower reduction potential in comparison with unsubstituted quinone compounds. As expected, electron-withdrawing groups have an opposite effect, increasing the reduction potential. The effect of the position of the substituents is also significant, for example, compound **29** shows a larger influence than compound **30**. These results are reasonable, because the introduction of substituents leads to a change in the charge distribution in the quinone structure, and therefore it influences the reduction potential: electron withdrawing substituents facilitate reduction stabilising the negative charge, whereas electron donating substituents destabilise it. The same reasoning can be applied to the introduction of a series of conjugated double bonds or an aromatic ring: both modifications dislocate the negative charge of the quinone core, leading to a decrease of reduction potential. These results suggest that the reduction potential of quinone compounds can be modulated by the presence of substituents in the aromatic ring, and as a consequence, the stability/toxicity of quinones/semiquinones/hydroquinones might be predicted *a priori*. This prediction has been considered for the design of novel compounds, that are in a particular redox potential range to show the cycling oxidation and reduction between the two redox centre, NQO1 and complex III, without ROS generation.

In particular, according to the results obtained (Chapter 6), two compounds have been designed and synthesised, **38** and **39**. The compounds have strong EWGs in position 3 (F and SCF₃), which drastically increase the reduction potential of the compounds as shown in the table.

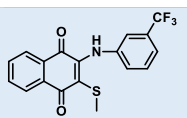
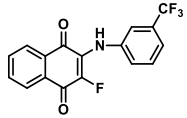
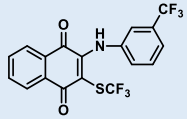
Compounds	Homo red	Lumo red	E° <i>Gaussian</i>	E° (exp)
 37	-0.20226	-0.07805	0.483	Not available
 38	-0.21153	-0.05335	0.600	Not available
 39	-0.21353	-0.0645	0.630	Not available

Table 3 Predicted reduction potential of designed quinone compounds

2.1.8 Conclusion

A variety of computational studies were performed in order to identify suitable substrates for NQO1 enzyme and, at the same time, Complex III. The position of docked ligands into the two enzyme pockets allowed us to determine the important surrounding residues. In particular, compound **19** showed a favourable binding mode in the NQO1 pocket:

- The naphthoquinone core lies parallel to the isoalloxazine ring
- The naphthoquinone position is stabilised by a hydrogen bonding interaction with the Tyr-126
- The naphthophenyl forms a hydrophobic interaction with the Trp-105.
- The phenyl moiety forms a hydrophobic interaction with the Met141

Unfortunately, the lack of crystal structures containing native ubiquinone molecule bound in the Qo site makes it more difficult the study of binding mode, whose mechanism is still contentious. However, the presence of crystal structures containing inhibitors allowed us to determine the essential features of the binding pocket. The Qo site is mainly hydrophobic pocket, that forms a sort of deep cavity inside of protein. The compound **19** could be well accommodated in different rational configurations with the naphthoquinone core inside of the cavity and the sidechain close to the opening to the phospholipid membrane. This binding mode is similar to the postulate binding of ubiquinone; the hydroquinone head close to the 2Fe-2S cluster in order to allow the electrons transfer and the long chain anchored to the lipid membrane. Interesting, the strong interaction between the phenyl moiety of compound **19** and Phe274 could be essential for the correct position of the naphthoquinones into the pocket.

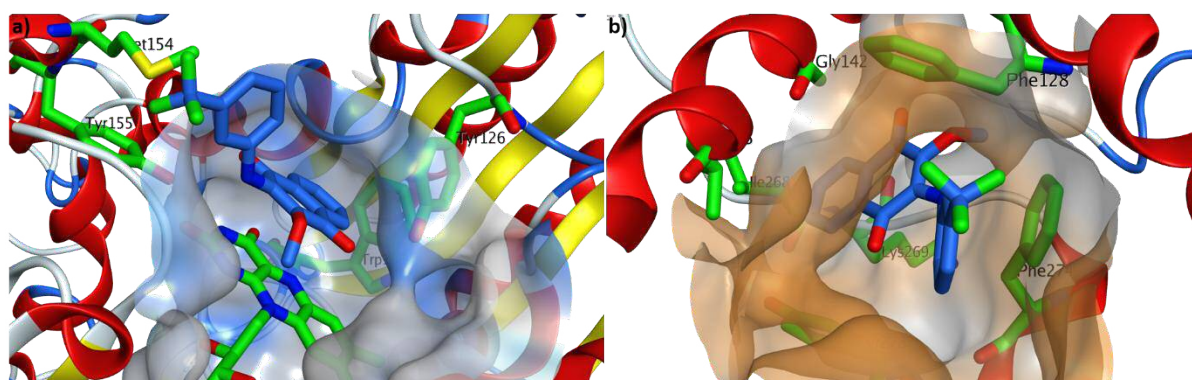
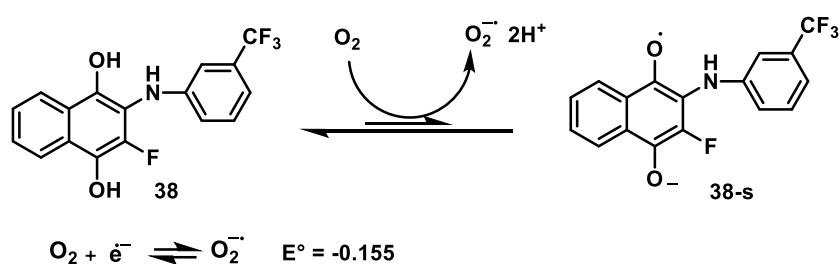


Figure 24 Predicted binding mode for the compound 19. The Figure 24 show **19** (in blue) in the NQO1-binding site and in the Complex III-binding site, respectively a and b. The amino acid residues involved in the binding are highlighted in green

Furthermore, it was demonstrated that the cytotoxic properties of quinones is in part related to the stabilisation energy after electron accepting¹¹⁹. DFT quantum chemical calculations were used in this project to study the structure-toxicity relationship of naphthoquinones derivatives. According to our DFT study, the electron withdrawing group lead to higher reduction potentials (positive), which might lead to a more easily reduction of the quinone by NQO1. Moreover, a more positive reduction potential, stabilising the hydroquinone form, affects the equilibrium position for the reaction hydroquinone/semi-quinone, which will lie to the left, disfavours the formation of superoxide, with a potential reduction above the spontaneous formation of O_2^- (Scheme 1).



Scheme 1 Schematic representation of semiquinones formation in presence of oxygen

**CHAPTER 3 OPTIMISATION
OF BIOCHEMICAL AND
BIOLOGICAL ASSAYS USING
IDEBENONE**

3.1 Biological evaluations

Quinone compounds have received considerable interest as potential therapeutic drugs and many studies have shown they are versatile organic compounds with a wide range of biological activities, including antimalarial¹²⁰, antibacterial¹²¹, antifungal¹²², antioxidant¹⁰³, anti-diabetic¹²³ and anticancer¹⁰⁹. Most studies addressing the biological potential of naphthoquinones relate to their ability to accept and donate electrons and consequently interact with oxidoreductases^{103,106,108,117,118}. In this study, we investigated a further potential application of naphthoquinones, namely as cytoprotection agents, in addition to electron carriers. Thus, the focus was on the development of rational testing strategies for evaluating not only the beneficial effects of studied naphthoquinone (ATP rescue), but also potential adverse effects, in particular pro-oxidant and cytotoxicity (Figure 25). The rationale for using multiple bioassays to assess potential biological activity was based on the versatile nature of quinones, the coexistence of the hydroquinone and quinone form in biological systems, the corresponding interaction with several oxidoreductases, in addition to possible anti-oxidant and/or pro-oxidant activity. Assessment of the activities of the test compounds in all qualitative and quantitative bioassays, even if in some case limited (Chapter 4.1.2), provided useful information on the structure-activity relationships of this family and the overall consensus of the biological results was used to select the most promising compounds for further *ex-vivo* / *in vivo* evaluation.

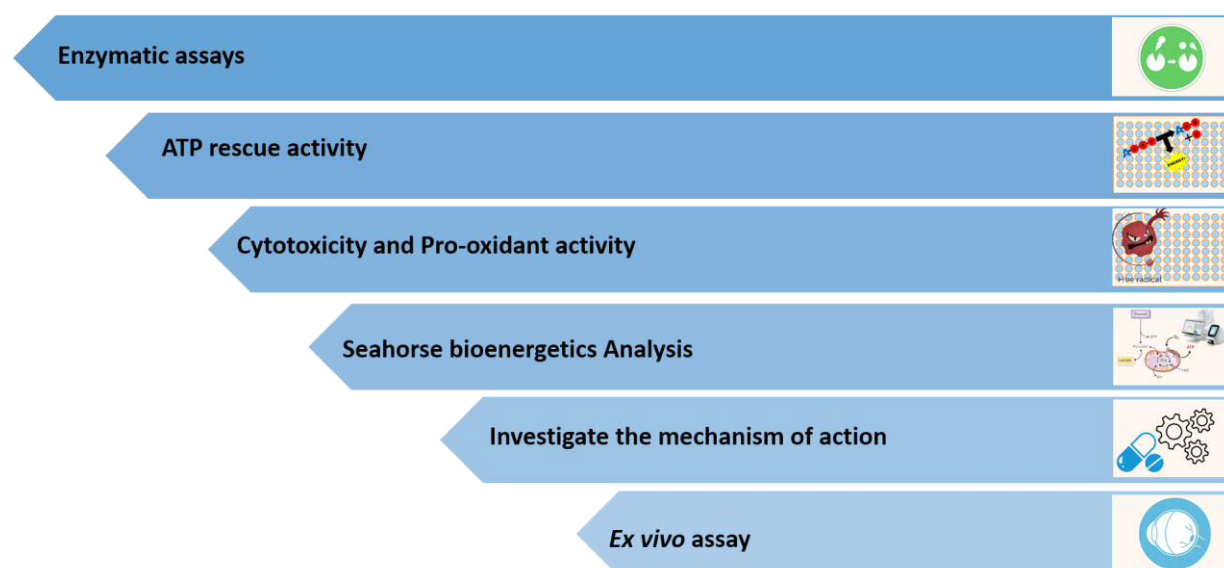


Figure 25 Experimental workflow and selective criteria to screen the identified compounds

The activities of the test compounds were determined relative to idebenone, which is currently the gold standard for the treatment of LHON disease. Performance superior to idebenone would indicate improved bioenergetics in the presence of a mitochondrial complex I impairment.

In vitro studies revealed that idebenone is capable of interacting with different proteins, in some cases with deleterious consequences (Chapter 1.5). It was suggested the observed beneficial effects of idebenone (stimulation of ATP formation, antioxidant capacity, scavenging of free radicals, protecting against lipid peroxidation,) are mainly attributable to its metabolic activation by NQO1. On the other hand, non-specific binding to other proteins, such as complex I, calcium-activated chloride channels (ANO1, TMEM16A), leads to deleterious effects of idebenone. Consequently, the studied compounds were evaluated in different enzymatic and cell-based assays in order to identify compounds that showed a better overall pharmacological profile than idebenone.

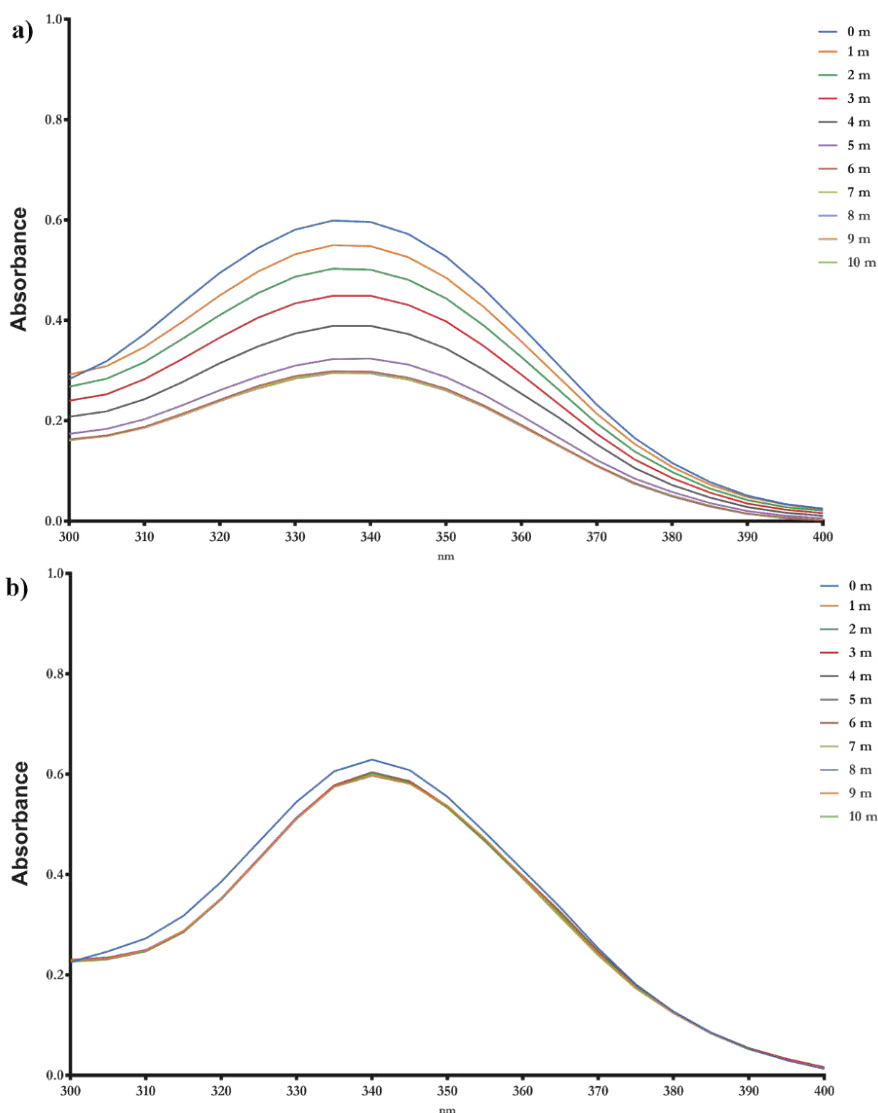
3.1.2 Overview of the enzymatic assays optimised and used in the study

The compounds selected from the virtual screening were firstly tested to assess whether they can be substrates of the NQO1 enzyme by employing NADH and spectrophotometric monitoring of NADH depletion. This assay allowed us to discriminate the compounds according their affinity for the NQO1 enzyme: compounds with low affinity cannot be activated in their hydroquinone form, and consequently showing the postulate biological activity. Moreover, previous study showed that Idebenone can act as competitive inhibitor of complex I and as agonist of complex II,^{61,63} so it was interesting to evaluate if the selected compounds showed a similar profile. Therefore, the compounds were assessed for their ability to act as electron acceptors from complex I or complex II, in isolated mitochondria, by employing NADH and succinate as electron donor for complex I and complex II, respectively. The 2,6 dichlorophenol indophenol (DCPIP) was used as electron acceptor, and the enzymatic activity was followed by spectrophotometric monitor of DCPIP depletion.

3.1.2.1 NQO1 activity in the presence of a quinone

Since the restoration of ATP levels of idebenone correlates with the NQO1 activity of this compound, all the new compounds were tested for their ability to be reduced by this enzyme.⁹⁹ *In vitro* assays using recombinant NQO1 enzyme provided a suitable model system to evaluate

the NQO1-quinone interaction. The reduction of quinone into hydroquinone can be followed by the decrease of NADH absorbance at 340 nm, according to the following reaction:



The CoQ₁ a well know analogue of ubiquinone and substrate of NQO1, was used as positive control¹²⁴. The results showed a constant decrease of absorbance at 340 nm until the complete conversion of quinone into hydroquinones after 10 minutes. Dicoumarol, an inhibitor of NQO1, was used to confirm the NADH oxidation depend on the NQO1-quinone activity.

Figure 26 UV/VIS spectral analysis of NADH oxidation by NQO1 in presence of idebenone. The NADH level was detected following the absorbance variations at 340 nm in 1 ml cuvette containing: 5mM Tris-HCl pH 7.4, 0.7 mg/ml bovine serum albumin (BSA), NQO1 1 μg/ml, 50 μM quinone and 100 μM NADH Each value was detected after NQO1 addition. The Figure **a** shows the decrease of NADH level in presence of CoQ₁, the Figure **b** shows the decrease of NADH level in presence of CoQ₁ and Dicoumarol (20 μM)

Idebenone was tested in the same condition using 4 different concentrations (5, 10, 25 and 50 μM). The results demonstrated that idebenone is a suitable substrate of NQO1, with a consistent reduction of NADH with the increase of idebenone concentration. The enzymatic activity was calculated as $\mu\text{mol min}^{-1}\text{mg}^{-1}$ of protein according to the following equation:

$$\text{Enzyme activity } (\mu\text{mol min}^{-1}\text{mg}^{-1}) = (\Delta \text{ Absorbance}/\text{min}) / [(\text{extinction coefficient} \times \text{volume of sample used in ml}) \times (\text{sample protein concentration in mg ml}^{-1})]$$

In detail, the activities were obtained by measuring the rate of absorbance ($\Delta \text{ Absorbance}/\text{min}$) in the linear region of the curve dividing by the extinction coefficient (in this case NADH = $6.22 \text{ mM}^{-1}\text{cm}^{-1}$) and the amount of enzyme used in the assay.

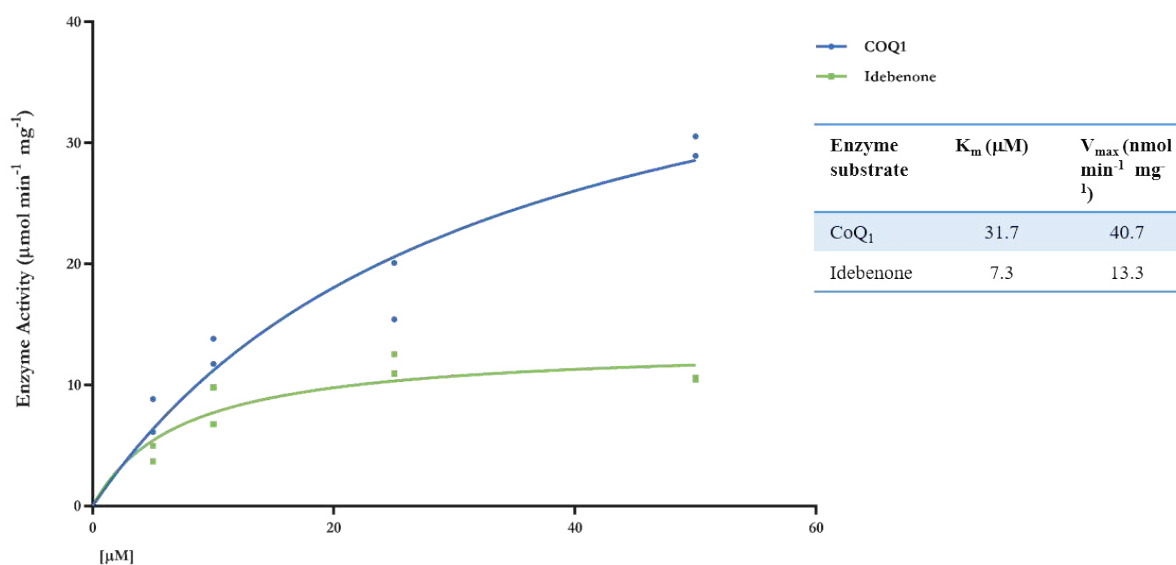
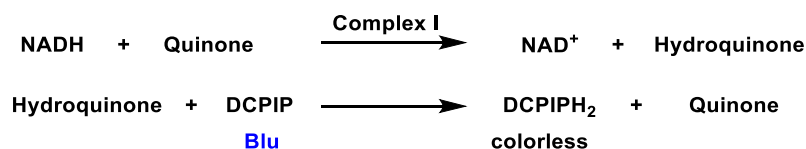


Figure 27 Michaelis-Menten plot depict oxidation of NADH by NQO1 in presence of Idebenone or CoQ₁.

3.1.2.2 Complex I and complex II activity in the presence of a quinone

Despite the beneficial effect of idebenone in restoring ATP in complex I impairment conditions,⁷³ previous studies report that idebenone inhibits complex I due to a slow dissociation from the binding-site and that it can increase the production of superoxide.⁶² The ability of the new analogs to interact with complex I was studied according to a modification of the protocol reported by Spinazzi et al.,¹²⁵ using CoQ₁ as reference compound, and 2,6 dichlorophenol indophenol (DCPIP) as acceptor of electron. The transfer of electrons can be

followed by the decrease of absorbance at 600 nm, due to the reduction of DCPIP, turning it from blue (oxidised form) to colourless (reduced form).



The use of DCPIP to assess the complex I activity of quinones rely on its capacity to absorb light at higher wavelength than NADH, thus avoiding a possible interference from the studied quinones (Chapter 4.1.2). This approach was not possible for NQO1 enzyme, due to the direct reduction of DCPIP by the enzyme ¹²⁶.

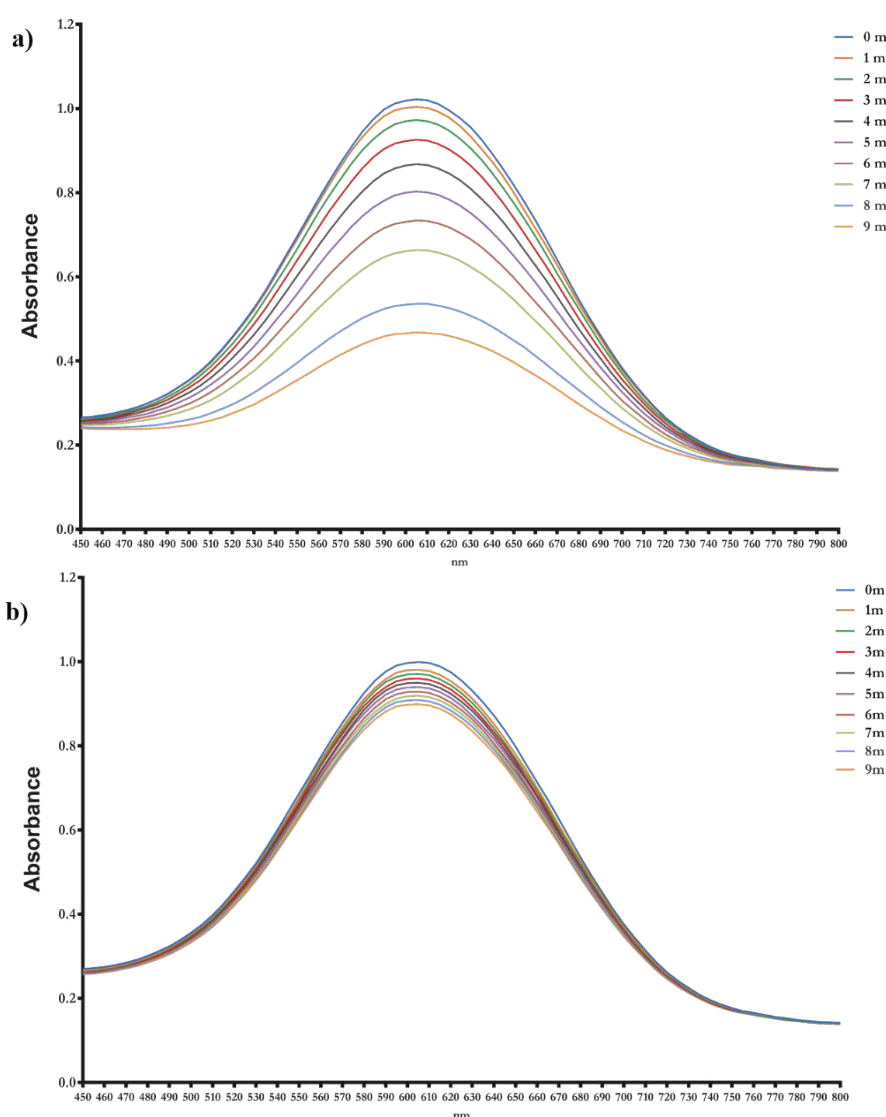


Figure 28 UV/VIS spectral analysis of DCPIP reduction by Complex I in presence of CoQ₁. The DCPIP level was detected following the absorbance variations at 600 nm in 1 ml cuvette containing: 50 mM Tris-HCl pH 7.4, 3 mg/ml bovine serum albumin (BSA), 20 μg/ml mitochondrial protein, 50 μM quinone and 100 μM NADH, 52 μM DCPIP, 300 μM KCN. Each value was detected after NADH addition. The Figure a shows the decrease of DCPIP level in presence of CoQ₁, the Figure b shows the decrease of DCPIP level in presence of CoQ₁ and Rotenone (10 μM)

The results obtained show that idebenone can interact with complex I, even if the kinetics of the reaction was different in comparison with CoQ₁. Rotenone, a known inhibitor of complex I, was used to validate this assay.

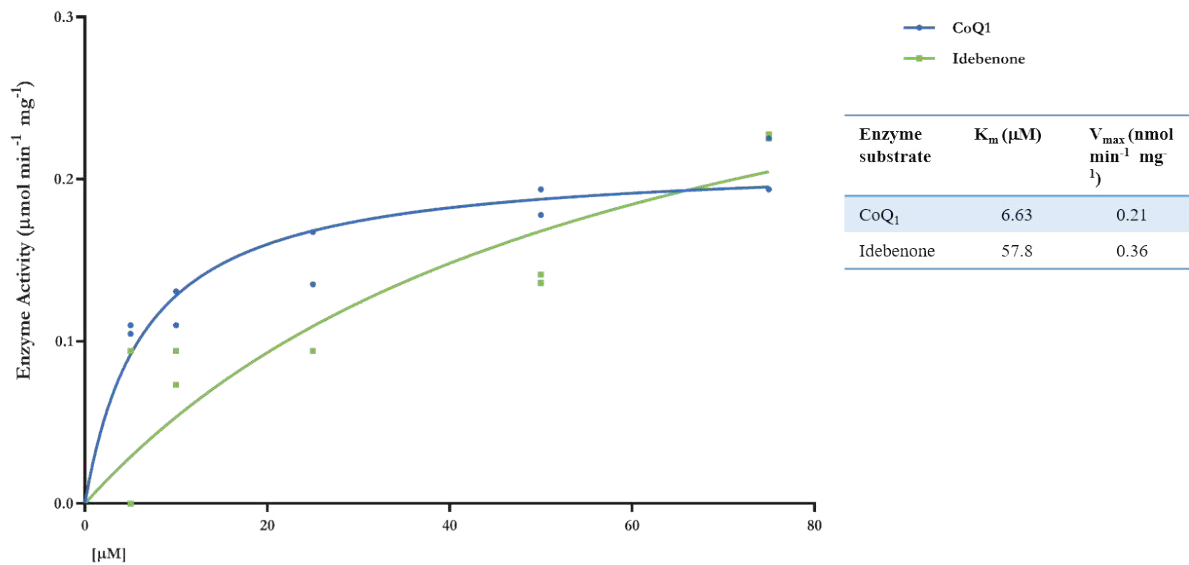


Figure 29 Michaelis -Menten plot depicts the reduction of DCPIP by Complex I in presence of Idebenone or CoQ₁.

Since idebenone inhibits complex I^{61,63}, the enzymatic activity was tested in the presence of CoQ₁ and idebenone, in order to evaluate if idebenone could work as competitive inhibitor. Thus the experiment was repeated in the same condition described previously (50 mM Tris-HCl pH 7.4, 3 mg/ml (BSA), 20 $\mu\text{g/ml}$ mitochondrial protein, 5-75 μM CoQ₁, 100 μM NADH, 52 μM DCPIP, 300 μM KCN), but adding 10 μM of idebenone in each cuvette. The results were in line with works by others^{61, 63}, confirming that idebenone inhibits mitochondrial respiration, via complex I.

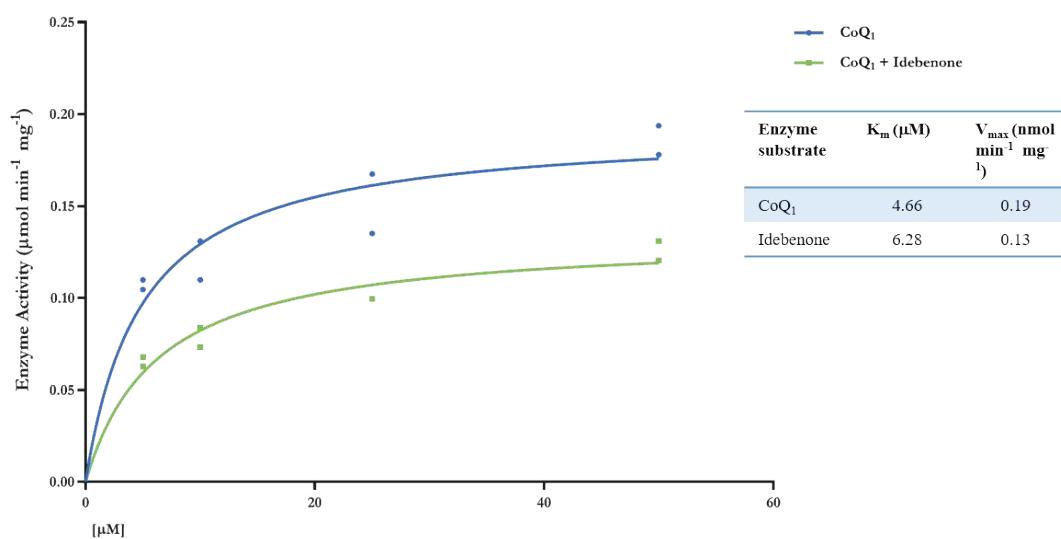


Figure 30 Michaelis -Menten plot depicts the reduction of DCPIP by Complex I in the presence of Idebenone and CoQ₁.

3.1.2.3 Idebenone activity dependent on complex II

Even if the reduction of idebenone by NQO1 was thoroughly demonstrated in various experiments, it is unlikely, that NQO1 is the only oxidoreductases that can react with idebenone; indeed different studies reported the idebenone is a substrate of other two oxidoreductases: complex II and glycerol-3-phosphate dehydrogenase (G3PDH)¹²⁷. In the light of this study, it is interesting to test if the naphthoquinone analogs maintain the same behaviour of idebenone. Complex II activity was analysed using the oxidation of succinate with an artificial electron DCPIP.

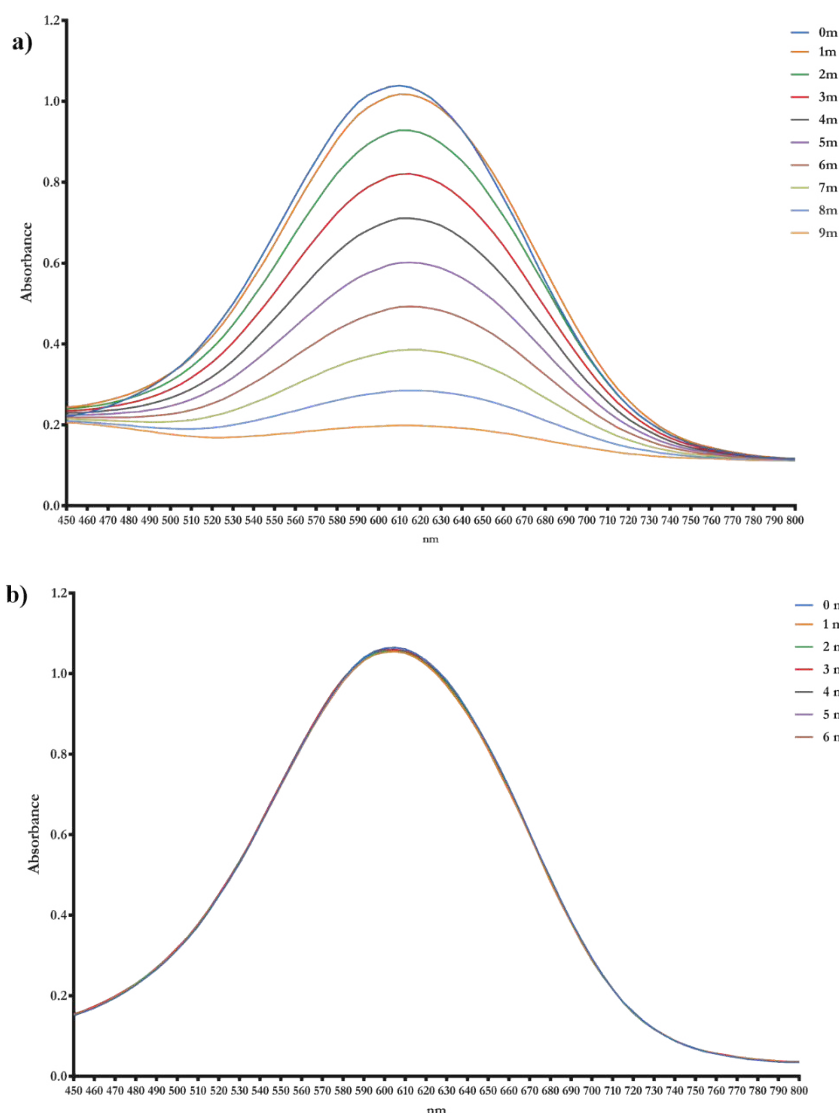


Figure 31 UV/VIS spectral analysis of DCPIP reduction by Complex II in presence of CoQ₁. The DCPIP level was detected following the absorbance variations at 600 nm in 1 ml cuvette containing: 25 mM Tris-HCl pH 7.4, 1 mg/ml bovine serum albumin (BSA), 20 μg/ml mitochondrial protein 50 μM quinone, 25mM Succinate, 52 μM DCPIP, 300 μM KCN. Each value was detected after DCPIP addition. The Figure **a** shows the decrease of DCPIP level in presence of CoQ₁, the Figure **b** shows the decrease of DCPIP level in presence of CoQ₁ and TTFA (500 μM)

The complex II result (Figure 31) showed a rapid decrease of DCPIP concentration in presence of CoQ₁ and idebenone, demonstrating the high affinity of benzoquinones for complex II enzyme. TFFA, complex II inhibitor was used to validate the assay

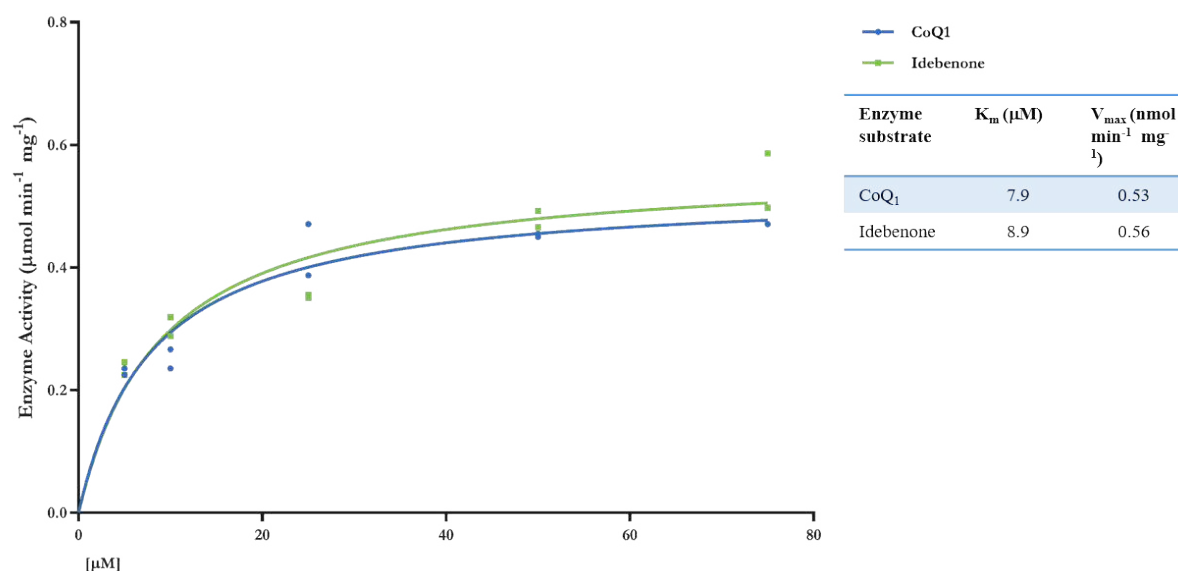


Figure 32 Michaelis -Menten plot depicts the reduction of DCPIP by Complex II in presence of idebenone or CoQ₁.

3.2 Overview of the cell based assays optimised and used in the study

The mere fact that a compound was able to interact or not with the target enzymes was not sufficient to qualify them as a relevant idebenone analogs. In vitro cell culture assays can provide more useful information on various cellular responses from exposure to a compound. Firstly, it was of crucial importance to assess whether the selected compounds can bypass the complex I dysfunction and sustain electron transport chain (ETC) by serving as electron donor to complex III. The re-established electron flow in ETC could be directly monitored evaluating the increase of mitochondrial respiration using the XF 96 analyser (section 3.2.1.2) or indirectly by the rescue of cellular ATP level under inhibition of complex I (section 3.2.1.1). The ability of compounds to affect the mitochondrial ETC activity in cells was used as the main parameter to assess their potential use in the treatment of LHON disease. The other important parameter to select the most promising compounds was the evaluation of their cytotoxicity. In fact, in

several studies quinones compounds showed significant toxic effect in different cell lines,^{106,107} mostly due to an increase of ROS level in cells. This potential toxic effects have been evaluated testing the ability of compounds to increase the level of reactive oxygen species in the cells, using the CellROX green reagent and ROS-Glo H₂O₂ assay, and monitoring the cell viability by MTT assay.

3.2.1 Selection of cell lines

Retinal ganglion cell disorders are implicated in numerous diseases, besides DOA and LHON diseases, they are involved in glaucoma, Friedreich's ataxia and diabetic retinopathy¹²⁸. But, despite their importance, the study of retinal ganglion cells (RGCs) is extremely difficult due to the small percentage of cells present in the retina and the current isolation protocol, which can provide only a limited yield of pure retinal ganglion cells^{129,130}. Therefore, the use of primary retinal ganglion cells for a large screening of compounds activity would have required a considerable quantity of tissue and time, not compatible with the aims of this study.

The RGC-5¹³¹ cell line has been widely used as a model to study the biology of retinal ganglion cells for years, but in the last years, many researchers have raised some concerns.^{132,133} Indeed, RGC-5 was initially characterised as derivative from rat retinal ganglion cell, but several studies indicate that the expression of certain proteins was not associated with these cells, but it seems a similar to 66W1 cells, mouse photoreceptors print.¹³⁴ The debate on this cell line is still open, and it seems it will not find an early end, the corresponding author dissociating himself from the original work, in the light of these recent studies.¹³⁵

Unfortunately, nowadays, fewer and fewer people are using this cell line as it has become extremely hard to publish any results, since many journals tend to reject articles with results related to RGC-5.

To date there is no validated alternative to RGC-5 to study retinal ganglion cells, making the choice of cell line for this project more challenging. The *in vitro* activity of idebenone has been investigated using several cell lines with variable results, including RGC-5 cell line, whose uncertainty of their nature contributes to the ambiguity on the idebenone results⁷³. The activity of idebenone strictly depends on the presence of NQO1 in the cells, showing a significant ATP rescue activity in cells expressing high level of NQO1, such as HepG2. On the other hand, idebenone consistently failed to rescue ATP levels in human embryonic kidney cells

(HEK293), human neuroblastoma cells (SH-SY5Y) and human keratinocyte cell line (HaCaT), all characterized by low NQO1 expression. In order to have a reasonable comparison between the novel identified compounds and idebenone, it was decided to test them on two different cell lines: HepG2¹³⁶ and SH-SY5Y¹³⁷.

HepG2, a human hepatocellular liver carcinoma cell line, is often used as a tool to screen for drug toxicity, and it is characterised by a high presence of detoxification enzymes, such as NQO1. This cell line was selected for the preliminary evaluation of toxicity and bioactivity of the novel compounds.

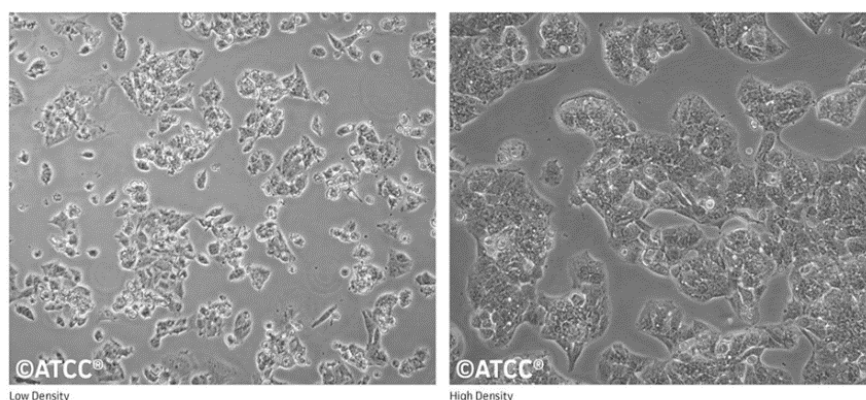


Figure 33 Images of HepG2 cell line¹³⁸

SH-SY5Y, human neuroblastoma, is a cell line widely used as model for study neuron cell lines, and neurodegenerative diseases. The cells are characterized by low level of NQO1 expression¹³⁹.

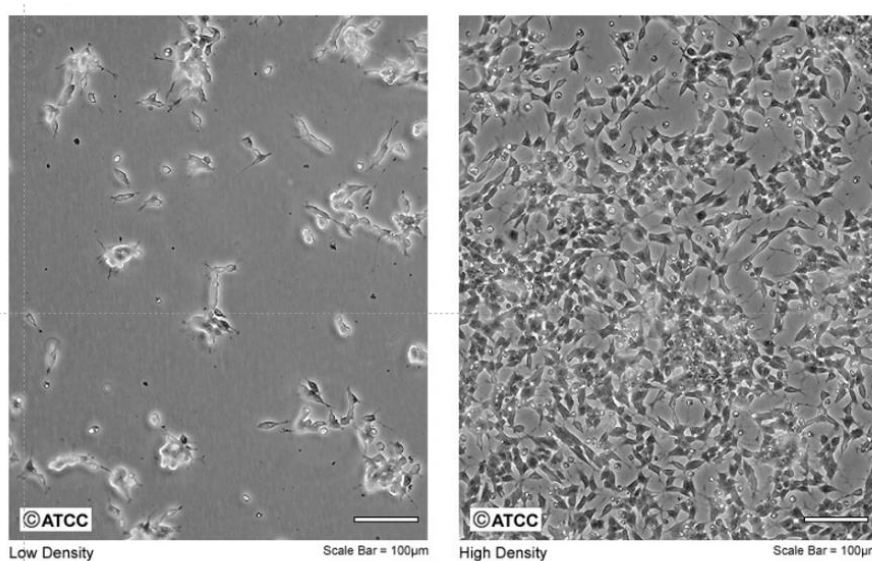


Figure 34 Images of SH-SY5Y cell line¹³⁸

3.2.1.1 Rescue of ATP level under inhibition of complex I

In mostly tumour-derived cells, such as HepG2 and SH-SY5Y cells, when glucose is abundant, they can utilise glycolysis alongside oxidative phosphorylation (OXPHOS) to sustain their growth in anaerobic conditions, reducing their sensitivity to mitotoxicants. On the other hand, when the level of glucose is low, highly effective ATP production is only mitochondria-dependent. However, without the contribution of glycolysis, energy production decreases over the time leading the cellular death.

Rotenone, a complex I inhibitor, was used for the suppression of mitochondria-dependent ATP production to recreate the “disease condition”. The glucose was removed from the media for a set time, which did not alter the energy production, but “activates” the Rotenone toxicity. Indeed, in the absence of glucose, any impairment in the electron transport chain drastically reduces ATP production (Figure. 35). In HepG2 cells, the removal of glucose for 2 hours did not alter ATP production, but the treatment of Rotenone 25 μ M reduced ATP levels almost completely at the same time (3 +/- 5% compared to untreated cells). This experimental method could easily be used to study the potential activity of compounds in mitochondrial ATP production, when OXPHOS is inhibited.

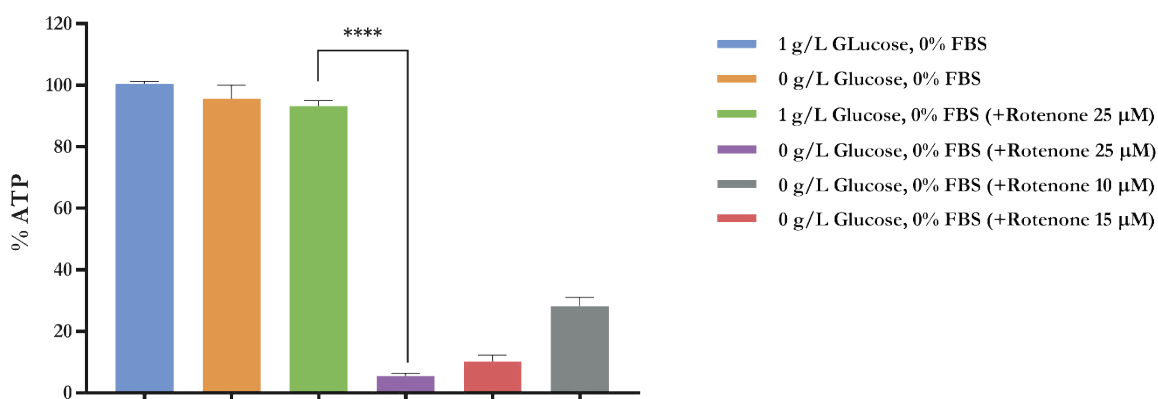


Figure 35 Influence of glucose on Rotenone toxicity. HepG2 cells were cultivated in medium containing 1g/l glucose or glucose-free medium in presence or absence of Rotenone. ATP level was defined as percentage of ATP in untreated cells, cultivated in medium containing 1g/l glucose. Bars represent mean \pm SEM of three independent measurements. Data were analysed using Two-way ANOVA test [F (2, 9) = 140.3, P<0.0001], followed by Sidak's post hoc test for multiple comparisons and adjusted P values were calculated (**** = $p \leq 0.0001$ 0 g/L glucose, 0% FBS (+Rotenone 25 μ M) versus 1 g/L glucose, 0% FBS (+Rotenone 25 μ M))

To determine if idebenone compounds could rescue ATP levels, cells were treated with different concentration of idebenone for 2 hours in glucose-free media, in the presence of 25 μM of Rotenone. The results show that idebenone was able to fully rescue the ATP level at a concentration of 10 μM

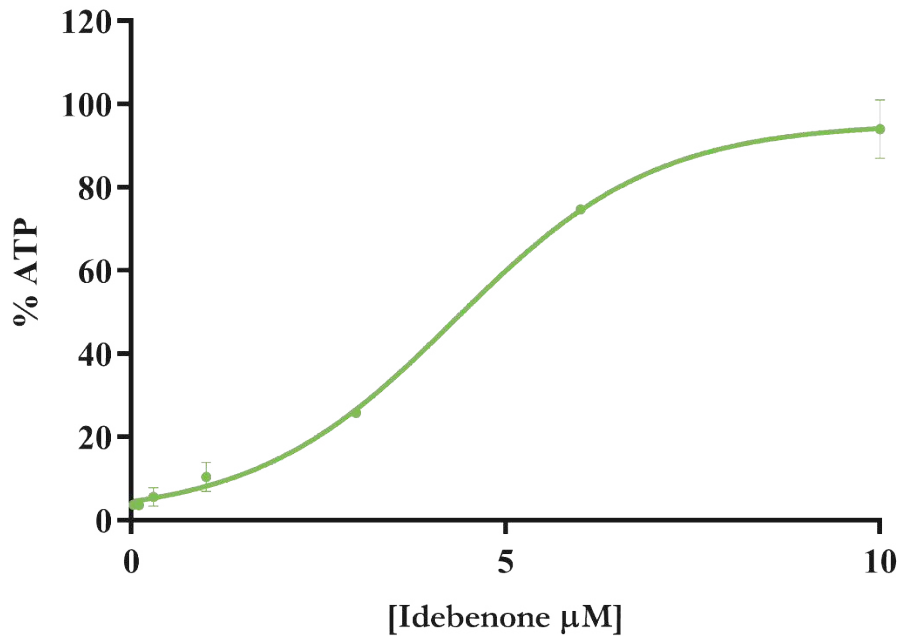


Figure 36 ATP rescue dose response curve for Idebenone. Bars represent mean \pm SEM of at least three independent measurements.

The effect of idebenone was lost when the function of NQO1 or complex III was inhibited by Dicoumarol and Antimycin (or Myxothiazol), suggesting that idebenone could affect the mitochondrial metabolism only if these two enzymes are available.

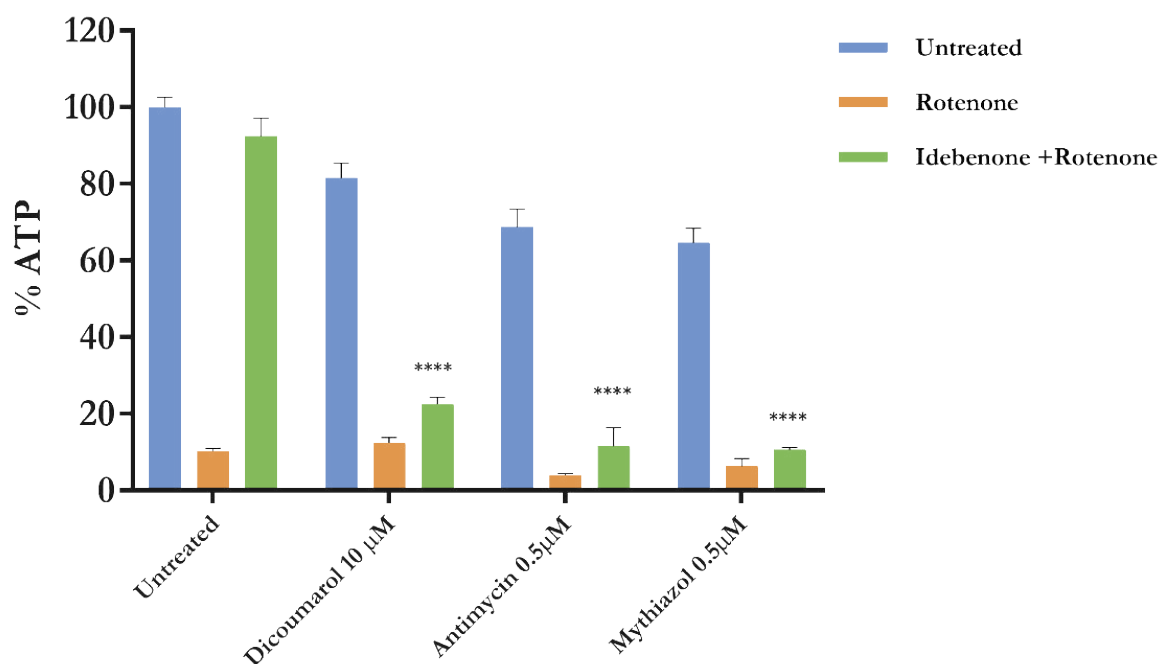


Figure 37 Influence of NQO1 and complex III inhibitors in the idebenone activity. HepG2 cell were incubated with Rotenone (25 μM), Antimycin (1 μM), Mythiazol (0.5 μM) and Dicoumarol (10 μM) in presence or absence of idebenone (10 μM) for 2h . ATP levels expressed as percentage of ATP in DMSO-treated cells in absence of rotenone (untreated). Bars represent mean ± SEM of three independent measurements. Data were analysed using Two-way ANOVA test [$F(6, 23) = 37.93, P < 0.0001$], followed by Tukey's post hoc test for multiple comparisons, *P* values were calculated versus Untreated (Idebenone+ Rotenone), **** = $p \leq 0.0001$.

According to this experimental setup for HepG2, the idebenone was tested on SH-SY5Y cell line, but it resulted ineffective (Figure. 38). The failure of restoring ATP levels was attributed to the poor NQO1 expression in these cells, as confirmed in our experiment using the western-blot technique (Chapter 2.2.10).

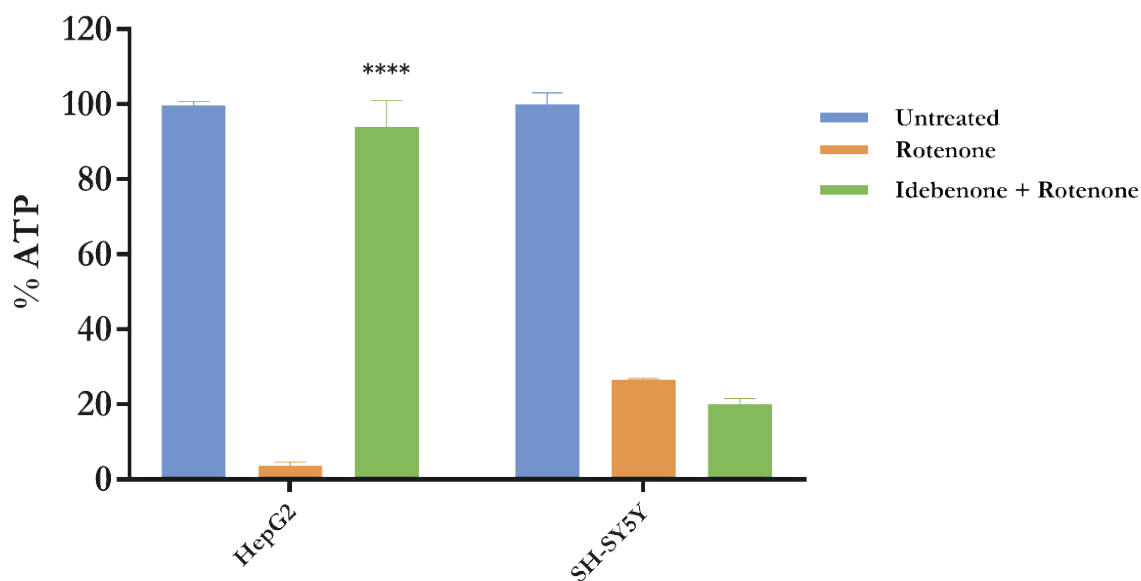


Figure 38 The comparison of ATP rescue activity of idebenone in HepG2 cell line and SH-SY5Y. The two cell lines were treated with Rotenone (25 μ M) in presence or absence of idebenone (10 μ M). ATP levels expressed as percentage of ATP in DMSO-treated cells in absence of rotenone (untreated). Bars represent mean \pm SEM of at least three independent measurements. Data were analysed using Two-way ANOVA test [F (2, 7) = 75.65, $P < 0.0001$], followed by Tukey's post hoc test for multiple comparisons, P values were calculated versus Untreated, **** = $p \leq 0.0001$

3.2.1.2 Seahorse bioenergetics analysis

During oxidative phosphorylation, production of ATP requires a continuous consumption of oxygen, as final electron acceptor in the electron transport chain. The set of metabolic reactions that consume oxygen is called mitochondrial respiration, and it is a direct parameter to assess the mitochondria condition¹⁴⁰. An alteration in the mitochondrial metabolism has a drastic impact on the consumption of oxygen, with a decrease of basal respiration as well as ATP production. Recently an innovative instrument was developed to monitor the cell respiration using an oxygen-dependent fluorescence probe, that can monitor the oxygen concentration in the medium: the seahorse xf 96 analyzer¹⁴¹. This instrument measures the two major energy-producing pathways of the cell simultaneously: mitochondrial respiration (oxygen consumption) and glycolysis (extracellular acidification). Using a piston-sensor close to the cells seeded in the plate, it is possible to monitor the oxygen uptake in that volume and control the respiration with two automatic injections of drugs: oligomycin, and rotenone/antimycin.

Briefly, the basal bioenergetics state of the cells is determined being followed by two consecutive injections. The first being oligomycin, an inhibitor of complex V ATPase, followed by rotenone and antimycin, which blocks complex I or complex III respectively, causes the complete blockage of the electron transport chain. At this point, the remaining residual OCR is due to non-mitochondrial respiration (Figure. 39).

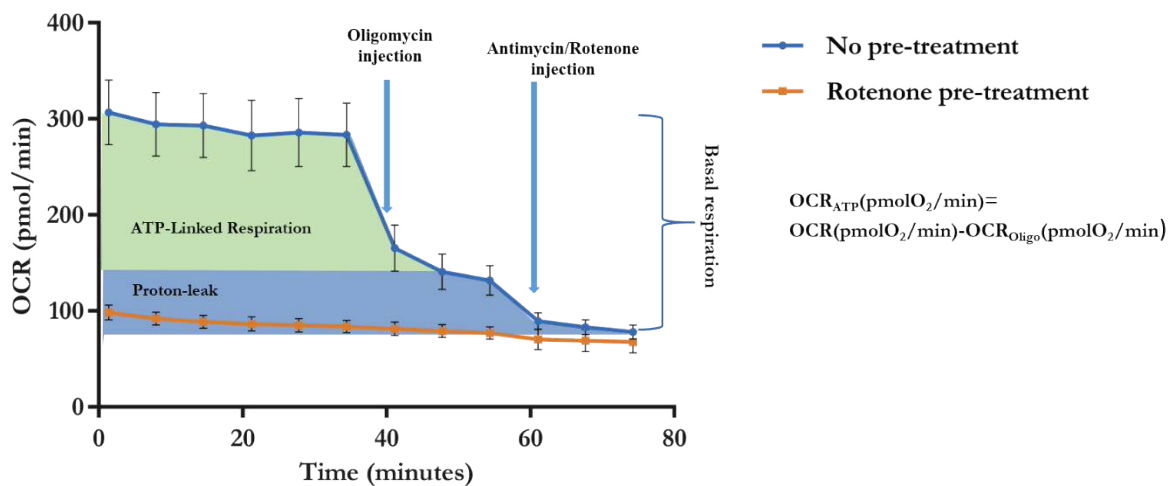


Figure 39 Seahorse assay. HepG2 cell were incubated in presence of Rotenone (Rotenone pre-treatment 0.5 μM) or absence of Rotenone (No-Rotenone pretreatment) for 45 minutes in no- CO_2 incubator at 37 $^\circ\text{C}$, before starting the assay. After 45 minutes, the basal oxygen consumption rate (OCR) was measured, followed by the injection of oligomycin 1 μM and Antimycin/Rotenone 1 μM . Oxygen consumption rate (OCR) is measured before and after the addition of inhibitors to derive several parameters of mitochondrial respiration. Data are means \pm SEM of $n = 6$ independent biological replicates.

In the case of mitochondrial dysfunctions this physiological trend is disturbed,¹⁴¹ in particular when the cells are pre-treated with rotenone the basal respiration is lower compared to the untreated cells, due to inhibition of complex I and consequently reduction of oxygen consumption. Compounds that can provide electrons bypassing the complex I, may possess the ability to re-establish the oxygen consumption at a physiological level. In our experiment, when idebenone was injected, there was an immediate increase of OCR, supporting the hypothesis that in the absence of complex I, idebenone allows the “bypass” by shuttling electrons from alternative donors to complex III (Figure. 40).

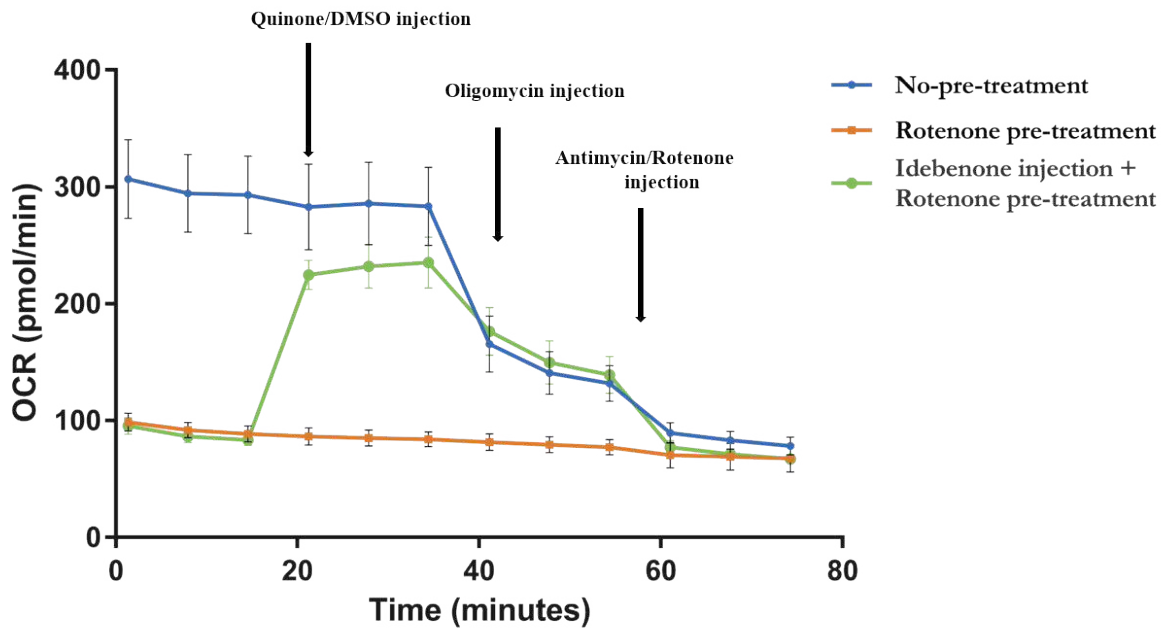


Figure 40 Influence of Rotenone on Oxygen consumption rate and OCR rescue by idebenone. Graph shows the rescue of OCR after idebenone injection (10 μM) in Rotenone pre-treatment sample. DMSO injection was used as control in the No pre-treatment samples and Rotenone pre-treatment sample. After DMSO/idebenone injection, oligomycin 1 μM , Antimycin/Rotenone 1 μM was injected in order to exclude OCR not correlated with the mitochondrial electron transport chain. Data are means \pm SEM of n = 6 independent biological replicates.

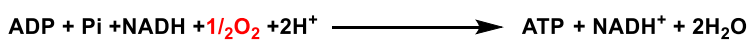
In mammalian cells the total ATP production is the result of oxidative phosphorylation (OXPHOS), that occurs in mitochondria, in addition to glycolysis. The seahorse is able to measure the contribution of both pathways simultaneously converting the change of the proton production (glycolysis) and oxygen consumption (OXPHOS) after the drugs injections. In fact, during glycolysis one molecule of glucose can be converted in lactate, producing ATP, water and protons.



Consequently, the contribution of glycolysis in the total production can be calculated by the acidification of assay media.

$$\text{glycolytic ATP Production Rate (pmol ATP/min)} = \text{Glycolytic Proton Efflux Rate (pmol H}^+/\text{min)}$$

In the case of oxidative phosphorylation instead, ATP production can be calculated by the consumption of oxygen



In conclusion, the total ATP produced is the sum of both pathways. In our study, idebenone was only able to increase the mitochondria respiration without influencing the glycolysis pathway; therefore, the total ATP produced after idebenone injection in pre-treatment Rotenone cells is the results of the ATP rescue in mitochondria (Figure 41).

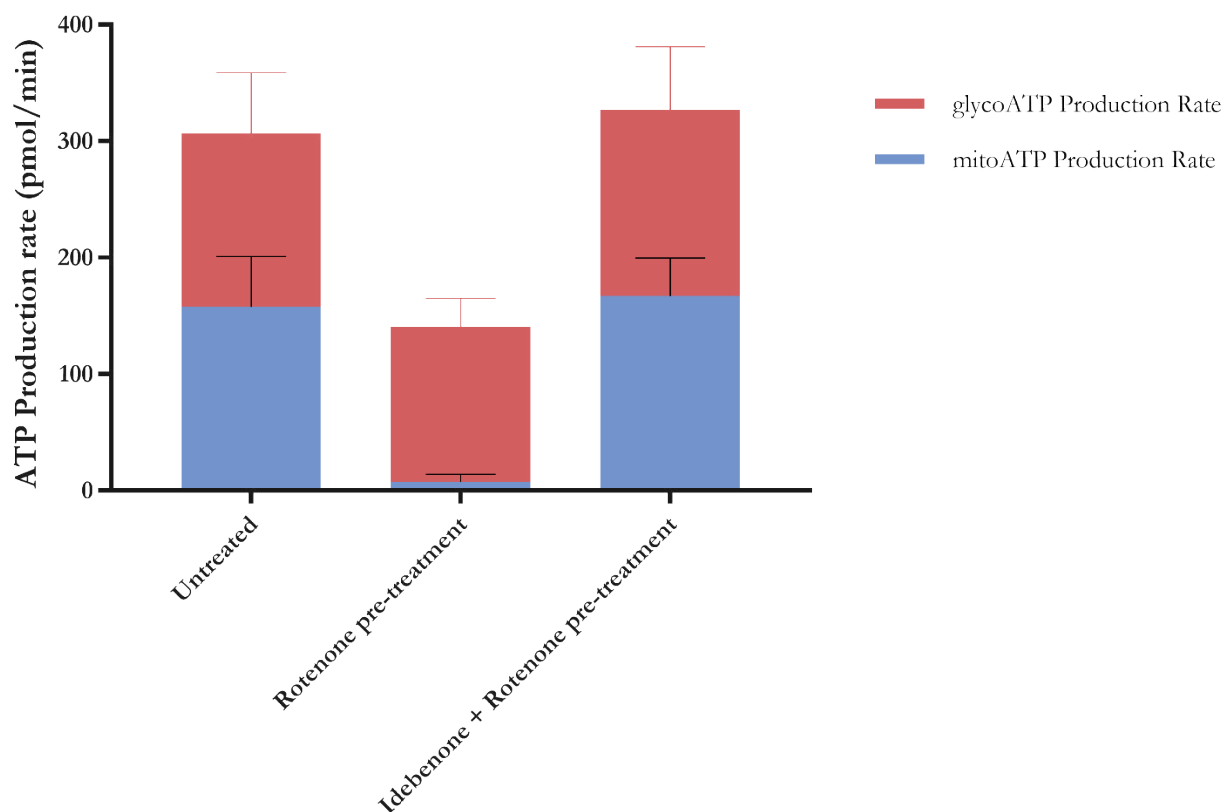
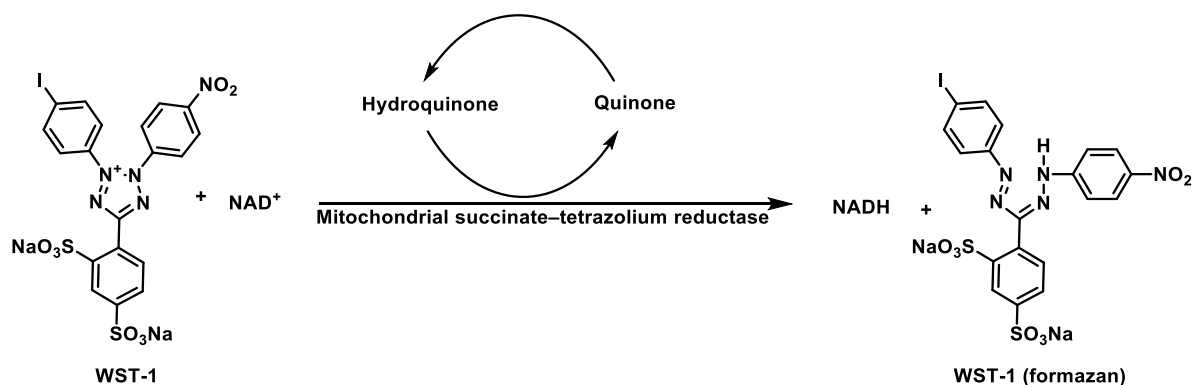


Figure 41 Rescue of mitoATP production by idebenone. The graph illustrates the quantitative metabolic shift from glycolysis (red) to mitochondrial respiration (blue) after idebenone injection in Rotenone pre-treatment samples. Data are means \pm SEM of $n = 6$ independent biological replicates.

3.2.1.3 Quinones reduction in cells

Since the idebenone and synthesised compound were quickly reduced by NQO1 in a cell-free environment, it was of interest to demonstrate the reduction of quinones by NQO1 in living cells. In 2009, Tan and Berridge reported the use of WST-1 to monitor the quinone reduction by NQO1 in cells¹⁴². WST-1 is a water soluble cell-impairment tetrazolium dye, used for the quantification of cell viability. This tetrazolium salts required an electron coupling reagent (i.e. 1-methoxy-PMS) and is cleaved to formazan dye by the succinate-tetrazolium reductase which exists in the mitochondrial respiratory chain and is active only in viable cells¹⁴³



In this study, WST-1 is converted into the corresponding formazan dye upon reduction by hydroquinones, which mediates the WST-1 reduction by electron donation and corresponding re-oxidation into quinones. This capacity of quinone to reduce WST-1 was used to assess whatever quinones can be reduced by other oxidoreductases except for NQO1 in cells, testing the compounds in the presence or not of Dicoumarol (NQO1 inhibitor). The results show that idebenone is highly metabolised by NQO1. In fact, WST-1 was significantly reduced in comparison with the control in presence of Dicoumarol. The assay was repeated in SH-SY5Y cells, not surprising, no conversion of WST-1 was detected in this cell line, confirming lack of activity of idebenone due to the absence of its reduced form. Menadione in the presence of pure isolated NQO1 was used as positive control for the assay.

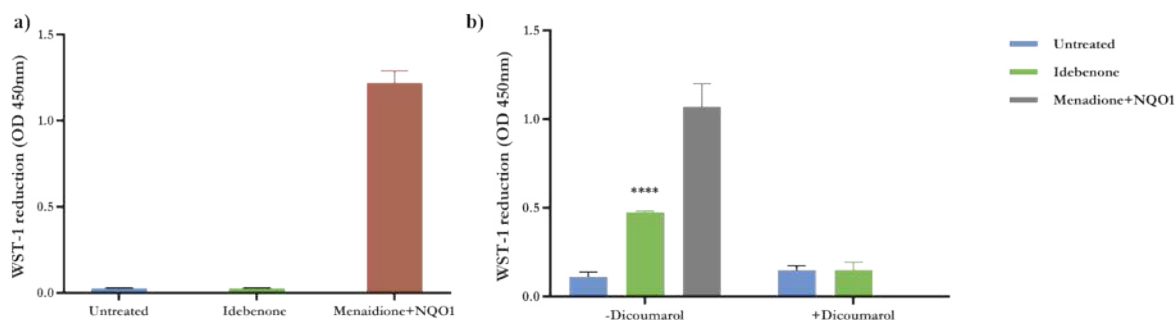


Figure 42 Idebenone reduction in SH-SY5Y and HepG2 cell line. Quinone reduction was measured using the WST-1 assay. The graph **a** and **b** show the absorbance detected in SH-SY5Y and HepG2 cell lines respectively, after the incubation with a PBS solution of 450 μ M of WST-1 in presence or absence of idebenone. In HepG2 Dicoumarol (20 μ M) was added to confirm the idebenone reduction by NQO1. Menadione in presence of recombinant NQO1 in free-cell environment was used as positive control. A one-way ANOVA was conducted to compare the idebenone reduction graph **a** [F (2, 14) = 326.0, $P < 0.0001$] graph **b** [F (2, 15) = 67.17, $P < 0.0001$] followed by Tukey's post hoc test for multiple comparisons, P values were calculated versus Untreated

3.2.1.4 Quinone cytotoxicity evaluation

1,4 Naphthoquinones have been widely studied for their cytotoxic activity and possible development as anticancer compounds.¹⁰⁹ They can show the cytotoxic activity as pro-oxidant, like plumbagin and juglone, which are excellent redox cyclers, which cause generation of reactive oxygen species (ROS) in cells and consequently oxidative cellular stress.¹¹⁰ Naphthoquinones with a free position in conjugation to one of the carbonyls, such as menadione, may react with glutathione (GSH), via a so-called Michael addition reaction, causing a significant depletion of this important antioxidant and co-factor of detoxification enzymes in cells exposed to these compounds (Figure. 43).¹¹⁰

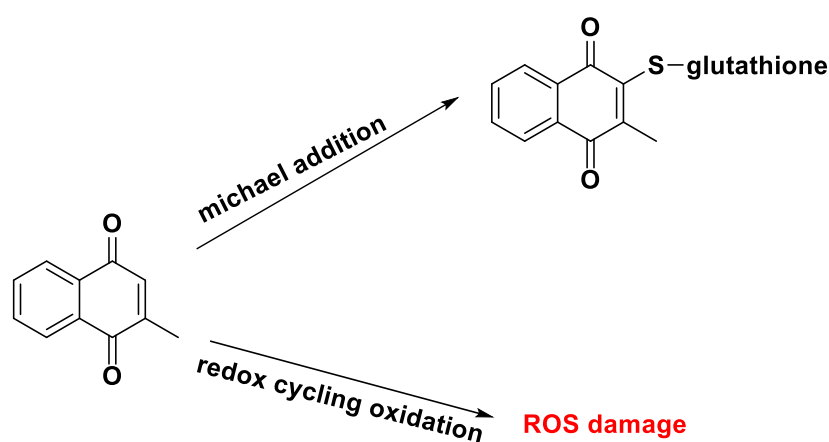


Figure 43 Schematic representation of naphthoquinones cytotoxicity.

To investigate the possible cytotoxicity of interesting naphthoquinones, the compounds were tested at a concentration of 25 μM using HepG2 and SH-SY5Y. These cell lines are characterized by the different expression of NQO1, which plays a critical role in the metabolism/activation of the interesting quinones, this diversity leads to a different equilibrium between the oxidative quinone forms in the two cell lines: the compounds are mainly in hydroquinone form in HepG2; instead they are in the oxidized (quinone) in SH-SY5Y. The different expression of NQO1 may explain the cytotoxicity of idebenone. Idebenone did not show any cytotoxicity in HepG2 at 25 μM , but in SH-SY5Y at this concentration, the cell viability is reduced by 45-50% after 1-day incubation (Figure. 44). These results are in agreement with the literature,¹⁴⁴ the toxicity in neuron cells may be explained as the inhibition of complex I, and consequently production and accumulation of ROS species. In the presence of high concentrations of NQO1, the toxicity was not evident because idebenone was metabolised into idebenol, electron carrier and antioxidant.

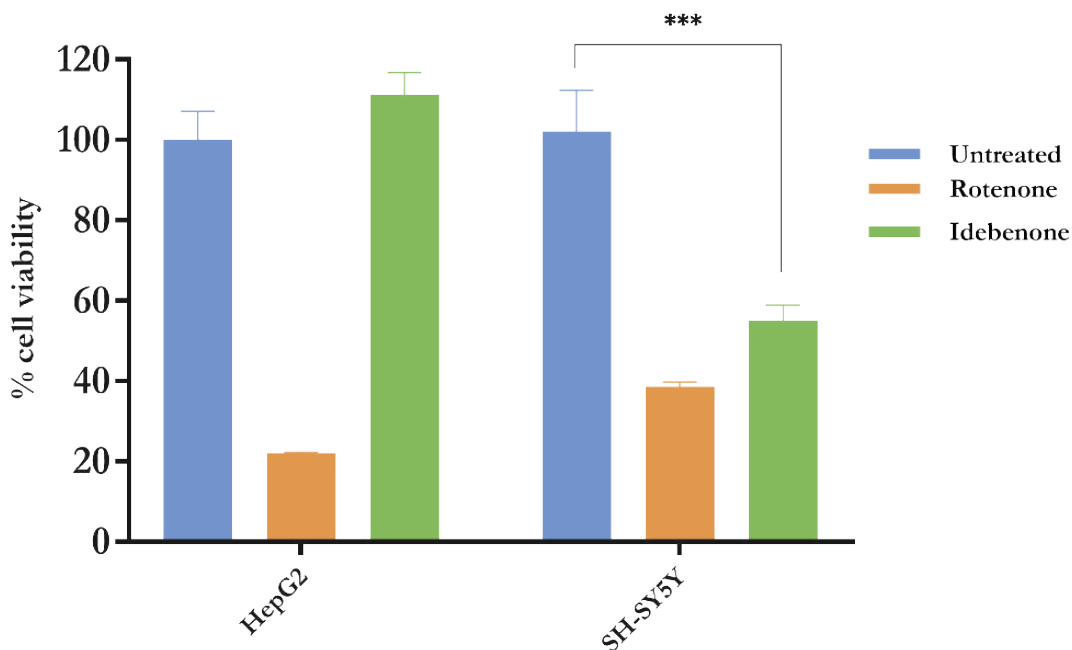


Figure 44 The idebenone cytotoxicity on HepG2 and SH-SY5Y. The graph shows the effect of idebenone incubation on cell viability after 24 hours' incubation. Rotenone was used as positive control, and the cell viability was determined as percentage of untreated cells. Bars represent mean \pm SEM of at least three independent measurements, Data were analysed using Two-way ANOVA test [$F(2, 12) = 21.94, P < 0.0001$], followed by Tukey's post hoc test for multiple comparisons, P values were calculated versus untreated **** = $p \leq 0.0001$

The idebenone toxicity might be strictly correlated with the inhibition of complex I and the consequent production of ROS. In order to confirm that hypothesis, the cytotoxicity assay was repeated in presence of *N*-acetyl cysteine (NAC) a known antioxidant, when NAC was added to the culture media, idebenone has not shown any significant toxic effect, suggesting that Idebenone induces the cytotoxic through ROS accumulation in the cells (Figure. 45).

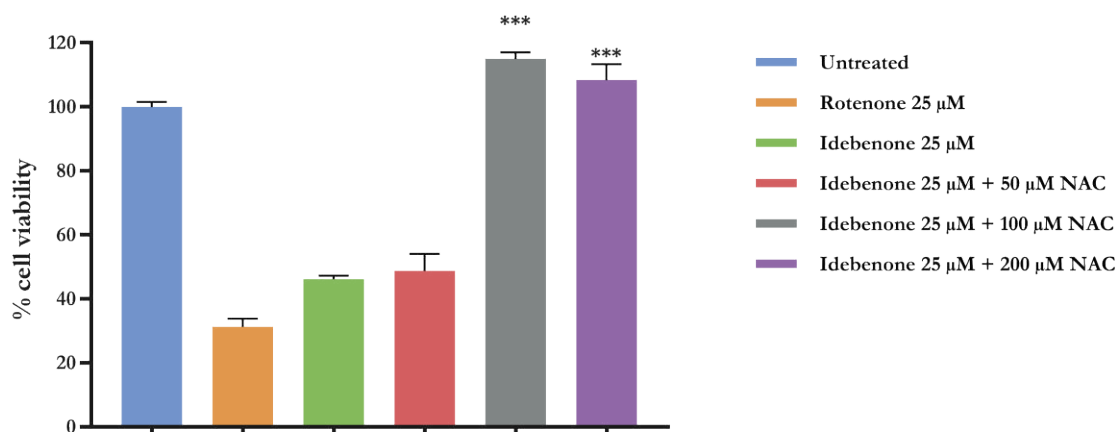


Figure 45 Cell viability of SHSY-5Y cells exposed to idebenone and various concentrations of NAC for 24h. The graph shows the increase of cell viability when cells were incubated with idebenone and various concentration of NAC. Bars represent mean \pm SEM of at least three independent measurements. Data were analysed using one-way ANOVA test [F (6, 21) = 154.6 P<0.0001], followed by Dunnet's post hoc test for multiple comparisons, *P* values were calculated versus Idebenone 25 μ M

3.2.1.4 Pro-oxidant effect of quinones

Pro-oxidant effects of naphthoquinones have been described in several of publications, as they can undergo bio-reductive activation by two pathways, a 1-electron (semiquinone) or a 2 electron reduction (hydroquinone), and interact with oxygen, resulting in the production of superoxide radical anions. The superoxide is an unstable free radical and a primary by-product of mitochondrial respiration. The CellROX® Green reagent is a novel fluorogenic probe, cell-permeant and non-fluorescent in the oxidized form, while in its reduced state it exhibits a photostable fluorescence.¹⁴⁵ It can undergo to this redox activation through interaction with superoxide ROS species.

As mentioned in Chapter 2.1.6 the naphthoquinones can undergo redox cycling in the cell, causing the accumulation of excess superoxide that is, in turn, converted to H₂O₂ by superoxide dismutase in the cytoplasm (CuZnSOD, SOD1) or in mitochondria (MnSOD). The ROS-Glo™ H₂O₂ Assay was used to evaluate the level of H₂O₂ in the cells. This assay is a sensitive bioluminescent assay capable of detecting the level of H₂O₂ in the cells through a formation of luciferase precursor, upon reaction with hydrogen peroxide¹⁴⁶ (Figure.46).



Figure 46 The ROS-Glo™ H₂O₂ Assay workflow. The H₂O₂ Substrate reacts directly with H₂O₂ to create the Luciferin Precursor which, in turn, is converted to luciferin after adding the ROS-Glo Detection Solution. The luciferase presents in the detection solution produces light signal proportional to the amount of H₂O₂ in the sample.

Given the reduction of quinones by NQO1, a cytosol enzyme, this probe provides useful information about the pro-oxidant activity of novel compounds in the cytoplasm. Menadione a well know naphthoquinone ROS-inducer was used as positive control for both assays^{143,146}.

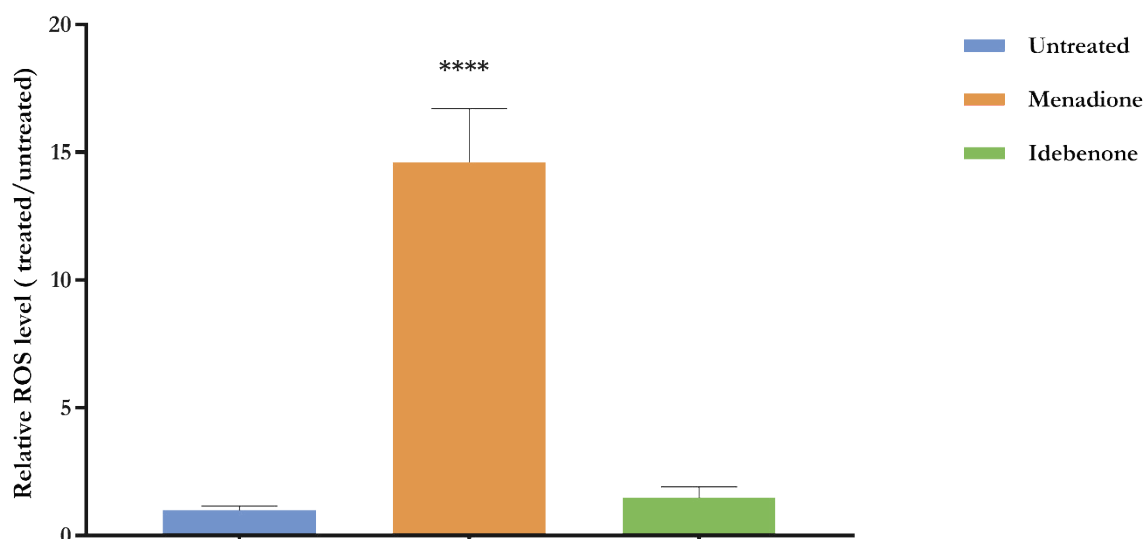


Figure 47 Quantification of ROS using CellROX® Green Reagent. The graph a shows the relative ROS level detected using CellROX Reagent, normalised to untreated cell. Menadione (25 µM) was used as positive control. Mean background value from cell-free wells incubated dye was subtracted from signals. Bars represent mean ± SEM of at least three independent measurements Data were analysed using one-way ANOVA test [F (2, 24) = 199.1P<0.0001], followed by Dunnet's post hoc test for multiple comparisons, *P* values were calculated versus untreated **** = *p* ≤ 0.0001

Although idebenone was described as an antioxidant, reducing the lipid peroxidation, it was of interest to determine if exposure to idebenone could increase the level of ROS, in particular in SH-SY5Y, in which idebenone showed a cytotoxic effect at 25 µM. As expected, idebenone did not show a pro-oxidant effect on HepG2, but surprisingly after 6 h incubation with

idebenone, only at high concentration (100 μM) a consistent increase of H_2O_2 level was detected in SH-SY5Y cell line.

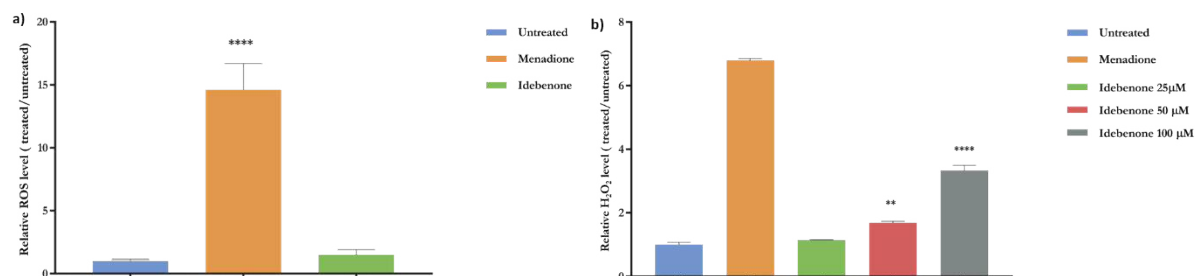


Figure 48 Quantification of H_2O_2 using ROS-Glo™ H_2O_2 The graph a shows the relative H_2O_2 level detected using ROS-Glo™ H_2O_2 , normalised to the untreated cell. Menadione (25 μM) was used as positive control. Mean background value from cell-free wells incubated dye was subtracted from signals. Bars represent mean \pm SEM of at least three independent measurements. Data were analysed using one-way ANOVA test graph a [F (2, 30) = 53.26 P<0.0001], graph b [F (4, 10) = 680.1 P<0.0001] followed by Dunnet's post hoc test for multiple comparisons, P values were calculated versus untreated **** = $p \leq 0.0001$

3.3 Conclusion

In conclusion, we optimised a series of enzymatic and cell-based assays that can be used as a tool to identify novel Idebenone analogs. Based on previous work, we focused on developing and optimising the assays using idebenone as a positive control.^{64,65,136,138,141} Firstly, we evaluated the idebenone affinity to the NQO1 and mitochondrial oxidoreductases such as complex I and complex II, that might be responsible for the activation of the quinones compounds into their active hydroquinone form. The results showed that the enzymatic assays were sensitive and reproducible: the rate of the enzyme-catalysed reactions was dependent on the Idebenone concentrations, and it was suppressed by the presence of selective inhibitors. Secondly, the biological effect of idebenone was evaluated in several cell-based assays. The quantification of ATP using the luciferase assay and the evaluation of cytotoxicity through the MTT assay showed consistent and reliable results, and they could be widely applied to evaluate several compounds rapidly. Finally, more sophisticated biological assays such as the evaluation of mitochondria respiration by XF96 analyser and detection of ROS level in cells could elucidate the mode of action of selected compounds. The overall consensus of these biological

results were used to select the most promising compounds for further *ex-vivo* /*in vivo* evaluation.

CHAPTER 4

**BIOLOGICAL EVALUATION OF
COMPOUNDS SELECTED BY
VIRTUAL SCREENING**

4.1 Hit identification

A hit molecule can be defined as a compound which has shown the desired activity in a compound screening. In this study, the virtual screening techniques have been combined with a bioassay-based validation to identify initial hit compounds for further medicinal chemistry optimisation. From the computational studies, naphthoquinone compounds have been identified as an interesting class of organic compounds, which might easily bind NQO1, accepting two electrons and consequently transferring them to the mitochondrial complex III, (Chapter 2). In order to validate the virtual screening results, 21 compounds have been selected and tested initially for their affinity for NQO1 using the recombinant enzyme. Successively, they have been tested whatever they can be substrates of mitochondrial oxidoreductase complex I and complex II, and finally, if they are able to bind the complex III after being reduced by NQO1. The preliminary enzymatic assays have shown a consistent interference of compounds, limiting the study of the mechanism of action and proving qualitative information rather than a quantitative value on their binding affinities of the studied enzymes (5.1.2). Moreover, the 21 compounds have been further evaluated for their potential biological response, in particular, they have been tested for their ability to rescue the ATP level under inhibition of complex I (by rotenone) and cytotoxicity, monitoring the cell viability by MTT. These assays were used to select a hit compound to optimise (Figure 49)

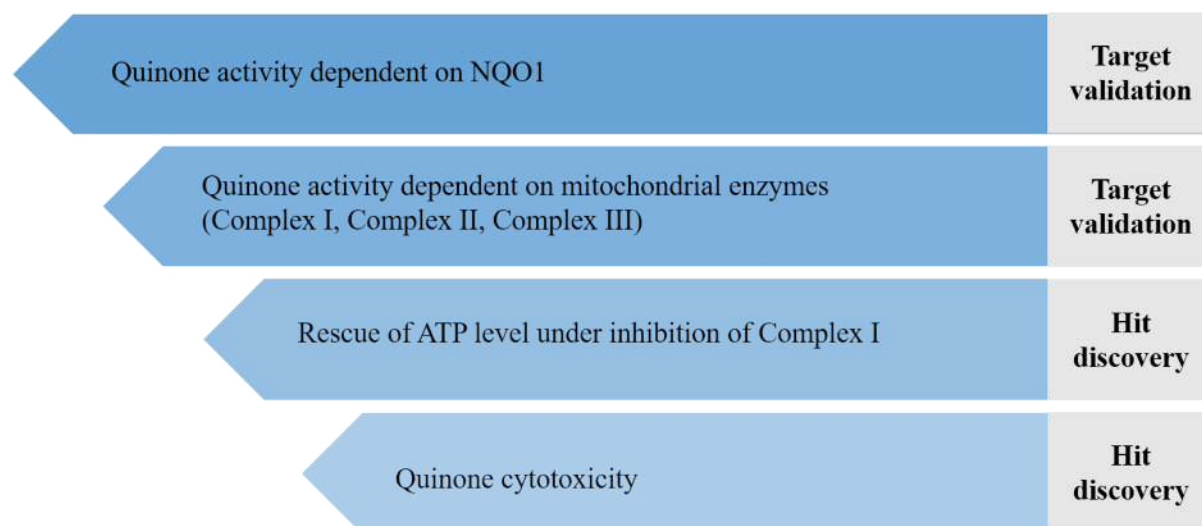


Figure 49 Experimental workflow used to select the hit compound

4.1.1 Results of enzymatic assays of virtual screening compounds

Since NQO1 plays a key role in the activation of idebenone, all compounds selected from virtual screening were tested for their ability to be reduced by this enzyme. The results obtained suggest that even if naphthoquinones are excellent NQO1 substrates, not all the quinones were reduced by the enzyme in a cell-free environment, in particular, the two 2-amino-1,4-naphthoquinone (**9**, **11**, **12**, **13**), which do not show a substituent in position 3, are inactive (Figure 50).

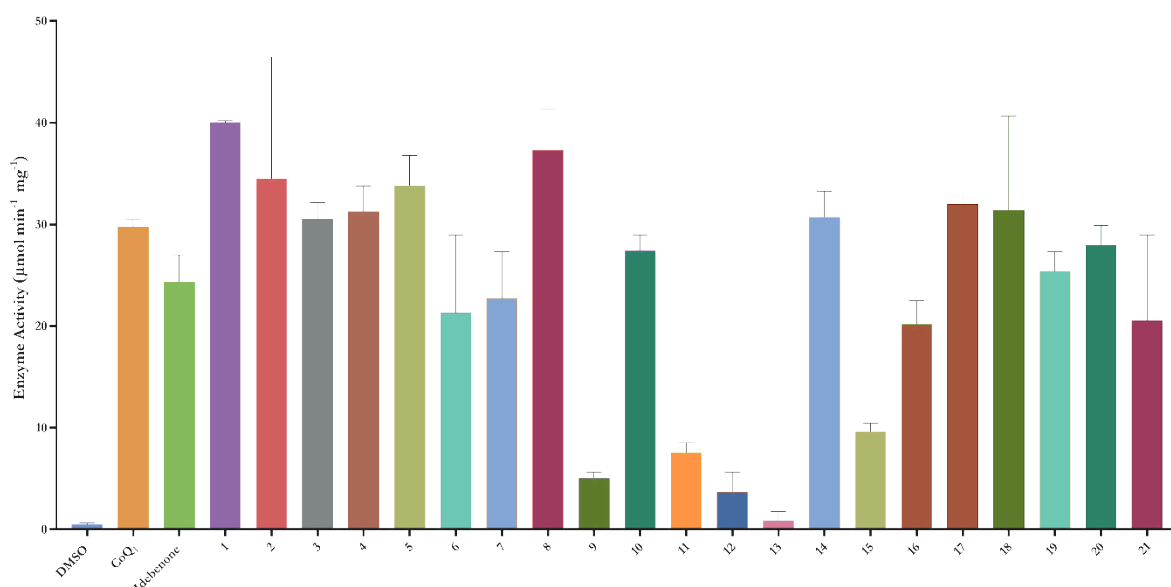


Figure 50 Results of the NQO1 assay. The graphs show the NQO1 enzymatic activity correlated with the quinones reduction. The assays contained 5mM Tris-HCl pH 7.4, 0.7 mg/ml bovine serum albumin (BSA), NQO1 1µg/ml, 50 µM quinone and 100 µM NADH. The enzymatic activity is expressed as variation of absorbance at 340 nm in 1 minute according the protein concentration (equation Chapter 3.1.2.1). Columns display mean activity ± SEM of three independent measurements. Data were analysed using one-way ANOVA test [F (23, 24) = 7.67, P<0.0001], followed by Dunnet's post hoc test for multiple comparisons, *P* values were calculated versus DMSO, * = $p \leq 0.05$, ** = $p \leq 0.01$, *** = $p \leq 0.001$, **** = $p \leq 0.0001$

The explanation may be found on the different reduction potential of these compounds, rather than the presence of phenyl ring. Indeed, **13** and **14**, that differ for the only presence of a chlorine at position 3, show a different activity, with **14** quickly reduced from NQO1.

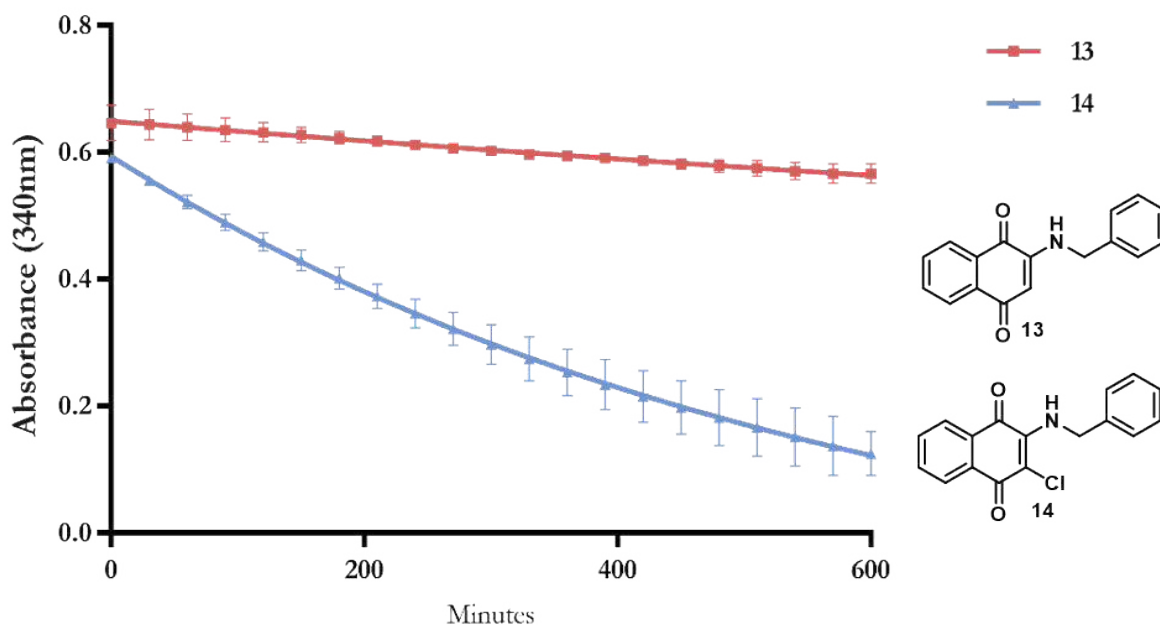


Figure 51 Comparison between 14 and 13 in the NQO1 assay. The graphs show the decrease of absorbance at 340nm due to consumption of NADH and the structure difference between **14** and **13**. The assay was carried out in in 1 ml cuvette containing: 25 mM Tris-HCl pH 7.4, 0.7 mg/ml bovine serum albumin (BSA), 50 μ M quinone, 1 μ g/ml NQO1, 100 μ M NADH. Each data point represents as means \pm SEM of two independent measurements.

Nevertheless, comparing the activity of naphthoquinones, it is evident that they show a particular trend: they are able to oxidise more NADH than they could do under the assay conditions. In other words, the reaction between NADH and the quinone catalysed by NQO1 is a two-electron transfer with a 1:1 stoichiometry,⁶⁵ which means a quinone is able to oxidise only the same amount of moles of NADH. In the assay, the reaction had a super-stoichiometric conduct, which led to a total consumption of NADH also at a lower concentration of the quinone. One possible explanation is that these compounds can be re-oxidised in the presence of molecular oxygen and generate a cyclic reaction, which terminates only when all NADH is consumed (Figure 52).

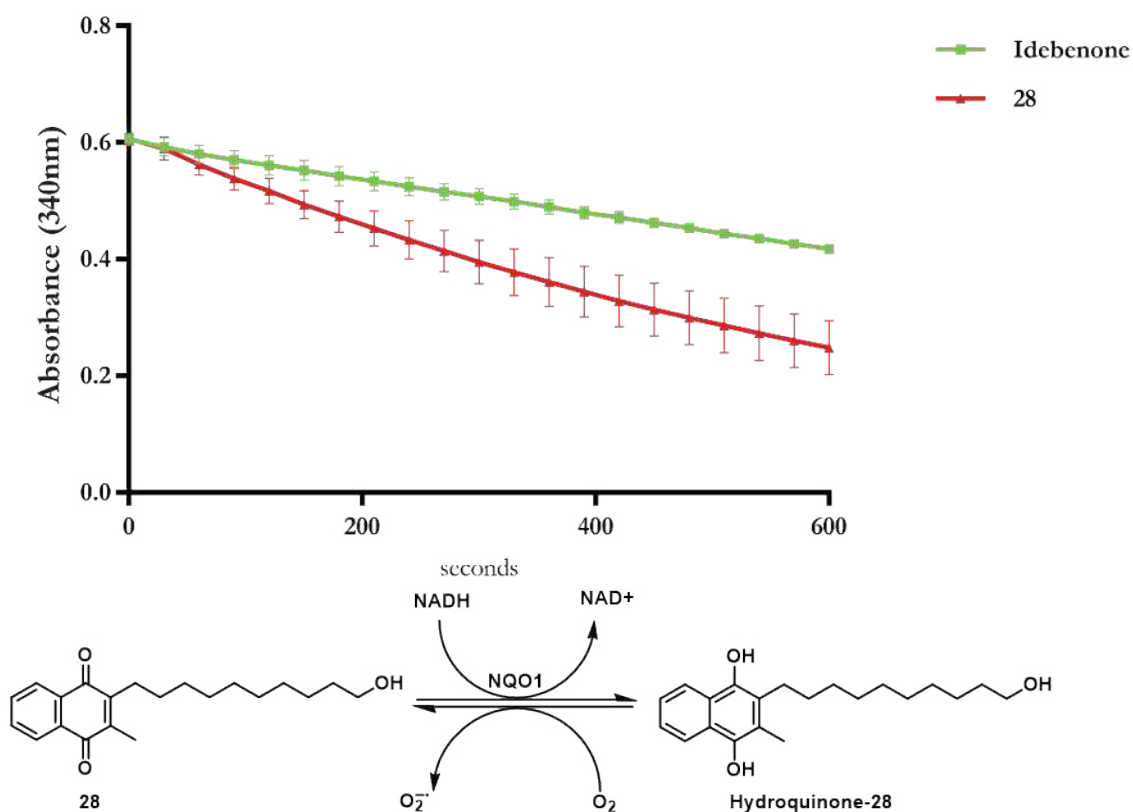


Figure 52 Cyclic reaction of NADH- re-oxidation. The Figure shows super-stoichiometric conduct of **28** due to the re-oxidation. The assay was carried out in in 1 ml cuvette containing: 25 mM Tris-HCl pH 7.4, 0.7 mg/ml BSA, 50 μ M quinone, 1 μ g/ml NQO1, 100 μ M NADH. Each data point represents as means \pm SEM of two independent measurements.

In order to demonstrate the re-oxidation event for these compounds in the presence of oxygen, the NQO1 assay was repeated removing the oxygen from the reaction environment using a sealed-tube cuvette and sparging with argon for 20 minutes. The results, showed in Figure 53, demonstrate that the reaction under these conditions does not show a super-stoichiometric conduct, since the decrease of NADH depends on the concentration of the quinone used.

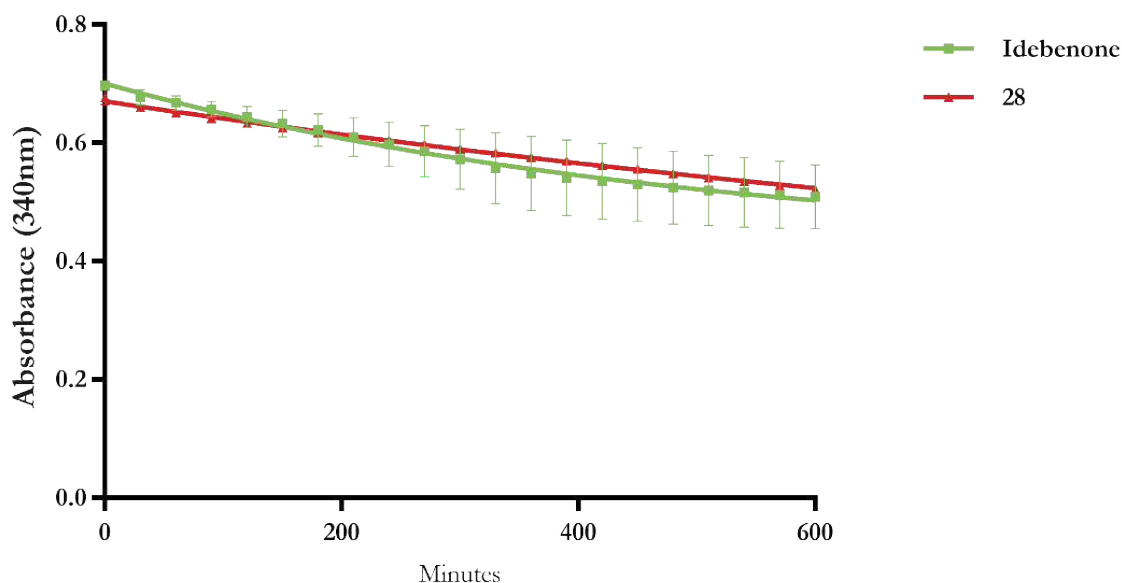


Figure 53 Effect of oxygen on the re-oxidation reaction The Figure shows the NQO1 results for **28** and idebenone in Argon-saturated solution. The enzyme activity was calculated following the addition of NQO1 after bubbling a seal-tube cuvette with argon for 20 minutes. The assay was carried out in in 1 ml cuvette containing: 25 mM Tris-HCl pH 7.4, 0.7 mg/ml BSA, 50 μ M quinone, 1 μ g/ml NQO1, 100 μ M NADH. Each data point represents as means \pm SEM of three independent measurements.

Due to the unknown absorption of the reduced form of compounds, the possibility that the corresponding hydroquinones interfere with the assay could not be excluded. Further, the well-known instability of hydroquinones limited their use for *in vitro* assays, for this reason, a proper comparison of the quinone activity could not be carried out. However, these explorative results, even if they are limited, provide useful information about the high affinity of naphthoquinones compounds for the NQO1 enzyme.

As previously mentioned (Chapter 2.3) idebenone can bind not only the NQO1 but complex I, II, and complex III. Hence, the naphthoquinones selected from virtual screening were tested for their ability to interact with these enzymes. The results showed that naphthoquinones are insufficient substrates for complex I and complex II, with the exception of less bulky naphthoquinones, like Menadione and compounds **6,7**.

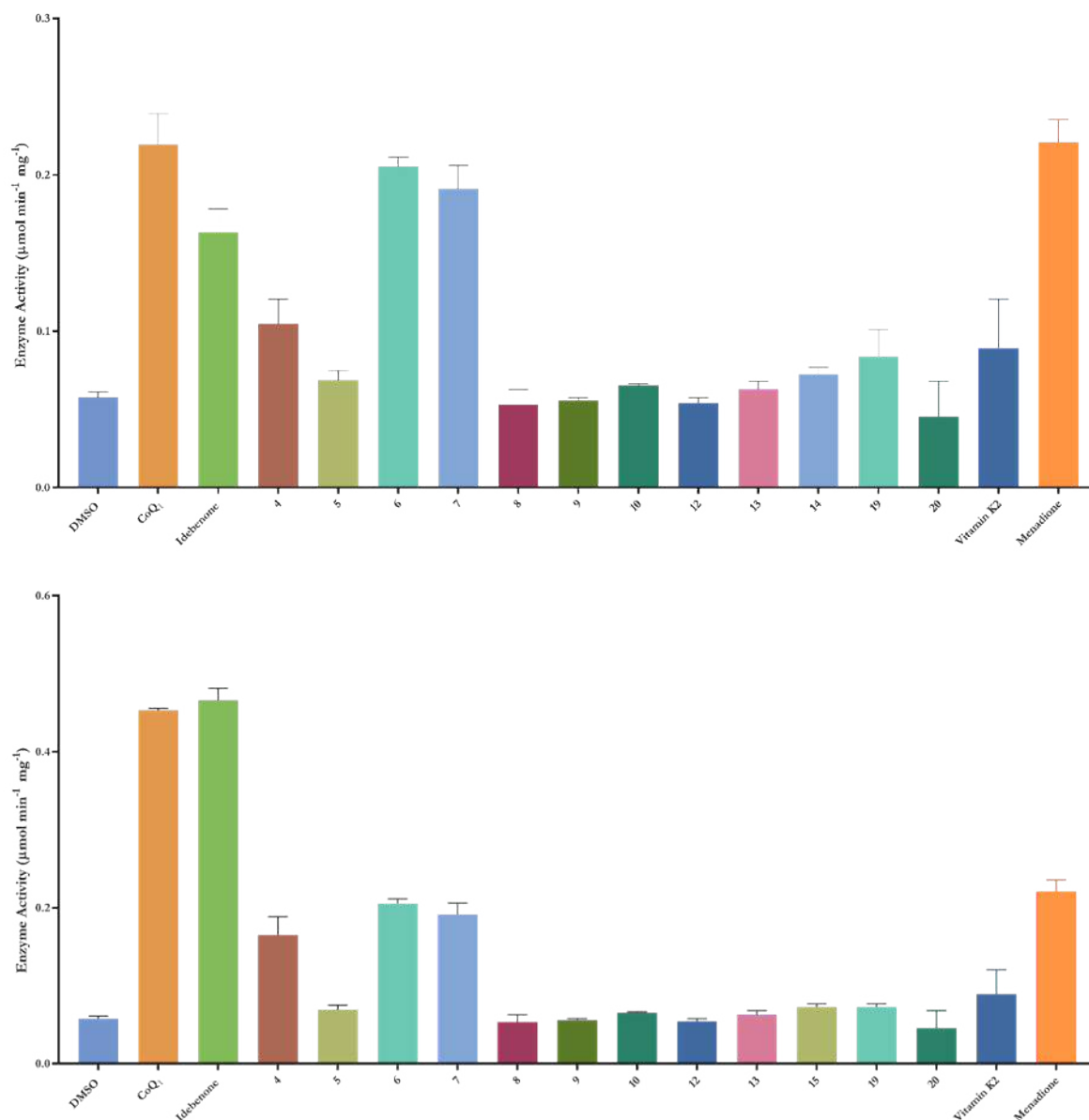


Figure 54 Results of the Complex I and Complex II assay. The graphs a and b show the Complex I and Complex II enzymatic activity correlated with the quinones reduction, respectively. The enzymatic activity is expressed as variation of absorbance at 600 nm in 1 minute according the protein concentration (equation Chapter 3.1.2.1). Columns display mean activity \pm SEM of three independent measurements. Data were analysed using one-way ANOVA test graph **a** [$F(16, 21) = 16.54$], graph **b** [$F(17, 19) = 101.1, P < 0.0001$] followed by Dunnet's post hoc test for multiple comparisons, P values were calculated versus DMSO, * = $p \leq 0.05$, ** = $p \leq 0.01$, *** = $p \leq 0.001$, **** = $p \leq 0.0001$

In particular, the change of the core from quinone to naphthoquinone, modulates the affinity of idebenone for complex I, as indicated by the different results obtained for **28** and idebenone, which differ only in the core (Figure 55).

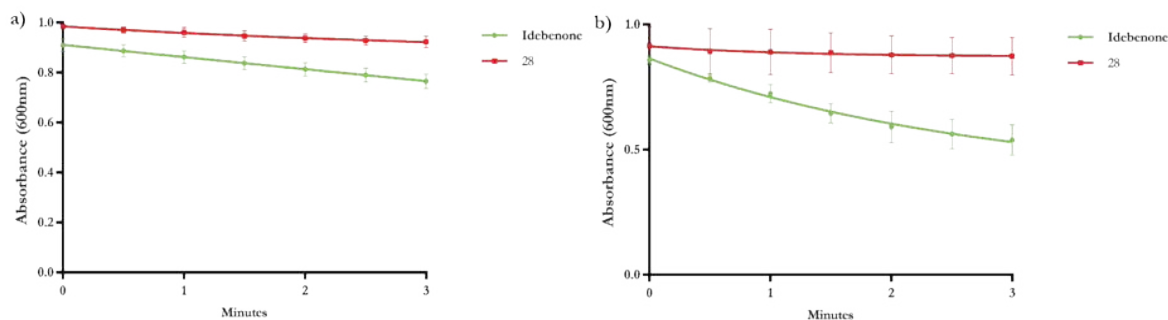


Figure 55 Comparison between idebenone and 28 in the complex I and complex II assay. The graphs show the decrease of absorbance at 600nm due to reduction of DCPIP in presence of quinone. The graph a show the complex I activity of idebenone and compound 28, while graph b shows the corresponding complex II activity. Each data point represents as means \pm SEM of three independent measurements.

These initial findings indicate that these naphthoquinone compounds might be associated with a different activity profile in comparison with idebenone. In fact, despite a significant turnover by NQO1, they do not have any interaction with complex I and complex II, making these compounds selective for the NQO1 oxidoreductase

4.1.1.1 NQO1-complex III assay and cytochrome c reduction

As previously mentioned (Chapter 1.3.2), recent studies suggest that idebenone in its reduced form (Idebenol) can donate its electrons to the complex III, re-establishing the correct electron flow in the electron transport chain. In this study, an *in vitro* model was used to evaluate the transfer of electrons between NQO1 and complex III using quinones as electron carrier. In particular, the assay was performed using isolated purified NQO1 enzyme, mitochondria, cytochrome c (final electron acceptor), quinone (electron carrier) and rotenone (complex I inhibitor), resuspended all in the same buffer (Phosphate Buffer). The reaction is started by the injection of NADH (initial electron donor), and it is monitored spectrophotometrically by measuring the reduction of cytochrome c at 550 nm. The majority of naphthoquinones, tested in the NQO1-complex III assay, showed a quicker and intense increase in absorbance at 550 nm, initially suggesting that these compounds could bind easily the Qo-binding site of complex III (Figure 56). But interestingly, while dicoumarol inhibited the activity of these compounds, antimycin A had no effect (Figure. 57). Furthermore, the reduction of cytochrome c by

naphthoquinone compounds was still evident after removing mitochondria from the reaction buffer.

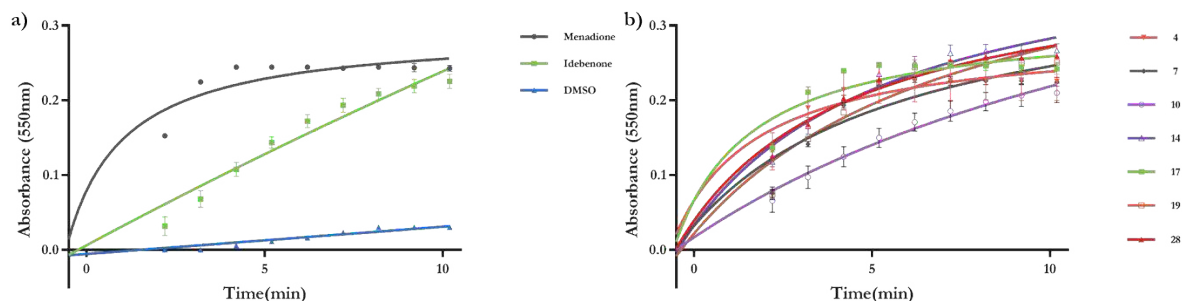


Figure 56 Results obtained for the NQO1-complex III assay by selected naphthoquinones. The graphs show the increase of absorbance at 550 nm due to the reduction of cytochrome c. The reduced cytochrome c level was detected in 1 ml cuvette containing: 25 mM Tris-HCl pH 7.4, 1 mg/ml bovine serum albumin (BSA), 20 $\mu\text{g/ml}$ mitochondrial protein, 50 μM quinone, 54 μM cytochrome c, 1 $\mu\text{g/ml}$ NQO1, 100 μM NADH, 500 μM KCN, 10 μM Rotenone. Each value was detected after NQO1 addition. Data point represents as means \pm SEM of three independent measurements.

These two experiments suggested that hydroquinone forms of the selected naphthoquinones were capable of reducing cytochrome c. The direct reduction of cytochrome c by naphthoquinones can be attributed to the formation of the superoxide anion ($\text{O}_2^{\cdot-}$) and a possible pro-oxidant activity of the selected compounds. This result was in line with the re-oxidation capacity of naphthoquinones, described earlier (Chapter 2.2.1) and with the results reported in the literature for Menadione¹⁴⁷. After reduction by NQO1, the naphthoquinone compounds can donate electrons to oxygen-generating superoxide, which can directly reduce a molecule of cytochrome c (Figure. 57 c). Another possibility is that the naphthoquinol can itself directly reduce cytochrome c, converting into semi-naphthoquinone.

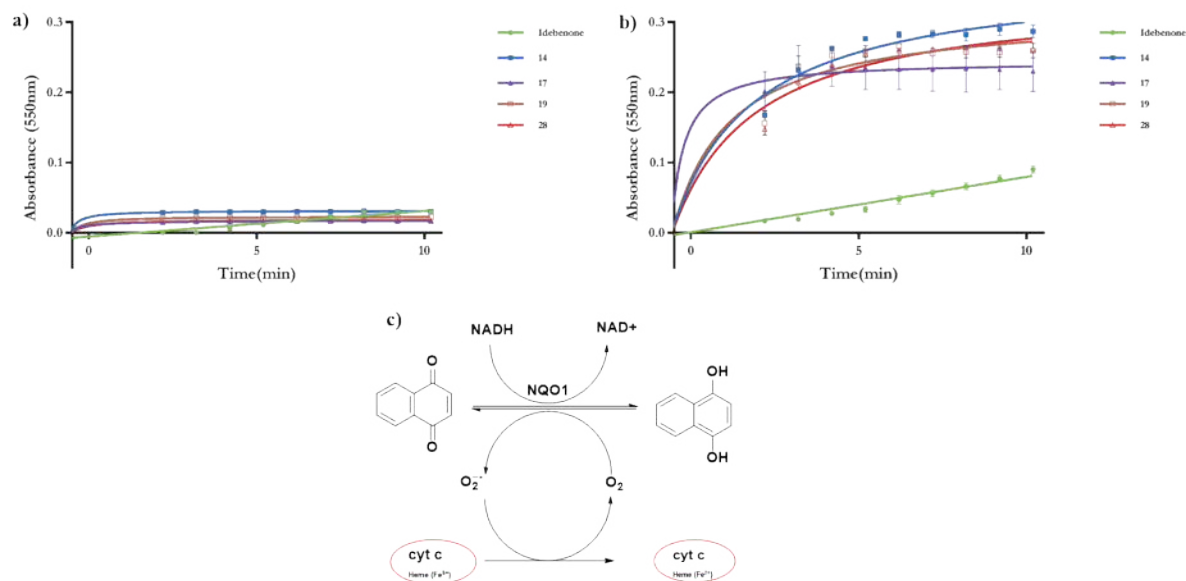


Figure 57 Results obtained for the NQO1-complex III assay in presence of Antimycin A or Dicoumarol. The graphs a and b show the increase of absorbance at 550 nm in the presence of inhibitor of complex III or inhibitor of NQO1 respectively. Figure c shows a schematic representation of the reduction of cytochrome c, that may occur in the absence of mitochondria.

4.1.2 Quinones interference in enzymatic assays and assay limitations

Naphthoquinones are a class of chromophore-bearing organic compounds capable of absorbing light at different wavelengths, as a result of the presence of several conjugated double bonds in the molecules. The absorption spectra of studied naphthoquinones revealed that this family showed different absorption peaks covering a range from approximately 400 to 550 nm in the UV-vis spectra. This peculiar property limits the study of the MAO of these family, since they directly interfere with the detection methods used in the enzymatic assays. Figure 58 shows the UV-vis spectra of **92** in quinone and hydroquinone form, determined using 5 different concentrations of NaBH_4 as reducing agent. Interestingly, in fully reduced form the compound did not show absorbance at 500 nm, meanwhile the hydroquinones spectra showed an increase at 350 nm compared to the full oxidised form. This change in absorbance from oxidised to reduced interferes with the study of NQO1 and complex III activity. In fact, NADH has the absorption peak at 340 nm and cytochrome c at 550 nm; moreover, the naphthoquinones are unstable in the hydroquinone form, and the re-oxidant occurs in few minutes in the presence of oxygen, Chapter (4.1.10.3), which constantly alters the equilibrium between the two redox states. Due to these limitations, an accurate study of MOA and a proper comparison of the quinone activities was not possible; alternative methods will be considered in future such as Isothermal Titration Calorimetry technique (ITC), which will allow us to determine the

biomolecular bindings of naphthoquinones¹⁴⁸. As a consequence, most experiments of this thesis concerning the mode of action of studied compounds were conducted in cells, using selective inhibitors for NQO1 and complex III, as described in Chapter 3

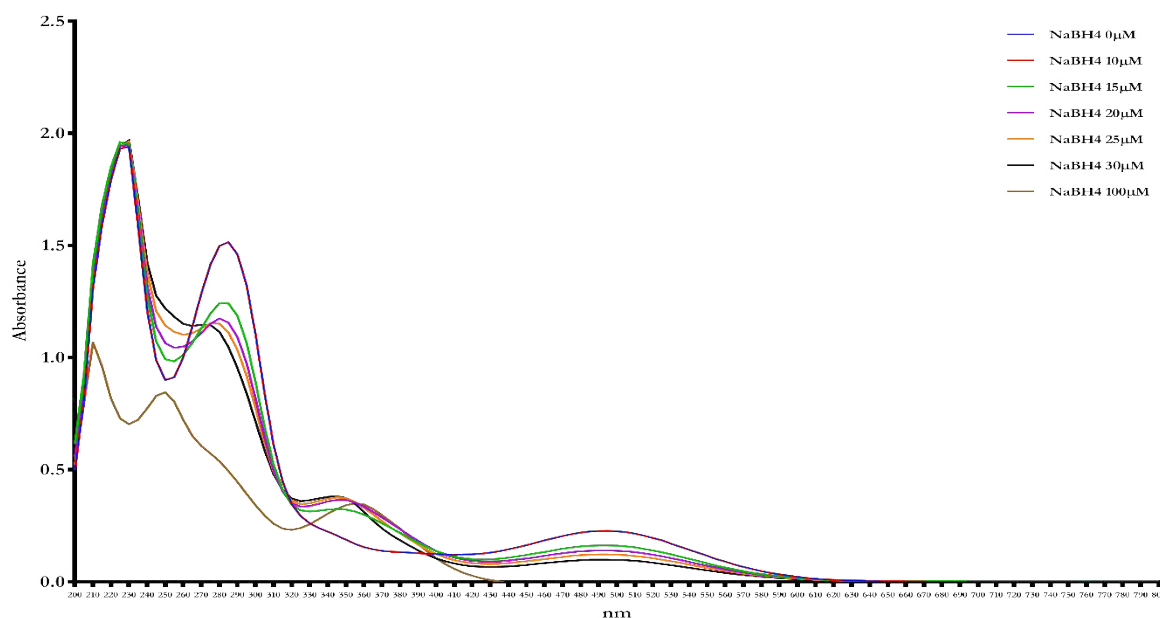


Figure 58 Change in absorbance spectrum of 92 according to the amount of reducing agent (NaBH₄) added

4.1.2 Results of cell based -assay of virtual screening compounds

To determine if selected compounds had the potential to rescue ATP levels, cells were treated with 5 μ M of quinones (or DMSO control) for 2 hours in free-glucose media, in presence of 25 μ M of Rotenone. The preliminary results showed that most of the selected naphthoquinones could recover ATP production, in particular, compounds **4,7,10,14** and **19** almost re-established the same concentration of ATP of idebenone (Figure 59). The lack of the substituent in position 3 produced a significant decrease of ATP production (**9,12,13**), confirming the low NQO1 activity of these compounds.

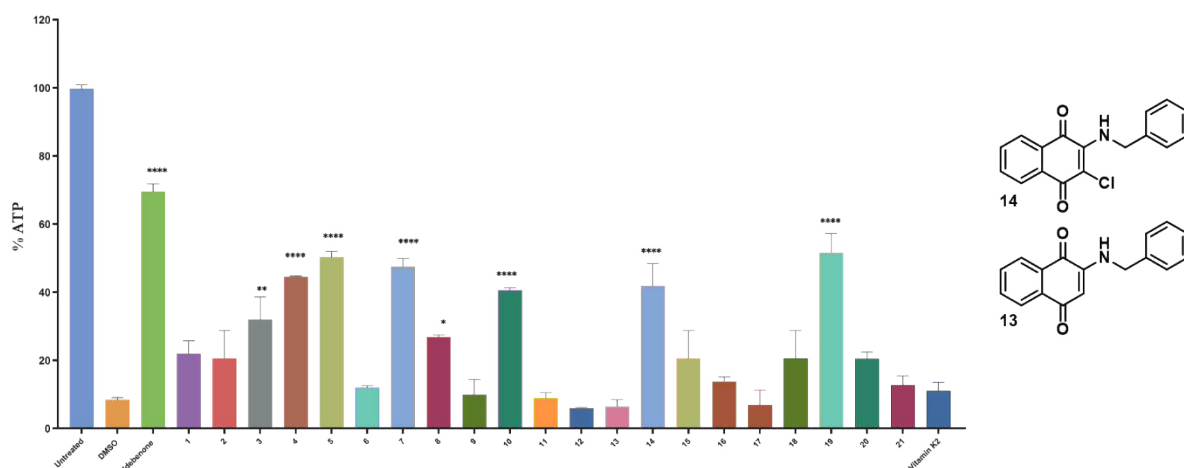


Figure 59 Efficacy of ATP rescue in the presence of rotenone by quinones at 5 μ M. ATP rescue activity of quinones was determined in rotenone-treated HepG2 cells. ATP levels expressed as percentage of ATP in DMSO-treated cells in absence of rotenone (untreated). Data represent mean \pm SEM of at least three independent measurements. Data were analysed using one-way ANOVA test [F (24, 173) = 222.0, $P < 0.0001$], followed by Dunnet's post hoc test for multiple comparisons, P values were calculated versus DMSO, * = $p \leq 0.05$, ** = $p \leq 0.01$, *** = $p \leq 0.001$, **** = $p \leq 0.0001$

The most active compounds were re-tested at a lower concentration (1 μ M), showing that quinones with a benzyl ring in position 2 (**7,14,19**) had a significant ATP rescue activity (Figure 60). This data was in line with the study of complex III: the phenyl moiety may be an important feature in the interaction with the Qo hydrophobic pocket of the enzyme.

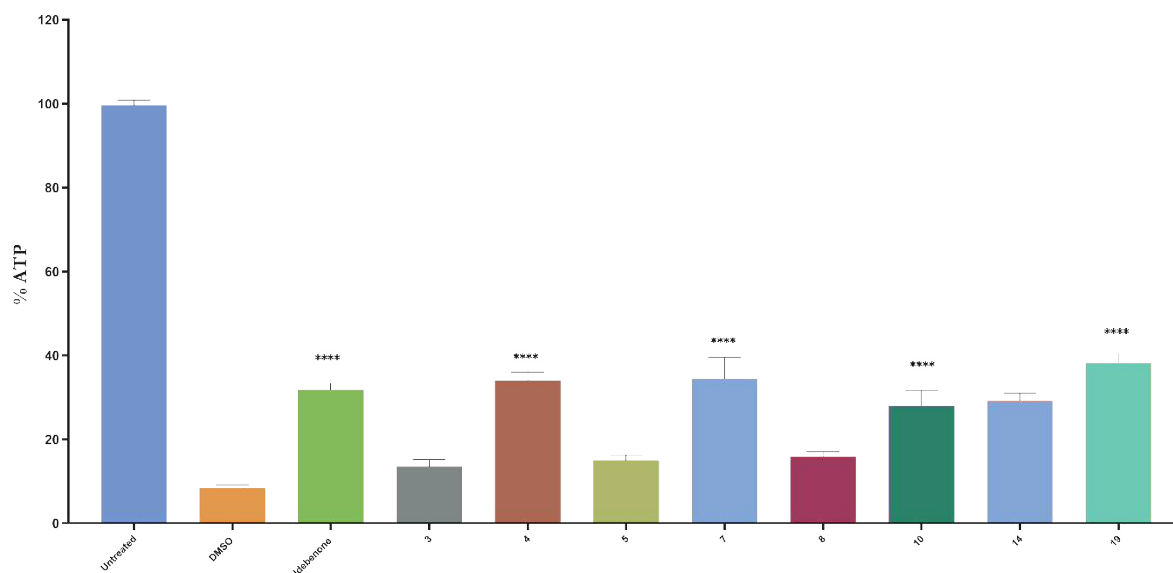


Figure 60 Efficacy of ATP rescue in presence of rotenone by quinones at 1 μ M ATP rescue activity of quinones was determined in rotenone-treated HepG2 cells. ATP levels expressed as percentage of ATP in DMSO-treated cells in absence of rotenone (untreated). Bars represent mean \pm SEM of at least three independent measurements. Data were analysed using one-way ANOVA test [F (21, 348) = 121.2, $p \leq 0.0001$], followed by

Dunnet's post hoc test for multiple comparisons, *P* values were calculated versus DMSO, * = $p \leq 0.05$, ** = $p \leq 0.01$, *** = $p \leq 0.001$, **** = $p \leq 0.0001$

The compounds that showed significant ATP rescue activity, even at 1 μM , were further tested to determine whether they show a cytotoxic effect using HepG2 and SH-SY5Y cell lines. Naphthoquinone compounds showed a moderately toxic effect at 25 μM with a decrease of 10-20% of cell viability compare to the untreated cells in HepG2, with the exception of **1** and **3**, but interesting the majority of the naphthoquinones showed a lower toxicity than idebenone in the SH-SY5Y cell line. The results suggested that the toxicity of these compounds is related to the higher affinity of naphthoquinone to NQO1 than other oxidoreductases, as complex I (Figure. 61).

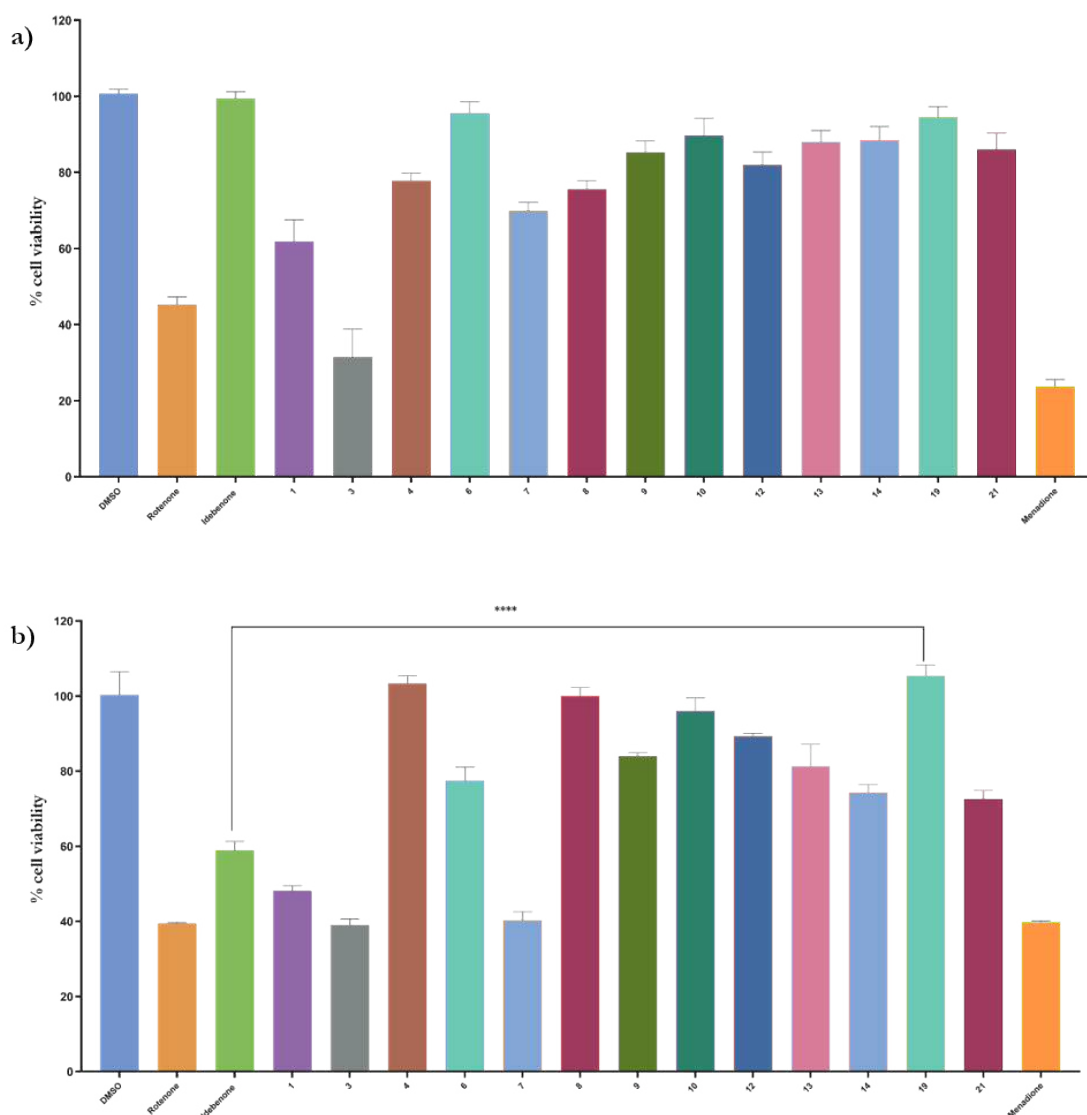


Figure 61 Cytotoxicity of quinones selected from virtual screening on HepG2 and SH-5YSY. The graphs **a** and **b** show the quinone cytotoxicity in HepG2 and SH-SY5Y cell line respectively. Both cell lines were treated with 25 μ M of compounds and incubated for 24 hours at 37 °C. The cell viability was determined as percentage of untreated cells. Bars represent mean \pm SEM of at least three independent measurements. Data were analysed using one-way ANOVA test: graph **a** [F (2, 14) = 326.0, P<0.0001] graph **b** [F (16, 37) = 69.56, P<0.0001] followed by Dunnet's post hoc test for multiple comparisons, *P* values were calculated versus DMSO, * = $p \leq 0.05$, ** = $p \leq 0.01$, *** = $p \leq 0.001$, **** = $p \leq 0.0001$

4.1.3 Conclusion: biological results obtained using compounds indicated from virtual screening

The naphthoquinones selected from the virtual screening exercise was an interesting class of compound. The majority of naphthoquinone selected from the virtual screening were good NQO1 enzyme substrates, showing a low affinity for complex I and complex II, unlike Idebenone (Table 3). This higher affinity for NQO1 than mitochondrial oxidoreductases was attributed to the change of core from quinone to naphthoquinone. However, the results also show that the reduction potential is a fundamental feature of these family; the only difference of chlorine in position **3** between **13** and **14** drastically change the NQO1 activity. These difference in NQO1 affinity of compounds was also evident in the cell-based assay: the compounds that showed high NQO1 affinity such as **10,14** and **19**, they also showed significant ATP rescue activity.

Compound ID	Enzymatic activity ($\mu\text{mol min}^{-1} \text{mg}^{-1}$)			Cell based assays		
	NQO1	Complex I	Complex II	% ATP rescue HepG2*	% Cytotoxicity HepG2**	% cytotoxicity SH-SY5Y**
DMSO	0.48	0.06	0.06	8.3	45.2	39.4
Idebenone	24.36	0.19	0.47	69.5	99.0	47.5
1	40.03			22.0	61.8	48.1
2	34.49			20.6		
3	30.55			32.0	31.4	39.0
4	31.27	0.10	0.16	44.6	77.8	103.4
5	33.84	0.07	0.07	40.3		
6	21.30	0.21	0.21	11.9	95.5	77.5
7	22.75	0.19	0.19	47.6	70.0	40.2
8	37.30	0.05	0.05	26.9	75.7	100.0
9	5.06	0.06	0.06	10.0	85.3	84.0
10	27.41	0.07	0.07	40.6	89.7	96.0
11	7.56			8.9	82.1	
12	3.70	0.05	0.05	5.9	88.0	89.3
13	0.88	0.06	0.06	6.4	88.5	81.3
14	30.15	0.07	0.08	41.9		74.3
15	9.65			20.6		
16	20.18			13.8		
17	31.99			6.8		
18	31.43			20.6	86.0	
19	25.40	0.08	0.07	51.6	94.5	105.5
20	27.97	0.05	0.05	20.4	86.0	72.5
21	20.58			12.8		

Table 4 Summarize of naphthoquinones bioactivity. *Efficacy of ATP rescue in the presence of rotenone by quinones at 5 μ M. the ATP level expressed as percentage of ATP in DMSO treated cells in the absence of rotenone (untreated). ** Cytotoxicity of compounds at 25 μ M the cell viability expressed as a percentage of untreated cells

In particular, the naphthoquinone **19** was a promising compound to study structure-activity relationships, in order to identify compounds with complex I bypass factors and ATP rescue activity, avoiding the idebenone side-effects due to the interaction of quinone compounds with the mitochondria complex I. This compound showed comparable rescue of ATP production to idebenone, in complex I impairment conditions, but despite a significant turnover by NQO1, it did not have any interaction with complex I and complex II, unlike compounds **4** and **7**. It is hypothesised that this pharmacological activity is due to direct interaction with complex III of the electron transport chain and increased mitochondrial respiration. Encouragingly, compound **19** showed no cytotoxic in the SH-SY5Y cell line, where lower levels of NQO1 protein were found, in contrast to idebenone (cell viability reduced by ~40%). Overall, for these reasons, **19** was selected as hit compound for further optimisation.

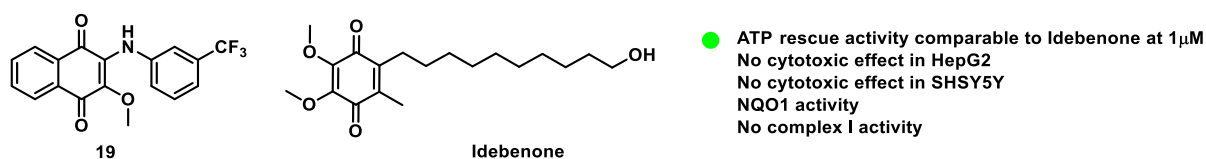


Figure 62 Summarize of naphthoquinones bioactivity. The figure shows the structures of naphthoquinones selected by virtual screening and highlighted their biological activity

CHAPTER 5

**SYNTHESIS OF NOVEL 1,4-
NAPHTHOQUINONES**

5.1 Design of novel naphthoquinones

In order to design novel analogs able to improve the efficacy of compound **19**, changes on the original structure were considered on the basis of the molecular modelling studies performed and the results obtained in the biological evaluation (Chapter 4). In particular, given the importance of the quinone core for the activity, this functional group was retained, and the hit optimisation of **19** was performed by modifying the substituents on the quinone core using the general diversification strategy depicted in Figure 63. Firstly, starting from the 2-amino-1,4-naphthoquinone scaffold of **19**, a series of 22 analogs were synthesised modifying the length of the linker between the benzoquinone core and phenyl ring in order to determine the minimum structural requirement. Next, substituent variation at different positions of the ring was investigated with the aim to increase the activity, improving the penetration and affinity of the molecule to enzyme pockets. In particular, strong EWG groups such as F, CF₃ and SF₅ were added to the aniline ring to enhance π - π stacking interactions by reduction of electrostatic repulsion between π clouds of the aniline ring and Phe 274 in the complex III binding pocket (chapter 2.1.8). Furthermore, the effect of substituents in position 2 was investigated, to study the influence of EWG and EDG on the reduction potential of the analogs and, consequently the potential relation with the cytotoxicity profile of this family. Finally, the replacement of the aromatic ring fused to the quinone with different heterocycles was explored to study their effect on the π - π interactions with the NQO1 enzyme and/or improve the water solubility.

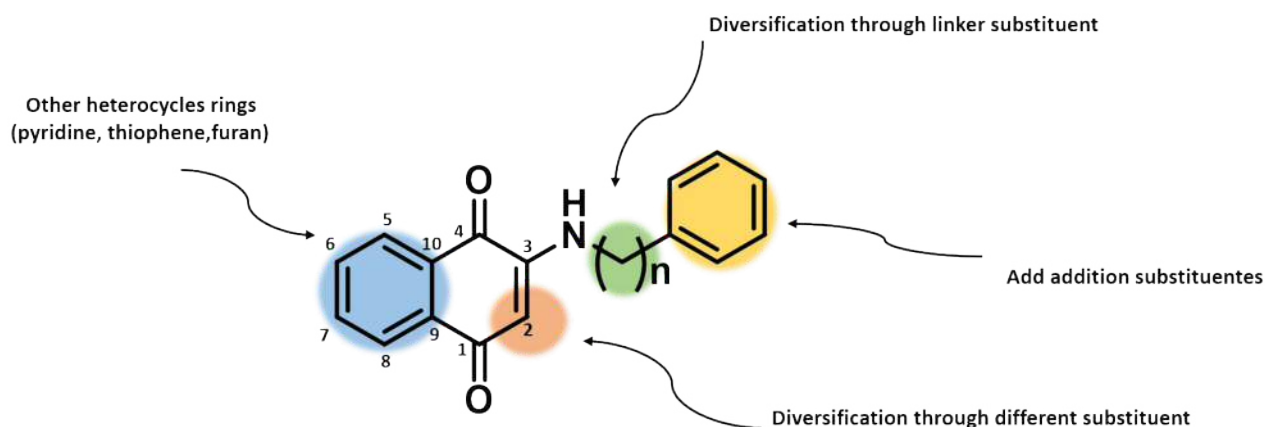
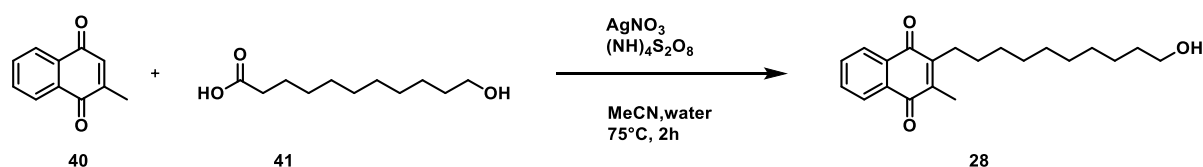


Figure 63 General strategy for identifying **19** analogs, showing 2-amino-1,4-naphthoquinone scaffold and four regions for diversification

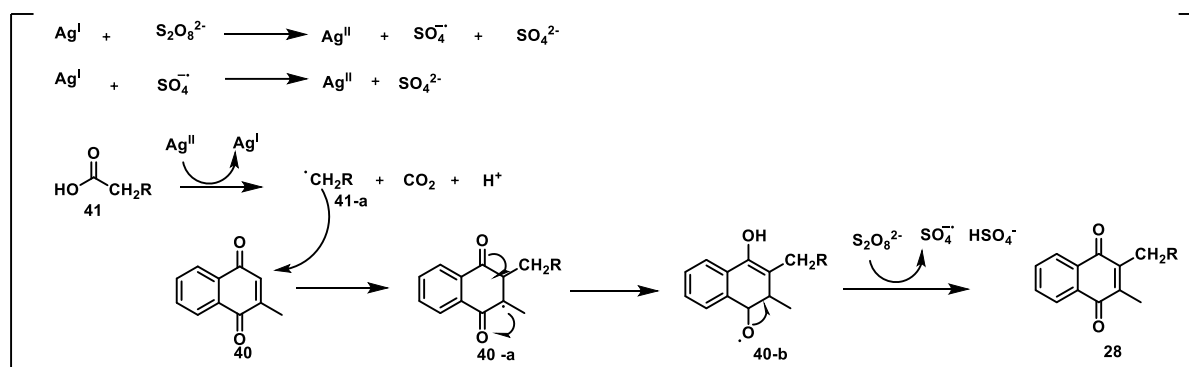
5.1.1 Design and synthesis of idebenone naphthoquinone analog (28)

Our initial strategy was based upon that of Vos *et al*¹⁴⁹ who reported that vitamin K₂ acts as an electron carrier in eukaryote cells, having made the observation that the addition of vitamin K₂ increased ATP levels in complex I-knockdown cells as well in cells affected by Rotenone-induced toxicity. The authors suggested that this activity was due to the interaction of vitamin K₂ with complex II and the consequent transfer of electrons to complex III. Based on these interesting findings, along with the results obtained from the computational studies (Chapter 2, a novel compound was designed (**28**), in which the vitamin K₂ core was combined with the side-chain of idebenone.



Scheme 3 Schematic reaction for idebenone analog **28**

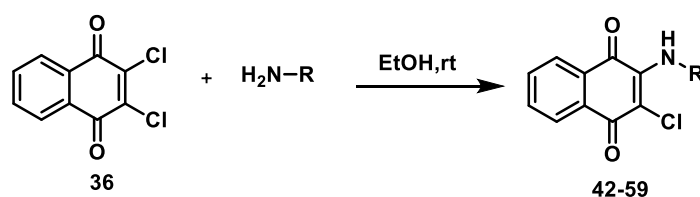
Compound **28** was synthesised according to a modified literature procedure.¹⁵⁰ This synthetic route lead to the final compound with a single-step reaction through the Minisci reaction¹⁵¹, a radical substitution on an aromatic compound (Scheme 3). The postulated mechanism of reaction involves the redox reaction between the Ag(I) cation, which is oxidised to an Ag(II) cation by peroxydisulfate. Next, the carboxylic acid group of **41** reacted with the Ag(II) cation to form an alkyl radical **41-a**, subsequently undergoing radical addition to naphthoquinone **40** forming a coupling intermediate **40-a**, which can transfer to the hydroquinol radical **40-b**. Finally, the hydroquinol radical is oxidised to **28** by peroxydisulfate (Scheme 4). This reaction is applicable to a wide range of alkyl carboxylic acids and represents a straightforward and inexpensive way to obtain numerous idebenone analogs.



Scheme 4 Mechanism of the Menisci reaction

5.1.2 Design and synthesis of 2-chloro-3-amino-1,4-naphthoquinones analogs

This series of naphthoquinone analogs was designed in order to investigate the necessary minimum structure requirement for their activity. The general scaffold of these derivatives is composed of a naphthoquinone core, crucial for the activity, linked with different aromatic amines. The 2,3 dichloro-1,4-naphthoquinone was selected as starting material because of its stability and versatility. The 2,3 dichloro-1,4-naphthoquinone has two carbon electrophilic centers which are highly activated by two carbonyl groups, and can easily undergo nucleophilic substitution, according to the addition-elimination mechanism¹⁵². All of these compounds were synthesised via a nucleophilic substitution reaction, treating 2,3-dichloro-1,4-naphthoquinone with an excess of the corresponding amine, in ethanol (Scheme 5). This synthetic route allowed the synthesis of numerous compounds quickly (~2h) and with a reasonable yield (Table 4).



Scheme 5 Schematic reaction for the synthesis of 2-chloro-3-amino-1,4-naphthoquinones

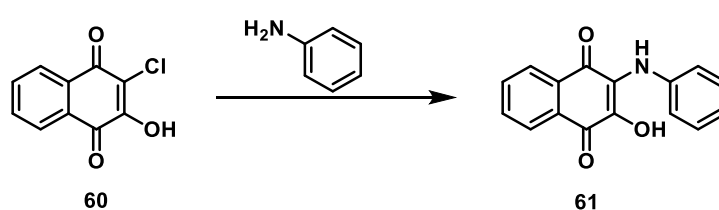
No.	42	43	44	45	46	47	48	49	50
structure									
yield	73%	90%	71%	44%	66%	38%	15%	36%	40%
No.	51	52	53	54	55	56	57	58	59
structure									
yield	34%	32%	38%	31%	35%	76%	78%	69%	94%

Table 5 Chemical structure details of synthesized compounds 42-59

5.1.3 Design and synthesis of 3-anilino-2-chloronaphthalene-1,4-dione analogs

After the first substitution and formation of the 2-amino-3-chloro-1,4-naphthoquinone derivative, the reactivity of naphthoquinone core was reduced, due to the increase of electronic density in the ring - the second substitution can occur only in the presence of strongly nucleophilic molecules, such as thiolate or if an EWG group effect is incorporated in the molecules substitution¹⁵². Therefore, another strategy for replacing the second chlorine atom was explored: a transition-palladium-catalysed amination of 2-chloro-naphthoquinone - a Buchwald–Hartwig amination¹⁵³.

Initially, the amination reaction was performed according to the procedure described by Lei Wang and collaborators using (PdCl₂ dppf)/dppf as catalyst and ligand, sodium tert-butoxide as base and toluene as solvent at 80°C for 12 h¹⁵⁴. However, under these conditions, only the starting material was recovered. However, using 3-chloro-2-hydroxynaphthalene-1,4-dione (**60**) as starting compound, different conditions were used to improve the Buchwald-Hartwig coupling, summarised in table 5

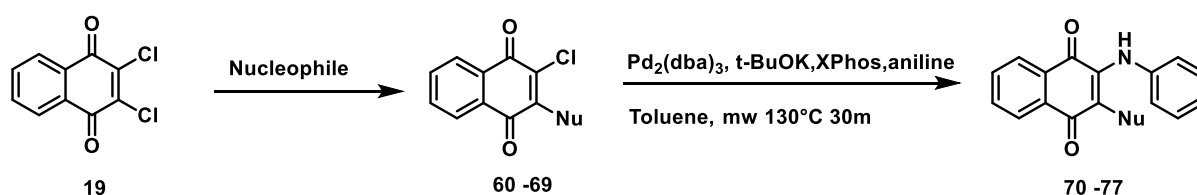


Scheme 6 Schematic synthesis of 2-hydroxy-3-(phenylamino) naphthalene-1,4-dione

Entry	Catalyst	Ligand	Solvent	Base	Yield
1	2% PdCl ₂ (dppf)	5% dppf	Toluene 80°C 12 h	t-BuONa	Starting material
2	2% Pd ₂ (dba) ₃	5% XPhos	Toluene 100°C 12 h	t-BuOK	Traces of product ^a
3	2% Pd ₂ (dba) ₃	5% XPhos	Toluene 130°C mw 30 m	t-BuOK	34%
4	2% Pd ₂ (dba) ₃	5% XPhos	Toluene 150°C mw 30 m	t-BuOK	Degradation ^b
5	2% Pd ₂ (dba) ₃	5% XPhos	NMP 150°C mw 30 m	t-BuOK	Degradation ^b
6	10% Pd ₂ (dba) ₃	10% XPhos	Toluene 130°C mw 30 m	t-BuOK	76%
7	10% Pd ₂ (dba) ₃	10%BrettPhos	Toluene 130°C mw 30 m	t-BuOK	68%

Table 6 Optimization Buchwald-Hartwig coupling. Conditions: 10% Pd₂(dba)₃, 10% BrettPhos, t-BuOK (1.5 eq) Naphthoquinone (1.0 eq), aniline (1 eq), toluene (1.0 mL), 130 °C, 30 minutes, 300 watts. ^a traces of product have been detected using the uplc-mass. ^b No presence of starting material and product, presence of undefined by-products

The microwave irradiation at 130°C, 300 Watt, successfully produced the desired product in good yield over a shorter period of time (30 minutes). Microwave-assisted reactions had several advantages: microwave heating is more reproducible compared to conventional heating because of uniformity of irradiation, it directly affects the kinetic energy of molecules and the shorter period of time compared to the conventional heat makes the microwave reaction cleaner due to the reduced presence of by-products formed for long-heat reaction. Therefore, the compounds were synthesised via the synthetic routes described in Scheme 7. Briefly, after the nucleophilic substitution with the appropriate nucleophile, the corresponding intermediate was treated with aniline as described above (Entry 6 Table 5). The results are summarised in Table 6

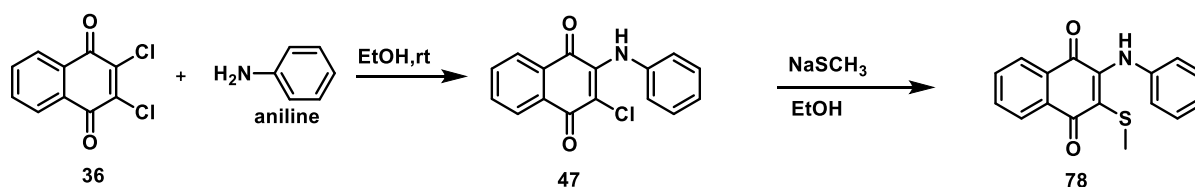


Scheme 7 Synthetic route for compounds 70-77

No. intermediate	Nucleophile	Reaction conditions ^a	Yield	No. final compound	Reaction conditions	Yield
60	KOH	H ₂ O	83%	61	Entry 6 table5	76%
62	MeOH	K ₂ CO ₃ , THF	73%	70	Entry 6 table5	80%
63	EtOH	K ₂ CO ₃ , THF	72%	71	Entry 6 table5	64%
64	n-PrOH	K ₂ CO ₃ , THF	75%	72	Entry 6 table5	67%
65	i-PrOH	K ₂ CO ₃ , THF	76%	73	Entry 6 table5	63%
66	PhOH	K ₂ CO ₃ , THF	63%	74	Entry 6 table5	59%
67	MeNH ₂	EtOH	93%	75	Entry 6 table5	45%
68	EtNH ₂	EtOH	95%	76	Entry 6 table5	35%
69	i-PrNH	EtOH	92%	77	Entry 6 table5	49%

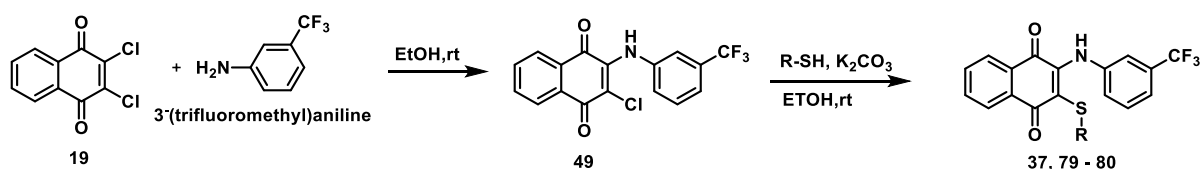
Table 7 Reagents and reagent condition synthesis compounds 61-77. Reaction condition: 2,3 dichloro-1,4 naphthoquinones (1 eq), nucleophile (1.5 eq), base (1.5 eq) solvent (0.3 M) Reaction conditions: 10% Pd₂(dba)₃, 10% BrettPhos, t-BuOK (1.5 eq) Naphthoquinone (1.0 eq), aniline (1 eq), toluene (1.0 mL), 130 °C, 30 minutes, 300 watts.

The analog **78**, which has a thiomethoxy in position **2**, was instead synthesised through two sequential nucleophilic substitutions due to the better nucleophilic reactivity of thiolate compared to alkoxide or amine scheme 8



Scheme 8 Synthesis of compound **78**

According to the positive results of compound **78** (Chapter 6), three analogs were synthesised using the same synthetic route, Scheme 9 table 7



Scheme 9 Synthesis of compound 37, 79-80

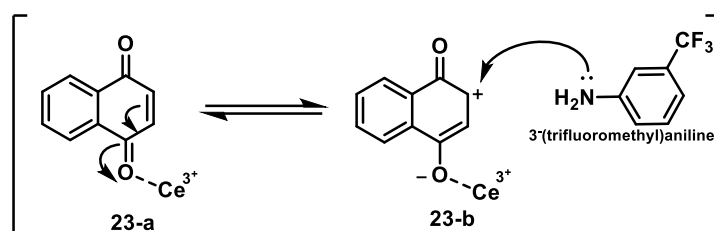
No.	37	79	80
structure	H_3C —	$\text{H}_3\text{CH}_2\text{C}$ —	$(\text{H}_3\text{C})_2\text{HC}$ —

Table 8 chemical structure details of synthesized compound 37, 79-80

5.1.4 Design and synthesis of 2-fluoro-3-((3(trifluoromethyl)phenyl) amino) naphthalene-1,4-dione (38)

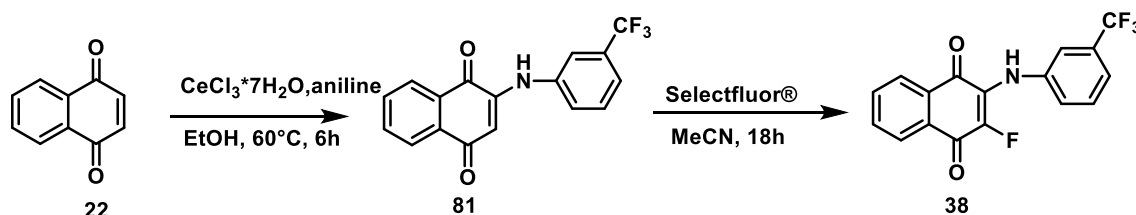
The redox property of quinones is crucial for their toxicity, and it can be determined by the stability of the anion free-radical generated after the electron transfer, as described in Chapter 2. The hydroquinone structures with a strong EWGs (**38** and **39**) have a HOMO/LUMO energy comparable to the idebenone so these molecules might be more stable in their reduced states than other naphthoquinones with reduction potentials above the range necessary for spontaneous generation of superoxide radical anion.

Compound **39** was synthesised starting with 1,4 naphthoquinones, using CeCl_3 as catalyst to facilitate the nucleophilic addition of the 3-(trifluoromethyl)aniline. In fact, the cerium salt is able to coordinate the carbonyl oxygen in the naphthoquinone core, removing electron density from the ring and increasing the electrophilicity of carbons, facilitating the nucleophile attack.



Scheme 10 Mechanism of nucleophilic attack using CeCl_3 as catalyst

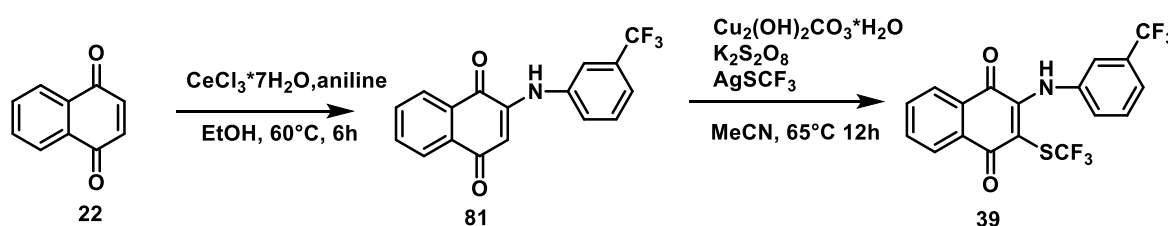
The installation of fluorine was conducted using Selectfluor® (Air Products and Chemicals) as electrophilic fluorinating agent¹⁵⁵. The Selectfluor® reagent has been intensely used in recent years, as N-F reagent (nitrogen-fluoro reagent) due to the safe and easy to handle and its strong nucleophilic reactivity. In fact, due to the low electrophilicity of C-2 in the quinone **81**, strong fluorinating reagents were necessary to achieve a successful fluorine installation in position 2 (Scheme 11).



Scheme 11 Synthesis of compound 38

5.1.5 Design and synthesis of 2-((3-(trifluoromethyl) phenyl) amino)-3-((trifluoromethyl)thio) naphthalene-1,4-dione (**39**)

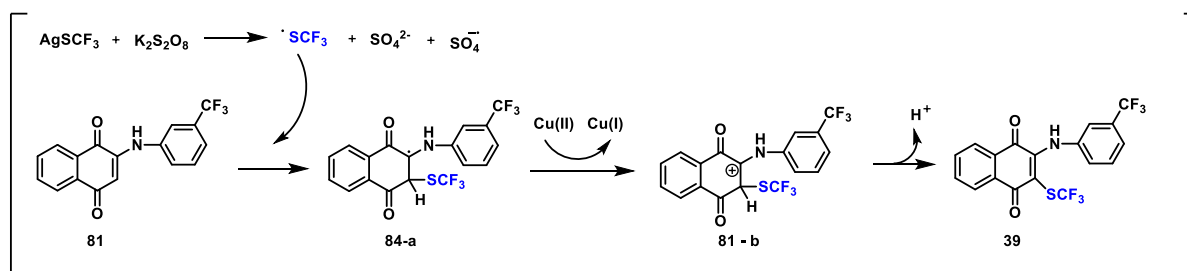
The trifluoromethylthiol group (SCF_3) is an increasingly important functionality in pharmaceutical due to its high lipophilicity and strong electronegativity. The presence of SCF_3 group in position 2 of the naphthoquinone core, has proven to be one of the most efficient EWGs able to increase the standard reduction potential of these family drastically. For that reason, the compound was designed and synthesised according to the Scheme 12



Scheme 12 Synthesis of compound 39

Briefly, the compound **39** was synthesised via a radical pathway starting by the intermediate **81**, and AgSCF_3 .¹⁵⁶ The postulated reaction mechanism involves the SCF_3 radical, formed in situ through the oxidation of AgSCF_3 by $\text{K}_2\text{S}_2\text{O}_8$. Once the SCF_3 radical is formed and released it undergoes addition to quinone **81** for the generation of intermediate **81-a**, which is further

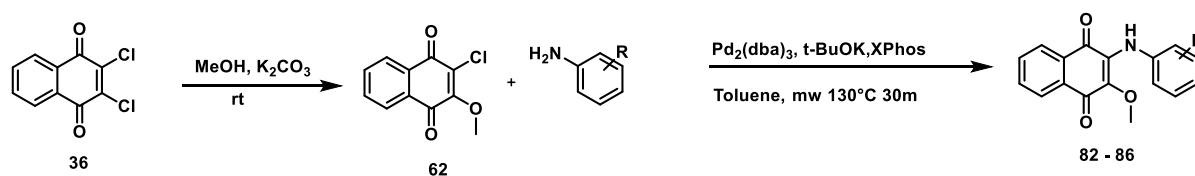
oxidised by copper salt to form SCF₃ intermediate **81-b**. Finally, deprotonation of intermediate **81-b** afforded the desired product **39** (Scheme 13).



Scheme 13 Mechanism of trifluoromethylthiolation of quinone **39**

5.1.6 Design and synthesis of 3-anilino-2-methoxynaphthalene-1,4-dione analog (**82-85**)

The analogs of 3-anilino-2-methoxynaphthalene-1,4-dione were synthesised according to the procedure described in Chapter 5.4. After the nucleophilic substitution of 2,4 dichloro naphthoquinone, the Buchwald-Hartwig reaction worked well, and the desired products were obtained in good yields.



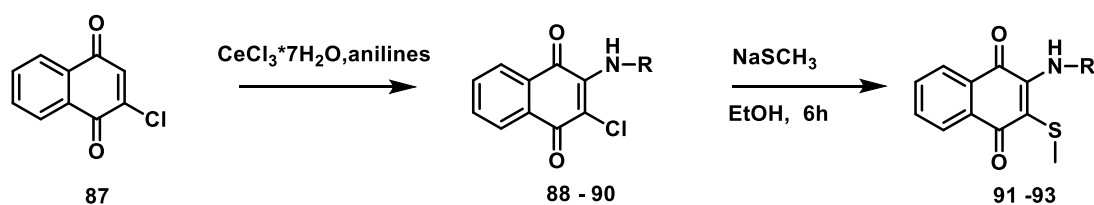
Scheme 14 Synthesis of compound **82-86**

No.	82	83	84	85	86
structure					

Table 9 Chemical structure details of synthesized compound **82-86**

5.1.8 Design and synthesis of 3-anilino-2-thionaphthalene-1,4-dione (37) analogs

The synthetic route for the synthesis of 3-anilino-2-thionaphthalene-1,4-dione (37) analogs involved a slightly different strategy to that shown in scheme 14. In fact, the compounds **91-93** could not be synthesised through nucleophilic substitution due to the poor nucleophilic reactivity of fluoro-3-trifluoromethylanilines, as the presence of an additional EWG in the aniline ring drastically reduce the π -electron density on the nitrogen. The nucleophilic substitution of 2,3-dichloro-naphthoquinones lead to only a ~25% of conversion. Therefore, compounds were obtained by nucleophile addition of the corresponding chloro-naphthoquinone in the presence of CeCl_3 , followed by nucleophilic substitution of chlorine with NaSCH_3 . Although all the desired products were obtained, the yields were limited in part by the nucleophilic substitution of chlorine in the first steps.

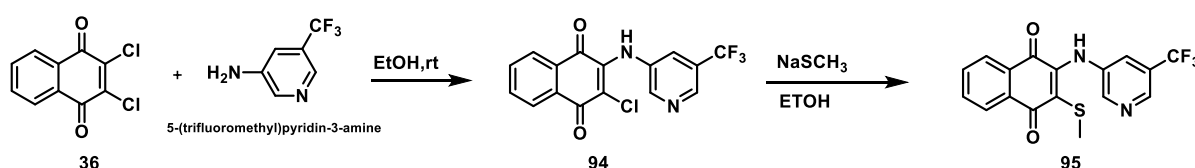


Scheme 15 Synthesis of compounds 91-93

No. intermediate	88	89	90
No. final	91	92	93
structure			

Table 10 Chemical structure details of synthesized compound 88-93

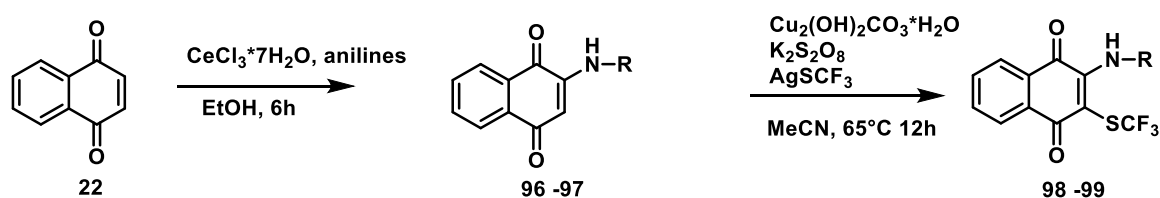
Compound **95** was synthesised using the procedure described 3.3, through two sequential nucleophilic substitutions.



Scheme 16 Synthesis of compound 95

5.1.9 Design and synthesis of analogs of 32-((3-(trifluoromethyl) phenyl) amino)-3-((trifluoromethyl)thio) naphthalene-1,4-dione (39)

Two analogs of compound **39** were prepared by reaction of 1,4 naphthoquinones with the 4-fluoro-3-(trifluoromethyl) aniline or 2-(trifluoromethyl)-pyridin-4-amine in the presence of CeCl_3 as catalyst, as reported in Scheme 17. After purification of the intermediate, the final product was obtained via SCF_3 radical addition, as described in Chapter 3.1.5.



Scheme 17 Synthesis of compounds 98-99

No. intermediate	96	97
No. final	98	99
structure		

Table 11 Chemical structure details of synthesised compounds 96-99

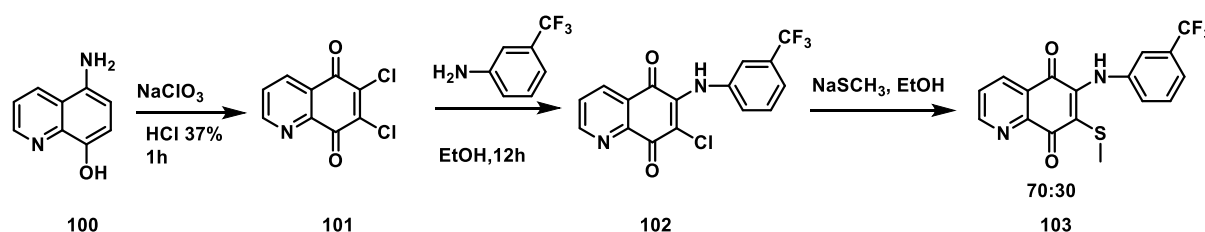
5.1.10 Scaffold-hopping approach

In order to develop novel analogs able to improve the efficacy of **19**, a scaffold-hopping approach was considered on the basis the biological results obtained from the previously synthesised compounds (Chapter 6). The goal of this strategy was the discovery of structurally novel compounds, modifying the central core structure of the known active molecules¹⁵⁷. Since the modifications made on the side chains did not show a significant increase of activity associated with the hit compound **19**, (Chapter 6), the core structure was modified to improve

the binding affinity with the enzyme. The central scaffold is directly involved in interactions with the target protein, a change in the scaffold might lead to an improved binding affinity. Two scaffold-hopping strategies were used: heteroatom replacement, replacing a carbon with a nitrogen, compound **103**, **104**, **105** and heterocyclic rings replacement, modifying the ring size, compound **109**, **113**. This series of analogs are part of families (quinoline-5,8-dione and benzothiophene-4,7-dione), that were recently identified as excellent substrates for the quinone reductase (NQO1) enzyme and they have been investigated for their antitumor, antiviral and broad-spectrum antimicrobial properties^{158,159,160,161}.

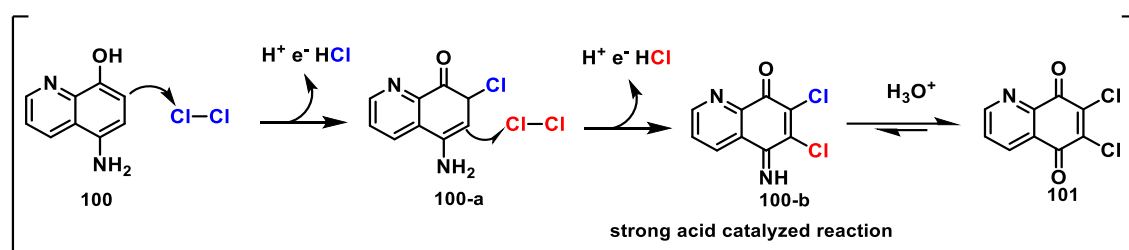
5.1.10.1 Synthesis of 7-(methylation)-6-((3 (trifluoromethyl)phenyl) amino) quinoline-5,8-dione

The family of quinolinequinones were synthesised using the synthetic route shown Scheme 18



Scheme 18 Synthesis of compound 103

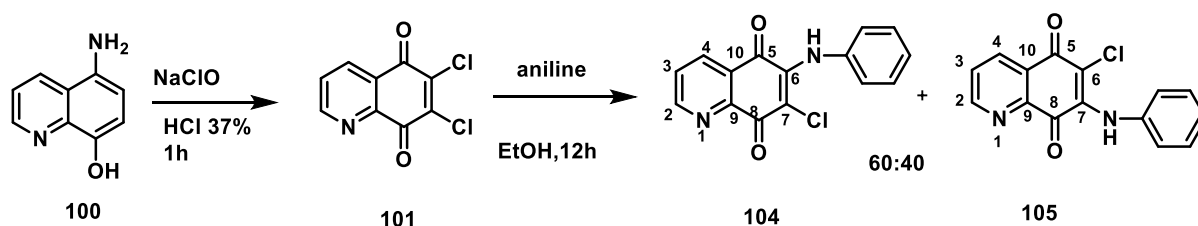
Briefly, 6,7-dichloroquinoline-5,8-dione was prepared by oxidative chlorination of the commercially available 5-aminoquinolin-8-ol with NaClO₃/ HCl (37%). Chlorine, generated *in situ* from sodium chlorate and hydrochloride via a redox reaction, reacted as a nucleophile with the aminoquinolinol, and sequentially the hydration of imine intermediate generated the dichloroquinoleidone as shown in the Scheme 19.



Scheme 19 Mechanism of oxidative chlorination of 5 aminoquinolin-8-ol

The dichloro-naphthoquinone was then treated with the aniline to give a mixture of the 6- and 7-substituted product with a ratio of 60:40 (A: B) scheme 19. Here, the nucleophilic substitution can occur on electrophilic carbon 6 or 7 generating two regioisomers. The different ratio and the preference for isomer 6 can in part be explained by the electron-withdrawing effect of the nitrogen atom and carbonyl in position 8, which increases the reactivity of the carbon in position 6. To confirm the regioselectivity of the two regioisomers, they were isolated by flash column chromatography and characterised by NMR proton, comparing that with previous studies mentioned in literature¹⁶².

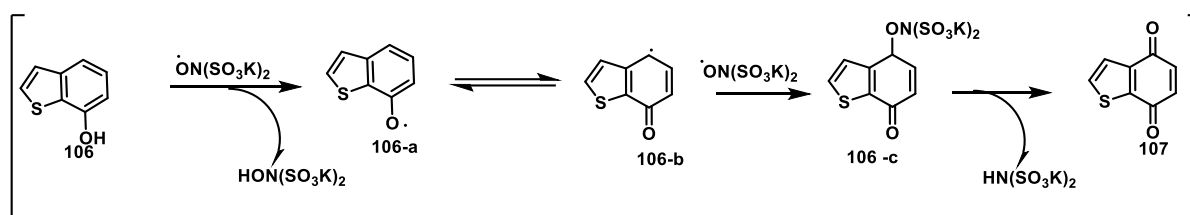
The treatment of dichloro naphthoquinone with 3-(trifluoromethyl) aniline, followed by sodium thiomethylate (NaSCH₃) gave the desired product **103** (Scheme 19). The compound was characterised and tested as a mixture of the two regioisomers



Scheme 20 Synthesis of compounds 104-105

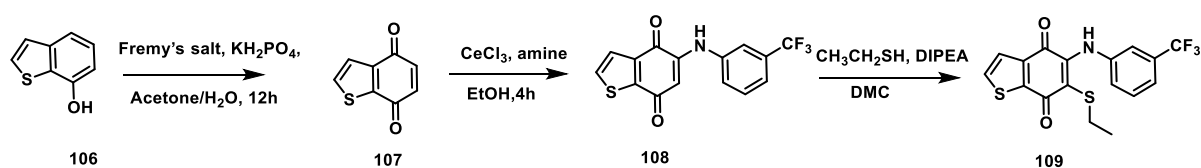
5.1.10.2 Synthesis of 6-(ethylthio)-5-((3-(trifluoromethyl) phenyl) amino) benzofuran-4,7-dione and 5-(ethylthio)-6-((3-(trifluoromethyl) phenyl) amino) benzo[b]thiophene-4,7-dione

Compound **109** was synthesised starting from benzofuran-7-ol (**106**). The first step of the reaction involved the oxidative conversion of the starting material into corresponding the quinones using Fremy's salt (potassium nitrosodisulfonate), which is a radical oxidising agent and extensively employed to oxidise phenols to quinones as in Scheme 21.



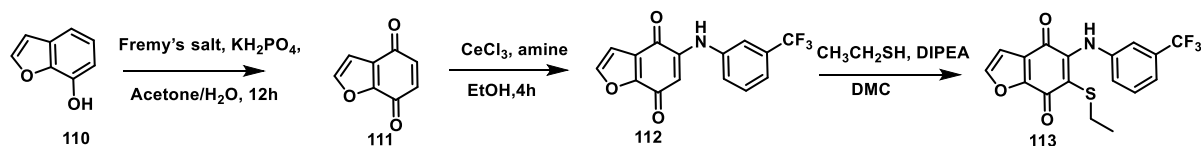
Scheme 21 Mechanism of oxidative conversion of 106 to 107

The second step was the nucleophilic addition of 3-(trifluoromethyl) aniline using CeCl_3 as catalyst to generate the intermediates **108**. The corresponding intermediates were initially treated with NaSCH_3 to obtain the corresponding thioderivate, but the reaction was unsuccessful. Hence, the nucleophilic addition was repeated using ethanethiol as nucleophile and DIPEA as base in ethanol at room temperature. Under these conditions, it was possible to isolate the product in good yield and short time. The failure in the addition of NaSCH_3 might be explained by the difference of nucleophilicity between ethanethiol and methanethiol and the volatility of the derivate methanethiol that limit the use of this reagent.



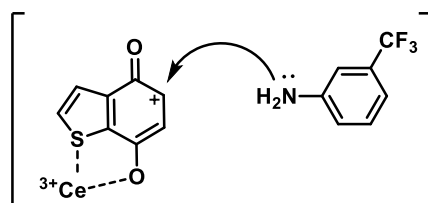
Scheme 22 Synthesis of compound 109

The bioisostere **113** was synthesized starting from benzofuran-7-ol **110**, following the same synthetic route, scheme 23.



Scheme 23 Synthesis of compound 113

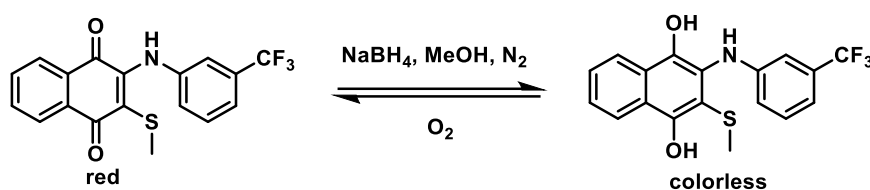
In both reactions, one-regioisomer was predominant. Here, the presence of a Lewis acid, such as CeCl_3 affected the regioselectivity of the reaction, favouring the nucleophilic attack in position 2. A possible explanation might be the chelation of the Lewis acid to oxygen or sulphur atom and carbonyl of the quinone core, thus increasing the electrophilicity of the carbonyl and the reactivity at the position 5.



Scheme 24 Mechanism of nucleophile addition

5.1.10.3 Attempt to isolate the 2-(methylthio)-3-((3-(trifluoromethyl) phenyl) amino) naphthalene-1,4-diol

In this project, the quinone compounds might be considered as prodrug compounds that require NQO1 to be activated into hydroquinone, the active form. In fact, the hydroquinones work as electron carrier transferring electrons to complex III, re-establishing the electron flow in the ETC and consequentially the ATP production. In order to investigate the mechanism of action of the studied naphthoquinones, several attempts were made to isolate the derivate hydroquinones, using NaBH₄ or Na₂S₂O₄ as reducing agent, but unfortunately, the re-oxidation occur in less than 10 minutes at room temperature in the presence of oxygen. This conversion is visible as the solution changes from coloured to colourless due to the loss of conjugated double bonds, and consequently UV-vis absorption. The use of UPLC showed the reduction of quinone to hydroquinone occurred in few minutes without generating by-products, and the process is reversible unless the reaction is kept under nitrogen. The UV spectra of the oxidised and reduced forms were studied.



Scheme 25 Schematic representation of hydroquinone synthesis

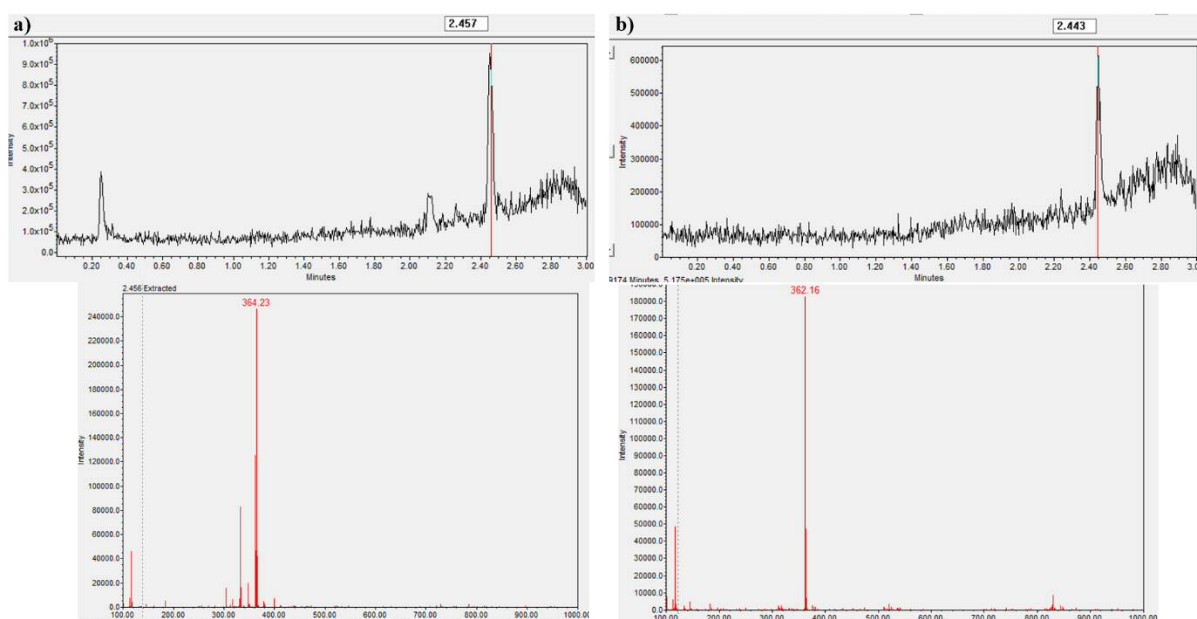
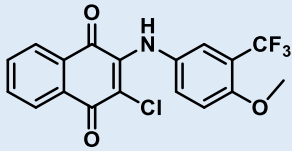
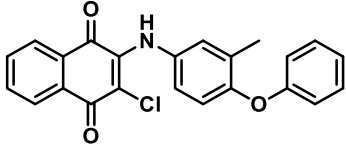
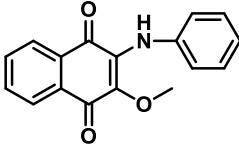
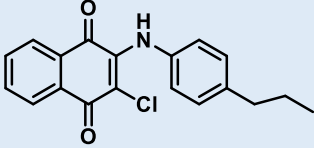
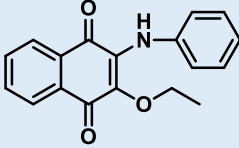
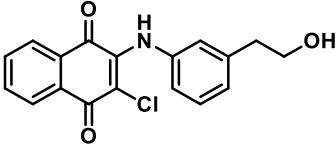
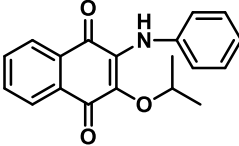
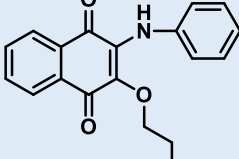
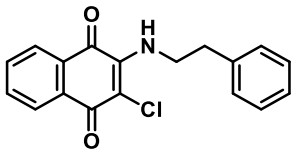
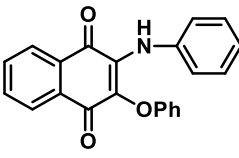
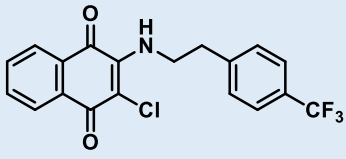
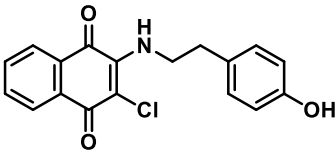
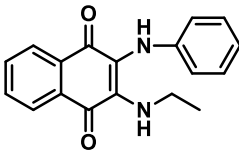
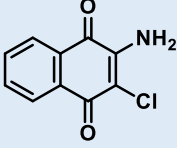
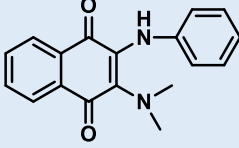


Figure 64 UPLC chromatograms of compound 37 in reduced and oxidized forms. The Figures a and b show the mass chromatogram of 37 in hydroquinone form (UPLC-MS Rt: 2.46 MS (ESI)-: 364[M-H]⁻) and in quinone form (UPLC-MS Rt: 2.44 MS (ESI)-: 362[M-H]⁻)

5.2 Conclusion

To summarise, 50 compounds were designed and successfully synthesised. Among them, 18 are NCEs (new chemical entities). This series of naphthoquinones compounds provide useful information on SAR of this family and their stability. Different synthetic strategies have been applied to obtain derivatives of **19** in few steps of reaction, with reasonable yield.

ID_Number	Structure	ID_Number	Structure
28		45	
37		46	
38		46	
39		48	
42		49	
43		50	

44		51	
52		70	
53		71	
54		72	
55		73	
56		74	
57		75	
58		76	
59		77	

61		78	
79		93	
80		95	
82		98	
83		99	
84		103	
85		104	
86		105	
91		109	

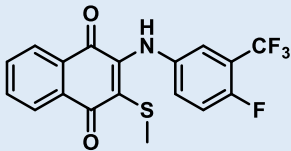
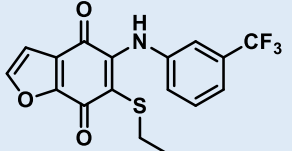
92		114	
----	---	-----	---

Table 12 Overview chemical structure synthesized compounds

CHAPTER 6

**BIOLOGICAL EVALUATION OF
DESIGNED AND
SYNTHESISED COMPOUNDS**

6.1 Hit-to-Lead workflow

The aim of this stage of the work was to rationally modify selected hit compound **19** in order to study the structure–activity relationships of this family and produce more potent and selective compounds which can be suitable candidates for further in *ex-vivo/in vivo* biological evaluation. According to the results from the virtual screening work, and the identified limitations of the enzymatic assays, a second bioassay workflow was used to screen the synthesised compounds. The synthesised compounds were tested in a series of cell-based assays aimed at investigating their biological activities in HepG2 and SH-SY5Y cell lines. ATP rescue and cytotoxicity were the two main assays used to explore the structure-activity relationships of synthesized naphthoquinones in order to identify the best derivatives of **19**. According to the modification made on the scaffold, the SAR study can be divided into 4 subgroups: SAR-1, SAR-2, SAR-3 and SAR-4. The combined results of these two assays were used to select the best candidates for further investigation *in vitro* assays as shown in Figure 65.

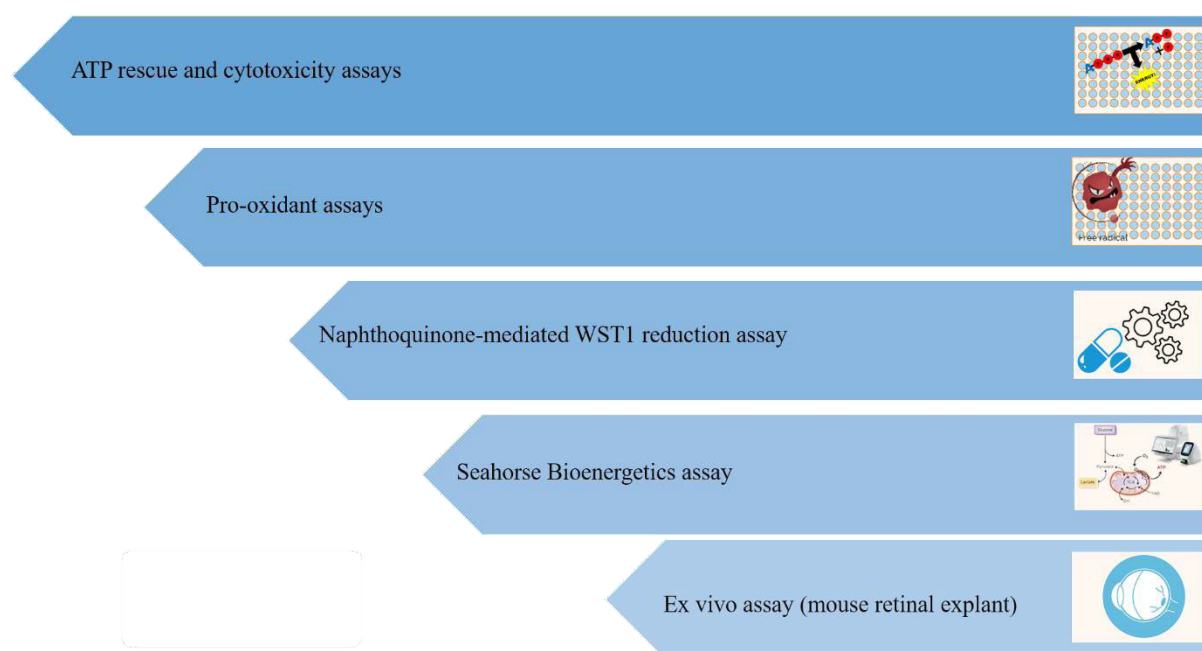


Figure 65 Experimental workflow used to screen the synthesized compounds

6.1.1 Results and discussion: ATP rescue and cytotoxicity SAR-1

The first attempt at optimising **19** was performed according to the Scheme 63. The biological data obtained from the commercially available compounds showed that naphthoquinones having a phenyl moiety in position 3, demonstrated significant ATP rescue in comparison with the control (**7,10,14,19**). Firstly, to determine the minimum structural requirement of the 2-amino-1,4-naphthoquinone scaffold, the phenyl ring was removed (**59**) and several analogs were synthesised modifying the length of the linker between the benzoquinone core and phenyl ring (**47,55,56**) (Figure 66).

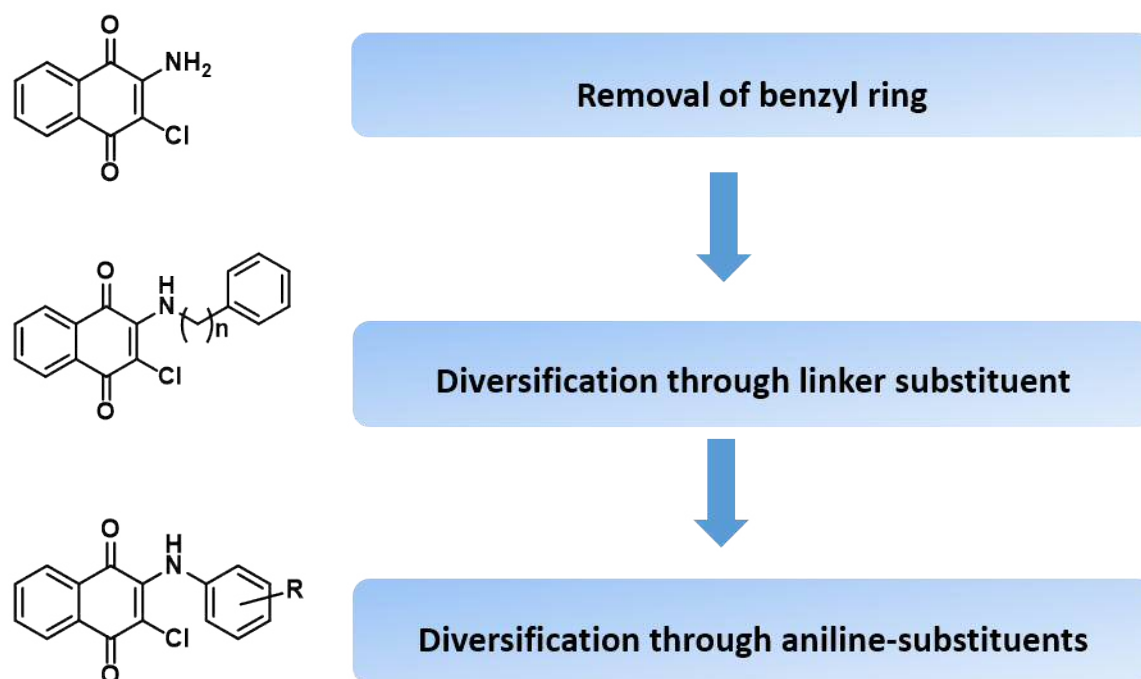


Figure 66 Schematic representation of SAR-1 scaffold modification strategy

The results obtained showed the importance of phenyl moiety (Figure 67). While the removal of benzyl ring completely suppressed the ATP rescue activity (**55**), removal or addition of a methyl group in the linker region did not alter the potency. Interestingly, the replacement of a hydrogen with a methyl in the linker slightly decreased the activity of **14**.

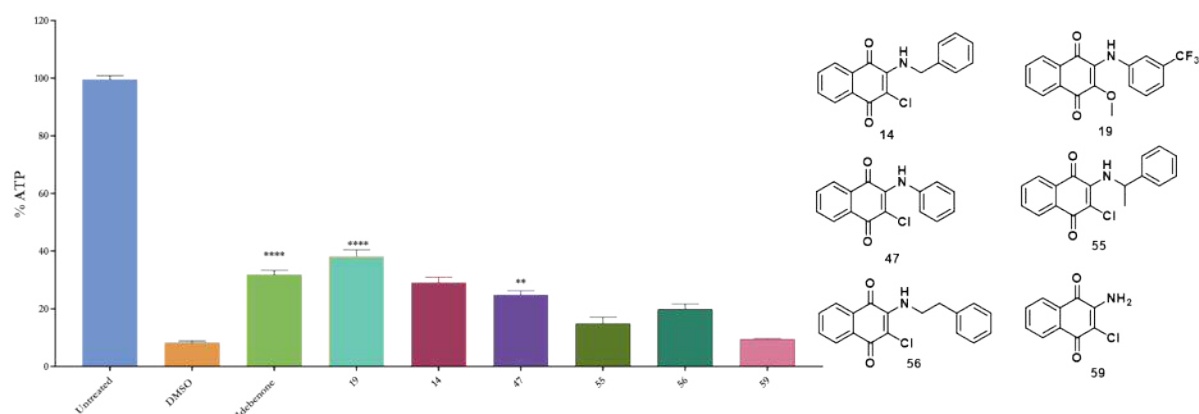


Figure 67 Efficacy of ATP rescue in presence of rotenone by naphthoquinones 14,47,55,56,39 ATP rescue activity of quinones was determined in rotenone-treated HepG2 cells. ATP levels expressed as percentage of ATP in DMSO-treated cells in absence of rotenone (untreated). Bars represent mean \pm SEM of at least three independent measurements. Data were analysed using one-way ANOVA test [F (20, 338) = 125.7, $p \leq 0.0001$], followed by Tukey's post hoc test for multiple comparisons, P values were calculated versus DMSO, * = $p \leq 0.05$, ** = $p \leq 0.01$, *** = $p \leq 0.001$, **** = $p \leq 0.0001$

The importance of the trifluoromethylene substituent on the phenyl ring was also investigated, and the corresponding analogs with and without the CF_3 on the phenyl ring were synthesised (46,49,57). Instead, compounds 50 and 57 were designed and synthesised to study the influence of trifluoromethylene position on benzyl ring. To have a wider overview on the effect of substituent on the phenyl ring, a series of derivatives 14, 47 and 56 were synthesised and tested (38-50).

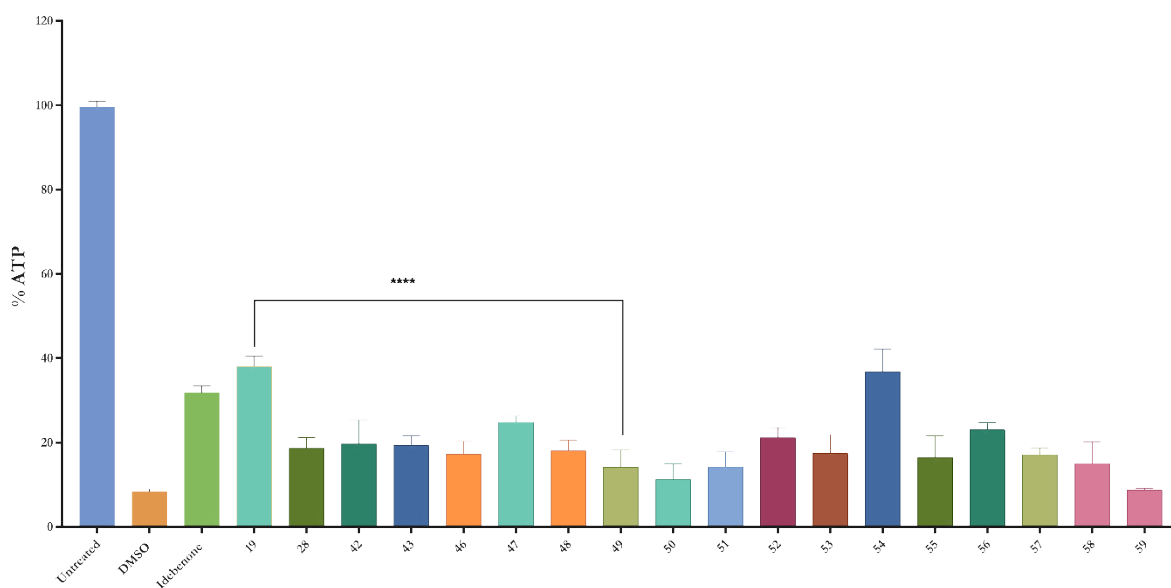


Figure 68 Efficacy of ATP rescue in presence of rotenone by naphthoquinones synthesized (SAR-1) ATP rescue activity of quinones was determined in rotenone-treated HepG2 cells. ATP levels expressed as percentage

of ATP in DMSO-treated cells in absence of rotenone (untreated). Bars represent mean \pm SEM of at least three independent measurements. Data were analysed using one-way ANOVA test [$F(20, 326) = 126.5, p \leq 0.0001$], followed by Tukey's post hoc test for multiple comparisons, P values were calculated versus 19, * = $p \leq 0.05$, ** = $p \leq 0.01$, *** = $p \leq 0.001$, **** = $p \leq 0.0001$

Unfortunately, none of the synthesised quinones manifested a better activity in ATP rescue than **19**. In particular, **49**, which differs by the presence of chlorine instead of OCH₃ at position 2, showed a significant decrease in activity, making the methoxy group a better substituent than chlorine. The **28** showed a lower ATP rescue than idebenone suggesting the replacement of the core from benzoquinone to naphthoquinone drastically changed the structure-activity relationship of this family.

Interestingly, compound **54** showed a comparable activity to idebenone and **19**. The compound was designed and synthesised as an analog of idebenone and **28**, to include an aniline moiety into the hydroxyl alkyl side chain in agreement with the computational study (Chapter 2.1.5).

This series of compounds showed higher cytotoxicity than **19**. In particular, **54** and **48** were cytotoxic in both cell line, with drastically reduced cell viability. Compounds **47** and **50** having an aniline substituent in position **3** showed lower toxicity than the corresponding phenylethylamine analogs (**56**, **58**) in SH-SY5Y cell line, while comparable toxicity with the benzylamine analogs (**14**, **49**).

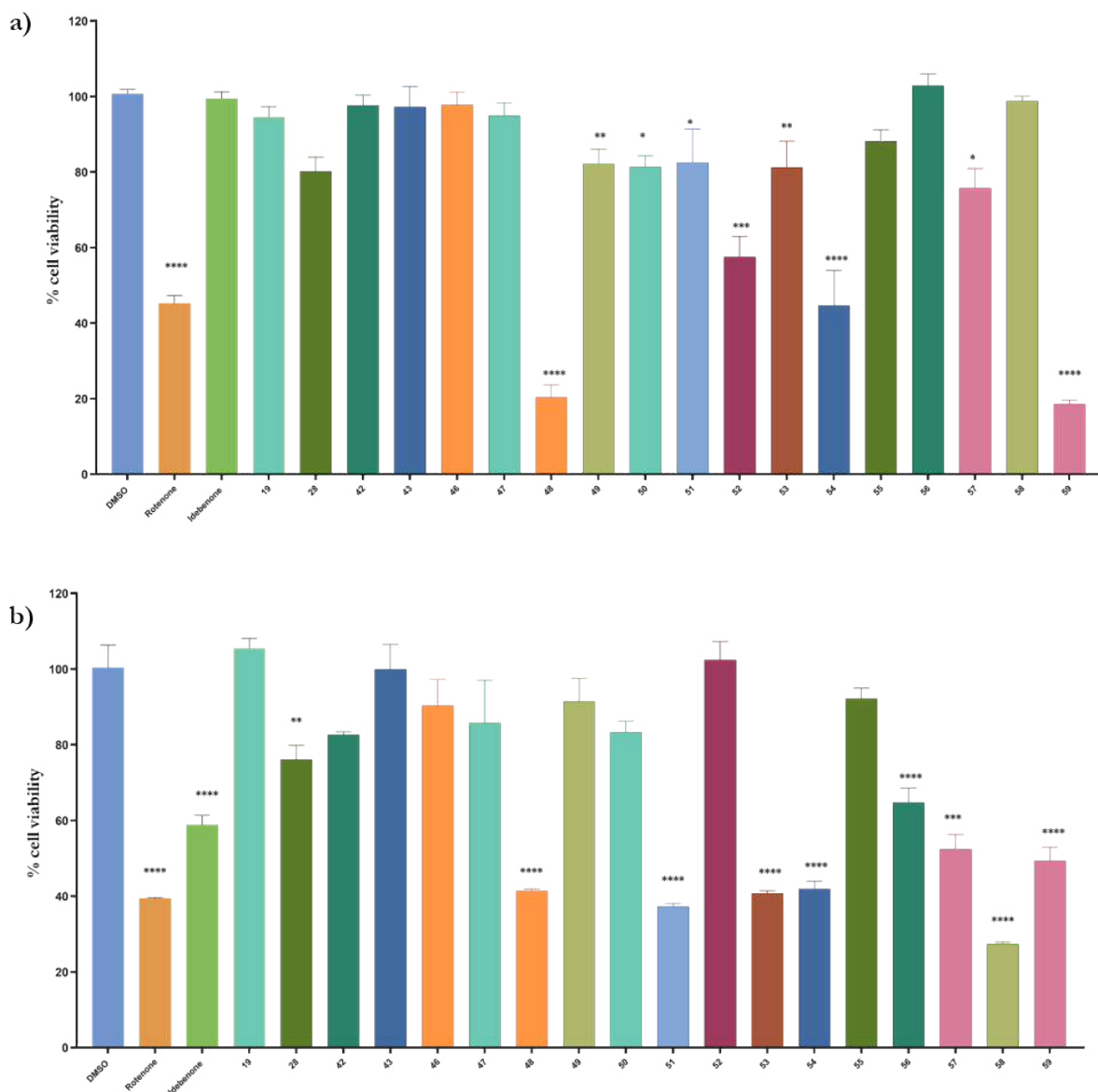


Figure 69 Cytotoxicity of naphthoquinones synthesized (SAR-1) on HepG2 and SH-5YSY. The graphs **a** and **b** show the quinone cytotoxicity in HepG2 and SH-SY5Y cell line respectively. Both cell lines were treated with 25 μ M of compounds and incubated for 24 hours at 37 $^{\circ}$ C. The cell viability was determined as percentage of untreated cells. Bars represent mean \pm SEM of at least three independent measurements. A one-way ANOVA was conducted to compare the idebenone reduction graph **a** [$F(20, 370) = 35.58, P < 0.0001$] graph **b** [$F(16, 37) = 69.56, P < 0.0001$] followed by Dunnett's post hoc test for multiple comparisons, P values were calculated versus untreated, * = $p \leq 0.05$, ** = $p \leq 0.01$, *** = $p \leq 0.001$, **** = $p \leq 0.0001$.

6.1.2 Results and discussion: ATP rescue and cytotoxicity SAR-2

According to the results of the previous study (SAR-1), it was evident that the chlorine group was not a good substituent; therefore, a second-stage SAR analysis was planned in order to investigate the effect of the substituent at position 2 (Figure 70). The aniline derivative of **19** without CF_3 on aniline ring (**47**) was used as starting point to study the effect of substituents.

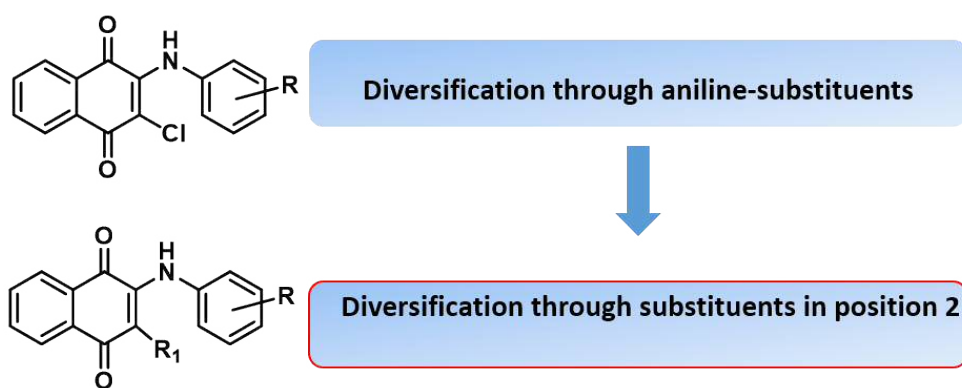


Figure 70 schematic representation of SAR-2 scaffold modifications made

Cleavage of the methyl ether drastically reduced the ATP rescue (**61**). The effect of bioisostere replacement of methoxy group with the methylamine and thiomethyl, **75** and **78** respectively, had different effects. Compound **75** decreased the potency; whereas **78** had comparable result to **70**.

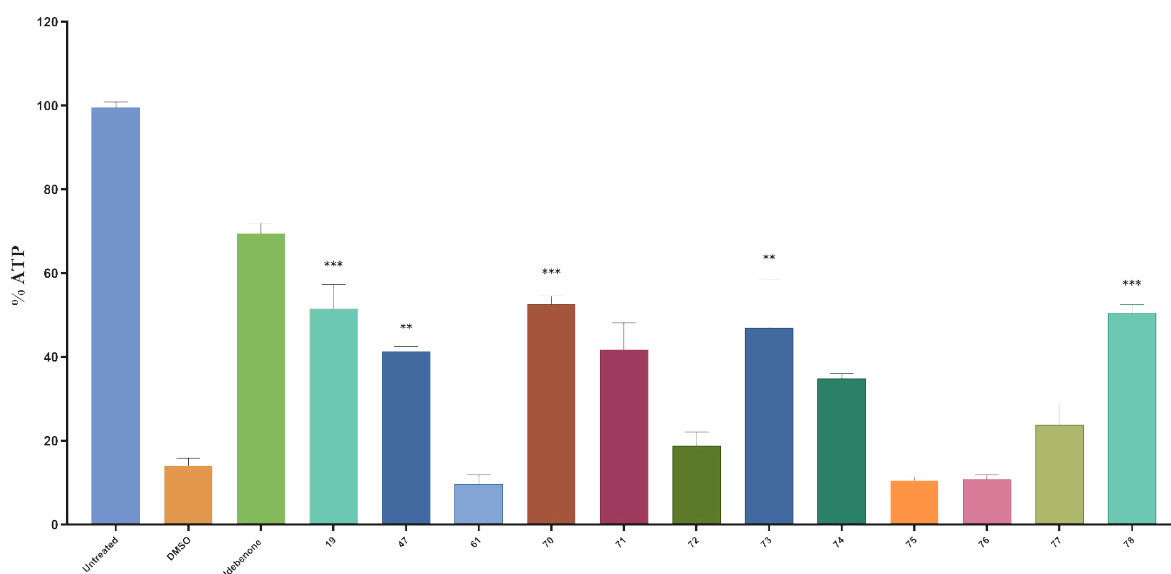


Figure 71 Efficacy of ATP rescue in presence of rotenone by synthesized naphthoquinones (SAR-2) at 5 μ M. ATP rescue activity of quinones was determined in rotenone-treated HepG2 cells. ATP levels expressed as percentage of ATP in DMSO-treated cells in absence of rotenone (untreated). Bars represent mean \pm SEM of at least three independent measurements. Data were analysed using one-way ANOVA test [$F(14, 18) = 31.90, p \leq 0.0001$], followed by Dunnet's post hoc test for multiple comparisons, P values were calculated versus DMSO, * = $p \leq 0.05$, ** = $p \leq 0.01$, *** = $p \leq 0.001$, **** = $p \leq 0.0001$

This trend was observed for the other analogs synthesised, where **76** and **77** showed lower ATP rescue than their ether and thio-derivates. The replacement of methyl ether with an ethyl ether

71, n-propyl ether **73** did not improve the activity, on the contrary, isopropyl ether **72** and phenyl ether **74** decreased the activity showing that sterically hindering groups are not beneficial.

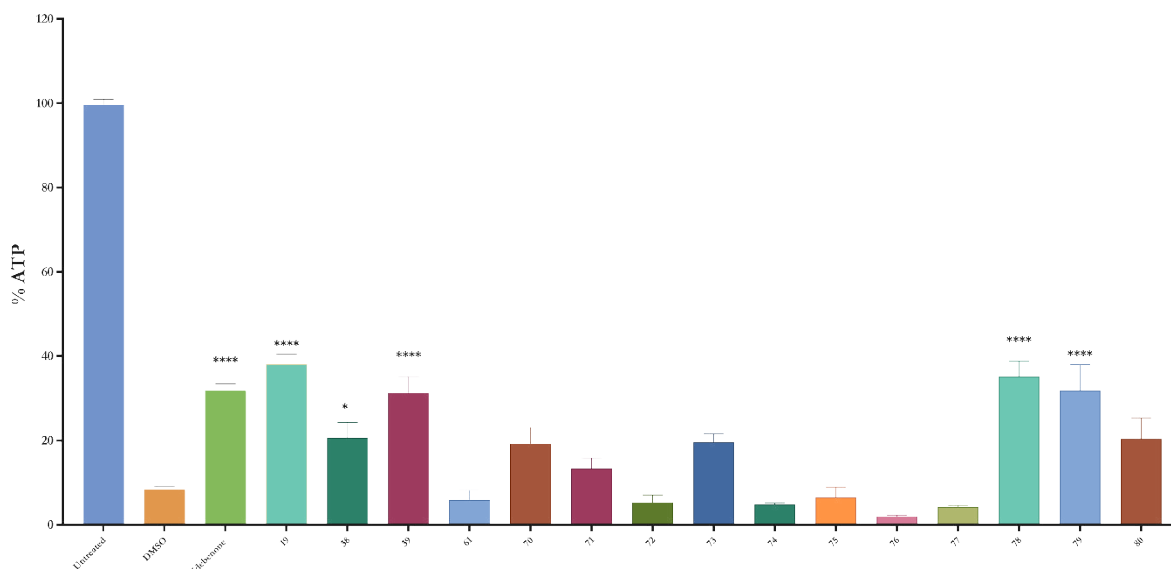


Figure 72 Efficacy of ATP rescue in presence of rotenone by synthesized naphthoquinones (SAR-2) at 1 μM ATP rescue activity of quinones was determined in rotenone-treated HepG2 cells. ATP levels expressed as percentage of ATP in DMSO-treated cells in absence of rotenone (untreated). Bars represent mean \pm SEM of at least three independent measurements. Data were analysed using one-way ANOVA test [F (18, 322) = 123.4, $P < 0.0001$], followed by Dunnet's post hoc test for multiple comparisons, P values were calculated versus DMSO, * = $p \leq 0.05$, ** = $p \leq 0.01$, *** = $p \leq 0.001$, **** = $p \leq 0.0001$

In order to clarify the drastically reduced activity of amino derivate, naphthoquinone **75** and **76** were tested to determine whether they can be substrates of the NQO1 enzyme. The enzymatic results showed no oxidation of NADH over 10 minutes, making of **75** and **76** poor substrates of NQO1. A difference in the binding modes cannot justify the significant difference in the NQO1 activity between **75** and the corresponding analogs **70** and **78**, the NQO1 possesses a highly plastic active site, which can accommodate quinone compounds of different sizes (Chapter 2). A possible explanation might be found again in the different reduction potential of these compounds. In fact, although the replacement of methoxy or thiomethyl group to methylamine causes minimal steric perturbations, the effect in the electron density distribution is significant. The addition of another EDG group in the quinone core might drastically reduce the ability to accept electrons, and therefore they could not be metabolised into hydroquinones by NQO1.

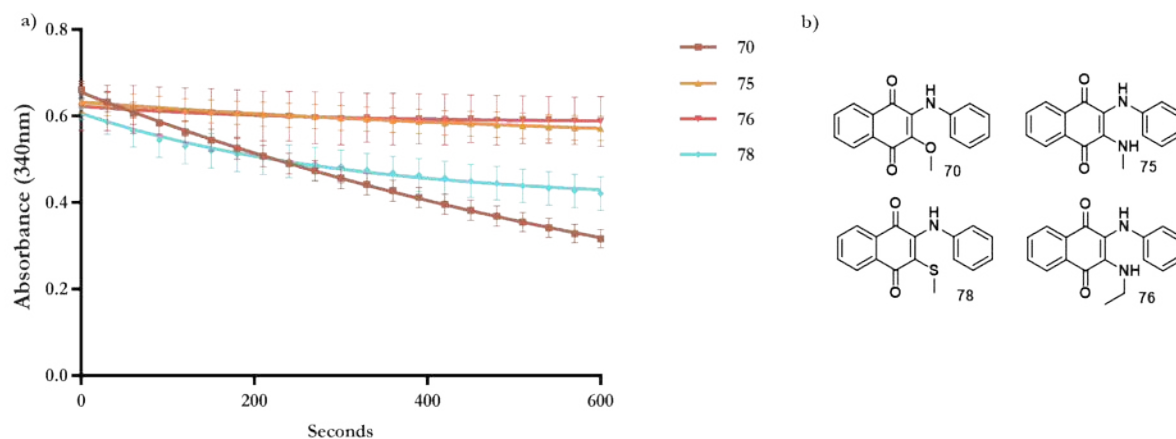


Figure 73 NQO1 activity of compounds 70,75,76,78. The graphs show the decrease of absorbance at 340nm due to consumption of NADH and the structure of compound 70, 75,76 and 78. The assay was carried out in in 1 ml cuvette containing: 25 mM Tris-HCl pH 7.4, 0.7 mg/ml BSA, 50 μ M quinone, 1 μ g/ml NQO1, 100 μ M NADH. Each data point represents as means \pm SEM of two independent measurements.

Due to the interesting profile of **78**, the compound **39** was synthesised and tested. The compounds **39** have a SCF_3 group in position 2, this group was extensively used in medicinal chemistry in the recent years for its unique quality: the fluorinated carbon adjacent to a sulphur atom increases lipophilicity, bioavailability and reduces the rate of oxidative metabolism. The introduction of a more electronegative group was further investigated with compounds **38** in order to clarify the EWG effect in the naphthoquinone ring. However, despite the hypothesised improved stability of the reduced form (Chapter 2), this family of analogs that possesses strong EWG group did not show the anticipated increase of activity; on the contrary, they showed a significant increase of cytotoxicity.

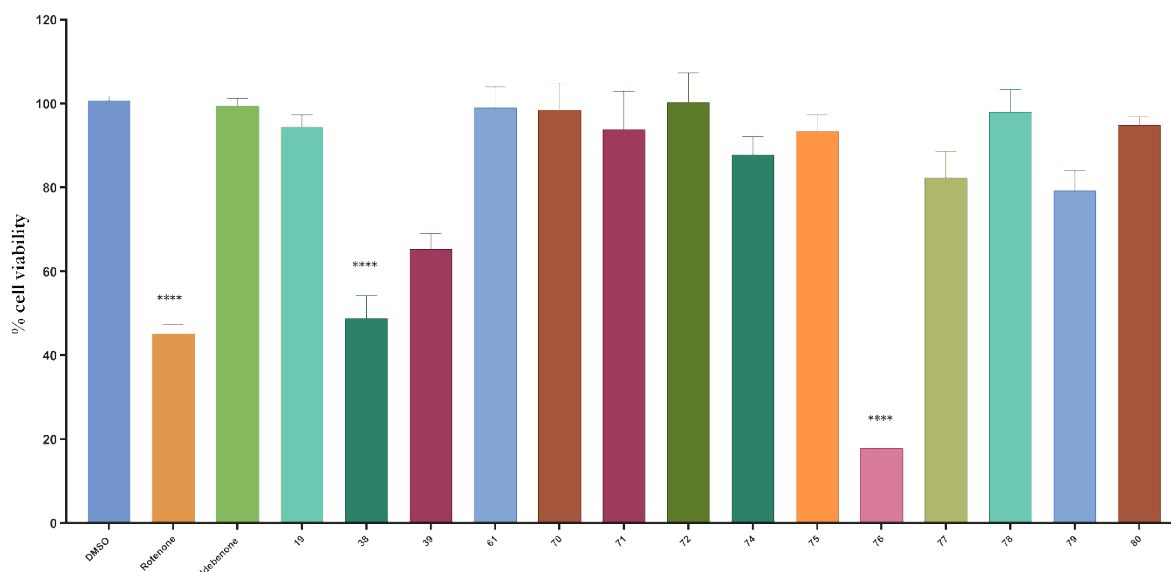


Figure 74 Cytotoxicity of naphthoquinones synthesized (SAR-2) on HepG2. The graph shows the quinone cytotoxicity in HepG2. Cells were treated with 25 μ M of compounds and incubated for 24 hours at 37 °C. The cell viability was determined as percentage of untreated cells. Bars represent mean \pm SEM of at least three independent measurements. Data were analysed using one-way ANOVA test [F (17, 371) = 40.56, $P < 0.0001$], followed by Dunnett's post hoc test for multiple comparisons, P values were calculated versus DMSO, * = $p \leq 0.05$, ** = $p \leq 0.01$, *** = $p \leq 0.001$, **** = $p \leq 0.0001$

This result is not in agreement with our hypothesis of quinol stability: the cytotoxic properties of quinones are related to the stabilisation energy after electron accepting. When an EWG is added to the molecule, the electrophilicity of reduced form (the ability to donate electrons) decreases, and consequently, the corresponding hydroquinone should be more stable and less toxic. Interestingly compound **38** and **39** showed cytotoxic effect also on SH-SY5Y cell line, suggesting a toxic effect in their oxidised/quinone form. The striking difference between a strong electron donor group (**75**) and a strong electron withdrawing group (**38**) in position 2 highlighted the importance of redox property of this family. A naphthoquinone with high standard electron potential as **38** might "steal" electrons from biological redox centers, such as cytochromes, iron-sulfur clusters, and cupredoxins, inhibiting metabolic output. However, **75**, which possesses a low standard electron potential, is not able to accept electrons, and therefore remains inactive. A mild redox naphthoquinone instead might be able to generate a useful cycle between oxidised and reduced forms using specific physiologic redox centers, showing a beneficial pharmacological effect.

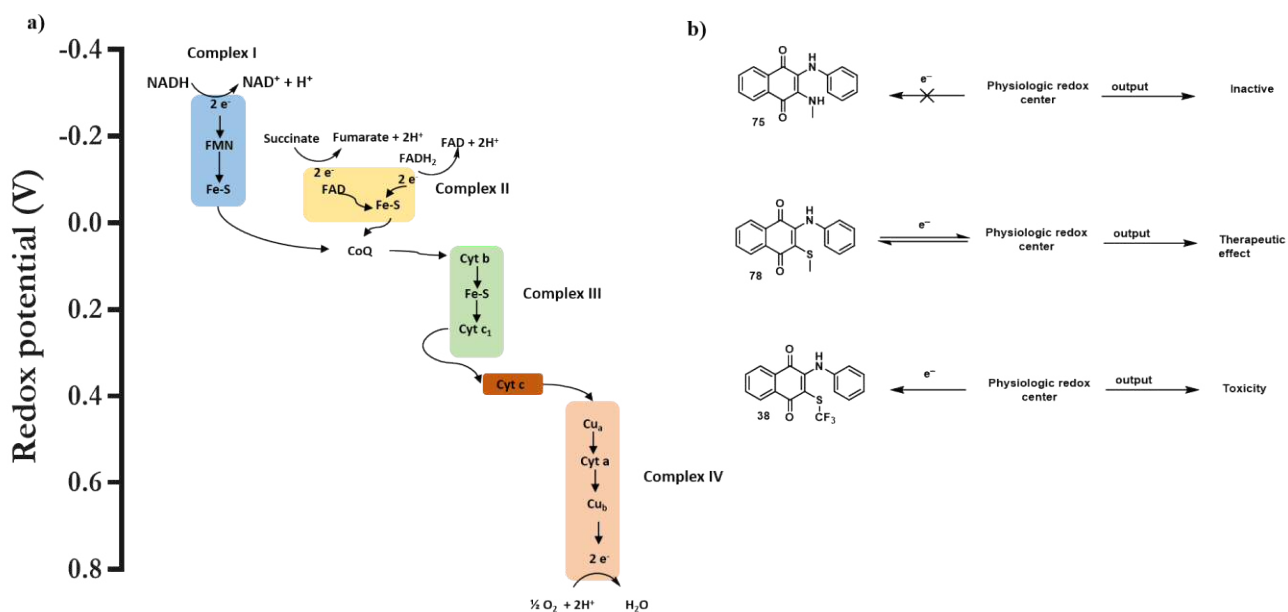


Figure 75 Schematic representation of redox potential changes in ETC and hypothesized redox effect of different naphthoquinones. The Figures show the possible outcome of studied naphthoquinones according their redox property and the redox potentials of the different components of the electron transport chain

6.1.3 Results and discussion ATP rescue and cytotoxicity SAR-3

In previous biological experiments, compounds **70**, **71** and **78** were identified as promising candidates to investigate as potential novel analogs. Hence, the introduction of different aniline derivatives in position **3** on the naphthoquinone core was further evaluated combining the positive results obtained from the previous SARs.

Compound **54** demonstrated a higher active profile compared to the other 2-chloro-naphthoquinones, but also exhibit an increase of cytotoxicity. Hence, compounds **84**, **85** were synthesised and tested in order to maintain the activity but limiting the toxicity, replacing the Chlorine in position 2 with the methoxy group. These compounds did not show a particular improvement in activity either in cytotoxicity as shown in Figure 76. The results suggested that the toxicity is due to the presence of hydroxyl group in the aniline ring. Therefore, other anilines derivates were explored.

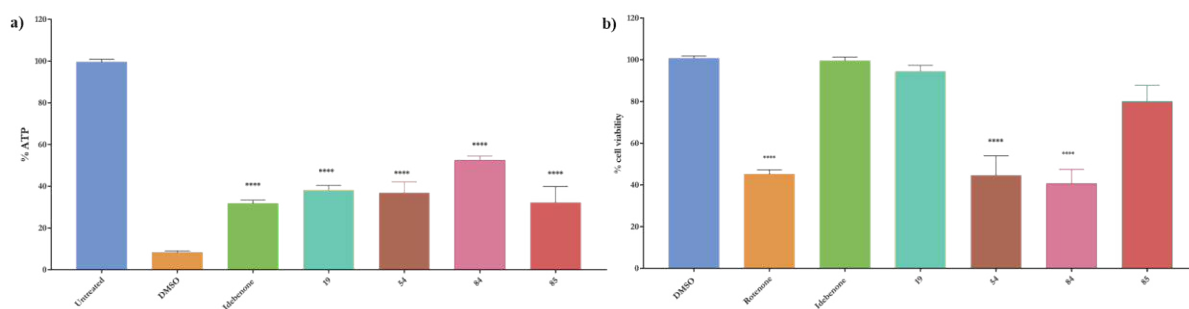


Figure 76 Efficacy of ATP rescue in presence of rotenone and cytotoxicity of naphthoquinones 54,84,85. The graph **a** shows. ATP rescue activity of quinones was determined in rotenone-treated HepG2 cells, treating the cells with 1 μM of quinones in presence of 25 μM of Rotenone. ATP levels expressed as percentage of ATP in DMSO-treated cells in absence of rotenone (untreated). The graph **b** shows the quinone cytotoxicity in HepG2. Cells were treated with 25 μM of compounds and incubated for 24 hours at 37 $^{\circ}\text{C}$. The cell viability was determined as percentage of untreated cells. Bars represent mean \pm SEM of at least three independent measurements. Data were analysed using one-way ANOVA test **a** [F (18, 381) = 93.09, $P < 0.0001$] graph **b** [F (18, 488) = 32.48] followed by Dunnet's post hoc test for multiple comparisons, P values were calculated versus DMSO, * = $p \leq 0.05$, ** = $p \leq 0.01$, *** = $p \leq 0.001$, **** = $p \leq 0.0001$

The simultaneous insertion of 2 SCH_3 and 3 CF_3 -aniline groups in naphthoquinones core was investigated to address if there is a synergistic effect of the two substitutions and thus an improvement in activity. These insertions resulted in comparable profile activity to **19** and **78** but overall not significant.

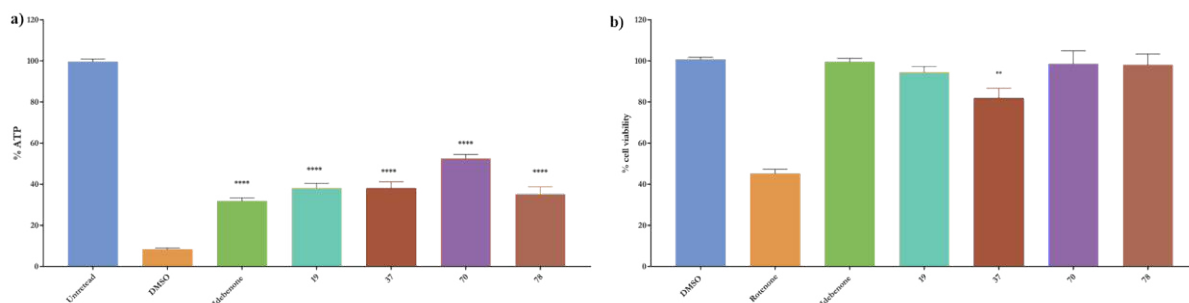


Figure 77 Efficacy of ATP rescue in presence of rotenone and cytotoxicity of naphthoquinones 37,70,76 The graph **a** shows. ATP rescue activity of quinones was determined in rotenone-treated HepG2 cells, treating the cells with 1 μM of quinones in presence of 25 μM of Rotenone. ATP levels expressed as percentage of ATP in DMSO-treated cells in absence of rotenone (untreated). The graph **b** shows the quinone cytotoxicity in HepG2. Cells were treated with 25 μM of compounds and incubated for 24 hours at 37 $^{\circ}\text{C}$. The cell viability was determined as percentage of untreated cells. Bars represent mean \pm SEM of at least three independent measurements. Data were analysed using one-way ANOVA test **a** [F (14, 318) = 131.6, $P < 0.0001$] graph **b** [F (18, 488) = 32.48, $P < 0.0001$] followed by Dunnet's post hoc test for multiple comparisons, P values were calculated versus dms, * = $p \leq 0.05$, ** = $p \leq 0.01$, *** = $p \leq 0.001$, **** = $p \leq 0.0001$

The further step was the introduction of fluorine atom in *ortho*, *para* and *meta* positions of the aniline ring **86**, **91**, **92**, **93**, **98**. The introduction of a fluorine atom significantly alters the

physicochemical properties of the compound due to its high electronegativity and lipophilicity. Hence, we studied the influence of the additional of further EWG than CF₃ in the aniline ring and if the increase of lipophilicity may increase the membrane permeability, and consequently the activity.

As shown in Figure 78, the introduction of fluorine was generally unsuccessful, as the compounds showed no improvement in ATP rescue activity compared to the **19**. Recently, the SF₅ has been used as a replacement for trifluoromethyl due to its better chemical and thermal stability¹⁶³. Consequently, in order to evaluate whether the introduction of a different EWG may affect the activity of compound, CF₃ was replaced with the SF₅ group, compound **83**, but this modification did not show a significant increase of ATP rescue activity.

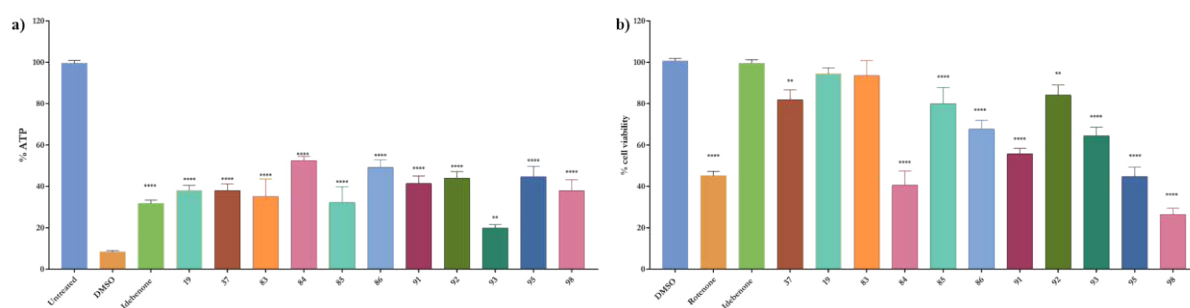


Figure 78 Efficacy of ATP rescue in presence of rotenone and cytotoxicity of synthesized naphthoquinones (SAR-3) The graph **a** shows. ATP rescue activity of quinones was determined in rotenone-treated HepG2 cells, treating the cells with 1 μ M of quinones in presence of 25 μ M of Rotenone. ATP levels expressed as percentage of ATP in DMSO-treated cells in absence of rotenone (untreated). The graph **b** shows the quinone cytotoxicity in HepG2. Cells were treated with 25 μ M of compounds and incubated for 24 hours at 37 $^{\circ}$ C. The cell viability was determined as percentage of untreated cells. Bars represent mean \pm SEM of at least three independent measurements. Data were analysed using one-way ANOVA test **a** [F (14, 318) = 131.6, P<0.0001] graph **b** [F (18, 488) = 32.48, P<0.0001] followed by Dunnet's post hoc test for multiple comparisons, *P* values were calculated versus dmso, * = $p \leq 0.05$, ** = $p \leq 0.01$, *** = $p \leq 0.001$, **** = $p \leq 0.0001$

6.1.4 Results and discussion ATP rescue and cytotoxicity SAR-4

The final attempt in the hit optimisation scheme was performed according to two avenues:

- 1) the introduction of a heteroatom in aniline ring **82**, **95** and **99** and in the naphthoquinone core **103**, **104** and **105**.
- 2) A scaffold-hopping strategy: the replacement of benzene ring with a small ring containing a heteroatom as thiophene and furane, respectively **109** and **114**.

Both strategies resulted in a series of compounds that showed an increase of ATP rescue, but also high toxicity.

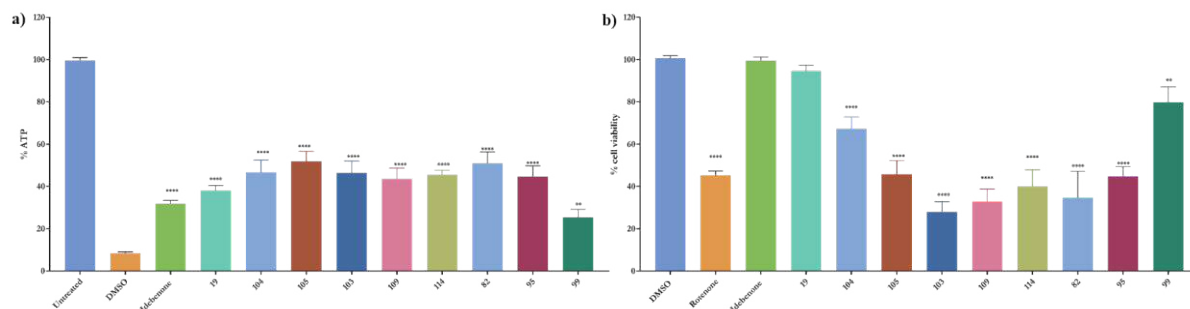


Figure 79 Efficacy of ATP rescue in presence of rotenone and cytotoxicity of synthesized naphthoquinones (SAR-4) The graph a shows the ATP rescue activity of quinones was determined in rotenone-treated HepG2 cells, treating the cells with 1 μ M of quinones in presence of 25 μ M of Rotenone. ATP levels expressed as percentage of ATP in DMSO-treated cells in absence of rotenone (untreated). The graph b shows the quinone cytotoxicity in HepG2. Cells were treated with 25 μ M of compounds and incubated for 24 hours at 37 $^{\circ}$ C. The cell viability was determined as percentage of untreated cells. Bars represent mean \pm SEM of at least three independent measurements. Data were analysed using one-way ANOVA test a [F (9, 266) = 204.4, P<0.0001] graph b [F (10, 285) = 81.03, P<0.0001] followed by Dunnet's post hoc test for multiple comparisons, P values were calculated versus DMSO, * = p \leq 0.05, ** = p \leq 0.01, *** = p \leq 0.001, **** = p \leq 0.0001

6.1.5 Conclusion ATP rescue assay and cytotoxicity assay

Taking into consideration all the biological data obtained for the 50 naphthoquinone derivatives of **19**, an analysis of the structure-activity relationships was performed. Molecules retaining the aniline group in position **3** showed slightly better activity than benzylamine and phenylethylamine analogs. A complete lost of activity was observed when an electron donating group was introduced in position **2**, on the other hand, the presence of strong electron withdrawing groups increased the cytotoxicity of these family. The presence of a hindering group in position **2** decreased activity, while replacement of methoxy group **47** with a thiomethyl group **78**, slightly improved activity. Consequently, for methoxy-derivatives and thiol-derivatives, changes on aromatic were explored. Overall, the introduction of fluorine or the replacement of CF₃ with SF₅ was associated with activity and cytotoxicity retention. Instead, the introduction of nitrogen in the naphthoquinone core or the replacement with heterocyclic rings improved the ATP rescue activity, but they also showed higher cytotoxicity than **19**. In order to select the top candidates for further investigation in vitro assays, the ATP rescue activity and cytotoxic effect of all synthesized compounds were considered and analysed. Figure 80

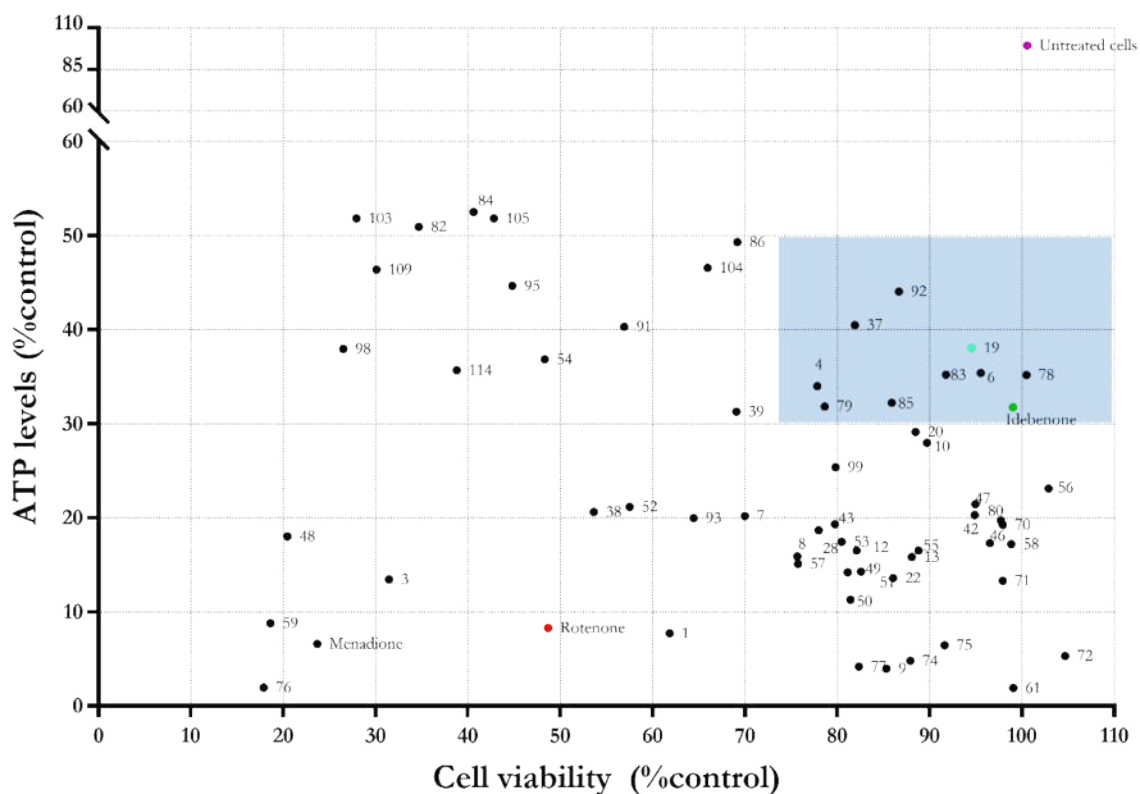


Figure 80 Overview of the results obtained for the ATP rescue activity and cytotoxicity of studied naphthoquinones. The graph shows the correlation between the ATP rescue activity of synthesised compounds, at 1 μM and their cytotoxicity at 25 μM . The red dot shows the cytotoxicity effect of rotenone and the remaining ATP level after the rotenone incubation in free-glucose media. The green dots show the ATP rescue and cytotoxic results obtained treating the cell with 19 (best compound selected by virtual screening) and idebenone.

The Figure 80 shows that 9 compounds have similar ATP rescue activity than idebenone at 1 μM and low toxicity profile at 25 μM . In addition, these compounds were tested at lower concentration in the ATP rescue assay (100 nM) and in the cytotoxicity assay (10 μM), in order to investigate if they could retain the activity.

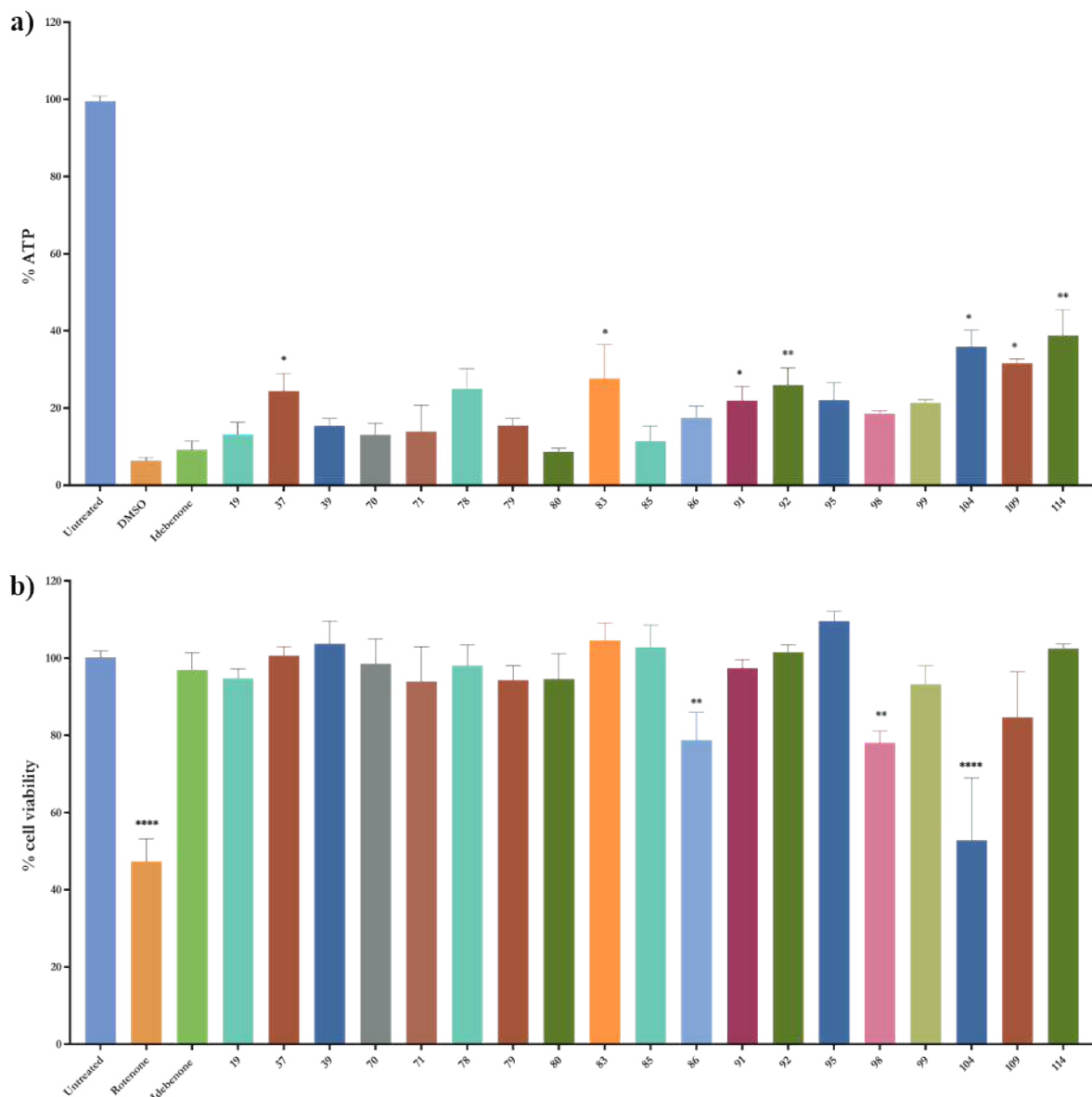


Figure 81 Efficacy of ATP rescue in presence of rotenone and cytotoxicity of selected naphthoquinones. The graph a shows the ATP rescue activity of quinones was determined in rotenone-treated HepG2 cells, treating the cells with 1 μM of quinones in presence of 25 μM of Rotenone. ATP levels expressed as percentage of ATP in DMSO-treated cells in absence of rotenone (untreated). The graph b shows the quinone cytotoxicity in HepG2. Cells were treated with 25 μM of compounds and incubated for 24 hours at 37 $^{\circ}\text{C}$. The cell viability was determined as percentage of untreated cells. Bars represent mean \pm SEM of at least three independent measurements. Data were analysed using one-way ANOVA test a [F (21, 96) = 37.85, $P < 0.0001$] graph b [F (28, 266) = 11.93, $P < 0.0001$] followed by Dunnet's post hoc test for multiple comparisons, P values were calculated versus dms0, * = $p \leq 0.05$, ** = $p \leq 0.01$, *** = $p \leq 0.001$, **** = $p \leq 0.0001$

Interestingly, Figure 81 shows idebenone is not able to rescue the ATP level under complex I inhibition at 100 nM concentration, but 7 compounds (37, 83, 91, 92, 104, 109 and 114) have a significant ATP rescue effect with a low cytotoxic profile, except for 104, which shows significant cytotoxicity even at 10 μM .

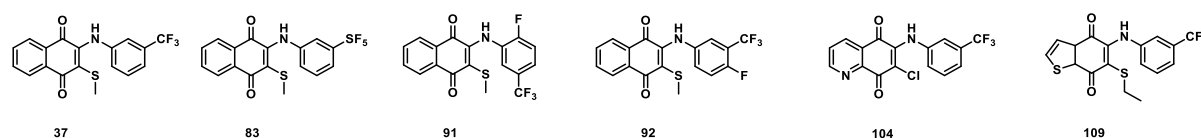


Figure 82 Chemical structures of compounds showing significant ATP rescue activity at 100nM

6.1.6 Results and discussion Pro-oxidant activity

As mentioned in Chapter 2, the naphthoquinones are reported in the literature as cytotoxic drug generating superoxide species in the cells and consequentially led to oxidative stress damage. The naphthoquinones selected in the previous ATP rescue and cytotoxic assays, have been tested for their capacity to generate ROS in the cells. Menadione, a well known pro-oxidant naphthoquinone, was used as control in both the development of both assays in this study.

Interesting, compounds **54**, **86**, **104** and **114** despite a high cytotoxic effect, did not show any particular increase of mitochondrial ROS level in comparison with Menadione, but they are able to produce a significant amount of ROS in the cytoplasm, as shown in Figure 83. On the other hand, compound **7** has the opposite effect; it can generate a high amount of ROS in the mitochondria but limited in the cytoplasm. These results are in line with the cytotoxic detected with the MTT assay. **54**, **86** and **104** might be easily reduced by NQO1 and in their reduced form may be unstable producing reactive oxygen species in the cytoplasm. Instead, Menadione and **7** might be mitochondrial pro-oxidant due to the interaction with mitochondrial complex I as showed in the enzymatic assay (Chapter 5.1.1) Moreover, Menadione and other naphthoquinone showing a free position in conjugation to one of the carbonyls, can cause a depletion of glutathione due to a nucleophilic attack via Michael addition reaction

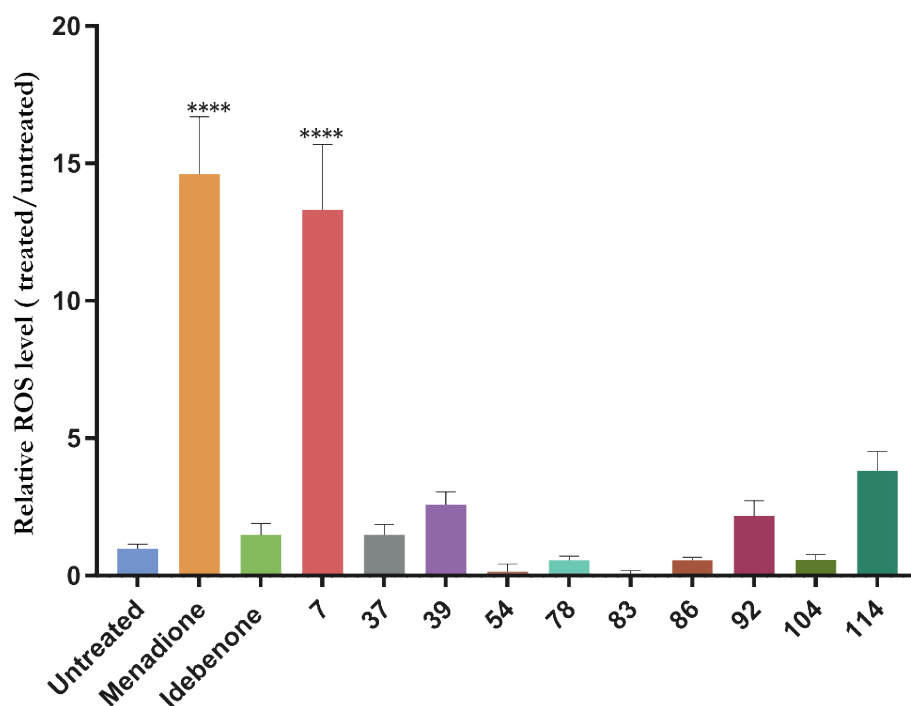


Figure 83 Evaluation of intracellular ROS induce by naphthoquinones. The graph a shows the relative ROS level detected using CellROX Reagent, normalised to untreated cell. Menadione (25 μ M) was used as positive control. Mean background value from cell-free wells incubated dye was subtracted from signals. Bars represent mean \pm SEM of at least three independent measurements. Data were analysed using one-way ANOVA test [F (15, 107) = 27.78, $P < 0.0001$], followed by Dunnet's post hoc test for multiple comparisons, P values were calculated versus DMSO, * = $p \leq 0.05$, ** = $p \leq 0.01$, *** = $p \leq 0.001$, **** = $p \leq 0.0001$

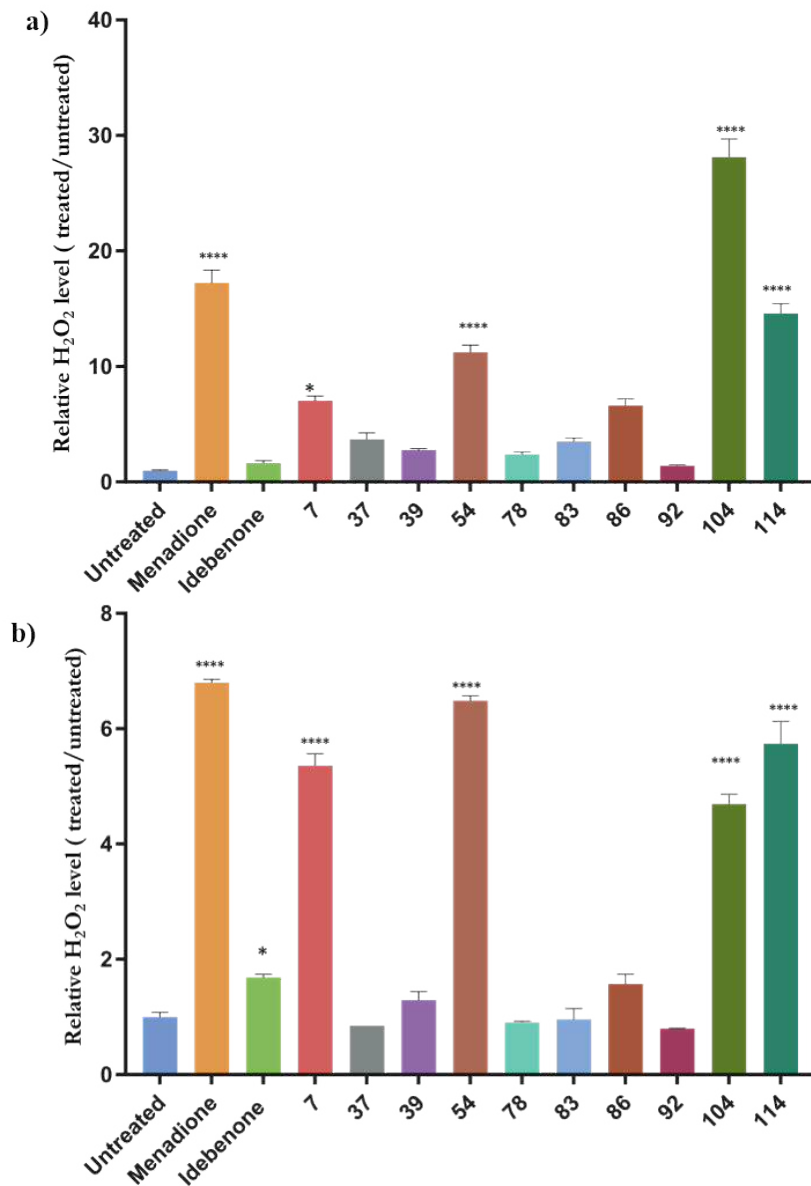


Figure 84 Evaluation of intracellular H₂O₂ induces by naphthoquinones in HepG2 and SH-SY cells. The graphs show the relative H₂O₂ level detected using ROS-Glo™ H₂O₂, normalised to the untreated cell. Menadione (25 μM) was used as positive control. Mean background value from cell-free wells incubated dye was subtracted from signals. Bars represent mean ± SEM of at least three independent measurements. Data were analysed using one-way ANOVA test **a** [[F (13, 91) = 142.7, P<0.0001] graph **b** [F (13, 28) = 247.1, P<0.0001] followed by Dunnet's post hoc test for multiple comparisons, *P* values were calculated versus dms0, * = *p* ≤ 0.05, ** = *p* ≤ 0.01, *** = *p* ≤ 0.001, **** = *p* ≤ 0.0001

6.1.7 Quinone reduction in cells

The tetrazolium dye WST-1 was used to detect quinone-mediated NQO1 activity (Chapter 4.2.1.3). As mentioned in the enzymatic results (Chapter 5.1.1), the naphthoquinones are good substrates of NQO1 with a low affinity for the mitochondrial enzymes, but that not exclude a possible reduction from other oxidoreductases present in the cells. For this reason, the assay was performed in the two different cells, HepG2 and SH-SY5Y in order to detect cell-specific reduction rates of the selected naphthoquinones. As reported in Figure 85, all naphthoquinones were highly reduced in HepG2, only if NQO1 is available. In fact, in presence of Dicoumarol, WST-1 was not converted into its formazan structure due to the lack of electron mediator (hydroquinone). The same result was obtained using cell lines featuring very low NQO1 expression as SH SY5Y, the addition of naphthoquinone did not result in an increase of absorption at 450 nm. The fact that each substrate for NQO1 exhibited individual turnover rates depends on different affinities of substrates towards the recombinant enzyme.

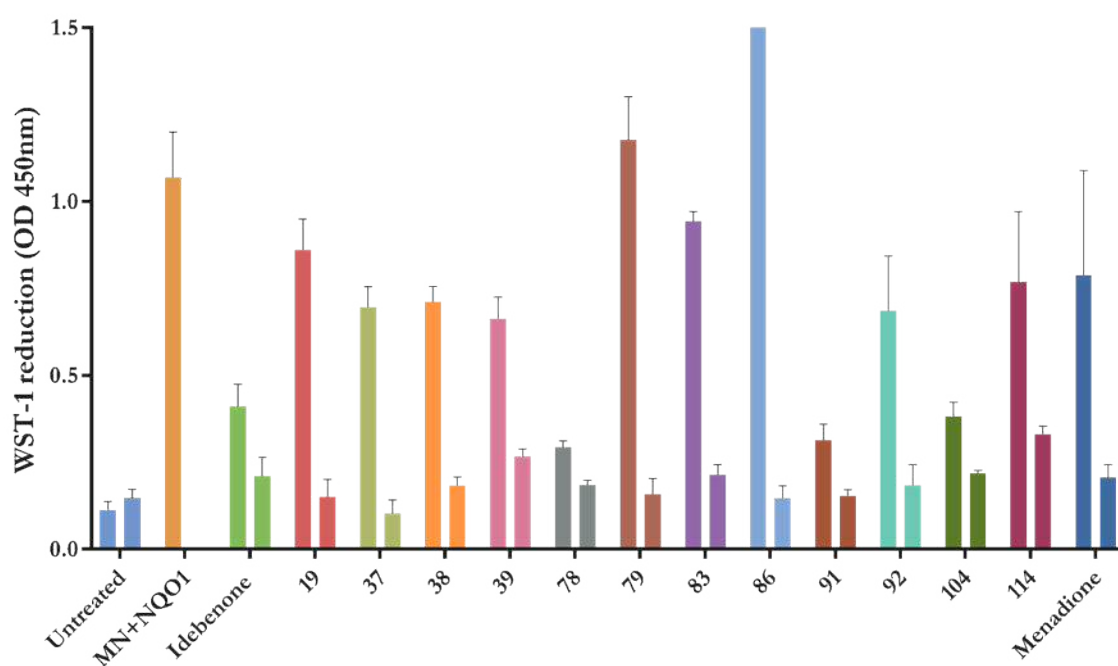


Figure 85 WST-1 reduction in presence of hydroquinone as electron donator in HepG2 cell line in presence of absence of Dicoumarol. The graph shows the variations of absorbance at 450 nm due to the reduction of WST-1 in HepG2 cell lines respectively, in presence or absence of quinones. Dicoumarol (20 μ M) was added to confirm the quinone reduction by NQO1. Menadione in presence of recombinant NQO1 in free-cell environment was used as positive control. Data were analysed using Two-way ANOVA test [$F(2, 15) = 67.1, P < 0.0001$], followed by Sidak's post hoc test for multiple comparisons and adjusted P values were calculated versus untreated (**** = $p \leq 0.0001$)

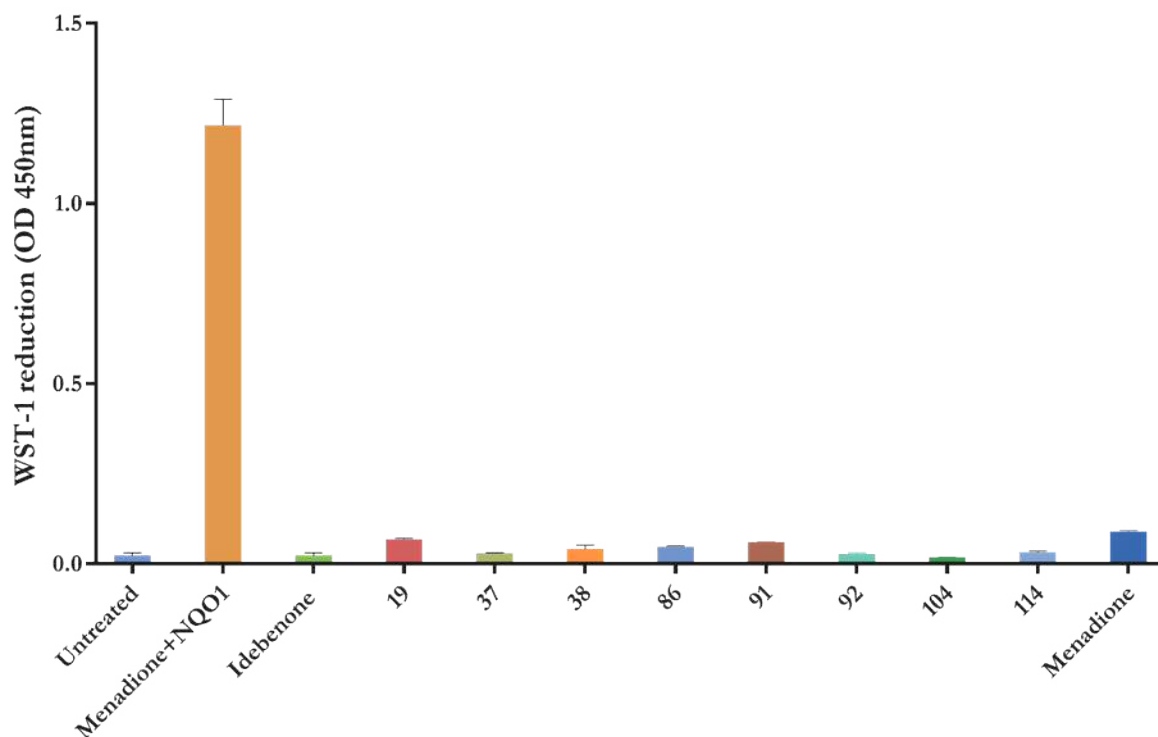


Figure 86 WST-1 reduction in presence of hydroquinone as electron donor in SH-SY5Y cell line. The graph shows the variations of absorbance at 450 nm due to the reduction of WST-1 in SH-SY5Y cell lines in presence or absence of quinones. Menadione in presence of recombinant NQO1 in free-cell environment was used as positive control. Data were analysed using one-way ANOVA test [$F(2, 14) = 326.0, P < 0.0001$], followed by Dunnet's post hoc test for multiple comparisons, P values were calculated versus untreated **** = $p \leq 0.0001$

6.1.8 Seahorse bioenergetics analysis

The naphthoquinones were tested for their capacity to affect oxygen consumption, and the data show all the selected naphthoquinones cause an oligomycin-sensitive increase in oxygen consumption, indicating that they have complex I-bypass activity. In particular, the comparison between the mitoATP production rate and GlycoATP production rate showed that naphthoquinones increase only the production of ATP correlated to mitochondria respiration. The rotenone pre-treatment blocks the oxidative phosphorylation through complex I inhibition, shifting the burden of ATP supply entirely to glycolysis, and consequently increasing glycolytic rate. After quinone injection, this trend was reversed, the ATP production related to the oxidative phosphorylation increased, suggesting a reactivation of electron flow in mitochondrial ETC.

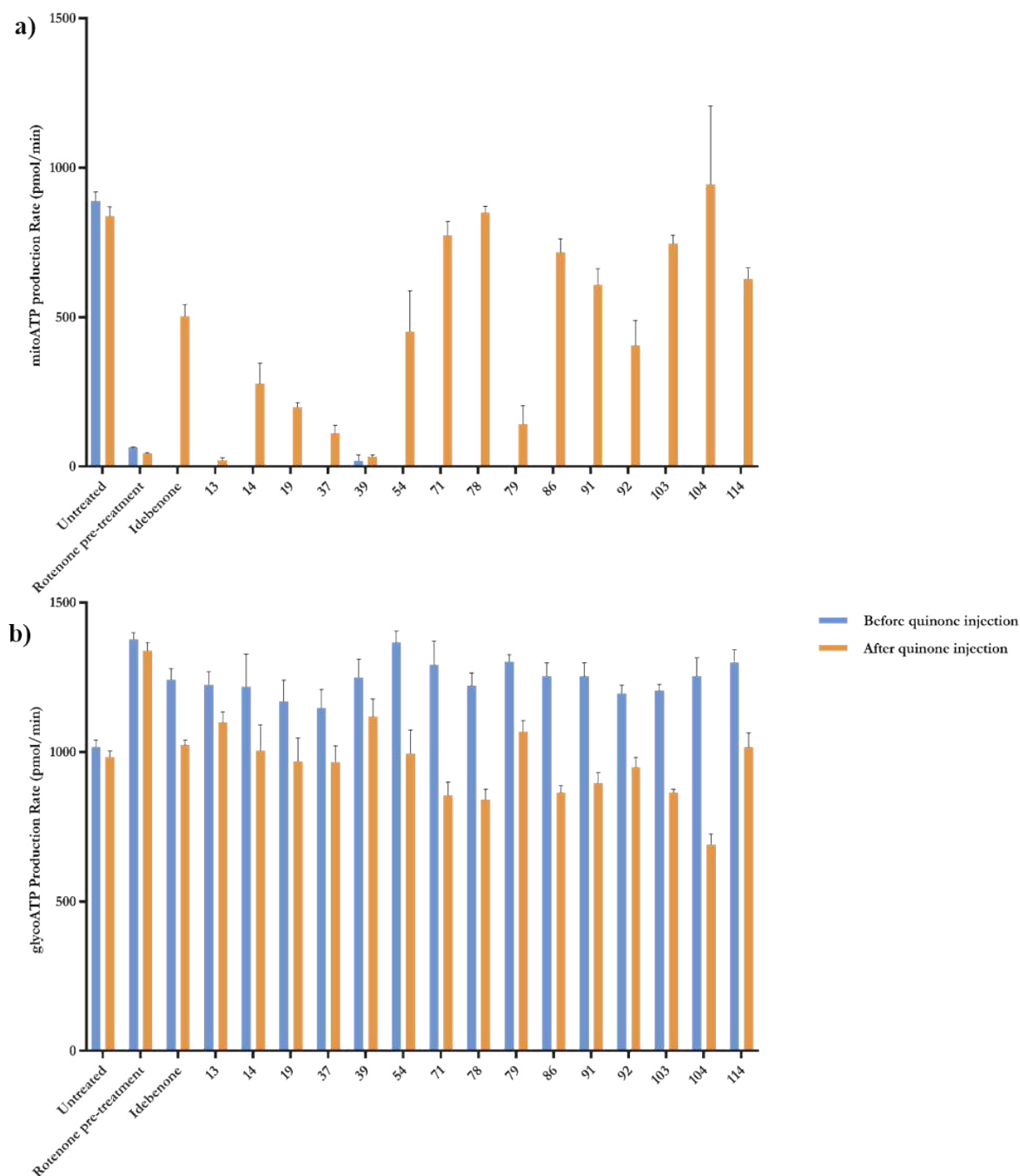


Figure 87 Comparison between the mitoATP production rate and GlycoATP production after quinone injection. The graphs show the difference of mitoATP production rate and glycoATP production before quinone injection (blue) and after quinone injection (orange) in Rotenone pre-treatment sample. No rotenone pre-treated cells (untreated) was used as control. Data are means \pm SEM of $n = 6$ independent biological replicates

The naphthoquinones **71**, **78**, **86**, **103** and **104** showed a higher rescue of mitochondria respiration than other naphthoquinones. **13** did not show an increase of OCR, confirming its inactivity in the ATP assay due to the lack of NQO1 interaction, as reported in the enzymatic

assay (Chapter 5.1.1). Overall, the seahorse data are in line with the results obtained in the ATP rescue assay, confirming the interaction of naphthoquinone with the mitochondria electron transport chain.

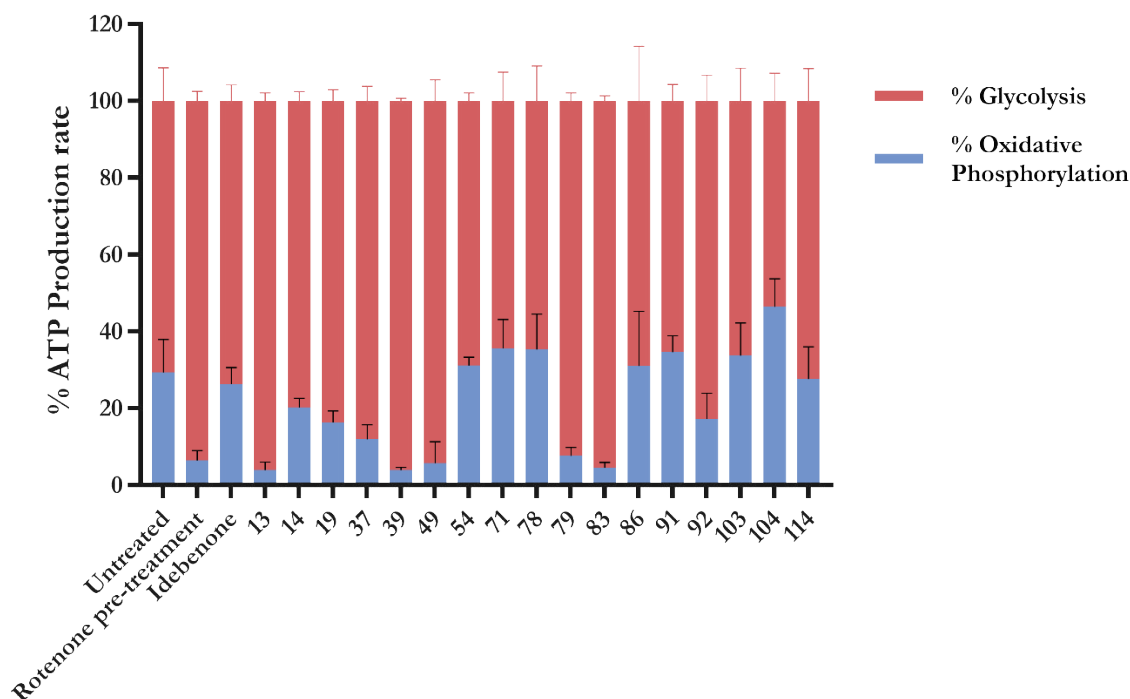


Figure 88 Total ATP production rate of naphthoquinones in presence of Rotenone. The graph shows the contribution of mitochondrial ATP and glycolytic ATP production rates in live cells after naphthoquinones injection in Rotenone pre-treated samples. The mitochondrial ATP was defined as change in the percentage of the total ATP production. Bars represent mean \pm SEM of at least three independent measurements. Data were analysed using Two-way ANOVA test [$F(19, 74) = 9.822, P < 0.0001$], followed by Tukey's post hoc test for multiple comparisons, P values were calculated versus Rotenone pre-treatment

However, despite showing a substantial increase of mitochondrial respiration, **104** did not entirely respond to OXPHOS inhibitors, indicating they might affect the oxygen consumption in other ways and its activity cannot be considered significant. Indeed, one potential limitation of this test is the fact that naphthoquinones can promote the generation of reactive oxygen species (ROS), with resulting consumption of oxygen not correlated with mitochondrial metabolism. The compounds **104** and **78** show a higher significant increase of OCR than other selected naphthoquinones, but **104** is only modestly sensitive to oligomycin, confirming that this compound has a pro-oxidant and consequently a cytotoxicity activity, as already reported in Chapter 5.1.5.

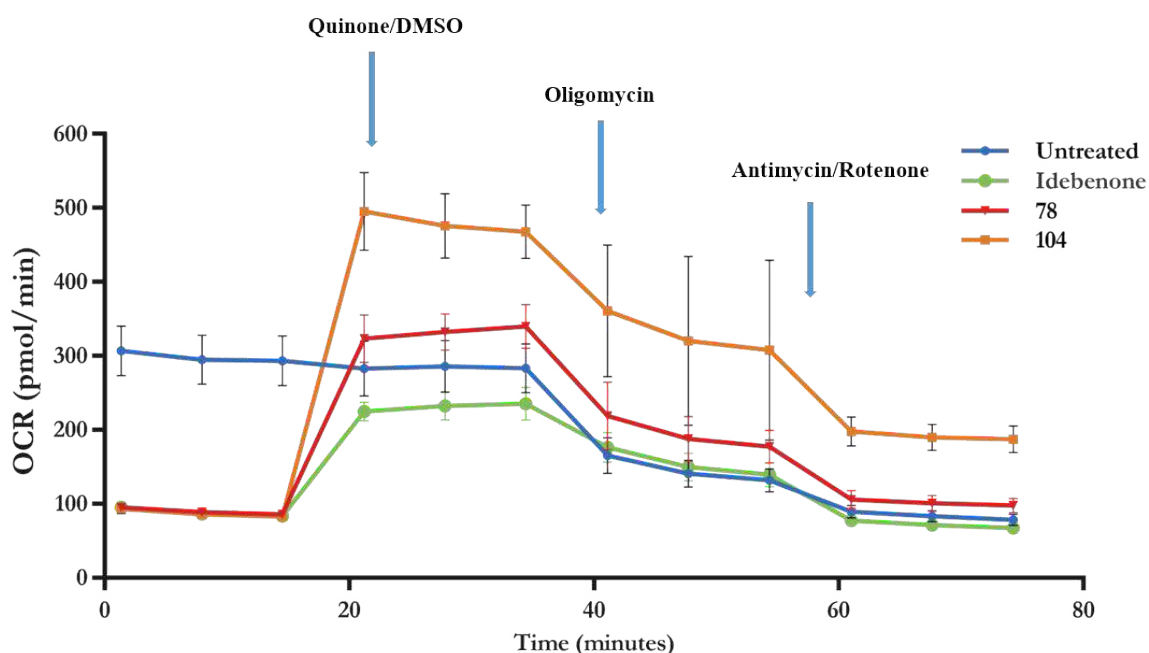


Figure 89 OCR rescue by 78,104 and idebenone in complex I impairment. Graph shows the rescue of OCR after quinone injection (10 μ M) in Rotenone pre-treatment sample. DMSO injection was used as control in the No pre-treatment samples and Rotenone pre-treatment sample. After DMSO/quinone injection, oligomycin 1 μ M, Antimycin/Rotenone 1 μ M was injected in order to exclude OCR not correlated with the mitochondrial electron transport chain. Data are means \pm SEM of n = 6 independent biological replicates

6.1.9 Dose-response curve ATP rescue and cytotoxicity

Compound **37** and **92** showed promising results in several biological assays:

- Rescue of ATP level under inhibition of complex I
- Rescue of mitochondrial respiration under inhibition of complex I
- Low cytotoxicity profile
- No pro-oxidant activity

For this reason, a concentration-Response studies were performed to determine the half maximal efficacy response (EC_{50}) and the half maximal inhibitory concentration (IC_{50}) using 7 data points. The calculation was performed on two different cell lines: HepG2 and SH-SY5Y, which express different level of NQO1.

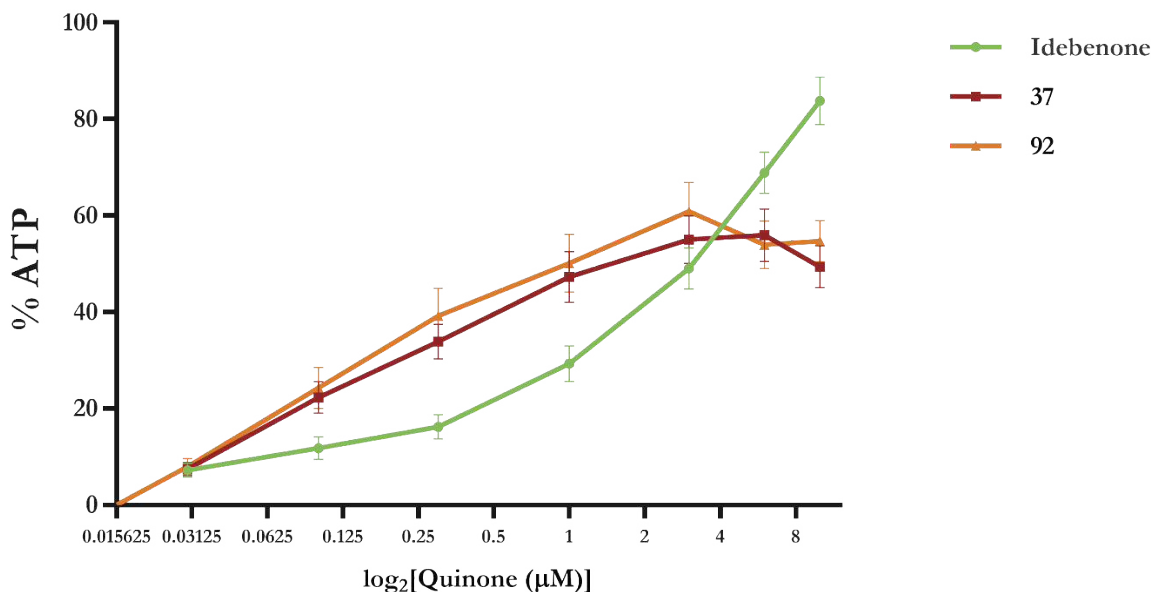


Figure 90 Dose response curve and EC₅₀ values for idebenone, 37 and 92. Dose response curves of ATP in HepG2 cells in presence of Rotenone (25 µM) and 7 different concentrations of quinone. Each plot point reflects data obtained from 4 independent experiments mean ± SEM

37 and **92** showed a higher activity than idebenone at lower concentration 100 nM-1 µM, but they reached a plateau-phase early. Meanwhile, idebenone was able to almost entirely rescue the ATP level - **37** and **92** did not show a complete ATP rescue at higher concentration. This result suggests that **37** and **92** might be partial agonists, which showed higher potency than idebenone, but lower efficacy. Indeed, the decrease of activity at 10 µM could not be correlated with the toxic effect of compounds. The naphthoquinones **37** and **92** showed low toxicity in SH-SY5Y and HepG2 cell lines, with an IC₅₀ 34 µM and 32 µM respectively.

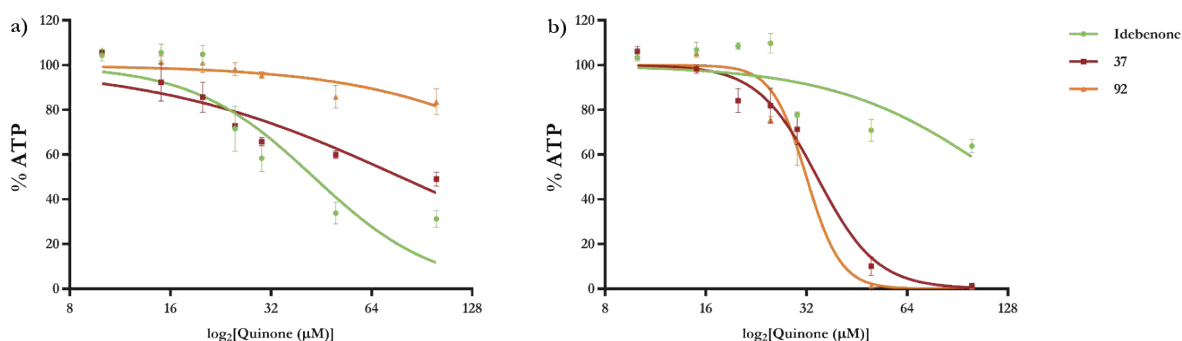


Figure 91 Dose response curve for idebenone, 37 and 92 in SH-SY5Y and HepG2. Dose dependent curve of quinone (10-100 μM) treatment on HepG2 and SH-SY5Y cells for 24 h. Each value is a ratio of the level in the treated cells to that in the control cells. Bars represent mean \pm SEM of at least three independent measurements.

Our study suggested that these compounds are acting as cytosolic-mitochondrial electron carrier rescuing the ATP level under inhibition of complex I. If the ATP rescue–activity depend on these enzymes the rescue should be sensitive to inhibition of complex III and NQO1, Myxothiazol and Antimycin were used as inhibitor of complex III and Dicoumarol as inhibitor of NOQ1; they were added to cells simultaneously with rotenone and DMSO or quinones. In all the cases the ATP rescue of compounds was lost, confirming the direct involvement of two enzymes in the **37** and **92** activity.

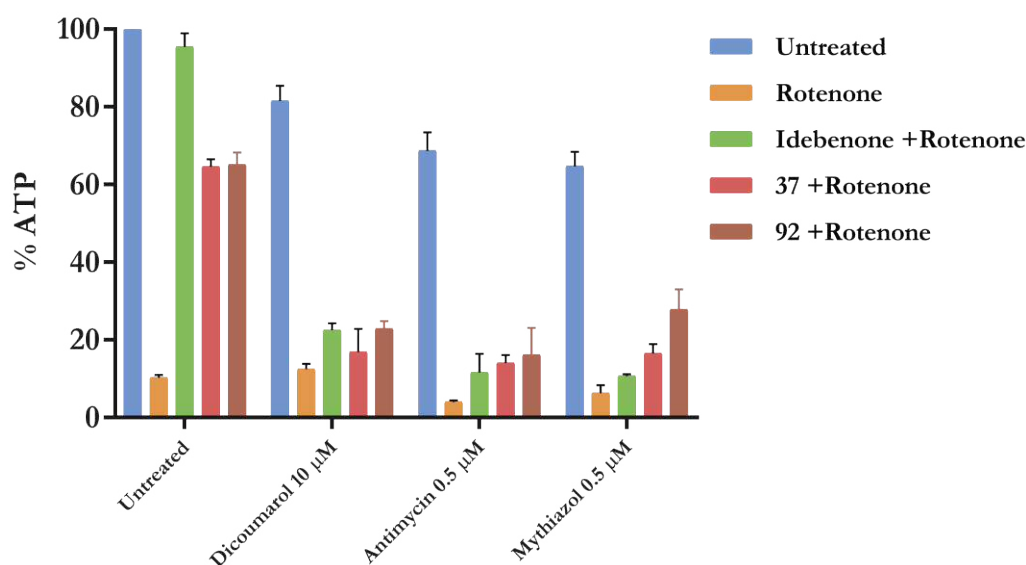


Figure 92 Efficacy of ATP rescue in presence of rotenone by idebenone, 37 and 92 at a concentration of 10 μM and the influence of inhibitors. The ATP rescue activity of idebenone (10 μM) in presence of Rotenone (25 μM), ATP levels expressed as percentage of DMSO-treated cells in the absence of rotenone. The effect of Dicoumarol, Antimycin, Myxothiazol on the ATP rescue activity of idebenone. Bars represent mean \pm SEM of two independent measurements. Data were analysed using Two-way ANOVA test [F (12, 39) = 17.32, $P < 0.0001$], followed by Tukey's post hoc test for multiple comparisons, P values were calculated versus Rotenone pre-treatment

6.2 Upregulation of the NQO1 Expression and ATP results

The expression of NQO1 enzyme may limit the potential therapeutic effect of these novel compounds as evident by the results obtained in the SH-SY5Y cell line. The expression of different detoxification enzymes, including NQO1, is known to be up-regulated by an Nrf2-dependent mechanism. The nrf-2 pathway can be stimulated by different phytochemical

inducers, the most potent are Organosulfur compounds as Lipoic acid and Sulforaphane¹⁶⁴ (Figure. 93).

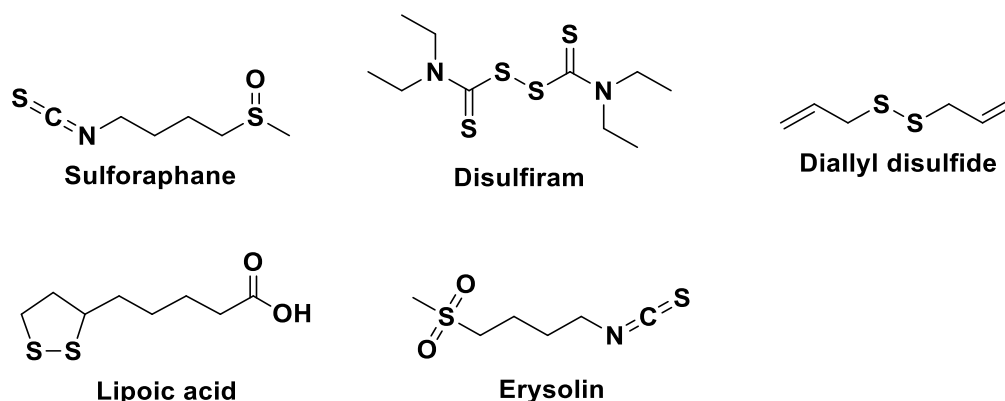


Figure 93 Chemical Structures of NQO1 inducers

α -lipoic acid (LA) is a thiol antioxidant present in numerous vegetables, such as broccoli, spinach, and tomatoes; it is an essential cofactor for pyruvate dehydrogenase complex and other enzymes, which components the aerobic metabolism. LA and its reduced form, dihydrolipoic acid (DHLA), can act as direct antioxidant or indirect, recycling other cellular antioxidants, such as glutathione. Recently, it was reported that the expression of NQO1 can be modulated by LA and DHLA in neuroblastoma SH-SY5Y cells¹⁶⁵. Given the antioxidant activity and the induction of NQO1 as lipoic acid, the low expression of NQO1 in neurons, as well in other tissue, may be bypassed by a treatment with this molecule.

In previous works, researchers have demonstrated that a concentration of lipoic acid up to 500 μ M was able to increase the concentration of NQO1 in SH-SY5Y cell line¹⁶⁵. In order to assess a dose curve response of lipoic acid in these two cells line, a western blot analysis was used. In this study, the activity of lipoic acid was examined at 5 different concentrations (1000 μ M, 2000 μ M, 3000 μ M, 5000 μ M). Incubation with LA for 48 h resulted in a significant induction of cellular NQO1, in particular, a concentration of 1 mM of LA-induced nearly 3.5-fold increase in SH-SY5Y (Figure. 94). The treatment with 5mM of LA did not show any increase of NQO1 expression, likely due to the toxic effects and loss of cell viability at this high dose. From these results, it is evident the NQO1 expression in SH-SY5Y drastically increase after treatment with lipoic acid

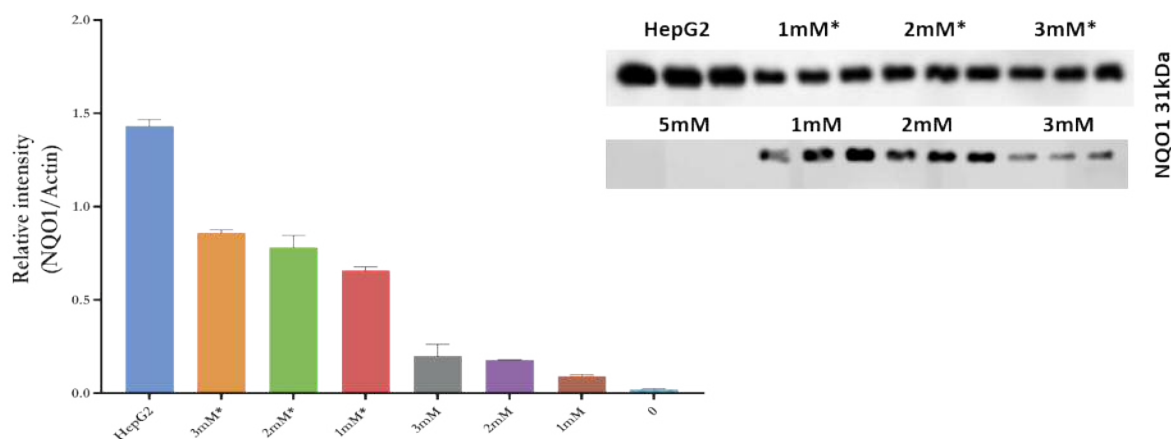


Figure 94 Protein expression of NQO1 induced by lipoic Acid. The graph shows the relative NQO1 level in SH-SY5Y after lipoic acid treatment. The Cells were cultured with 0.1% DMSO alone or with various concentrations of lipoic acid for 48 h (*cells were treated with fresh Lipoic acid after 24h). The NQO1 protein was determined by immunoblot assay. A total of 30 μ g protein for each sample was used. The protein was quantified by densitometry. Bars represent mean \pm SEM of experiment in triplicates

Idebenone did not show any positive results on SH-SY5Y, and a concentration over 25 μ M reduce the cell viability. The low activity/toxicity effect may be correlated to the lack of NQO1 and indirect interaction with complex I and production of ROS. In order to demonstrate this hypothesis, idebenone and interesting naphthoquinones were tested after having induced NQO1 with 3mM of lipoic acid. The results showed quinones failed to rescue the ATP production, suggesting there is a strict correlation between NQO1 protein expression and the biological activity of these compounds. These results are in agreement with the study conduct by Gueven and collaborators ⁶⁴, in which they compared the activity of idebenone in several cell line expressing different NQO1 mRNA levels.

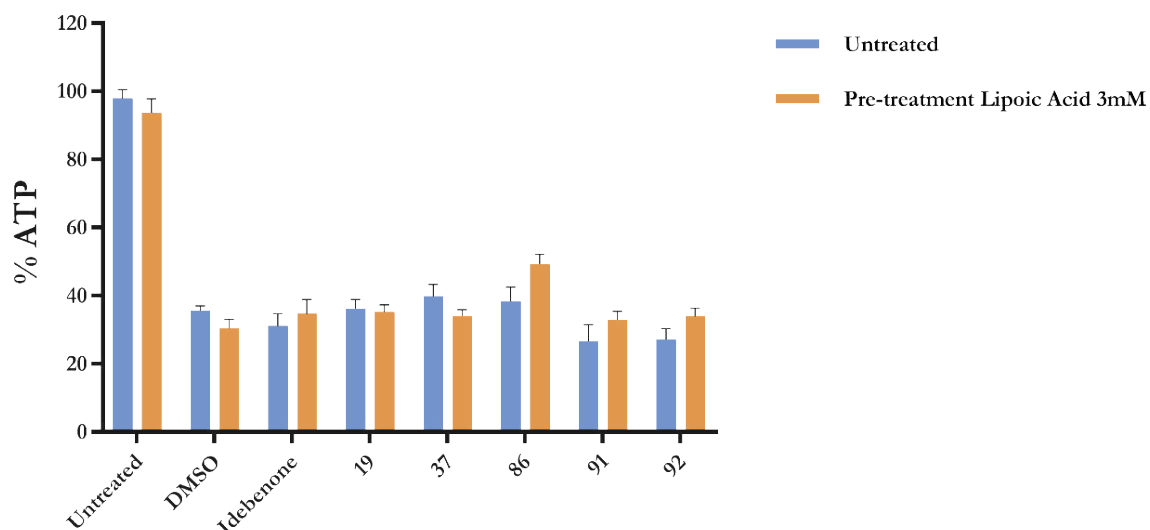


Figure 95 ATP rescue activity by idebenone and naphthoquinone after inducing NQO1. Graph shows the difference between the ATP rescue activity in presence of Rotenone after Lipoic acid pre-treatment (orange) or No pre-treatment (untreated). The SH-SY5Y cells were incubated in presence or absence of Lipoic acid (3 mM) for 48h before testing the quinone activity. After 48h Rotenone (25 μ M) and quinones (5 μ M) were added at same time and the cells were incubated for 6h before evaluating the ATP level using CellTiter-Glo®. Bars represent mean \pm SEM of at least three independent measurements.

6.3 Discussion Ex-vivo studies of compounds 37 and 92

All the assays and the related results shown in this section were conducted by Dr. Kathy Bernie, and they were acquired in the permission of Prof. Marcela Voltubra, Dr. Malgorzata Rozonaswa and Dr. Kathy Bernie, Cardiff University.

Compounds **37** and **92** were further tested *ex vivo* using mouse explant retina to assess whatever they are able to rescue rotenone-induced retinal ganglion cell loss. Firstly, different retina sections were examined to study the levels of NQO1 expression in the murine retina and specifically in the RGC cells. Overall, strong immunoreactivity was found predominantly in the RGC cell layer and the photoreceptor layer (Figure 96), suggesting the quinones can be metabolised into hydroquinones in the retinal ganglion cells.

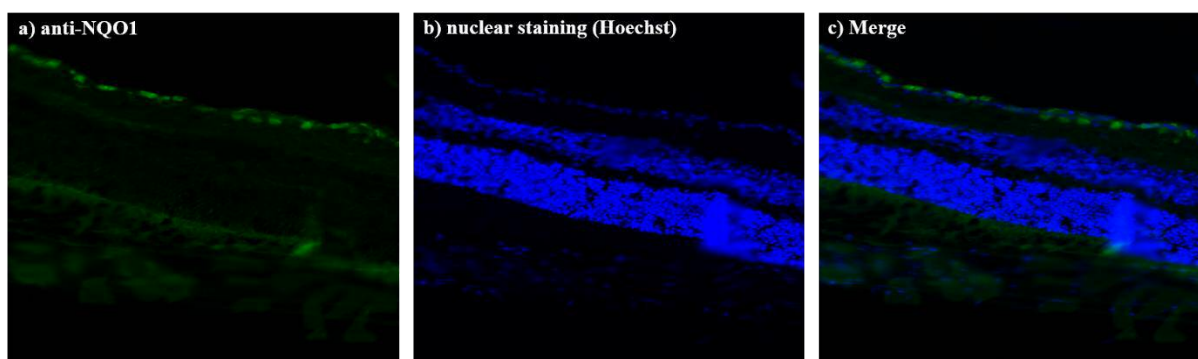


Figure 96 NQO1 expression in retina layer. The Figure shows the Distribution of NQO1 in the mouse retina stained with rabbit anti-NQO1 (green) and nuclear staining using Hoechst (blue) antibodies.

Successively, the naphthoquinones were tested on retina explant to assess their rescue rotenone-induced RGC loss. Briefly, explant retina was cultured for 24 hours in the presence of Rotenone (100 μ M) and compounds before quantifying the RGC degeneration measured by immunochemistry. The graph showed that **92** has proved a superior therapeutic efficacy than idebenone, almost completely rescuing the retinal ganglion cells.

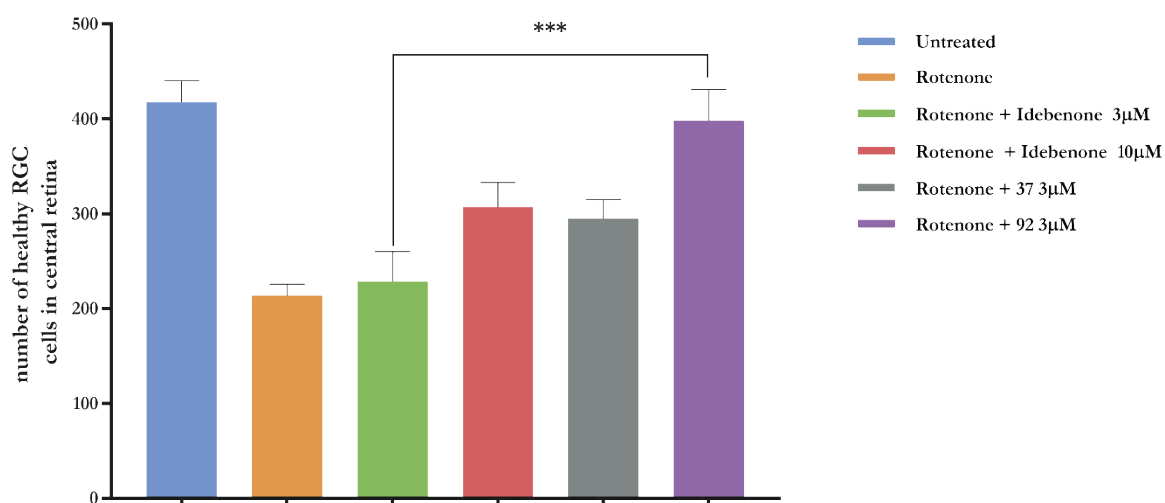


Figure 97 Treatment of retinal explants with selected naphthoquinones (37, 92). The graph shows the rescue of retinal ganglion cells (RGC) by quinones in presence of rotenone. RBPMS (RNA-binding protein with multiple splicing) was used as marker to enable RGC counting in retina explants after 24 hours. Data were analysed using one-way ANOVA test [$F(5, 81) = 7.075, p \leq 0.0001$], followed by Tukey's post hoc test for multiple comparisons, P values were calculated versus Rotenone +Idebenone 3 μ M

6.4 Conclusion: biological results obtained using synthesised compounds

Taking into consideration all the biological data obtained from the five different cell-based assays described above, consistency of activity was found among the test compounds. In summary, compounds showing significant ATP rescue activity at 1 μ M (e.g. **85**, **86**, **91**, **92**, **103**) also demonstrated increased oxygen consumption rate under inhibition of complex I using the Seahorse XF96 analyser (Chapter 6.1.8), suggesting direct interaction of these compounds with mitochondrial respiration. Moreover, these compounds exhibited high affinity for the NQO1 enzyme as shown in the WST-1 assay, which confirmed the involvement of this enzyme in compound activity, as was hypothesised in the computational studies (Chapter 2). These data were then cross-referenced with the results obtained from the cytotoxicity and pro-oxidant assays to pinpoint the most promising compound (**92**) to take forward and define the structure-activity relationship of this family, as depicted in Figure 95.

Although **92** did not in fact provide the highest activity in terms of ATP and OCR rescue, this compound showed important reduced cytotoxic and pro-oxidant effects compared to more active naphthoquinones. Based on this combination of properties, compound **92** was selected as lead compound for further ex-vivo and in vivo evaluations.

SAR analysis of **92** highlighted the importance of a number of specific features for the activity, including (1) the aniline substituent in position 2, which might increase the affinity with the mitochondrial complex III (Chapter 2.1.8); (2) the presence of CF₃ in the aniline ring, which might increase the overall membrane permeability of the molecule; (3) the presence of a mild EDG such as SCH₃, which might affect the electronic behaviour and consequently the potential reduction of the molecule. The results obtained from the structural modifications of the studied naphthoquinones suggested that the biological effect is strongly determined by the electrophilic capacities of the entire molecule rather than particular structural features. The standard reduction potential of naphthoquinones determines the reduction by oxidoreductases, influencing their ATP rescue capacity and cytotoxicity. The model described in this study, although limited by the number of naphthoquinones used, showed a cut-off above which the naphthoquinone showed significant cytotoxicity, and below which the compounds are inactive due to the lack of reduction by NQO1.

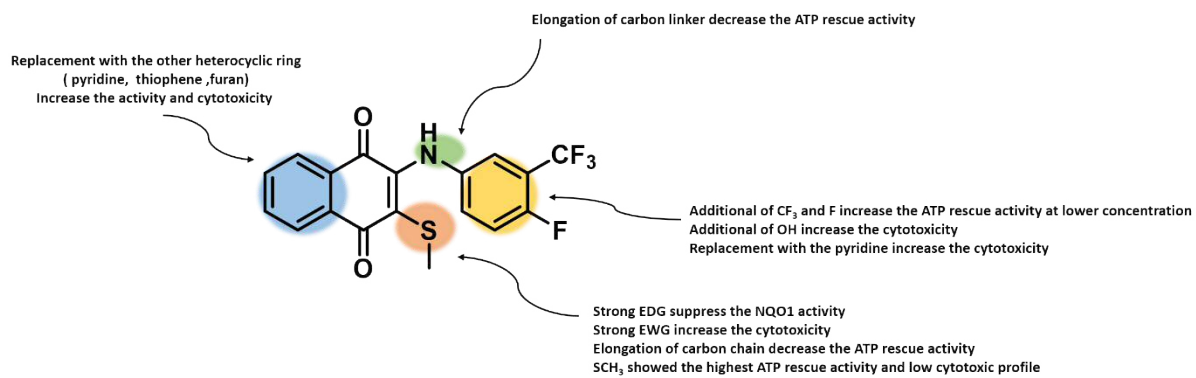


Figure 98 Chemical structure of compound 92 and the general overview of the SAR study

CHAPTER 7

**CONCLUSION AND FUTURE
PERSPECTIVES**

7.1 Conclusion

The naphthoquinones identified in this study are an interesting class of compounds, which possess unique properties. They showed to possess a “bypass complex I function” and be capable of rescuing OXPHOS activity in several assays, despite a low toxic profile. These observed effects of naphthoquinones are mainly attributed to their interaction with NQO1 and mitochondrial complex III.

Molecular modelling techniques have been used to explore the feature involved in the binding with both enzymes, and to design naphthoquinones, which have a specific affinity. Taking into consideration these computational studies, several compounds have been synthesised with the aim to improve the activity of idebenone, the current gold standard for LHON diseases.

50 compounds were successfully synthesised to study the SAR of these naphthoquinone family, revealing the key structural factors for tuning their biological activities. Among them, 4 novel compounds showed very promising mitochondrial rescue properties at low concentrations – each being superior to the current gold standard, idebenone. Moreover, it was very encouraging to find the majority of the compounds evaluated in this project demonstrated a lack of cytotoxic effects using the neuron cell line SH-SY5Y, demonstrating a better cytotoxic profile than idebenone. In particular, one of these, **92** demonstrated superior therapeutic efficacy than idebenone in an *ex vivo* model of mitochondrial optic neuropathy, and thus is believed to be particularly good candidate for *in vivo* studies.

A study of the mechanism of action was performed for the best compound **92**. Although the activity of the compound was lost when NQO1 and complex III were inhibited in cell-based assay (Chapter 6.1.9), a further confirmation using the isolated enzymes are needed. In fact, data from the enzymatic assays used in this work suggest the possible specific interaction of the identified naphthoquinone with the NQO1 and complex III, but they are limited by the interference of the compounds, which did not allow us to determine their binding constant and provide definitive evidence of their interaction. However, based on this proposed possible mechanism, the naphthoquinones identified in this study are versatile class of compounds, that potentially can be drug treatments for several diseases. In fact, mitochondrial complex I deficiency can be a direct cause of mitochondrial diseases such as LHON, but it was shown to play a central role in neurodegenerative diseases such as Parkinson's disease, Alzheimer's disease and Mitochondrial Encephalomyopathy, Lactic Acidosis, Stroke-like episodes (MELAS)⁵⁴. The observed *in vitro* results clearly show these class of compound could prevent

the cell death induced by the ATP lost and possible achieve an amelioration in complex I deficiency phenotype diseases.

In conclusion, in the absence of alternative treatments, Idebenone is in the only drug approved for the treatment of LHON, but there is still uncertainty on its clinical benefit ⁶⁸; the data presented in this thesis show that compound **92** may be a potential new drug treatment in the area of great clinical need.

7.2 Future perspectives

The 50 naphthoquinone synthesised in this study provide useful information on the biological activity of these family, but further substitution and chemical modifications may better define the structure-activity relationship and the role of the standard reduction potential in their biological effect. The most interesting compounds will be further investigated *in vitro* using primary retinal ganglion cells and *ex vivo* using mouse retina. In particular, compound **92**, although it showed a lower efficacy than idebenone, it demonstrated a far superior retinal ganglion cells rescue in the explant mouse retina. These results might be explained by a higher potency at lower concentration than idebenone and/or better drug permeability, better NQO1 targeting than idebenone.

Pharmacokinetic and metabolic studies of idebenone showed a low bioavailability of parent Idebenone, with an intraocular concentration of 111 nM in the aqueous humour after a single oral administration of 60 mg/kg of idebenone to male mice^{72,73}. According to these data, the novel identified compound might be within the therapeutic range shown to be more effective in protecting cells from rotenone-induced cell death than idebenone, and with significantly lower toxic side effects. This hypothesis needs to be further investigated using *in vivo* model, but for the potential use of **92** as a treatment for mitochondrial optic neuropathies, a true benefit of the drug can only be realised through effective delivery to the retina. In fact, previous metabolic studies showed that CYP enzymes are primarily responsible for the rapid metabolism of quinone, reducing their bioavailability¹⁶⁶.

This rapid metabolism can severely limit the application of compounds as therapeutic agents in complex I deficient diseases; unfavourable pharmacokinetics is the most common reason for a drug therapy failure. However, in the last years, several drug delivery systems have been formulated to overcome the challenges associated with drug metabolism. Liposomes, microspheres, solid lipid nanoparticles, cyclodextrins have been successfully used to enhance the solubility, stability, safety and bioavailability of drug molecules¹⁶⁷.

A specific delivery system of **92** to the cells of the retina over a sustained period (e.g. use of biodegradable nanoparticles in eye drops) may improve ocular drug bioavailability, prolonging precorneal residence time, maximising ocular permeability and minimising the necessary therapeutic dose¹⁶⁸.

CHAPTER 8

METHODS AND MATERIALS

8.1 Statistic analysis

Statistical analysis was performed with Prism 7.1 software (Prism version 7.00 for Windows, GraphPad Software, La Jolla California USA):

- 1) Anova, Dunnet's multiple comparisons, Sidak's multiple comparisons and Tukey's multiple comparisons: to compare each compound against the other and each compound against the positive controls, respectively.
- 2) Michaelis-Menten enzyme kinetics: to determine enzyme's K_m (substrate concentration that yield a half-maximal velocity) and V_{max} (maximum velocity).

8.2 Mitochondrial isolation

Mitochondria were isolated from heart and brain of mice as described in the Overview of mitochondrial bioenergetics / Vitor M.C. Madeira¹⁶⁹ with slight modifications.

This method is based on the typical differential centrifugation procedure. Fresh brain and heart were rapidly washed and minced on the glass dishes. The next step is the homogenization, crucial for the quality and quantity of mitochondria isolated from tissues and it is different between hard and soft tissue. Two different procedures were carried out.

- The brain tissue, once was it chopped into fragments, was homogenized at 4°C using a cold small glass Potter-Elvehjem containing 10 mL of brain isolation buffer BIB (225 mM mannitol (Sigma), 75 mM sucrose (Sigma), 5 mM HEPES (Sigma), 1 mg/mL BSA (Sigma), 1 mM EDTA pH7.4 (Sigma)).
- The brain homogenate was transferred to a fresh pre-chilled 10ml tube and centrifuged at 2000 x g at 4°C for 4 minutes.
- The supernatant was decanted and the pellet was re-suspended in BIB and subject to a second centrifugation.
- The two supernatants were combined and transferred to a fresh pre chilled 30ml tube and centrifuged at 12,000 x g for 10 minutes at 4°C.

- The supernatant was discarded and the pellet was re-suspended in brain resuspension buffer BRB, (225 mM mannitol, 75 mM sucrose, 0.02 % digitonin (Sigma) and 5 mM HEPES pH 7.4) 12,000 × g for other 8 min.
- The resulting pellet was re-suspended in brain in 300 μL of buffer BRB(without digitonin), and stored at - 80°C.

Heart is a hard tissue and needs a different homogenization force to disrupt its cells, and in some procedures, the use of proteases is reported in order to improve effective disruption of the heart cells but with the risk to damage mitochondria.

- The heart homogenization took place with 4 homogenizations with a refrigerated Teflon-glass Potter-Elvehjem.
- The homogenate was transferred to a fresh pre-chilled 30 ml tube containing 20 mL of heart isolation buffer HIB (250 mM sucrose, 10 mM HEPES, 1 mg/mL BSA, 0.5mM EDTA pH7.4) and centrifuged at 12000 x g at 4°C for 8 minutes.
- The pellet was recovered and transferred to a smaller glass manual Potter-Elvehjem homogenizer containing 10 ml of HIB and promoted a gentle homogenization
- The homogenate was transferred to a fresh pre-chilled 10ml tube and centrifuged at 2000 x g at 4°C for 10 minutes.
- The supernatant was collected at centrifuged at centrifuge at 12,000 × g for other 8 min.
- The new supernatant was discarded, and the pellet was resuspended in 20 mL of re-suspended heart buffer HBR (250 mM sucrose, 10 mM HEPES, pH 7.4) at centrifuged at 12,000 x g for 8min
- The isolated mitochondria were resuspended in 300 μL HRB and stored at -80°C.

8.3 Determination of protein concentration-bicinchonic acid assay (BCA)

Protein concentrations of mitochondria were measured using a commercial protein assay kit (Thermo Scientific). BSA standards and mitochondria were plated in triplicate in a flat bottomed 96-well plate and incubated for 30 minutes at room temperature. The plate was read at 562 nm wavelength. A standard curve was determined from a set of know concentrations of bovine albumin serum (0.1 mg/mL, 0.25 mg/mL, 0.5 mg/mL, 0.75 mg/mL, 1 mg/mL, 2 mg/mL) and used to extrapolate the relative concentration of protein extracts.

8.4 Investigation of interactions of quinone compounds with NQO1

Reduction of quinones by recombinant NQO1 was evaluated according to a procedure reported by Haefel *et al*⁹⁹. The NQO1 assay was performed using the CLARIOstar® microplate reader measuring the change in absorbance of NADH (Sigma) at 340nm. In each well was added the reaction buffer containing 25 mM Tris-HCl pH 7.4, 0.7 mg/mL BSA, NQO1 1µg/mL (Sigma), 50 µM quinone. Since quinones showed an absorbance at 340nm, the absorbance at time zero was evaluated before adding NADH (100 µM) to the reaction buffer. The reaction started with the added of NQO1 and the decrease of absorbance at 340 nm was followed for 5 minutes. Specificity of the assay was confirmed using dicoumarol (Sigma) at a concentration of 20 µM. The Michaelis menten curves were determined using the Hitachi U-2900 UV-Vis spectrophotometer. The reaction was performed in 1-ml cuvettes (10 mm) at room temperature using the same reaction buffer (25 mM Tris-HCl pH 7.4, 0.7 mg/mL BSA, NQO1 1µg/mL, NADH 100 µM). The quinone activity was tested using 4 different concentrations (5, 10, 25 and 50 µM) and the decrease of absorbance at 340 nm was followed for 5 minutes.

8.5 Investigation of interactions of quinone compounds with Complex I

Complex I activity was analysed using the artificial electron acceptor 2,6 dichlorophenolindophenol, DCPIP (Sigma). The quinone was reduced to quinol in presence of NADH by complex I, the resulting quinol reduced DCPIP, turning it from blue to colourless. The expected absorbance of DCPIP at 600 nm was calculated from the extinction coefficient of DCPIP $19.1 \times 10^3 \text{ M}^{-1}\text{cm}^{-1}$. Enzyme activity was measured as a decrease in absorbance at 600 nm during 10 minutes at room temperature, using the CLARIOstar® microplate reader. The assay was performed following the procedure described by Spinaza *et al*¹²⁵, with modifications. In each well of flat bottomed 96-well micro plate was added the reaction buffer (50 mM buffer phosphate pH 7.4, 3 mg/mL BSA, 20 µg/ml bovine hearth isolated mitochondria, 300 µM KCN (Sigma), 80 µM DCPIP). The compounds were tested at a concentration of 80 µM, and NADH was added at a concentration of 100 µM. The specificity of the assay was confirmed using rotenone (Sigma) at a concentration of 10 µM. Isolated mitochondria were subject to three cycles of freeze-thawing in hypotonic buffer (10 mM Tris-

HCl) before measuring complex I in order to maximize the enzymatic rates. The Michaelis menten curve was determined using the Hitachi U-2900 UV-Vis spectrophotometer in 1ml cuvette, using the same protocol, with the exception of DCPIP concentration (52 μM).

8.6 Investigation of interactions of quinone compounds with Complex II

Complex II activity was analysed using the oxidation of succinate with DCPIP. The assay was performed at room temperature in 50 mM phosphate buffer pH 7.4 containing 10 mM succinate, 80 μM quinones, 3mg/mL BSA, 20 μg mitochondria and 300 μM KCN. Specificity of the assay was confirmed using TFFA (Sigma) at a concentration 20 μM . Isolated mitochondria were subject to three cycles of freeze-thawing in hypotonic buffer 10 mM Tri-HCl before measuring complex II activity. The Michaelis menten curve was determined using the Hitachi U-2900 UV-Vis spectrophotometer in 1ml cuvette, using the same protocol, with the exception of DCPIP concentration (52 μM).

8.7 Investigation of interactions of novel compounds with cytochrome c and Complex III in presence of NQO1

Complex III activity was analysed by measuring the change in absorbance at 550 nm of oxidized cytochrome c. The expected absorbance of 60 μM cytochrome c (Sigma) was calculated from the extinction coefficient ($18.5 \times 10^3 \text{ M}^{-1} \text{ cm}^{-1}$). The expected reduced cytochrome c was obtained adding few grams of sodium dithionite to a solution of oxidised cytochrome c in Tri-HCl. The reaction was performed at room temperature in 50 mM phosphate buffer pH 7.4 containing 60 μM quinones, 1 $\mu\text{g}/\text{mL}$ NQO1, 3 mg/mL BSA, 20 μg mitochondria and 300 μM KCN. The reaction was initiated by automated dispensing of the NADH solution (100 μM) into the wells. The tested quinone was reduced into quinol by NQO1, the potential binding of the quinol to complex III, was evaluated following the increase of absorbance at 550 nm, due to the reduction of cytochrome c. Specificity of the assay was confirmed using dicoumarol at a concentration 20 μM to inhibit the NQO1 activity or antimycin 10 μM to inhibit the complex III activity. The directly reduction of cytochrome by naphthoquinone was determined using the same protocol, but removing mitochondria from the reaction buffer.

8.8 Culturing of Cells

HepG2 cell line was kindly provided by Prof. Karl Hoffmann's lab, IBERS, (Aberystwyth University), while SH-SY5Y was provided Dr. Emma Kidd's lab (Cardiff University). Both cell lines were cultivated under normal culture conditions (37 °C, 5% CO₂, and 90% relative humidity [rH]). All media were supplemented with antibiotics (100 units/mL penicillin, 1 µg/mL streptomycin, (Gibco), Glutamax (Gibco) as 1% of volume in a mixed solution. fetal bovine serum (FBS, Gibco) was used as serum at a final concentration 10%. The cells were cultivated in flasks of 75 cm² with 15 mL of medium. Confluent adherent cells were washed once with PBS (Gibco) to remove FBS and cellular debris. Cells were then incubated to detachment with 0.25% Trypsin-EDTA (Gibco). Detached-cells were resuspended in growth media and harvested (125 x g; 5 min; RT). Cells were resuspended in their growth medium and split at a ratio of 1:3 to 1:5 depending on cell type.

8.9 Thawing and Freezing of Cells

Cells stored in liquid nitrogen were thawed at 37 °C in a water bath and resuspended in growth medium to a final volume of 15 ml. After harvesting by centrifugation (125 x g; 5 min; RT), the cells were resuspended in their growth medium and seeded into a flask. For cryopreservation of cells, they were resuspended in media containing 5% DMSO and 10% FBS and transferred into cryotubes (Nunc) at concentrations of 2,000,000 cells/mL. In a first step, cells were slowly frozen at -80 °C in an isopropanol-containing tube box for 24 h and then transferred to liquid nitrogen for long-term storage.

8.10 Compound Treatment Solution Preparation

Most compounds were stored at a stocks concentration 25.7 mM at -20 °C in DMSO; except for dicoumarol (in 0.1% sodium hydroxide). Stock solutions were diluted in DMSO to obtain a solution of 4 mM used to test compounds at concentration 1 µM or lower. The resulting DMSO solutions were diluted in the medium at a concentration 10X of the one used for the experiment. Finally, 10 µL of this solution was added on the top of cells for a maximum of 0.1% DMSO concentration.

8.11 Determination of ATP level

Cellular ATP levels were quantified by CellTiter-Glo® Luminescent Cell Viability Assay (Promega). The Kit was used as recommended by the manufacturer. Briefly, after treating the cells as described in the results section (3.2.1), 50 µL of CellTiter-Glo® were added in each wells and the 96 well plate was gently mixed on a shaker for 2 min in the CLARIOstar at 300 rpm. After 10 minutes of incubation at room temperature, the luminescence signal was quantified in the CLARIOstar, plate reader. The luminescence of each well was normalized according to untreated cells (in absence of rotenone).

8.11.1 Rescue of ATP level in HepG2 and SH-SY5Y

The day prior to the assay cells were seeded in 96-well plates (10×10^3) in DMEM (Gibco) containing 1g/L glucose supplemented with 1x penicillin/streptomycin, 1x Glutamax, 2% FBS. The day after, the media was replaced with fresh media DMEM (without glucose and FBS) containing rotenone 25 µM, tested compounds were added at same time. Cells were incubated at 37°C for 2 hours, before measuring the ATP content. using the Cell Titer Glo assay.

8.11.2 Rescue of ATP level SH-SY5Y

The day prior to the assay cells were seeded in 96-well plates (5×10^3) in DMEM: F12 (Gibco) containing 1g/L glucose supplemented with 1x penicillin/streptomycin, 1x Glutamax, 2% FBS. The day after the media was replaced with fresh media DMEM (without glucose and FBS) containing rotenone 25 µM, tested compounds were added at same time. Cells were incubated at 37°C for 5 hours. ATP content is measured using the Cell Titer Glo assay.

8.11.3 Rescue of ATP level SH-SY5Y after lipoic Acid treatment

The day prior to the assay cells were seeded in 96-well plates (5×10^3) in DMEM: F12 containing 1g/L glucose supplemented with 1x penicillin/streptomycin, 1x Glutamax, 2% FBS.

The day after the media was replaced with fresh media containing lipoic acid (sigma) 3mM and the plate was incubated for 72 h. After 72 h, the media was replaced with fresh media DMEM (0% glucose) containing rotenone 25 μ M, tested compounds were added at the same time (5 μ M). Cells were incubated at 37°C for 6 hours. ATP content is measured using the Cell Titer Glo assay (Promega). The CellTiter Glo reagent was added to each well at 50 μ L, and the plate is allowed to incubate for 10 minutes at room temperature. Following incubation, luminescence is measured using a CLARIOstar plate reader. The luminescence of each well was normalized according to untreated cells

8.12 Determination of cell viability assessed by MTT

To quantify the amount of live and dead cells, The MTT assay was used. The MTT (3-(4,5-dimethylthiazol-2-yl)-2,5-diphenyltetrazolium bromide (Sigma)) tetrazolium is a dye, that can be converted into a purple coloured formazan product by viable cells with active metabolism. The formazan product of the MTT tetrazolium accumulates as an insoluble precipitate inside cells. After removing the media, the precipitate can be solubilized in DMSO, and the absorbance at 570 nm can be read. The absorbance of each well was normalized according to untreated cells.

8.12.1 Cytotoxicity assay HepG2 assessed by MTT

The day prior to the assay cells were seeded in 96-well plates (10×10^3) in DMEM containing 1g/l glucose supplemented with 1x penicillin/streptomycin, 1x Glutamax, 2% FBS. The day after, the media was replaced with fresh media DMEM (2% FBS, 1g/L glucose) containing 25 μ M of tested compound. Cells were incubated at 37°C for 24 hours. After 24 hours, the media was removed, and 100 μ l of MTT solution (0.5 mg/mL) was added to each well. The plate was incubated for 3h at 37°C. After 3h the solution was removed, and the purple solid was dissolved adding 50 μ l of DMSO. The absorbance at 570 nM was read for each well

8.12.2 Cytotoxicity assay SH-SY5Y assessed by MTT

The day prior to the assay cells are seeded in 96-well plates (5×10^3) in DMEM: F12 containing 1g/l glucose supplemented with 1x penicillin/streptomycin, 1x Glutamax, 2% FBS. The day after, the media was replaced with fresh media DMEM: F12 (2% FBS, 1g/L glucose)

containing 25 μM of tested compound. Cells were incubated at 37°C for 24 hours. After this time, the media was removed, and 100 μl of MTT solution (0.5mg/mL) was added to each well. The plate was incubated for 3h at 37°C. After 3h the solution was removed, and the purple solid was dissolved adding 50 μl of DMSO. The absorbance at 570 nm was read for each well.

8.12.3 Determination of cell viability assessed by ATP quantification

Dose-cytotoxicity curve of idebenone, **37** and **92** was assessed by ATP quantification using CellTiter Glo assay. In order to confirm the results obtained by MTT assay, the dose cytotoxicity curve of the best compounds was assessed by CellTiter-Glo kit. The ATP detection assay using CellTiter-Glo is more sensitive and has the least amount of interference than the MTT assays, where the use of tetrazolium is less expensive¹⁷⁰. In both cell lines, the cells were treated using the same procedure described in the Chapter 7.12.1 and 7.12.2 for HepG2 and SH-SY5Y respectively. After the incubation with the tested compound for 24. The CellTiter Glo reagent was added to each well at 50 mL, and the plate is allowed to incubate for 10 minutes at room temperature. Following incubation, luminescence is measured using a CLARIOstar plate reader. The luminescence of each well was normalized according to untreated cells

8.14 Seahorse assay

Oxygen consumption rate is measured using Seahorse Extracellular Flux (XF) 96 Analyzer (Seahorse Bioscience, North Billerica, MA, USA). The oxygen consumption rate was measured before and after adding the pharmacological agents to respiring cells. Measurement of oxygen consumption over 3 min was made repeatedly. Three measurements were made and averaged to provide reliable measurements. For the first 18 minutes, basal respiration was measured, followed by the injection of tested quinone, oligomycin (Agilent Seahorse XF ATP Real-Time) and antimycin/rotenone (Agilent Seahorse XF ATP Real-Time) for the remaining 54 minutes, divided equally for all injections.

On the day of the experiment, the cell plate was washed two times with Seahorse assay media (Agilent Seahorse XF), (low-glucose (1 g/L), supplemented with 1x Glutamax, 1x pen-strep and adjusted to pH 7.4). The cell plate and the loaded chemical cartridge were both incubated at 37°C without CO₂ for 45 minutes before the start of the experiment. To testing the activity

of quinones compounds, Rotenone was dissolved in the assay media at a concentration of 0.5 μM , and the tested compound was injected before the three inhibitors.

Before testing the quinones activity, the cell density and concentration of drugs were optimized. The day prior to the assay, the cell is seeded 25×10^4 on plates. On the day of the experiment, the media was removed, and the cell plate was washed with Seahorse twice, before incubating the plate with assay media containing rotenone 0.5 μM . After incubating the cells for 45 minutes, the machine injected sequentially 10 μM of quinones, 1.5 μM oligomycin, 1 μM Antimycin separated by periods of mixing and measurement.

8.15 Determination of Reactive Oxygen Species by CellROX®

The fluorescent dye CellROX® Green reagent (Invitrogen) was used to quantify the level of mitochondrial ROS in cells. The dye passively diffuses and accumulates into cells in non-fluorescent oxidized form. In the presence of reactive oxygen species, the dye is reduced, and it changes to a fluorescent compound. This fluorescent signal has an emission of ~ 520 nm. The method was performed as instructed by the manufacturer. Briefly, HepG2 cells were seeded in black 96-well plates, and the day of the assay the media was replaced with a fresh media containing 25 μM of Menadione or interested compounds. After the incubation for 3h in the dark, the fluorescent dye was added at a concentration of 5 μM . Subsequently, cells are washed twice with 100 μl PBS, and fluorescence signals were measured immediately in 100 μl PBS (excitation: 485 nm, emission: 520 nm). Mean background value from cell-free wells incubated dye was subtracted from signals. An increase in fluorescence represented an increase in ROS level.

8.16 Determination of H_2O_2 level by the ROS-Glo™ H_2O_2

The reagent ROS-Glo™ H_2O_2 (Promega) was used to quantify the level of H_2O_2 in cells, used as indicator of ROS generation. ROS-Glo™ H_2O_2 assay was carried out as instructed by the manufacturer. Briefly, HepG2 cells were seeded in white 96-well plates, and the day of the assay the media was replaced with 80 μL of a fresh media containing 25 μM of Menadione or tested compounds, followed by 20 μL of H_2O_2 substrate dilution buffer (containing 125 μM of H_2O_2 substrate). The plates were incubated for 4h, and after that, 100 μL of ROS-GLO detection solution was added to the plates. The plates were incubated at room temperature for

another 20 minutes. Subsequently, the luminescence signals were measured immediately using the CLARIOstar plate reader. Mean background value from cell-free wells incubated dye was subtracted from signals.

8.17 Determination of quinone reduction by WST-1

The intracellular reduction of quinones was determined using the water-soluble tetrazolium salts WST-1((2-(4-iodophenyl)-3-(4-nitrophenyl)-5-(2,4-disulfophenyl)-2H- tetrazolium (Santa Cruz Biotechnology,). The conversion of salt into the corresponding formazan dye, upon reduction by hydroquinones, was followed by reading the increase of absorbance at 450 nm using the CLARIOstar plate reader. The assay was performed as described by Tan and Berridge work¹³⁴. Menadione cell-free NQO1 enzyme solution was used as positive control. In detail, 10 μ L of 4.5 mM Menadione DMSO-solution was added to 90 μ L of NQO1 enzyme solution containing 25mM Tris-HCl pH 7.4, 0.7 mg/ml bovine serum albumin (BSA), NQO1 1 μ g/mL, and 50 μ M Menadione.

8.17.1 Quinone reduction in SH-SY5Y cell line

The day prior to the assay, cells were seeded in 96-well plates (5×10^3) in DMEM: F12 containing 1g/l glucose supplemented with 1x penicillin/streptomycin, 1x Glutamax, 2% FBS. The day after, the media was replaced with HBSS containing 450 μ M WST-1 and 25 μ M of testing compounds. Cells were incubated at 37°C and WST-1 reduction was followed over a period of 8 hours. The mean background value from cell-free wells incubated dye was subtracted from signals.

8.17.2 Quinone reduction in HepG2 cell line

The day prior to the assay cells were seeded in 96-well plates (10×10^3) in DMEM containing 1g/l glucose supplemented with 1x penicillin/streptomycin, 1x Glutamax, 2% FBS. The day after, the media was replaced with HBSS containing 450 μ M WST-1 and 25 μ M of testing compounds, with or without dicoumarol (20 μ M). Cells were incubated at 37°C and WST-1

reduction was followed over a period of 4 hours. Mean background value from cell-free wells incubated dye was subtracted from signals.

8.18 Western blot

The quantification of a specific protein was determined using western blots. Briefly, cells were lysed in an RIPA lysis buffer (50 mM Tris pH 7.4 (Sigma), 1% NP-40 (Thermo Scientific), 150 mM NaCl (Sigma), 0.25% sodium deoxycholate (Sigma), 1 mM EDTA (Sigma) for 30 min on ice.

Gel chambers were assembled and filled with separation buffer (1.5 M Tris pH 8.8, 30% acrylamide (Bio-Rad), 10% SDS (Bio-Rad), and freshly added 0.1% APS (Sigma) and 1% TEMED (Bio-Rad)). Ethanol was added on top of the gel to smoothen the border. After the hardening of the gel, ethanol was removed and washed with water. Stacking buffer (1 M Tris pH 6.8, 30% acrylamide, 10% SDS, and freshly added 0.1% APS and 1% TEMED) was poured on top and mini-protean 15-well combs (Bio-Rad) was positioned. After the hardening of stacking gel, the comb was gently removed, and gaps were thoroughly rinsed with water. Gels were placed into electrophoresis rack, and the tank was filled with running buffer (25 mM Tris, 192 mM glycine, 10 % SDS). Protein samples were denaturised for 10 minutes at 100 °C. Approximately 30ug protein supernatant was applied to each well. Electrophoresis was performed at a constant current (25 mA/gel). The gel was carefully removed from the glass, and the protein was transferred to nitrocellulose membrane. The transfer was performed at a constant voltage (150V) in a tank filled with transfer buffer (25 mM Tris, 192 mM glycine, 20 % SDS, 20% methanol) at 4°C. Membrane was washed in TBST (50 mM Tris-HCl pH 7.4, 150 mM NaCl, 0.1% Tween 20 (Sigma)). After incubation for one hour in blocking buffer (5% milk powder in PBS), membranes were subjected to primary antibodies in cold blocking buffer overnight at 4 °C. the concentration of primary antibody was 1:1000 and 1:2000 for NQO1 (Anti-NQO1, Abcam) and actin respectively. The following day, the membranes were washed with PBS before secondary antibodies were added in blocking buffer for one hour. After washing the secondary antibodies, the relative amount of protein in different bands was analysed using software Molecular Imager Gel Doc XR+ imaging system.

8.19 Induce NQO1 lipoic acid in SH-SY5Y

The cells were plated on 6 well plates at a density of 1.000.000 cells/ml and were allowed to grow for 24 h. Fresh culture medium containing various concentrations of lipoic acid (Sigma) (1mM, 2mM, 3mM, 5mM) was added, and the cells were incubated for the indicated times (24 or 48h), adding or no fresh amount of lipoic Acid after 24h. Cells treated with 0.1% DMSO alone were used as controls. After lipoic acid treatment, the cells were washed twice with PBS, detached with trypsin and were then harvested, the pellet was resuspended in RIPA buffer with protease inhibitor cocktail (Sigma) and gently mixed for 30 minutes at 4°C. After 30 minutes, the solution was centrifuged at 13,000 rpm for 13 min. Protein concentrations were determined with the BCA Protein Assay Reagent kit.

CHAPTER 9

EXPERIMENTAL SECTION

9.1 COMPUTATIONAL METHODS

9.1.2 General information

A PC 1.80 GHz Intel Xeon (8 cores), running Ubuntu 14.04 LTS was used for molecular modelling studies. Two molecular modelling software were used: Molecular Operating Environment (MOE) 2015.10 and Maestro (Schrödinger version 10).

9.1.3 Protein preparation

All target structures were downloaded from the Protein Data Bank and completed with MAESTRO (Schrödinger version 10). In all of them, all water and co-crystallised molecules were removed, except for the ligand and FADH or HEME groups. Predicting protonation states of protein residues was calculated considering a temperature of 300K and a pH of 7.

9.1.4 Pharmacophore

For NQO1 target protein (PDB: 1D4A, 2F1O, 1GG5,) a pharmacophore was built with MOE 2015.10 protein ligand interaction fingerprints (PLIF). PLIF automatically detected the potential location features (annotation points), that constitute the pharmacophore query and binding interactions. Hydrophobic areas (Hs), aromatic rings (ARs), hydrogen bond acceptors (HBAs), aromatic rings (ARs) have been used as ligand annotation points, exclusion volumes (XVOLs) were added for binding site size definition. The prepared ligand conformations, originated from commercially available database of four different vendors (SPECS, Enamine, Life Chemicals and ChemDiv), were screened for structures that match the pharmacophore query. The molecule that matched at least three essential features of the total were saved.

9.1.5 Homology modelling

The homology model was computed with the Homology Model tool of MOE 2015.10 suite. The FASTA sequence of the protein (P00156) was downloaded from the Swiss-Prot database, and was modelled on the template crystal structure (PDB: 1ntz). Protein crystal structure was prepared before the homology modelling, removing water molecules and unwanted ligands.

9.1.6 Molecular Docking

All molecular docking studies were performed Maestro (Schrödinger version 10) Glide program. Prior docking, the receptor grids were built selected the co-crystallised ligands as center and a 12 Å grid length. The docking calculations were performed with standard precision and the selected compounds poses were visually with MOE 2015.10

9.1.10 Prediction of standard reduction potential

The prediction of standard potential reduction of quinone compounds was performed using Gaussian 09. Molecular structures were optimized at the B3LYP/6-31G(d) level of theory and the presence of water was simulated using the Conductor-like Polarizable Continuum Model (CPCM).

9.2 SYNTHESIS

9.2.1 General Information

The compounds selected by virtual screening were purchased from SPECS, ChemDiv and Life Chemicals. All chemical reagents and solvents used in the synthesis were purchased from Aldrich, Alfa Aesar, Flurochem, Enamine.

9.2.2 Thin Layer Chromatography

Silica gel plates (Merck Kieselgel 60F₂₅₄) were used and were developed by the ascending method. After solvent evaporation, compounds were visualized by irradiation with UV light at 254 nm and 366 nm.

9.2.3 Purification and isolation of final products

The final products and intermediate of reactions were purified by re-crystallisation in Ethanol or flash column chromatography. The purity of synthesized compounds was assessed by UPLC-MS, meanwhile the presence of residual solvent was assessed by NMR.

9.2.4 Column Chromatography

Chromatography was performed using a Biotage Isolera™ Prime with SNAP Cartridges KP-Sil column. Samples were applied as a concentrated solution in the same eluent. Fractions containing the product were identified by TLC, combined and the solvent removed in vacuum.

9.2.5 NMR Spectroscopy

¹H and ¹³C, NMR spectra were recorded on a Bruker AVANCE 500 spectrometer (500 MHz and 75 MHz respectively) and auto-calibrated to the deuterated solvent reference peak. Chemical shifts are given in δ relative to tetramethylsilane (TMS); the coupling constants (J) are given in Hertz. TMS was used as an internal standard ($\delta = 0$) for ¹H- NMR and CDCl₃ served as an internal standard ($\delta = 77.0$) for ¹³C- NMR.

9.2.6 UPLC-MS analysis

UPLC-MS analysis was conducted on a Waters UPLC system with both Diode Array detection, and Electrospray (+'ve and -'ve ion) MS detection. The stationary phase was a Waters Acquity UPLC BEH C18 1.7um 2.1x50mm column. The mobile phase was H₂O containing 0.1% Formic acid (A) and MeCN containing 0.1% Formic acid (B). Column temperature: 40°C. Sample diluent: acetonitrile. Sample concentration 10 µg/mL. Injection volume 2 µL. Three methods were used:

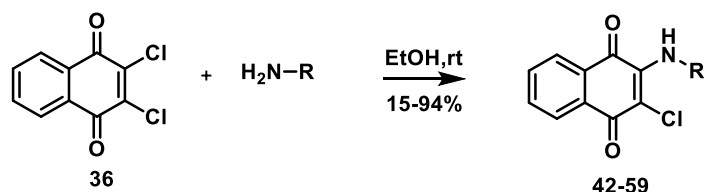
Linear gradient standard method A: 90% A (0.1 min), 90%-0% A (2.6 min), 0% A (0.3 min), 90% A (0.1 min); flow rate 0.5 mL/min.

Linear gradient standard method B: 90% A (0.1 min), 90%-0% A (2.1 min), 0% A (0.8 min), 90% A (0.1 min); flow rate 0.5 mL/min.

Linear gradient standard method C: 90% A (0.1 min), 90%-0% A (1.5 min), 0% A (1.4 min), 90% A (0.1 min); flow rate 0.5 mL/min.

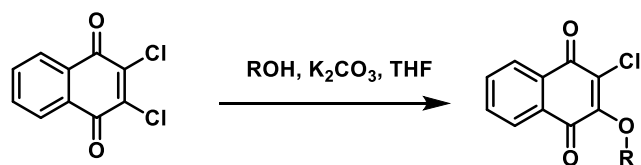
9.3 Chemistry: general procedure and compound characterization

General procedure 1: synthesis of 2-chloro-3-amino derivatives



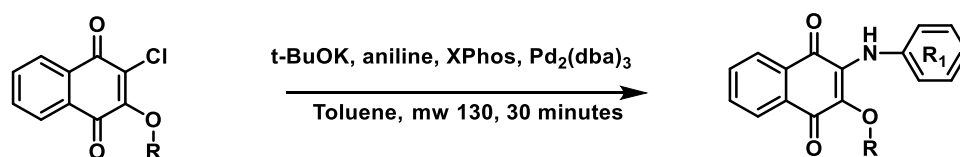
A mixture of 2,3-dichloronaphthoquinone and the corresponding amine 2 (1.5 eq) in absolute ethanol was stirred at room temperature and monitored by TLC until completion. The resulting mixture was concentrated in vacuum, and the residue was partitioned between a HCl 1 N solution and AcOEt. The organic layer was dried over anhydrous magnesium sulphate, filtered and concentrated. The crude product was purified using silica gel column chromatography, Biotage Isolera One system, using nHexane/EtOAc as eluent to afford the pure compound. In same reactions, the precipitated pure product was collected by vacuum filtration

General procedure 2 : synthesis of 2-alkoxy-3-chloro naphthoquinones



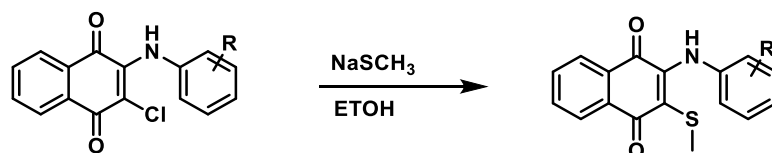
A mixture of 2,3-dichloronaphthoquinone, the corresponding alcohol (1.2 eq) and K_2CO_3 (1.2 eq) in THF (0.2 M) was stirred at room temperature for 12 h. The resulting mixture was concentrated in vacuum, and the residue was partitioned between a HCl 1N solution and AcOEt. The combined organic layers were dried over anhydrous magnesium sulfate, filtered and concentrated. The crude product was purified using silica gel column chromatography Biotage Isolera One system, using nHexane/EtOAc as eluent to afford the pure compound. . When possible, the precipitated pure product was collected by vacuum filtration without further purification

General procedure 3 : synthesis of 2-alkoxy-3-benzamine naphthoquinones



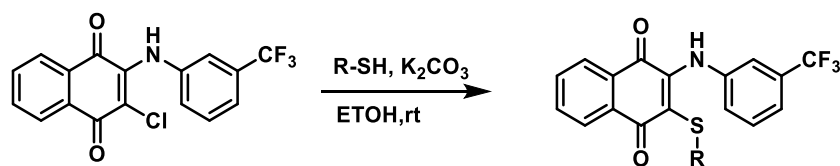
A microwave tube-with a magnetic stir bar was charged with t-BuOK (1.5 eq) naphthoquinone (1.0 eq), XPhos (10 mol %), Pd₂(dba)₃ (10 mol %) and the appropriate aniline (1.5 eq), sealed with a septum, and degassed by alternating vacuum evacuation and nitrogen (three times) before a anhydrous toluene (0.3 M) was added by a syringe. The reaction mixture was irradiated at the MW for 30 min at 130°C. After the reaction was complete, the mixture was dissolved in AcOEt, filtered on Celite and washed with HCl 2 N. The organic layer was dried over anhydrous magnesium sulfate, filtered and concentrated. The crude product was purified using silica gel column chromatography, Biotage Isolera One system, using nHexane/EtOAc as eluent to afford the final compound.

General procedure 4 : synthesis of 2-methylthio -3-benzamine naphthoquinones



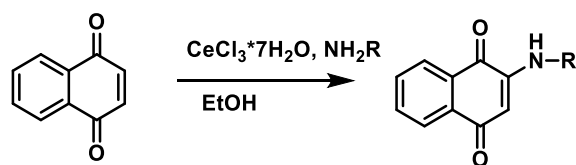
To a mixture of 2-chloro-3-amino-naphthoquinone (1 eq) in EtOH (0.3 M), sodium methanethiolate (2 eq) was added, and the reaction was stirred at room temperature for 3 h The resulting mixture was concentrated in vacuum, and the residue was partitioned between a water and AcOEt. The combined organic layers was dried over anhydrous magnesium sulfate, filtered and concentrated. The crude product was purified using silica gel column chromatography, Biotage Isolera One system, using nHexane/EtOAc as eluent to afford the final compound

General procedure 5 synthesis of 2-sulfanyl -3-benzammine naphthoquinones



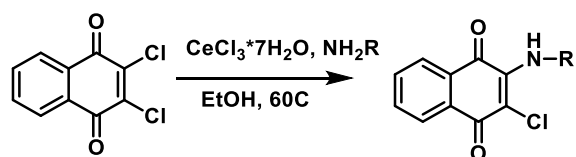
To a mixture of 2-chloro-3-((3-(trifluoromethyl) phenyl) amino) naphthalene-1,4-dione (1 eq) in EtOH appropriate Thiols (2 eq) and K_2CO_3 (2 eq) were added, and the reaction was stirred at room temperature. The resulting mixture was concentrated in vacuum, and the residue was partitioned between a water and AcOEt. The combined organic layers was dried over anhydrous magnesium sulfate, filtered and concentrated. The crude product was purified using silica gel column chromatography, Biotage Isolera One system, using nHexane/EtOAc as eluent to afford the final compound.

General procedure 6: synthesis of 2-aminonaphthalene-1,4-dione



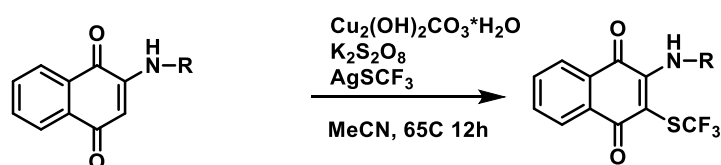
The 1,4 naphthoquinone (1.0 eq) was stirred with cerium trichloride heptahydrate (1.5 eq) in EtOH at room temperature. After 15 minutes, the appropriate aniline (1.5 eq) was added, and the reaction was stirred for 12 h. The resulting mixture was concentrated in vacuum, and the residue was partitioned between satd. aq. NH_4Cl and AcOEt. The combined organic layers were washed with HCl 6N and dried over anhydrous magnesium sulfate, filtered and concentrated. The crude product was purified using silica gel column chromatography, Biotage Isolera One system, using nHexane/EtOAc as eluent to afford the final compound. In some reactions, the precipitated pure product was collected by vacuum filtration.

General procedure 7: synthesis of 2-chloro-3-aminonaphthalene-1,4-dione



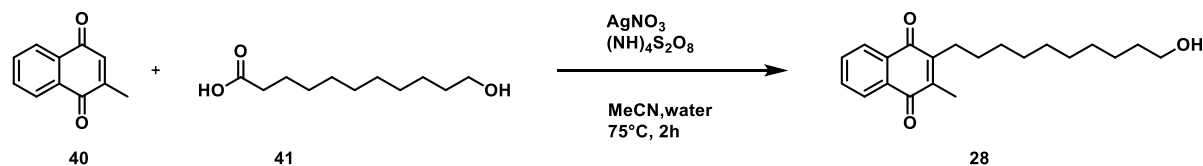
The 2-chloronaphthalene-1,4-dione (1.0 eq) was stirred with cerium trichloride heptahydrate (1.5 eq) in EtOH at room temperature. After 15 minutes, the appropriate aniline (1.5 eq) was added, and the reaction was stirred for 24 h at 60°C . The reaction mixture was cooled and the precipitated was collected by vacuum filtration.

General procedure 8: synthesis of 2-chloro-3-aminonaphthalene-1,4-dione



A Schlenk tube equipped with a magnetic stir bar was charged with naphthoquinones (1.0 eq), $\text{Cu}_2(\text{OH})_2\text{CO}_3 \cdot \text{H}_2\text{O}$ (1.5 eq), AgSCF_3 (3.0 eq) and $\text{K}_2\text{S}_2\text{O}_8$ (3.0 eq). The tube was sealed with a septum, and degassed by alternating vacuum evacuation and nitrogen (three times) before anhydrous CH_3CN (0.3 M) was added by a syringe. The mixture was stirred at 65°C overnight for 12 h. The solution was then cooled to room temperature and a satd. aq. NH_4Cl solution was added. The resulting mixture was filtered by Celite, eluted with DCM. Separated the organic layers, the water phase was extracted with DCM two times. The combined organic phases were dried over anhydrous magnesium sulfate, filtered and concentrated. The crude product was purified using silica gel column chromatography, Biotage Isolera One system, using nHexane/EtOAc as eluent to afford the final compound.

Synthesis of 2-(10-hydroxydecyl)-3-methylnaphthalene-1,4-dione (**28**)



To a solution of **40** (1 eq in acetonitrile/water 5 ml 4/1) was added 11-mono-carboxylic acids **41** (1.5 eq) and AgNO_3 (0.3 eq). The mixture was heated to 75°C and a solution of $\text{K}_2\text{S}_2\text{O}_8$ (2 eq) in distilled water 3mL was added dropwise over 10 minutes, then the reaction mixture was stirred for another 90minutes. The resulting mixture was cooled, evaporated and the residue was extracted with CH_2Cl_2 . The organic layer was washed with water, then dried over anhydrous Na_2SO_4 and evaporated under reduced pressure. The crude product was purified by flash column chromatography, Biotage Isolera One system, Cartridge: ZIP KP 20g, using nHexane/EtOAc, as eluent to afford the title compound.

T.L.C system: n-hexane-EtOAc 8:2 v/v, Rf: 0.62

Yellow solid

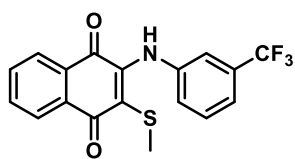
Yield: 30%

Purity: 95 %

$^1\text{H-NMR}$ (500 MHz, CDCl_3) δ ppm 8.12-8.10 (m, 2H, ArH), 7.33-7.71 (m, 2H, ArH), 3.67 (t, $J = 6.8$ Hz, 2H, CH_2OH), 2.66 (t, $J = 7.4$ Hz, 2H, CH_2), 2.22 (s, 3H, CH_3), 1.60-1.20 (m, 16H, CH_2).

$^{13}\text{C-NMR}$ (125 MHz CDCl_3), δ ppm 181.2, 180.4 (C=O), 144.4, 140.2 (C, C- aromatic), 135.0, 134.7, 132.8, 132.4, 126.0, 125.4 (CH, C-aromatic), 64.3 (OH), 32.4, 29.6, 28.5, 28.0, 27.7, 24.4, 23.3, 22.5, 21.4 (CH_2), 14.0 (CH_3)

2-(methylthio)-3-((3-(trifluoromethyl) phenyl) amino) naphthalene-1,4-dione (37)



General procedure 4

orange solid

T.L.C system: n-hexane-EtOAc 8:2 v/v, Rf: 0.63

Purification column chromatography hexane/AcOEt

Yield: 75%

Purity: 100 %

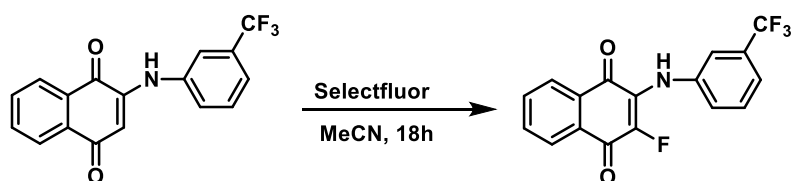
UPLC-MS method C: 2.46 MS (ESI)+: 364[M+H] +

¹H-NMR (500 MHz, DMSO) δ: 8.16 (dd, *J* = 7.6, 1.4 Hz, 1H, ArH), 8.10 (dd, *J* = 7.6, 1.4 Hz, 1H, ArH), 7.83 (s, 1H, NH), 7.75 (td, *J* = 7.5, 1.4 Hz, 1H, ArH), 7.72 – 7.66 (m, 1H, ArH), 7.45 (d, *J* = 7.9 Hz, 1H, ArH), 7.39 (d, *J* = 7.8 Hz, 1H, ArH), 7.26 (d, *J* = 3.3 Hz, 1H, ArH), 7.16 (dt, *J* = 8.0, 1.4 Hz, 1H, ArH), 2.12 (s, 3H, CH₃).

¹³C-NMR (125 MHz DMSO, δ 180.9, 180.3 (C=O), 142.9, 138.6 (C, C aromatic), 134.7 (CH, C-aromatic), 133.4 (C, C aromatic), 133.1, 131.0 (CH, C-aromatic), 130.8 (C, C aromatic), 130.4, 128.9, 126.8, 124.9, 124.6, 121.6, 120.8, 118.5 (CH, C-aromatic), 17.9(CH₃).

¹⁹F NMR (471 MHz, CDCl₃) δ -62.5.

Synthesis of 2-fluoro-3-((3-(trifluoromethyl) phenyl) amino) naphthalene-1,4-dione (38)



To a mixture of 2-((3-(trifluoromethyl) phenyl) amino) naphthalene-1,4-dione (1 eq) was dissolved in anhydrous MeCN (0.2 M) Selectfluor (2 eq) was added and the reaction was stirred for 18h at room. The resulting mixture was concentrated in vacuum and the residue was partitioned between satd. aq. NH₄Cl and AcOEt. The combined organic phases were dried over anhydrous magnesium sulfate, filtered and concentrated. The crude product was purified using silica gel column chromatography, Biotage Isolera One system, using nHexane/EtOAc, as eluent to afford the title compound.

Orange solid

T.L.C system: n-hexane-EtOAc 8:2 v/v, R_f: 0.44

Yield: 25%

Purity: 93%

UPLC-MS method c: Rt: 2.709, MS (ESI)-: 332.1-334.1[M-H]-

¹H-NMR (500 MHz, CDCl₃) δ ppm 8.17 (dd, *J* = 7.6, 1.3 Hz, 1H, ArH), 8.13 (dd, *J* = 7.7, 1.3 Hz, 1H, ArH), 7.80 (td, *J* = 7.5, 1.3 Hz, 1H, ArH), 7.72 (td, *J* = 7.6, 1.3 Hz, 1H, ArH), 7.48 (t, *J* = 7.9 Hz, 1H, ArH), 7.43 (d, *J* = 7.8 Hz, 1H, ArH), 7.37 (m, 1H, ArH), 7.21 – 7.18 (m, 1H, ArH).

¹³C-NMR (125 MHz CDCl₃), δ ppm 182.2, 182.1 (C=O), 175.9(C, C aromatic), 143.6, 141.5(C, C aromatic), 138.5, 135.3(CH, C-aromatic), 133.4(C, C aromatic), 131.3, 130.9, 129.4, 128.7, 126.8, 125.2, 121.6, 118.9(CH, C-aromatic).

¹⁹F NMR (471 MHz, CDCl₃) δ -62.13. 131.22

2-((3-(trifluoromethyl)phenyl)amino)-3-((trifluoromethyl)thio)naphthalene-1,4-dione (39)



General procedure 8

orange solid

T.L.C system: n-hexane-EtOAc 8:2 v/v, Rf: 0.28

Purification: column chromatography hexane/AcOEt

Yield: 70%

Purity: 100 %

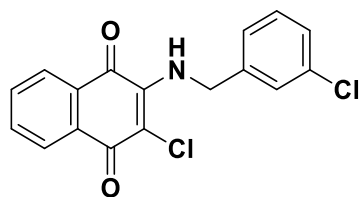
UPLC-MS method C: 2.48 MS (ESI)+: 418[M+H] +

¹H-NMR (500 MHz, DMSO) δ: 8.20 (dd, *J* = 7.8, 1.3 Hz, 1H, ArH), 8.15 (s, 1H, ArH), 8.11 (dd, *J* = 7.7, 1.3, 1H, ArH), 7.78 (td, *J* = 7.6, 1.4 Hz, 1H, ArH), 7.68 (td, *J* = 7.6, 1.3 Hz, 1H, ArH), 7.55 – 7.51 (m, 1H, NH), 7.48 (t, *J* = 7.8 Hz, 1H, ArH), 7.36 (d, *J* = 1.9 Hz, 1H, ArH), 7.28 (dd, *J* = 7.9, 1.9 Hz, 1H, ArH).

¹³C-NMR (125 MHz DMSO, δ: δ 180.3, 179.8(C=O), 150.4, 138.5 (C, C aromatic), 135.8 (CH, C-aromatic), 133.2 (C, C aromatic), 133.1, 129.9 (CH, C-aromatic), 129.8 (C, C aromatic), 128.9, 127.7, 127.3, 124.1, 122.8 (CH, C-aromatic).

¹⁹F NMR (471 MHz, CDCl₃) δ -41.3, -62.9.

2-chloro-3-((3-Chlorobenzyl) amino) naphthalene-1,4-dione (42)



General procedure 1;

brown solid

T.L.C system: n-hexane-EtOAc 8:2 v/v, Rf: 0.42

Purification: re-crystallation from EtOH

Yield: 73%

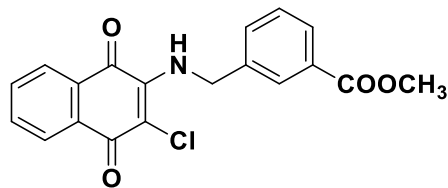
Purity: 99 %

UPLC-MS method B: Rt: 2.709, MS (ESI)-: 332.1-334.1[M-H]-

¹H-NMR (500 MHz, CDCl₃) δ 8.23-8.21 (m, 1H, ArH), 8.18 (d, J=7.7, Hz 1H, ArH), 8.08 (d, J = 7.6, Hz, 1H, ArH), 7.64– 7.62 (m, 1H, ArH), 7.76 (dt, J = 6.3, 1.4 Hz, 1H, ArH), 7.66 (t, J = 7.7, 1.2 Hz, 1H, ArH), 7.34-7.33 (m, 1H, ArH), 7.23-7.22 (m, 1H, ArH), 5.05 (s, 2H, CH₂)

¹³C-NMR (125 MHz CDCl₃) δ : 176.9, 176.1 (C=O), 140.1, 135.0 (C, C aromatic), 134.8, 134.7, 132.7, 132.5, 130.3, 129.7, 128.2, 127.8, 127.6, 126.9, 125.6 (CH, C-aromatic), 48.1(CH₂).

Methyl 3-(((3-chloro-1,4-dioxo-1,4-dihydronaphthalen-2-yl) amino) methyl) benzoate (43)



General procedure 1;

red solid

T.L.C system: n-hexane-EtOAc 8:2 v/v, Rf: 0.58

Purification: re-crystallation from EtOH

Yield: 90%

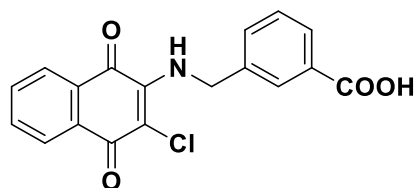
Purity: 100%

UPLC-MS method B: Rt: 2.507, MS (ESI)-: 356.2-358.2[M-H]-

¹H-NMR (500 MHz, CDCl₃) δ: 8.18 (d, J=7.6, Hz 1H, ArH), 8.08 (d, J = 7.6, 1, 3H, ArH), 7.78 (dt, J = 7.6, 1.2 Hz, 1H, ArH), 7.68 (dt, J = 7.8, 1.2 Hz, 1H, ArH), 7.43 (d, J=8.8 2H), 7.23-7.22 (m, 1H, ArH), 5.35 (s, 2H, CH₂), 3.94 (s, 1H, CH₃)

¹³C NMR (DMSO-d₆), δ: 176.9, 176.1 (C=O), 166.6(C=O), 148.2, 136.1 (C, C aromatic), , 132.7, 132.6, 130.3, 129.8, 127.2, 126.9 (CH, C-aromatic), 52.2(CH₂), 48.3(CH₃).

3-(((3-Chloro-1,4-dioxo-1,4-dihydronaphthalen-2-yl) amino) methyl) benzoic acid (44)



General procedure 1;

red solid

T.L.C system: n-hexane-EtOAc 8:2 v/v, Rf: 0.12

Purification: re-crystallation

Yield: 71%

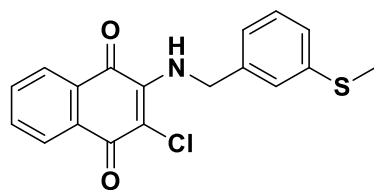
Purity: 100 %

UPLC-MS method B: Rt: 1.939, MS (ESI)+: 280.04[M+H] +

¹H-NMR (500 MHz, CDCl₃), δ: 10.12 (s, 1H, COOH) 8.18 (d, J=7.6, Hz, 1H, ArH), 8.08 (d, J = 7.6, 1, 3H, ArH), 7.78 (dt, J = 7.6, 1.2 Hz, 1H, ArH), 7.68 (dt, J = 7.8, 1.2 Hz, 1H), 7.43 (d, J=8.8 2H, ArH), 7.23-7.22 (m, 1H, NH), 5.45 (s, 2H, CH₂)

¹³C-NMR (125 MHz CDCl₃), δ: 176.9, 176.1 (C=O), 166.6(C=O), 148.2, 136.1 (C, C aromatic), 132.7, 132.6, 130.3, 129.8, 127.2, 126.9 (CH, C-aromatic), 52.2(CH₂).

2-chloro-3-((3-(methylthio) benzyl) amino) naphthalene-1,4-dione (45)



General procedure 1;

orange solid

T.L.C system: n-hexane-EtOAc 8:2 v/v, Rf: 0.31

Purification: column chromatography using as eluent nHexane/EtOAc

Yield: 44%

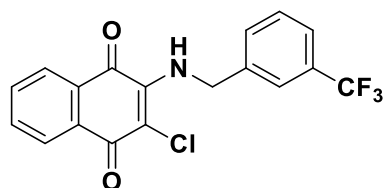
Purity: 92%

UPLC-MS method B: Rt: 2.706, MS (ESI)-: 344.2-146.1[M-H]-

¹H-NMR (500 MHz, CDCl₃) δ: 8.13-8.11 (m, 1H, ArH), 8.08 (d, J = 7.7, 1, 1H, ArH), 7.97 (d, J = 7.8 Hz, 1H, ArH), 7.75-7.73 (m, 1H, ArH), 7.67 (dt, J = 7.1, 1.1 Hz, 1H, ArH), 7.57 (dt, J = 7.8, 1.1 Hz, 1H, ArH), 7.20 (m, 1H, ArH), 7.23-7.22 (m, 1H, ArH), 4.94 (s, 2H, CH₂), 4.67 (s, 3H, CH₃)

¹³C-NMR (125 MHz CDCl₃), δ: 180.4, 176.1 (C=O), 138.5 (C, C aromatic), 134.9, 134.6 (CH, C-aromatic), 134.6 (C, C aromatic), 132.6, 130.9, 128.2, 127.8, 127.1, 126.8 (CH, C-aromatic), 58.4 (CH₂), 18.4 (CH₃).

2-chloro-3-((3-(trifluoromethyl) benzyl) amino) naphthalene-1,4-dione (46)



General procedure 1;

red solid

T.L.C system: n-hexane-EtOAc 8:2 v/v, Rf: 0.52

Purification: re-crystallation in EtOH

Yield: 66%

Purity: 100 %

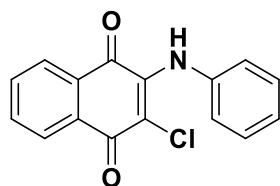
UPLC-MS method B: Rt: 2.306, MS (ESI)-: 368.2-370.2[M-H]-

¹H-NMR (500 MHz, CDCl₃) δ: 8.20(dd, J=7.78,1.0 1H, ArH), 8.09 (dd, J = 7.7, 1.1, 1H, ArH), 7.79 (dt, J = 7.6, 1.3 Hz, 1H, ArH), 7.60 (dt, J = 7.64,1.1 Hz, 1H, ArH), 7.20 (m, 1H, ArH),7.62-7.60 (m, 2H, ArH), 7.56-7.54 (m, 2H, ArH), 6.28(bs, 1H, NH) 5.15 (dd, 2H, CH₂)

¹³C-NMR (125 MHz CDCl₃), δ: 180.4, 176.6 (C=O), 143.4, 135.1 (C, C aromatic), 132.2, 132.6, 129.9, 126.2, 127.8, 127.0, 126.8(CH, C-aromatic), 48.2 (CH₂).

¹⁹F NMR (471 MHz, CDCl₃) δ -62.67.

2-chloro-3-(phenylamino) naphthalene-1,4-dione (47)



General procedure 1;

orange solid

T.L.C system: n-hexane-EtOAc 8:2 v/v, Rf: 0.52

Purification: column chromatography using as eluent nHexane/EtOAc

Yield: 38%

Purity: 100 %

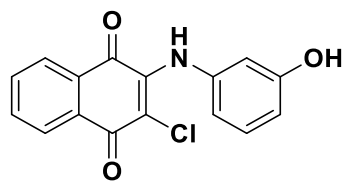
UPLC-MS method B: Rt: 2.535, MS (ESI)-: 284.0-285.8[M-H]-

¹H-NMR (500 MHz, CDCl₃) δ: 8.09(d, J=7.67,1.0 1H, ArH), 7.97 (dd, J = 7.44, 1.1, 1H, ArH), 7.68 (dt, J = 8.2, Hz, 1H, ArH), 7.57 (t, J = 6.86,1.1 Hz, 1H, ArH), 7.20 (m, 1H, ArH), 7.33-7.30 (m, 2H, ArH), 7.27-7.26 (m, 2H, ArH), 6.15 (bs, 1H, NH)

¹³C-NMR (125 MHz CDCl₃), δ: 180.4 (C=O), 137.9 (C, C aromatic), 134.95(CH, C-aromatic), 132.6 (C, C aromatic), 132.5, 129.8 (CH, C-aromatic), 129.1 (C, C aromatic), 128.1, 127.7, 126.8 (CH, C-aromatic).

2-chloro-3-((3-hydroxyphenyl)

amino) naphthalene-1,4-dione (48)



General procedure 1;

brown solid

T.L.C system: n-hexane-EtOAc 8:2 v/v, Rf: 0.35

Purification: column chromatography using as eluent nHexane/EtOAc

Yield: 15%

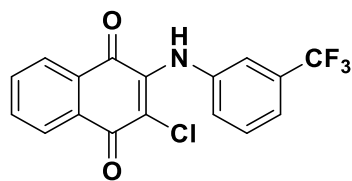
Purity: 94 %

UPLC-MS method B: Rt: 1.939, MS (ESI)⁺: 280.04[M+H]⁺

¹H-NMR (500 MHz, CDCl₃) δ: 9.08(s, 1H, OH), 8.11-8.09 (m, 1H, ArH), 8.05-8.02 (m, 1H, ArH), 7.93-7.90 (m, 1H, ArH), 7.87 (dt, J = 6.58, 1.51 Hz, 1H, ArH), 7.82 (dt, J = 7.31, 1 Hz, 1H, ArH), 7.72(t, J=7.7, 1H, ArH), 7.10(t=7.1 1H, ArH), 6.74-6.70(m, 1H, ArH)

¹³C-NMR (125 MHz CDCl₃), δ: 180.4 (C=O), 137.8 (C, C aromatic), 134.9(CH, C-aromatic), 132.6 (C, C aromatic), 129.6 (C, C aromatic), 129.1, 128.1, 127.7, 126.7, 125.6(CH, C-aromatic).

2-chloro-3-((3-(trifluoromethyl) phenyl) amino) naphthalene-1,4-dione (49)



General procedure 1;

red solid

T.L.C system: n-hexane-EtOAc 8:2 v/v, Rf: 0.48

Purification: re-crystallation from EtOH

Yield: 36%

Purity: 94 %

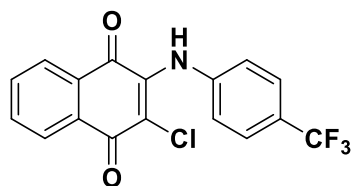
UPLC-MS method B: Rt: 2.314 MS (ESI)-: 352.2-354.1[M-H]-

¹H-NMR (500 MHz, CDCl₃) δ: 7.94-7.92(m, 1H, ArH), 7.66-7.62 (m, 2H, ArH), 7.53 (s, 1H, ArH), 7.49-7.45 (m, 2H, ArH), 7.36-7.35 (m, 2H, ArH),

¹³C-NMR (125 MHz CDCl₃), δ: 178.4 (C=O), 147.6 (C, C aromatic), 134.7, 134.3, 134.2 (CH, C-aromatic), 132.5 (C, C aromatic), 129.6, 127.8, 127.4, 124.8 (CH, C-aromatic),

¹⁹F NMR (471 MHz, CDCl₃) δ -62.82.

2-chloro-3-((4-(trifluoromethyl) phenyl) amino) naphthalene-1,4-dione (50)



General procedure 1;

red solid

T.L.C system: n-hexane-EtOAc 8:2 v/v, Rf: 0.48

Purification: re-crystallation from EtOH

Yield: 40%

Purity: 88%

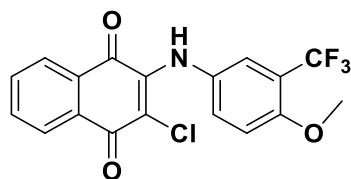
UPLC-MS method B: Rt: 2.412 MS (ESI)-: 352.2-354.4[M-H]-

¹H-NMR (500 MHz, CDCl₃) δ: 8.25(d, J=6.42 Hz, 1H, ArH), 8.18 (d=7.25, 2H, ArH), 7.83 (dt, J = 7.7 Hz, 1H, ArH), 7.78 (dt, J = 7.7,1 Hz, 1H, ArH),7.66 (d, J=7.9,2H, ArH), 7.16(d, J=8.2 2H, ArH)

¹³C-NMR (125 MHz CDCl₃), δ: 180.1, 176.2 (C=O), 138.5 (C, C aromatic), 134.4, 132.5(CH, C-aromatic), 132.6 (C, C aromatic), 130.6, 130.9, 129.2, 127.8, 127.3, 126.8, 125.6 (CH, C-aromatic).

¹⁹F NMR (471 MHz, CDCl₃) δ -62.13.

2-chloro-3-((4-methoxy-3-(trifluoromethyl) phenyl) amino) naphthalene-1,4-dione (51)



General procedure 1;

brown solid

T.L.C system: n-hexane-EtOAc 8:2 v/v, Rf: 0.55

Purification: column chromatography using as eluent nHexane/EtOAc

Yield: 34%

Purity: 100 %

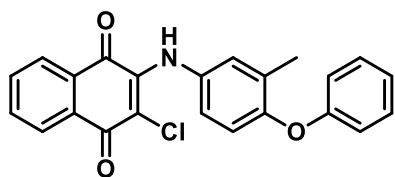
UPLC-MS method B: Rt: 2.408, MS (ESI)-: 382.2-384.1[M-H]-

¹H-NMR (500 MHz, CDCl₃) δ: 8.24 (d, J=7.11Hz, ArH), 8.16 (d=7.05, 2H, ArH), 7.81 (dt, J = 7.7 Hz, 1H, ArH), 7.73 (dt, J = 7.7,1 Hz, 1H, ArH), 7.62 (bs,1H, NH) ,7.37(d, J=7.9,2H, ArH), 7.26(d, J=8.2 1H, ArH), 3.97(s,1H, CH₃)

¹³C-NMR (125 MHz CDCl₃), δ: 180.3, 179.0 (C=O), 138.5 (C, C aromatic), 135.15, 133.04, 129.54, 127.21, 127.04, 123.92, 111.87(CH, C-aromatic), 56.27 (CH₃).

¹⁹F NMR (471 MHz, CDCl₃) δ -62.66.

2-chloro-3-(3-methyl-4-phenoxyphenoxy) naphthalene-1,4-dione (52)



General procedure 1;

red solid

T.L.C system: n-hexane-EtOAc 8:2 v/v, Rf: 0.69

Purification: column chromatography using as eluent nHexane/EtOAc

Yield: 32%

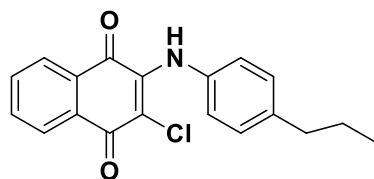
Purity: 94%

UPLC-MS method B: Rt: 2.700, MS (ESI)-: 280.04[M-H]-

¹H-NMR (500 MHz, CDCl₃) δ: 8.14 (dd, J = 7.7, 0.9 Hz, 1H, ArH), 8.07 (dd, J = 7.7, 0.9 Hz, 1H, ArH), 7.72 (td, J = 7.6, 1.3 Hz, 1H, ArH), 7.65 (td, J = 7.6, 1.3 Hz, 1H, ArH), 7.54 (s, 1H, ArH), 7.34 (d, J = 2.6 Hz, 1H, ArH), 7.31 – 7.23 (m, 2H, ArH), 7.10 (dd, J = 8.8, 2.7 Hz, 1H, ArH), 6.96 – 6.89 (m, 2H, ArH), 6.84 (d, J = 8.8 Hz, 1H, ArH), 1.47 (s, 3H, CH₃).

¹³C-NMR (125 MHz CDCl₃), δ: 179.5 (C=O), 138.5, 135.2 (C, C aromatic), 133.4, 133.2, 130.0, 129.0 (CH, C-aromatic), 127.3 (C, C aromatic), 127.1, 123.3, 120.5, 119.2 (CH, C-aromatic), 17.3 (CH₃).

2-chloro-3-((4-propylphenyl) amino) naphthalene-1,4-dione (53)



General procedure 1;

red solid

T.L.C system: n-hexane-EtOAc 8:2 v/v, Rf: 0.45

Purification: re-crystallation from EtOH

Yield: 38%

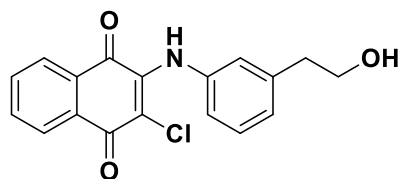
Purity: 90%

UPLC-MS method B: Rt: 2.704, MS (ESI)-: 280.04[M+H] +

¹H-NMR (500 MHz, CDCl₃) δ: 8.24(d, J=6.88 Hz, 1H, ArH), 8.14 (d, J=8.11 Hz, 1H, ArH), 7.85-7.83(m, 1H, ArH), 7.79 (dt, J = 7.5,1.70 Hz, 1H, ArH), 7.72 (dt, J = 7.4,1.4 Hz, 1H, ArH),7.19 (d, J=7.9 Hz, 2H, ArH), 7.16 (d, J=8.8 Hz 2H, ArH), 2.63(t, J=7.8 Hz, CH₂),1.72-1.60 (m, 2H, CH₂), 0.99(d, J=7.3 Hz, CH₃)

¹³C-NMR (125 MHz CDCl₃), δ: 177.4 (C=O), 140.5, 135.0 (C, C aromatic), 134.7, 132.9, 132.7, 129.9, 128.4(CH, C-aromatic), 127.8 (C, C aromatic), 127.1, 127.0, 124.3, 124.1(CH, C-aromatic), 37.5, 24.5(CH₂), 13.8(CH₃).

2-chloro-3-((3-(2-hydroxyethyl) phenyl) amino) naphthalene-1,4-dione (54)



General procedure 1;

red solid

T.L.C system: n-hexane-EtOAc 8:2 v/v, Rf: 0.10; n-hexane-EtOAc 2:8 v/v, Rf: 0.69

Purification: column chromatography using as eluent nHexane/EtOAc

Yield: 31%

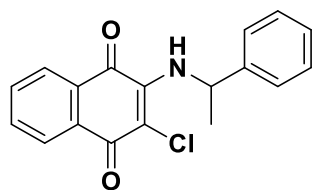
Purity: 94%

UPLC-MS method B: Rt: 1.962, MS (ESI)-: 328.2-330.2[M-H]-

¹H-NMR (500 MHz, CDCl₃): 8.22 (dd, J = 7.7, 0.9 Hz, 1H, ArH), 8.14 (dd, J = 7.6, 0.9 Hz, 1H, ArH), 7.78 (td, J = 26.4, 16.3, 1.3 Hz, 1H, ArH), 7.76 – 7.59 (m, 2H, ArH), 7.24 (d, J = 8.3 Hz, 2H, ArH), 7.06 (d, J = 8.2 Hz, 2H, ArH), 3.91 (t, J = 6.5 Hz, 2H, CH₂), 2.92 (t, J = 6.5 Hz, 2H, CH₂).

¹³C-NMR (125 MHz CDCl₃), δ: 180.5, 177.4 (C=O), 141.5, 136.2, 135.8(C, C aromatic), 135.1, 133.0(CH, C-aromatic), 132.6, 129.9(C, C aromatic), 129.0, 127.1, 127.0, 124.5(CH, C-aromatic), 63.5(CH₂), 38.7 (CH₃).

2-chloro-3-((1-phenylethyl) amino) naphthalene-1,4-dione (55)



General procedure 1;

orange solid

T.L.C system: n-hexane-EtOAc 8:2 v/v, Rf: 0.62

Purification: column chromatography using as eluent nHexane/EtOAc

Yield: 35%

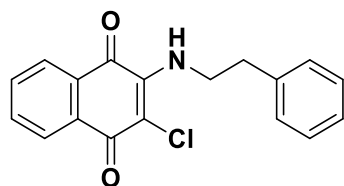
Purity: 100 %

UPLC-MS method B: Rt: 2.445, MS (ESI)-: 312.1-314.1 [M-H]-

¹H-NMR (500 MHz, CDCl₃) δ : 8.15 – 7.95 (m, 2H, ArH), 7.95 (dd, J = 7.7, 0.8 Hz, 1H, ArH), 7.64 – 7.56 (m, 1H, ArH), 7.56 – 7.46 (m, 1H, ArH), 7.31 – 7.25 (m, 2H, ArH), 7.20 (dt, J = 7.0, 2.4 Hz, 1H, ArH), 5.80 – 5.65 (m, 1H, ArH), 1.57 (d, J = 6.7 Hz, 3H, CH₃).

¹³C-NMR (125 MHz CDCl₃), δ : 180.5, 176.9(C=O), 143.8(C, C aromatic), 134.9, 132.6(CH, C-aromatic), 132.5, 129.8 (C, C aromatic), 128.9, 127.6, 126.9, 125.7(CH, C-aromatic), 53.4 (CH₂), 24.6 (CH₃).

2-chloro-3-(phenethylamine) naphthalene-1,4-dione (56)



General procedure 1;

red solid

T.L.C system: n-hexane-EtOAc 8:2 v/v, Rf: 0.59

Purification: re-crystallation from EtOH

Yield: 76%

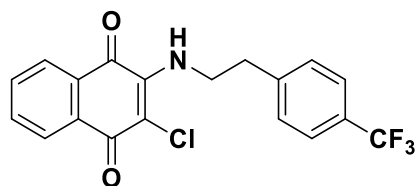
Purity: 100 %

UPLC-MS method B: Rt: 2.458, MS (ESI)-: 312.2-314.1 [M-H]-

¹H-NMR (500 MHz, CDCl₃) δ: 8.17 (dd, J = 7.7, 0.8 Hz, 1H, ArH), 8.04 (dd, J = 7.7, 0.9 Hz, 1H, ArH), 7.75 (td, J = 7.6, 1.3 Hz, 1H, ArH), 7.64 (td, J = 7.6, 1.2 Hz, 1H, ArH), 7.36 (t, J = 7.3 Hz, 2H, ArH), 7.27 (d, J = 8.1 Hz, 2H, ArH), 6.12 (s, 1H, NH), 4.15 (dd, J = 13.9, 6.9 Hz, 2H, CH₂), 3.02 (t, J = 7.2 Hz, 2H, CH₂).

¹³C-NMR (125 MHz CDCl₃), δ: 180.4 (C=O), 137.7 (C, C aromatic), 134.9, 134.7, 132.7 (CH, C-aromatic), 132.4 (C, C aromatic), 128.9, 128.8, 127.8, 126.9, 126.8, 126.8 (CH, C-aromatic), 46.0, 37.3 (CH₂).

2-chloro-3-((4-(trifluoromethyl) phenethyl) amino) naphthalene-1,4-dione (57)



General procedure 1;

orange solid

T.L.C system: n-hexane-EtOAc 8:2 v/v, Rf: 0.59

Purification: re-crystallation from EtOH

Yield: 78%

Purity: 88%

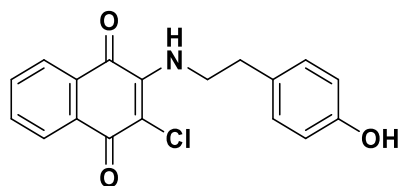
UPLC-MS method B: Rt: 2.525, MS (ESI)-: 380.2-382.2[M-H]-

¹H-NMR (500 MHz, CDCl₃) δ: 8.18 (dd, J = 7.7, 0.9 Hz, 1H, ArH), 8.05 (dd, J = 7.7, 0.9 Hz, 1H, ArH), 7.76 (td, J = 7.6, 1.3 Hz, 1H, ArH), 7.66 (td, J = 7.6, 1.3 Hz, 1H, ArH), 7.61 (m, 2H, ArH), 7.39 (d, J = 8.0 Hz, 2H), 6.10 (s, 1H, NH), 4.16 (dd, J = 14.3, 6.7 Hz, 2H, CH₂), 3.09 (t, J = 7.2 Hz, 2H, CH₂).

¹³C-NMR (125 MHz CDCl₃), δ: :180.4 (C=O), 137.7(C, C aromatic), 135.0, 134.7, 132.6 (CH, C-aromatic), 132.4(C, C aromatic), 128.9, 127.5, 127.3, 126.9, 126.5, 126.3, 125.3(CH, C-aromatic), 46.0, 37.3 (CH₂).

¹⁹F NMR (471 MHz, CDCl₃) δ -62.49.

2-chloro-3-((4-hydroxyphenethyl) amino) naphthalene-1,4-dione (58)



General procedure 1;

brown solid

TLC system n-hexane/AcOEt 2:8 v/v Rf:0.69

Purification: re-crystallation from EtOH

Yield: 69%

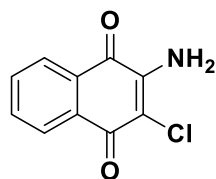
Purity: 92%

UPLC-MS method B: Rt: 2.055 MS (ESI)-: 228.1-330.2[M-H]-

¹H-NMR (500 MHz, CDCl₃) δ: 8.08 (d, J = 7.6 Hz, 1H, ArH), 7.94 (d, J = 7.2 Hz, 1H, ArH), 7.65 (d, J = 7.5 Hz, 1H, ArH), 7.56 (d, J = 6.7 Hz, 1H, ArH), 7.04 (d, J = 8.4 Hz, 2H, ArH), 6.73 (d, J = 8.4 Hz, 2H, ArH), 6.02 (s, 1H, NH), 4.00 (dd, J = 13.7, 6.8 Hz, 2H, CH₂), 2.85 (t, J = 7.1 Hz, 2H, CH₂).

¹³C-NMR (125 MHz CDCl₃), δ: 180.4 (C=O), 154.6(C, C aromatic), 134.9, 132.5, 130.0 CH, C-aromatic), 129.8(C, C aromatic), 126.8, 115.7 CH, C-aromatic), 46.2, 36.4 (CH₂).

2-amino-3-chloronaphthalene-1,4-dione (59)



General procedure

orange solid

T.L.C system: n-hexane-EtOAc 8:2 v/v, Rf: 0.11; : n-hexane-EtOAc 2:8 v/v, Rf: 0.69

Purification re-crystallation from EtOH

Yield: 78%

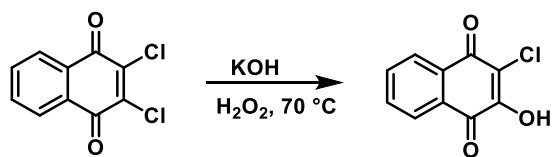
Purity: 95 %

UPLC-MS method B: Rt: 1.651

¹H-NMR (500 MHz, DMSO) δ 7.99 – 7.95 (m, 2H, ArH), 7.82 (td, *J* = 7.5, 1.4 Hz, 1H, ArH), 7.74 (td, *J* = 7.5, 1.3 Hz, 1H, ArH), 7.32 (s, 2H, NH₂).

¹³C-NMR (125 MHz DMSO, δ 179.74, 175.63, 180.4, 176.1 (C=O), 147.47, 135.36(C, C aromatic), 133.13, 132.76, 130.21, 126.72, 126.32, 109.31(CH, C-aromatic).

Synthesis of 2-chloro-3-hydroxynaphthalene-1,4-dione (60)



To a suspension of 2,3-dichloro-1,4-naphthoquinone (1 eq) in water (0.2 M), an aqueous solution of KOH (4.4 mM) was added carefully over 10 minutes, the reaction mixture was heated at 70 °C for 1h. Unreacted dichloro naphthoquinone was excreted with DCM and the remaining aqueous later was acidified with HCl. A yellow precipitate was obtained filtered and recrystallized using methanol, to afford the title compound.

Yellow solid

T.L.C system: n-hexane-EtOAc 8:2 v/v, R_f: 0.13; n-hexane-EtOAc 8:2 v/v, R_f: 0.59

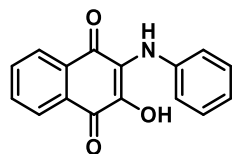
Yield:83%

Purity: 100 %

UPLC-MS method C: Rt: 1.47, MS (ESI)-: 205.1[M-H]-

¹H-NMR (500 MHz, CDCl₃) δ ppm 8.24 (dd, J = 7.7, 1.4 Hz, 1H, ArH), 8.17 (dd, J = 7.7, 1.4 Hz, 1H, ArH), 7.85 (td, J = 7.6, 1.4 Hz, 1H, ArH), 7.79 (td, J = 7.5, 1.3 Hz, 1H, ArH), 7.63 (s, 1H, OH).

2-hydroxy-3-(phenylamino) naphthalene-1,4-dione (61)



General procedure 3

orange solid

TLC system n-hexane/AcOEt 2:8 v/v Rf:0.59

Purification column chromatography hexane/AcOEt

Yield: 76%

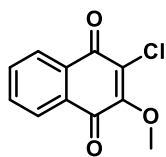
Purity: 96%

UPLC-MS method C: 1.14 MS (ESI)+: 266[M+H] +

¹H-NMR (500 MHz, DMSO) δ : 8.13 (dd, $J = 7.7, 1.4$ Hz, 1H, ArH), 8.05 (dd, $J = 7.7, 1.4$ Hz, 1H, ArH), 7.68 (dd, $J = 7.6, 1.4$ Hz, 1H, ArH), 7.65 (dd, $J = 7.6, 1.4$ Hz, 1H, ArH), 7.28 (dd, $J = 8.5, 7.4$ Hz, 2H, ArH), 7.15 (s, 1H, OH), 7.15 – 7.08 (m, 1H, ArH), 7.08 – 7.02 (m, 2H, ArH)

¹³C-NMR (125 MHz DMSO, δ : 183.2, 179.7 (C=O), 139.4, 138.7 (C, C aromatic), 134.6, 133.8 (CH, C-aromatic), 132.7, 132.2 (C, C aromatic), 130.17, 128.31, 126.31, 126.28, 124.06, 122.22(CH, C-aromatic)

2-chloro-3-methoxynaphthalene-1,4-dione (62)



General procedure 2

yellow solid

T.L.C system: n-hexane-EtOAc 8:2 v/v, Rf: 0.75

Purification: re-crystallation from MeOH

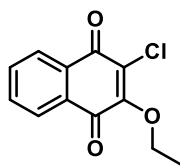
Yield: 73%

Purity: 100%

UPLC-MS MS method C: Rt: 2.21(ESI)+: 224[M+H] +

¹H-NMR (500 MHz, DMSO) δ: 8.15 – 8.05 (m, 1H, ArH), 8.06 – 7.97 (m, 1H, ArH), 7.78 – 7.58 (m, 2H, ArH), 4.25 (s, 3H, OCH₃).

2-chloro-3-ethoxynaphthalene-1,4-dione (63)



General procedure 2

yellow solid

T.L.C system: n-hexane-EtOAc 8:2 v/v, Rf: 0.75

Purification re-crystallation from EtOH

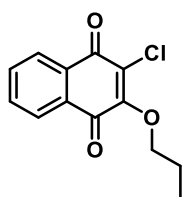
Yield: 71%

Purity: 100 %

UPLC-MS MS method C: Rt: 2.02 MS (ESI)+: 237[M+H] +

¹H-NMR (500 MHz, DMSO) δ : 8.11 – 8.04 (m, 1H, ArH), 8.06 – 7.93 (m, 1H, ArH), 7.71 – 7.63 (m, 2H, ArH), 4.56 (q, $J = 7.1$ Hz, 2H, CH₂), 1.40 (t, $J = 7.1$ Hz, 3H, CH₃).

2-chloro-3-propoxynaphthalene-1,4-dione (64)



General procedure 2

yellow solid

T.L.C system: n-hexane-EtOAc 8:2 v/v, Rf: 0.75

Purification: re-crystallation from MeOH

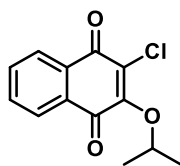
Yield: 75%

Purity: 98 %

UPLC-MS MS method C: Rt: 2.39 MS (ESI)⁺: 251[M+H]⁺

¹H-NMR (500 MHz, DMSO) δ : 8.12 – 8.05 (m, 1H, ArH), 8.07 – 7.96 (m, 1H, ArH), 7.72 – 7.61 (m, 2H, ArH), 4.47 (t, J = 6.5 Hz, 2H, CH₂), 1.77 (dt, J = 7.5, 6.5 Hz, 2H, CH₂), 1.00 (t, J = 7.4 Hz, 3H, CH₃).

2-chloro-3-isopropoxynaphthalene-1,4-dione (65)



General procedure 2

yellow solid

T.L.C system: n-hexane-EtOAc 8:2 v/v, Rf: 0.75

Purification: re-crystallation from MeOH

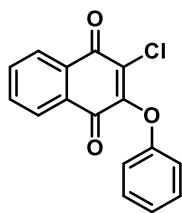
Yield: 73%

Purity: 100 %

UPLC-MS MS method C: Rt: 2.19 MS (ESI)+: 272[M+Na]

¹H-NMR (500 MHz, DMSO) δ : δ 8.15 – 8.12 (m, 1H, ArH), 8.10 – 7.90 (m, 1H, ArH), 7.73 – 7.68 (m, 2H, ArH), 5.21 – 5.10 (m, 1H, CH), 1.32 (d, J = 6.2 Hz, 6H, CH₃).

2-chloro-3-phenoxynaphthalene-1,4-dione (66)



General procedure 2

yellow solid

T.L.C system: n-hexane-EtOAc 8:2 v/v, Rf: 0.78

Purification re-crystallation from MeOH

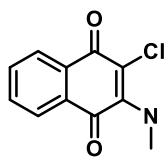
Yield: 63%

Purity: 84%

UPLC-MS MS method C: Rt: 2.36 MS (ESI)+: 272[M+Na]

¹H-NMR (500 MHz, DMSO) δ : 8.03 – 7.98 (m, 1H, ArH), 7.79 – 7.63 (m, 2H, ArH), 7.32 – 7.25 (m, 1H, ArH), 7.17 (d, $J = 7.4$ Hz, 2H, ArH), 7.12 – 7.06 (m, 2H, ArH), 6.99 – 6.93 (m, 1H, ArH),

2-chloro-3-(methyl-1 λ -azaneyl) naphthalene-1,4-dione (67)



General procedure: 1

red solid

T.L.C system: n-hexane-EtOAc 8:2 v/v, R_f: 0.58

Purification: re-crystallation from MeOH

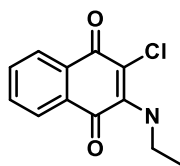
Yield: 93%

Purity: 100 %

UPLC-MS MS method C: Rt: 1.91 MS (ESI)⁺: 222[M+Na]

¹H-NMR (500 MHz, DMSO) δ : 8.08 (dd, $J = 7.8, 1.4$, Hz, 1H, ArH), 7.96 (dd, $J = 7.7, 1.4$, Hz, 1H, ArH), 7.66 (td, $J = 7.6, 1.4$ Hz, 1H, ArH), 7.55 (td, $J = 7.6, 1.3$ Hz, 1H, ArH), 3.38 (d, $J = 5.2$ Hz, 3H, CH₃).

2-chloro-3-(ethyl-1₂-azaneyl) naphthalene-1,4-dione (68)



General procedure: 1

red solid

T.L.C system: n-hexane-EtOAc 8:2 v/v, R_f: 0.58

Purification: re-crystallation from MeOH

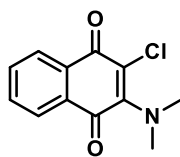
Yield: 95%

Purity: 100 %

UPLC-MS MS method C: R_t: 2.10 MS (ESI)⁺: 236[M+Na]

¹H-NMR (500 MHz, DMSO) δ: 8.14 – 8.04 (m, 1H, ArH), 7.96 (dd, *J* = 7.6, 1.3 Hz, 1H, ArH), 7.65 (td, *J* = 7.6, 1.3 Hz, 1H, ArH), 7.55 (td, *J* = 7.6, 1.3 Hz, 1H, ArH), 3.84 (qd, *J* = 7.2, 6.1 Hz, 2H, CH₂), 1.27 (t, *J* = 7.2 Hz, 3H, CH₃).

2-chloro-3-(dimethylamino) naphthalene-1,4-dione (69)



General procedure: 1

red solid

T.L.C system: n-hexane-EtOAc 8:2 v/v, Rf: 0.65

Purification: re-crystallation from MeOH

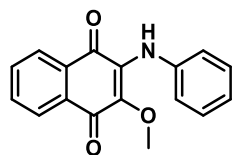
Yield: 85%

Purity: 92%

UPLC-MS MS method C: Rt: 2.29 MS (ESI)⁺: 250[M+Na]

¹H-NMR (500 MHz, DMSO) δ 8.08 (ddd, $J = 7.8, 1.3, 0.5$ Hz, 1H, ArH), 7.97 (ddd, $J = 7.6, 1.3, 0.5$ Hz, 1H, ArH), 7.65 (td, $J = 7.6, 1.3$ Hz, 1H, ArH), 7.55 (td, $J = 7.5, 1.3$ Hz, 1H, ArH), 1.25 (d, $J = 6.4$ Hz, 6H, CH₃).

2-methoxy-3-(phenylamino) naphthalene-1,4-dione (70)



General procedure 3

orange solid

T.L.C system: n-hexane-EtOAc 8:2 v/v, Rf: 0.69

Purification column chromatography hexane/AcOEt

Yield: 80%

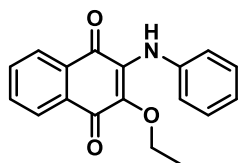
Purity: 100 %

UPLC-MS method C: 1.14 MS (ESI)+: 266[M+H] +

¹H-NMR (500 MHz, DMSO) δ : 8.11 (dd, $J = 7.7, 1.4$ Hz, 1H, ArH), 8.07 (dd, $J = 7.7, 1.4$ Hz, 1H, ArH), 7.72 (dd, $J = 7.6, 1.4$ Hz, 1H, ArH), 7.66 (dd, $J = 7.6, 1.4$ Hz, 1H, ArH), 7.31 (dd, $J = 8.5, 7.4$ Hz, 2H, ArH), 7.18 (s, 1H, NH), 7.15 – 7.08 (m, 1H, ArH), 7.08 – 7.02 (m, 2H, ArH), 3.52 (s, 3H, CH₃).

¹³C-NMR (125 MHz DMSO, δ : 183.2, 179.7 (C=O), 139.4, 138.7 (C, C aromatic), 134.6, 133.8 (CH, C-aromatic), 132.7, 132.2 (C, C aromatic), 130.17, 128.31, 126.31, 126.28, 124.06, 122.22(CH, C-aromatic), 59.92 (CH₃).

2-ethoxy-3-(phenylamino) naphthalene-1,4-dione (71)



General procedure 3

orange solid

T.L.C system: n-hexane-EtOAc 8:2 v/v, Rf: 0.67

Purification column chromatography hexane/AcOEt

Yield: 64%

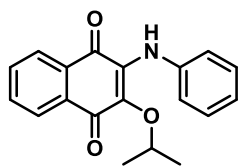
Purity: 100 %

UPLC-MS method C: 1.14 MS (ESI)+: 266[M+H] +

¹H-NMR (500 MHz, DMSO) δ : 8.11 (dd, $J = 7.6, 1.3$ Hz, 1H, ArH), 8.07 (dd, $J = 7.6, 1.4$ Hz, 1H, ArH), 7.72 (td, $J = 7.5, 1.3$ Hz, 1H, ArH), 7.70 – 7.62 (m, 1H, ArH), 7.36 – 7.28 (m, 2H, ArH), 7.16 – 6.94 (m, 3H, ArH), 3.74 (q, $J = 7.0$ Hz, 2H, CH₂), 0.85 (t, $J = 7.0$ Hz, 3H, CH₃).

¹³C-NMR (125 MHz DMSO, δ : 183.3, 179.9 (C=O), 143.3, 138.6 (C, C aromatic), 134.5 (CH, C-aromatic) 134.5 (C, C aromatic), 132.6 (CH, C-aromatic), 132.5 (C, C aromatic), 130.5 (CH, C-aromatic) 130.3, 128.9, 128.4, 126.2, 125.4, 124.1, 122.8 (CH, C-aromatic), 68.5 (CH₂), 14.6 (CH₃).

2-isopropoxy-3-(phenylamino) naphthalene-1,4-dione (72)



General procedure 3

orange solid

T.L.C system: n-hexane-EtOAc 8:2 v/v, Rf: 0.75

Purification column chromatography hexane/AcOEt

Yield: 63%

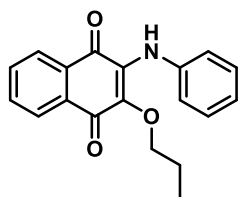
Purity: 99 %

UPLC-MS method C: 1.22 MS (ESI)+: 310[M+H] +

¹H-NMR (500 MHz, DMSO) δ : 8.11 (dd, $J = 7.6, 1.4$ Hz, 1H, ArH), 8.07 (dd, $J = 7.7, 1.4$ Hz, 1H, ArH), 7.74 – 7.69 (m, 1H, ArH), 7.65 – 7.60 (m, 1H, ArH), 7.41 (dd, $J = 5.0, 2.0$ Hz, 1H, ArH), 7.33 – 7.28 (m, 2H, ArH), 7.20 (bs, 1H, NH), 7.13 – 7.05 (m, 2H, ArH), 7.05 – 7.00 (m, 2H, ArH), 4.41 – 4.21 (m, 1H, CH), 0.88 (d, $J = 6.1$ Hz, 6H, CH₃).

¹³C-NMR (125 MHz DMSO, δ : 181.3, 178.4 (C=O), 141.4, 136.6 (C, C aromatic), 135.4 (CH, C-aromatic) 133.1 (C, C aromatic), 132.6 (CH, C-aromatic), 130.7 (C, C aromatic), 130.3 (CH, C-aromatic) 128.6, 128.5, 127.1, 126.5, 126.2, 124.4, 124.3, 123.6, 121.9, 120.8, 73.1 (CH), 19.9 (CH₃)

2-(phenylamino)-3-propoxynaphthalene-1,4-dione (73)



General procedure 3

orange solid

T.L.C system: n-hexane-EtOAc 8:2 v/v, Rf: 0.75

Purification: column chromatography hexane/AcOEt

Yield: 67

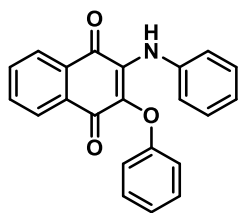
Purity: 92%

UPLC-MS method C: 2.45 MS (ESI)+: 308[M+H] +

¹H-NMR (500 MHz, DMSO) δ : 8.10 (dt, $J = 7.6, 0.9$ Hz, 1H, ArH), 8.09 – 8.04 (m, 1H, ArH), 7.72 (td, $J = 7.5, 1.3$ Hz, 1H, ArH), 7.64 (td, $J = 7.5, 1.4$ Hz, 1H, ArH), 7.33 – 7.27 (m, 2H, ArH), 7.15 (s, 1H, NH), 7.12 – 7.09 (m, 1H, ArH), 7.08 – 7.03 (m, 2H, ArH), 3.68 (t, $J = 6.7$ Hz, 2H, CH₂), 1.36 – 1.22 (m, 2H, CH₂), 0.65 (t, $J = 7.4$ Hz, 3H, CH₃).

¹³C-NMR (125 MHz DMSO, δ : 183.2, 179.8 (C=O), 143.3, 138.8(C, C aromatic), 134.5, 132.6 (CH, C-aromatic), 132.3 (C, C aromatic), 130.5 (CH, C-aromatic), 130.3 (C, C aromatic), 128.9, 128.2, 126.3, 126.2, 125.6, 123.9, 122.4 (CH, C-aromatic), 74.6, 22.8 (CH₂), 10.0 (CH₃).

2-phenoxy-3-(phenylamino) naphthalene-1,4-dione (74)



General procedure 3

orange solid

T.L.C system: n-hexane-EtOAc 8:2 v/v, Rf: 0.64

Purification column chromatography hexane/AcOEt

Yield: 59%

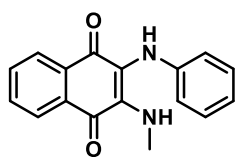
Purity: 94%

UPLC-MS method C: 2.34 MS (ESI)+: 342[M+H] +

¹H-NMR (500 MHz, DMSO) δ : 8.18 – 8.11 (m, 1H, ArH), 7.82 – 7.71 (m, 2H, ArH), 7.69 (dd, J = 7.6, 1.3 Hz, 1H, ArH), 7.17 (t, J = 7.8 Hz, 2H, ArH), 7.10 – 7.00 (m, 3H, ArH), 6.96 (dd, J = 7.4, 1.7 Hz, 2H, ArH), 6.90 (dd, J = 8.7, 1.1 Hz, 1H, ArH), 6.88 – 6.80 (m, 1H, ArH), 6.58 – 6.46 (m, 2H, ArH).

¹³C-NMR (125 MHz DMSO, δ : 183.5, 179.9 (C=O), 142.4, 138.9 (C, C aromatic), 135.53(CH, C-aromatic), 134.98(C, C aromatic), 132.79, 129.01, 128.04(CH, C-aromatic), 127.63(C, C aromatic), 127.11, 126.81, 126.55(CH, C-aromatic), 125.05(C, C aromatic), 124.20, 123.74, 121.99, 120.40, 119.32, (CH, C-aromatic),

2-(methyl-12-azaneyl)-3-(phenylamino) naphthalene-1,4-dione (75)



General procedure 3

orange solid

T.L.C system: n-hexane-EtOAc 8:2 v/v, Rf: 0.57

Purification column chromatography hexane/AcOEt

Yield: 45%

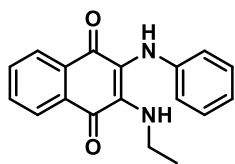
Purity: 89%

UPLC-MS method C: 1.16 MS (ESI)+: 279[M+H] +

¹H-NMR (500 MHz, DMSO) δ 8.21 – 7.99 (m, 2H, ArH), 7.63 (m, 1H, ArH), 7.32 – 7.15 (m, 2H, ArH), 6.98 – 6.84 (m, 2H, ArH), 6.75 (m, 2H, ArH), 6.42 (s, 1H, NH) 2.73 (dd, $J = 5.7$, 2.5 Hz, 3H, CH₃).

¹³C-NMR (125 MHz DMSO, δ 181.9, 181.1 (C=O), 143.68, 137.86(C, C aromatic), 134.06, 132.6 (CH, C-aromatic), 132.1, 130.9 (C, C aromatic), 129.0, 128.4, 126.2, 126.1, 120.4, 120.3, 116.5, 113.8 (CH, C-aromatic), 30.4 (CH₃).

2-(ethyl-1,2-azaneyl)-3-(phenylamino) naphthalene-1,4-dione (76)



General procedure 3

orange solid

T.L.C system: n-hexane-EtOAc 8:2 v/v, Rf: 0.60

Purification: column chromatography hexane/AcOEt

Yield: 35%

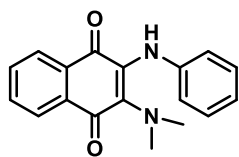
Purity: 96%

UPLC-MS method C: 1.21 MS (ESI)+: 293[M+H] +

¹H-NMR (500 MHz, DMSO) δ : 8.06 – 8.23 (m, 2H, ArH), 7.64 -7.62 (m, 2H, ArH), 7.43 – 7.41 (m, 2H, ArH), 6.98 – 6.84 (m, 2H, ArH), 6.42 (s, 1H, NH), 3.14 – 2.96 (m, 2H, CH₂), 0.96 (t, *J* = 7.2 Hz, 3H, CH₃).

¹³C-NMR (125 MHz DMSO, δ 188.9, 182.1 (C=O), 143.3, 143.3 (C, C aromatic), 134.8, 134.0 (CH, C-aromatic), 133.5 (C, C aromatic), 132.6, 130.5, 128.9, 127.4, 126.3, 126.2, 126.1, 125.4 (CH, C-aromatic), 37.8 (CH₂), 15.7 (CH₃).

2-(dimethylamino)-3-(phenylamino) naphthalene-1,4-dione (77)



General procedure 3

orange solid

T.L.C system: n-hexane-EtOAc 8:2 v/v, Rf: 0.65

Purification column chromatography hexane/AcOEt

Yield: 49%

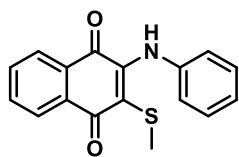
Purity: 100 %

UPLC-MS method C: 2.48 MS (ESI)+: 293[M+H] +

¹H-NMR (500 MHz, DMSO) δ : 8.09 – 7.89 (m, 2H, ArH), 7.62 (m, 2H, ArH), 7.39 – 7.18 (m, 2H, ArH), 7.19 – 7.06 (m, 1H, ArH), 7.04 – 6.95 (m, 1H, ArH), 6.91 – 6.71 (m, 2H, ArH), 2.74 (s, 6H, CH₃).

¹³C-NMR (125 MHz DMSO, δ : 182.1, 181.9 (C=O), 140.2, 133.5 (C, C aromatic), 133.3, 132.7 (CH, C-aromatic), 130.8 (C, C aromatic), 128.8 (CH, C-aromatic), 128.2 (C, C aromatic), 127.4, 126.3, 125.5, 121.8, 121.6 (CH, C-aromatic), 41.0 (CH₃).

2-(methylthio)-3-(phenylamino) naphthalene-1,4-dione (78)



General procedure 4

orange solid

T.L.C system: n-hexane-EtOAc 8:2 v/v, Rf: 0.67

Purification: column chromatography hexane/AcOEt

Yield: 78%

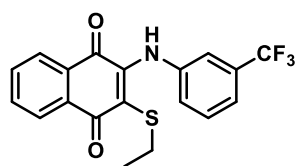
Purity: 100 %

UPLC-MS method C: 1.18 MS (ESI)+: 296[M+H] +

¹H-NMR (500 MHz, DMSO) δ : 8.08 (dd, $J = 7.8, 1.4$ Hz, 1H, ArH), 8.02 (dd, $J = 7.6, 1.4$ Hz, 1H, ArH), 7.74 (s, 1H, ArH), 7.67 (td, $J = 7.6, 1.4$ Hz, 1H, ArH), 7.60 (td, $J = 7.5, 1.4$ Hz, 1H, ArH), 7.35 – 7.25 (m, 2H, ArH), 7.15 – 7.04 (m, 1H, ArH), 7.04 – 6.80 (m, 2H, ArH), 2.04 (s, 3H, CH₃).

¹³C-NMR (125 MHz DMSO, δ : 180.4, 176.6 (C=O), 138.3 (C, C aromatic), 134.6 (CH, C-aromatic), 133.6 (C, C aromatic), 132.8, 128.5, 126.8, 126.7, 124.5, 122.1 (CH, C-aromatic), 17.5 (CH₃).

2-(ethylthio)-3-((3-(trifluoromethyl) phenyl) amino) naphthalene-1,4-dione (79)



General procedure 5

orange solid

T.L.C system: n-hexane-EtOAc 8:2 v/v, Rf: 0.64

Purification: column chromatography hexane/AcOEt

Yield: 73%

Purity: 100%

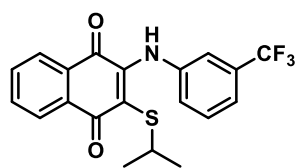
UPLC-MS method C: 2.53 MS (ESI)+: 378[M+H] +

¹H-NMR (500 MHz, DMSO) δ : 8.09 (dd, $J = 7.6, 1.3$ Hz, 1H, ArH), 8.03 (dd $J = 7.6, 1.5$ Hz, 1H, ArH), 7.74 (s, 1H, ArH), 7.68 (td, $J = 7.6, 1.4$ Hz, 1H, ArH), 7.67 – 7.59 (m, 1H, ArH), 7.38 (t, $J = 7.8$ Hz, 1H, ArH), 7.32 (d, $J = 7.8$ Hz, 1H, ArH), 7.09 (dt, $J = 8.1, 1.5$ Hz, 1H, ArH), 2.57 (d, $J = 7.4$ Hz, 2H, CH₂), 0.98 (t, $J = 7.4$ Hz, 3H, CH₃).

¹³C-NMR (125 MHz DMSO, δ 181.1, 180.2(C=O), 144.1, 138.9 (C, C aromatic), 134.7 (CH, C-aromatic), 133.4 (C, C aromatic), 133.1 (CH, C-aromatic), 130.5 (C, C aromatic), 128.9, 127.0, 126.8, 125.0, 120.9, 119.9, 118.8(CH, C-aromatic), 28.0(CH₂), 14.4 (CH₃).

¹⁹F NMR (471 MHz, CDCl₃) δ -62.35

2-(isopropylthio)-3-((3-(trifluoromethyl) phenyl) amino) naphthalene-1,4-dione (80)



General procedure 5

orange solid

T.L.C system: n-hexane-EtOAc 8:2 v/v, Rf: 0.64

Purification: column chromatography hexane/AcOEt

Yield: 69%

Purity: 99 %

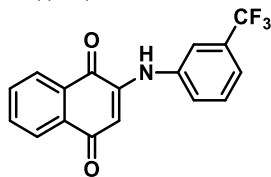
UPLC-MS method C: 2.58 MS (ESI)+: 378[M+H] +

¹H-NMR (500 MHz, DMSO) δ : δ 8.09 (dd, $J = 7.8, 1.4$ Hz, 1H, ArH), 8.01 (dd, $J = 7.7, 1.4$ Hz, 1H, ArH), 7.77 (s, 1H, ArH), 7.68 (td, $J = 7.6, 1.4$ Hz, 1H, ArH), 7.61 (td, $J = 7.5, 1.4$ Hz, 1H, ArH), 7.35 (dd, $J = 20.3, 7.8$ Hz, 2H, ArH), 7.09 (dt, $J = 7.6, 1.6$ Hz, 1H, ArH), 3.21 (p, $J = 6.7$ Hz, 1H, CH), 1.00 (d, $J = 6.7$ Hz, 6H, CH₃).

¹³C-NMR (125 MHz DMSO, δ : δ 181.1, 180.2 (C=O), 145.1, 139.0 (C, C aromatic), 134.6 (CH, C-aromatic), 133.3 (C, C aromatic), 133.0 (CH, C-aromatic), 130.7 (C, C aromatic), 128.9, 127.0, 126.8, 125.6, 121.1, 119.3, 37.9 (CH, C-aromatic), 24(CH₃).

¹⁹F NMR (471 MHz, CDCl₃) δ -62.45.

2-((3-(trifluoromethyl) phenyl) amino) naphthalene-1,4-dione (81)



General procedure 6

orange solid

T.L.C system: n-hexane-EtOAc 8:2 v/v, Rf: 0.65

Purification: column chromatography hexane/AcOEt

Yield: 84%

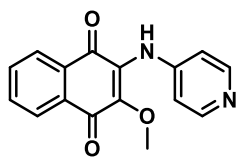
Purity: 92%

UPLC-MS method C: 2.29 MS (ESI)+: 318[M+H] +

¹H-NMR (500 MHz, DMSO) δ : 8.07 (dd, $J = 9.7, 7.8$ Hz, 2H, ArH), 7.72 (td, $J = 7.5, 1.3$ Hz, 1H, ArH), 7.63 (td, $J = 7.5, 1.4$ Hz, 1H, ArH), 7.55 (s, 1H, ArH), 7.49 (t, $J = 7.9$ Hz, 1H, ArH), 7.42 (dd, $J = 17.1, 8.2$ Hz, 2H, ArH), 6.35 (s, 1H, ArH).

¹⁹F NMR (471 MHz, CDCl₃) δ -62.5

2-methoxy-3-(pyridin-4-ylamino) naphthalene-1,4-dione (82)



General procedure 3

orange solid

Purification column chromatography hexane/AcOEt 2:8 v/v Rf:0.33

Yield: 82%

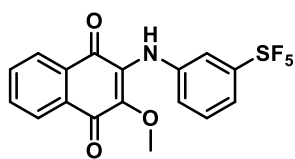
Purity: 99%

UPLC-MS method C: 1.31 MS (ESI)+: 281[M+H] +

¹H-NMR (500 MHz, DMSO) δ : 8.53 – 8.28 (m, 2H, ArH), 8.12 (ddd, J = 17.3, 7.6, 1.4 Hz, 2H, ArH), 7.73 (dtd, J = 27.9, 7.5, 1.4 Hz, 2H, ArH), 7.10 (s, 1H, ArH), 6.87 – 6.77 (m, 2H, ArH), 3.79 (s, 3H, CH₃).

¹³C-NMR (125 MHz DMSO, δ : 180.5, 179.6 (C=O), 149.1, 146.2 (C, C aromatic), 140.30, 134.88 (CH, C-aromatic), 134.3 (C, C aromatic), 133.2 (CH, C-aromatic), 130.3 (C, C aromatic), 127.2, 126.8, 124.6, 122.8 (CH, C-aromatic), 60.2 (CH₃).

2-methoxy-3-((3-(pentafluoro-16-sulfaneyl) phenyl) amino) naphthalene-1,4-dione (83)



General procedure 3

orange solid

T.L.C system: n-hexane-EtOAc 8:2 v/v, Rf: 0.65

Purification: column chromatography hexane/AcOEt

Yield: 78%

Purity: 98%

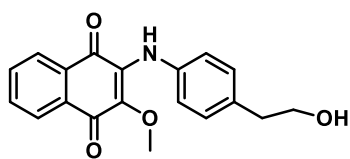
UPLC-MS method C: 2.47 MS (ESI)+: 406[M+H] +

¹H-NMR (500 MHz, DMSO) δ: 8.20 – 8.07 (m, 2H, ArH), 7.77 (td, *J* = 7.6, 1.4 Hz, 1H, ArH), 7.71 (td, *J* = 7.6, 1.4 Hz, 1H, ArH), 7.51-7.49 (m, 1H, ArH), 7.49 – 7.37 (m, 2H, ArH), 7.22 – 7.07 (m, 2H, ArH), 3.72 (s, 3H, CH₃).

¹³C-NMR (125 MHz DMSO, δ: 182.7, 179.8 (C=O), 176.6, 134.7(C, C aromatic), 133.1(CH, C-aromatic), 132.4, 131.9 (C, C aromatic), 128.4, 126.5, 124.5, 120.8, 119.3(CH, C-aromatic), 60.2 (CH₃).

¹⁹F NMR (471 MHz, CDCl₃) δ 62.79 (d, *J* = 150.1 Hz, 4F), 84.84-83.56 (m, 1F)

2-((4-(2-hydroxyethyl) phenyl) amino)-3-methoxynaphthalene-1,4-dione (84)



General procedure 3

orange solid

TLC system n-hexane/AcOEt 2:8 v/v Rf:0.69

Purification column chromatography hexane/AcOEt

Yield: 66%

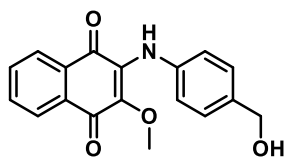
Purity: 100%

UPLC-MS method C: 1.92 MS (ESI)+: 324[M+H] +

¹H-NMR (500 MHz, DMSO) δ: 8.17 – 8.08 (m, 1H, ArH), 8.06 (dd, *J* = 7.8, 1.3 Hz, 1H, ArH), 7.73 (td, *J* = 7.6, 1.4 Hz, 1H, ArH), 7.65 (td, *J* = 7.5, 1.3 Hz, 1H, ArH), 7.23 – 7.11 (m, 3H, ArH), 7.11 – 6.90 (m, 2H, ArH), 3.87 (t, *J* = 6.6 Hz, 2H, CH₂), 3.53 (s, 3H, CH₃), 2.87 (t, *J* = 6.6 Hz, 2H, CH₂).

¹³C-NMR (125 MHz DMSO, δ 183.2, 179.6 (C=O), 137.3(C, C aromatic), 134.6(CH, C-aromatic), 134.3, 132.7(C, C aromatic), 132.2, 128.8, 126.3, 122.5(CH, C-aromatic), 63.6(CH₂), 60.0(CH₃), 38.6(CH₂).

2-((4-(hydroxymethyl) phenyl) amino)-3-methoxynaphthalene-1,4-dione (85)



General procedure 3

orange solid

TLC system n-hexane/AcOEt 2:8 v/v Rf:0.69

Purification column chromatography hexane/AcOEt

Yield: 65%

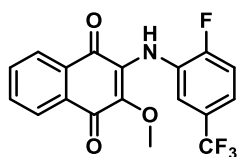
Purity: 93%

UPLC-MS method C: 1.86 MS (ESI)+: 310[M+H] +

¹H-NMR (500 MHz, DMSO) δ: δ 8.10 – 8.00 (m, 2H, ArH), 8.03 – 7.92 (m, 1H, ArH), 7.77 – 7.65 (m, 1H, ArH), 7.65 – 7.57 (m, 1H, ArH), 7.31 – 7.20 (m, 1H, ArH), 7.07 – 6.98 (m, 2H, ArH), 6.98 – 6.81 (m, 1H, ArH), 4.64 (d, *J* = 5.8 Hz, 2H, CH₂), 3.48 (s, 3H, CH₃).

¹³C-NMR (125 MHz DMSO, δ 183.2, 179.6 (C=O), 137.3, 134.6 (C, C aromatic), 134.3, 132.6, 132.2, 128.8, 126.3, 122.5 (CH, C-aromatic), 63.6(CH₂), 60.0 (CH₂).

2-((2-fluoro-5-(trifluoromethyl) phenyl) amino)-3-methoxynaphthalene-1,4-dione (86)



General procedure 3

orange solid

T.L.C system: n-hexane-EtOAc 8:2 v/v, Rf: 0.65

Purification column chromatography hexane/AcOEt

Yield: 72%

Purity: 91%

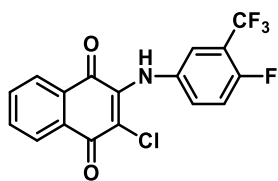
UPLC-MS method C: 2.45 MS (ESI)+: 366[M+H] +

¹H-NMR (500 MHz, DMSO) δ : δ 8.07 – 7.95 (m, 1H, ArH), 7.72 – 7.64 (m, 1H, ArH), 7.62 (dd, J = 7.5, 1.4 Hz, 1H, ArH), 7.59 – 7.52 (m, 2H, ArH), 7.35 (m, 2H, ArH), 6.96 (s, 1H, NH), 3.68 (s, 3H, CH₃).

¹³C-NMR (125 MHz DMSO, δ : 182.3, 179.9(C=O), 143.4, 134.8(C, C aromatic), 134.6, 133.1 (CH, C-aromatic), 132.3 (C, C aromatic), 131.9 (CH, C-aromatic), 130.5 (C, C aromatic), 130.0, 128.9, 128.4, 126.4, 126.3, 125.4, 121.5, 120.9, 115.5 (CH, C-aromatic), 60.24 (CH₃).

¹⁹F NMR (471 MHz, CDCl₃) δ -61.9, -121.3

2-chloro-3-((4-fluoro-3-(trifluoromethyl) phenyl) amino) naphthalene-1,4-dione (88)



General procedure 7

orange solid

TLC system n-hexane/AcOEt 8:2 v/v Rf:0.65

Purification column chromatography hexane/AcOEt

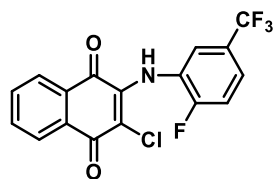
Yield: 83%

Purity: 100%

UPLC-MS method C: 2.20 MS (ESI)+: 370[M+H] +

¹H-NMR (500 MHz, DMSO) δ : 8.16 – 8.11 (m, 2H, ArH), 8.07 (dd, J = 1.4, 7.7 Hz, 1H, ArH), 7.77 – 7.70 (m, 1H, ArH), 7.66 (td, J = 1.4, 7.6 Hz, 1H, ArH), 7.52 (bs, 1H, NH) 7.26 (dd, J = 2.7, 6.1 Hz, 1H, ArH), 7.13 (t, J = 9.2 Hz, 1H, ArH).

2-chloro-3-((2-fluoro-5-(trifluoromethyl) phenyl) amino) naphthalene-1,4-dione (89)



General procedure 7

orange solid

TLC system n-hexane/AcOEt 8:2 v/v Rf:0.65

Purification column chromatography hexane/AcOEt

Yield: 80%

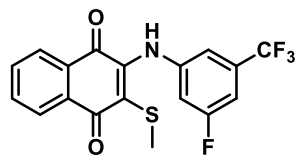
Purity: 100%

UPLC-MS method C: 2.18 MS (ESI)+: 370[M+H] +

¹H-NMR (500 MHz, DMSO) δ: 8.28-8.23 (m, 1H, ArH), 8.20 – 8.12 (m, 1H, ArH), 7.82 (td, *J* = 1.4, 7.6 Hz, 1H, ArH), 7.76 (td, *J* = 1.3, 7.5 Hz, 1H, ArH), 7.54 – 7.48 (m, 1H, ArH), 7.45 (s, 1H, NH), 7.39 (dd, *J* = 2.3, 7.3 Hz, 1H, ArH), 7.28 – 7.24 (m, 1H, ArH).

¹⁹F NMR (471 MHz, CDCl₃) δ -62.2, -118.0.

2-((3-fluoro-5-(trifluoromethyl)phenyl)amino)-3-(methylthio)naphthalene-1,4-dione (91)



General procedure 4

orange solid

T.L.C system: n-hexane-EtOAc 8:2 v/v, Rf: 0.67

Purification: column chromatography hexane/AcOEt

Yield: 63%

Purity: 97 %

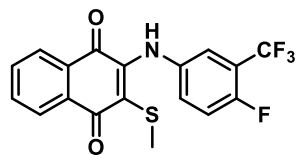
UPLC-MS method C: 2.48 MS (ESI)+: 382[M+H] +

¹H-NMR (500 MHz, DMSO) δ : 8.08 (dd, $J = 7.6, 1.3$ Hz, 1H, ArH), 8.03 (dd, $J = 7.7, 1.4$ Hz, 1H, ArH), 7.77 – 7.65 (m, 2H, ArH), 7.63 (dd, $J = 7.6, 1.4$ Hz, 1H, ArH), 7.10 (dd, $J = 7.7, 1.5$ Hz, 2H, ArH), 2.07 (s, 3H, CH₃).

¹³C-NMR (125 MHz DMSO, δ : 180.8, 180.21 (C=O), 143.5 (C, C aromatic), 135.3, 134.8(CH, C-aromatic), 134.5, 133.4 (C, C aromatic), 133.3, 133.1(CH, C-aromatic), 132.5, 130.5 (C, C aromatic), 127.3, 127.1, 127.0, 126.8, 116.8(CH, C-aromatic), 17.4 (CH₃).

¹⁹F NMR (471 MHz, CDCl₃) δ -61.5, -119.4.

2-((4-fluoro-3-(trifluoromethyl)phenyl)amino)-3-(methylthio)naphthalene-1,4-dione (92)



General procedure 4

orange solid

T.L.C system: n-hexane-EtOAc 8:2 v/v, R_f: 0.67

Purification column chromatography hexane/AcOEt

Yield: 68%

Purity: 94%

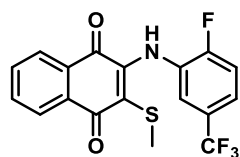
UPLC-MS method C: 2.46 MS (ESI)⁺: 382[M+H]⁺

¹H-NMR (500 MHz, DMSO) δ: δ 8.10 – 8.07 (m, 1H, ArH), 8.04 – 8.01 (m, 1H, ArH), 7.68 (td, *J* = 7.6, 1.4 Hz, 1H, ArH), 7.64 (s, 1H, NH), 7.61 (td, *J* = 7.5, 1.4 Hz, 1H, ArH), 7.20 (d, *J* = 2.1 Hz, 1H, ArH), 7.11 – 7.07 (m, 2H, ArH), 2.08 (s, 3H, CH₃).

180.9, 180.3 (C=O), 142.9 (C, C aromatic), 138.6, 134.7(CH, C-aromatic), 134.7, 133.4 (C, C aromatic), 133.3, 133.1(CH, C-aromatic), 131.5, 130.7 (C, C aromatic), 128.9, 126.7, 124.8, 124.6, 121.6, 120.6(CH, C-aromatic), 16.8 (CH₃).

¹⁹F NMR (471 MHz, CDCl₃) δ -61.5, -119.4.

2-((2-fluoro-5-(trifluoromethyl) phenyl) amino)-3-(methylthio) naphthalene-1,4-dione (93)



General procedure 4

orange solid

T.L.C system: n-hexane-EtOAc 8:2 v/v, Rf: 0.67

Purification column chromatography hexane/AcOEt

Yield: 65%

Purity: 100%

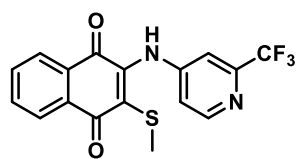
UPLC-MS method C:

¹H-NMR (500 MHz, DMSO) δ: 8.08 (dd, *J* = 7.6, 1.3 Hz, 1H, ArH), 8.03 (dd, *J* = 7.7, 1.4 Hz, 1H, ArH), 7.78 – 7.65 (m, 2H, ArH), 7.65 – 7.55 (m, 1H, ArH), 7.10 (dd, *J* = 7.7, 1.5 Hz, 2H, ArH), 2.07 (s, 3H, CH₃).

¹³C-NMR (125 MHz DMSO, δ: 180.8, 180.2 (C=O), 143.5, 135.3 (C, C aromatic), 134.8 (CH, C-aromatic), 133.4 (C, C aromatic), 133.1, 130.3, 127.3, 126.8, 120.6, 117.0, 116.8 (CH, C-aromatic), 17.4 (CH₃).

¹⁹F NMR (471 MHz, CDCl₃) δ -61.5, -119.4.

2-(methylthio)-3-((2-(trifluoromethyl) pyridin-4-yl) amino) naphthalene-1,4-dione (95)



General procedure 4

orange solid

Purification column chromatography hexane/AcOEt 2:8 v/v Rf:0.45

Yield: 75%

Purity: 95%

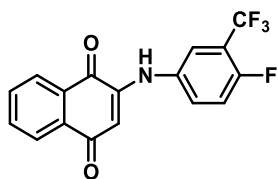
UPLC-MS method C: 2.20 MS (ESI)+: 365[M+H] +

¹H-NMR (500 MHz, DMSO) δ: 8.61 (d, *J* = 11.3 Hz, 1H, ArH), 8.16 (dd, *J* = 7.7, 1.3 Hz, 1H, ArH), 8.11 (dd, *J* = 7.6, 1.5 Hz, 2H, ArH), 7.86 (s, 1H, NH), 7.77 (td, *J* = 7.6, 1.4 Hz, 1H, ArH), 7.71 (td, *J* = 7.5, 1.4 Hz, 1H, ArH), 7.43 (t, *J* = 2.2 Hz, 1H, ArH), 2.14 (s, 3H, CH₃).

¹³C-NMR (125 MHz DMSO, δ 180.8, 179.9 (C=O), 146.1, 142.2 (C, C aromatic), 141.30, 134.8 (CH, C-aromatic), 133.3 (C, C aromatic), 133.2 (CH, C-aromatic), 130.3 (C, C aromatic), 127.1, 126.8, 124.6, 122.8 (CH, C-aromatic), 17.3 (CH₃).

¹⁹F NMR (471 MHz, CDCl₃) δ -62.5.

2-((4-fluoro-3-(trifluoromethyl) phenyl) amino) naphthalene-1,4-dione (96)



General procedure 6

orange solid

T.L.C system: n-hexane-EtOAc 8:2 v/v, Rf: 0.75

Purification column chromatography hexane/AcOEt

Yield: 85%

Purity: 90%

UPLC-MS method C: 2.31 MS (ESI)+: 366[M+H] +

¹H-NMR (500 MHz, DMSO) δ 8.23 (dd, $J = 7.6, 1.4$ Hz, 1H, ArH), 8.16 (dd, $J = 7.8, 1.4$ Hz, 2H, ArH), 7.85 – 7.79 (m, 1H, ArH), 7.79 – 7.68 (m, 1H, ArH), 7.62 (s, 1H, NH), 7.56 – 7.48 (m, 1H, ArH), 6.28 (s, 1H, ArH).

2-((4-fluoro-3-(trifluoromethyl) phenyl) amino)-3-((trifluoromethyl)thio) naphthalene-1,4-dione (98)



General procedure 8

orange solid

T.L.C system: n-hexane-EtOAc 8:2 v/v, Rf: 0.28

Purification column chromatography hexane/AcOEt

Yield: 77%

Purity: 100%

UPLC-MS method C: 2.48 MS (ESI)+: 436[M+H] +

¹H-NMR (500 MHz, DMSO) δ : δ 8.19 (dd, J = 7.7, 1.3 Hz, 1H, ArH), 8.14 – 8.02 (m, 2H, ArH), 7.78-7.76 (m, 2H, ArH), 7.70-7.66 (m, 1H, ArH), 7.37-7.35 (m, 1H, ArH), 7.30-7.27 (d, J = 3.5 Hz, 2H, ArH).

¹³C-NMR (125 MHz DMSO, δ): 180.1, 179.7 (C=O), 159.4, 157.3 (C, C aromatic), 150.5 (CH, C-aromatic), 135.8 (C, C aromatic), 134.8, 133.9 (CH, C-aromatic), 133.9 (C, C aromatic), 133.3, 133.0, 131.5, 129.9, 127.8, 127.3, 117.9, 117.8 (CH, C-aromatic).

¹⁹F NMR (471 MHz, CDCl₃) δ -41.1, -61.7, -114.7

2-((2-(trifluoromethyl) pyridin-4-yl) amino)-3-((trifluoromethyl)thio) naphthalene-1,4-dione (99)



General procedure 8

orange solid

T.L.C system: n-hexane-EtOAc 8:2 v/v, Rf: 0.28

Purification column chromatography hexane/AcOEt

Yield: 78%

Purity: 89%

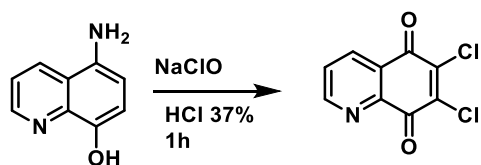
UPLC-MS method C: 2.29 MS (ESI)+: 419[M+H] +

¹H-NMR (500 MHz, DMSO) δ : 8.77 (d, $J = 1.9$ Hz, 1H, ArH), 8.60 (d, $J = 2.4$ Hz, 1H, ArH), 8.20 (dd, $J = 7.7, 1.3$ Hz, 1H, ArH), 8.17 – 7.99 (m, 2H, ArH), 7.80 (td, $J = 7.6, 1.3$ Hz, 1H, ArH), 7.71 (td, $J = 7.6, 1.3$ Hz, 1H, ArH), 7.66 (d, $J = 2.4$ Hz, 1H, ArH).

¹³C-NMR (125 MHz DMSO, δ) 180.8 176.6(C=O), 146.3, 142.2 (C, C aromatic), 135.9(CH, C-aromatic), 134.8 (CH, C-aromatic), 134.8 (C, C aromatic), 133.4 (CH, C-aromatic), 133.2 (C, C aromatic), 129.9, 127.8, 127.4, 125.4. (CH, C-aromatic),

¹⁹F NMR (471 MHz, CDCl₃) δ -40.8, -62.5.

Synthesis of 6,7-dichloroquinoline-5,8-dione (101)



Sodium chlorate (4 eq) was added over a period of 1 h to a solution of 5-aminoquinolin-8-ol (1 eq) in conc. HCl (37%, 0.3 M) at 55 °C. The reaction mixture stirred for 1 h before being diluted with water. The resulting yellow precipitate was collected and the water phase discarded. The precipitate was then re-crystallised in MeOH to afford the title compound.

Yellow solid

T.L.C system: n-hexane-EtOAc 8:2 v/v, R_f: 0.23

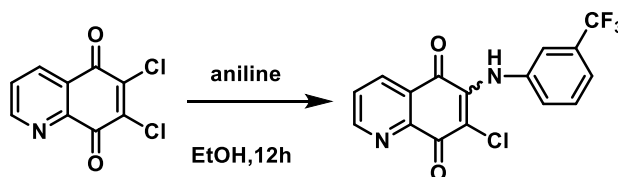
Yield: 56%

Purity: 100 %

UPLC-MS method C: R_t: 1.031, MS (ESI)⁺: 230.0-232.0[M+H]⁺

¹H-NMR (500 MHz, CDCl₃) δ ppm 9.11 (dd, *J* = 4.6, 1.7 Hz, 1H, ArH), 8.54 (dd, *J* = 7.9, 1.8 Hz, 1H, ArH), 7.77 (dd, *J* = 7.9, 4.7 Hz, 1H, ArH).

Synthesis of 7-chloro-6-((3-(trifluoromethyl) phenyl) amino) quinoline-5,8-dione (102)



A mixture of 6,7-dichloroquinoline-5,8-dione and 3-(trifluoromethyl) aniline (1.5 eq) in absolute ethanol was stirred at room temperature for 4h. The resulting mixture was concentrated in vacuum, and the residue was partitioned between a HCl 1N solution and AcOEt. The organic layer was dried over anhydrous magnesium sulphate, filtered and concentrated. The crude product was purified using silica gel column chromatography, Biotage Isolera One system, Cartridge: ZIP KP 30g, using nHexane/EtOAc as eluent to afford the title compound as a mixture of the two regioisomer (30:70)

Red solid

T.L.C system: n-hexane-EtOAc 8:2 v/v, Rf: 0.31

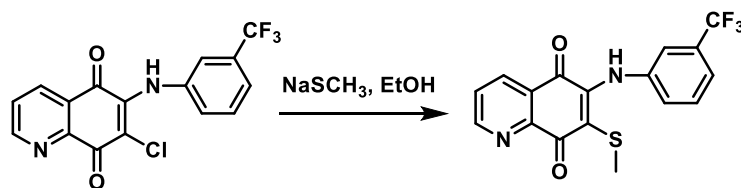
Yield: 56%

Purity: 87%

UPLC-MS method C: Rt: 2.061, MS (ESI)+: 353.1[M+H], 2.157, MS (ESI)+: 353.1[M+H],

¹H-NMR (500 MHz, CDCl₃) δ 9.09 (dd, *J* = 1.8, 4.7 Hz, 1H, ArH), 9.03 (dd, *J* = 1.7, 4.7 Hz, 1H, ArH), 8.46 (dd, *J* = 1.8, 7.9 Hz, 1H, ArH), 8.42 (dd, *J* = 1.8, 7.8 Hz, 1H, ArH), 7.75 (s, 1H, NH), 7.68 (m, 1H, ArH), 7.64 (m, 2H, ArH), 7.50 (m, 1H, ArH), 7.47 (m, 1H, ArH), 7.42 (m, 1H, ArH), 7.17 (m, 1H, ArH).

Synthesis of 7-(methylthio)-6-((3-(trifluoromethyl) phenyl) amino) quinoline-5,8-dione (103)



To a mixture of 7-chloro-6-((3-(trifluoromethyl) phenyl) amino) quinoline-5,8-dione in EtOH sodium methanethiolate was added and the reaction was stirred at room temperature. The resulting mixture was concentrated in vacuum, and the residue was partitioned between a water and AcOEt. The combined organic layers was dried over anhydrous magnesium sulfate, filtered and concentrated. The crude product was purified using silica gel column chromatography, Biotage Isolera One system, Cartridge: ZIP KP 30g, using nHexane/EtOAc as eluent to afford the title compound as a mixture of the two regioisomer (30:70).

Red solid

T.L.C system: n-hexane-EtOAc 8:2 v/v, Rf: 0.33

Yield:36%

Purity:100%

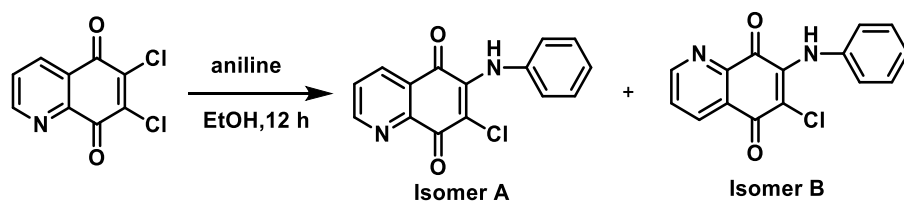
UPLC-MS method C: Rt: 2.085, MS (ESI)+: 365.2[M+H]⁺, 387.2 [M+Na]⁺

¹H-NMR (500 MHz, CDCl₃) δ 9.09 (dd, *J* = 1.8, 4.7 Hz, 1H, ArH), 9.03 (dd, *J* = 1.7, 4.7 Hz, 1H, ArH), 8.46 (dd, *J* = 1.8, 7.9 Hz, 1H, ArH), 8.42 (dd, *J* = 1.8, 7.8 Hz, 1H, ArH), 7.75 (s, 1H, ArH), 7.68 (m, 1H, ArH), 7.64 (m, 2H, ArH), 7.50 (m, 1H, ArH), 7.47 (m, 1H, ArH), 7.42 (m, 1H, ArH), 7.17 (m, 1H, ArH), 2.24 (s, 3H, CH₃)

¹³C-NMR (125 MHz CDCl₃), δ 176.6 (C=O), 155.1, 145.9 (C, C aromatic), 142.7, 138.6, 134.6 (CH, C-aromatic), 129.1 (C, C aromatic), 127.0, 124.9, 121.3, 121.2, 118.8, 106.9 (CH, C-aromatic), 17.4 (CH₃).

¹⁹F NMR (471 MHz, CDCl₃) δ -62.14.

Synthesis of 7-chloro-6-(phenylamino) quinoline-5,8-dione (104-105)



A mixture of 6,7-dichloroquinoline-5,8-dione and aniline (1.5 eq) in absolute ethanol was stirred at room temperature for 4 h. The resulting mixture was concentrated in vacuum, and the residue was partitioned between a HCl 1N solution and AcOEt. The organic layer was dried over anhydrous magnesium sulphate, filtered and concentrated. The crude product was purified using silica gel column chromatography, Biotage Isolera One system, using nHexane/EtOAc as eluent to afford the title compounds

Red solid

T.L.C system: n-hexane-EtOAc 8:2 v/v, Rf: 0.28

Yield: 73%

Purity: 100%

Isomer A

¹H-NMR (500 MHz, CDCl₃) δ 8.99 (dd, *J* = 4.7, 1.7 Hz, 1H, ArH), 8.52 (dd, *J* = 7.9, 1.7 Hz, 1H, ArH), 7.85 (bs, 1H, NH), 7.71 (dd, *J* = 7.9, 4.7 Hz, 1H, ArH), 7.44 – 7.34 (m, 2H, ArH), 7.14 – 7.07 (m, 2H, ArH).

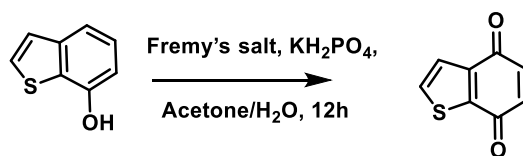
¹³C-NMR (125 MHz CDCl₃), δ ppm δ 179.4, 176.5 (C=O), 153.8 (CH, C-aromatic), 146.2, 141.9 (C, C-aromatic), 136.9, 134.9, 129.9, 128.5, 126.2, 124.6 (CH, C-aromatic).

Isomer B

¹H-NMR (500 MHz, CDCl₃) δ 9.06 (dd, *J* = 4.7, 1.8 Hz, 1H, ArH), 8.44 (dd, *J* = 7.8, 1.8 Hz, 1H, ArH), 7.78 (bs, 1H, NH), 7.65 (dd, *J* = 7.9, 4.7 Hz, 2H, ArH), 7.38 (dd, *J* = 8.4, 7.4 Hz, 2H, ArH), 7.16 – 7.05 (m, 2H, ArH).

¹³C-NMR (125 MHz CDCl₃), δ 180.1, 179.5 (C=O), 155.43 (CH, C-aromatic), 148.4, 137.04 (C, C-aromatic), 134.82, 128.56, 126.95, 126.91, 126.10, 124.43 (CH, C-aromatic).

Synthesis of benzo[b]thiophene-4,7-dione (107)



To a solution of benzo[b]thiophen-7-ol in Acetone, a solution of Fremy's salt in a 0.1 M of aqueous dipotassium phosphate was added, and the mixture was stirred for 12 h. The mixture was concentrated in vacuum and extracted with DCM 3 times. The combined organic layers was dried over anhydrous magnesium sulfate, filtered and concentrated. The formed yellow precipitate was collected by vacuum.

Yellow solid

T.L.C system: n-hexane-EtOAc 8:2 v/v, Rf: 0.28

Yield: 67%

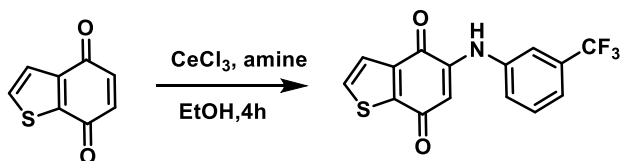
Purity: 100 %

UPLC-MS method C: Rt: 1.66, MS (ESI)+: 165.2[M+H] +

$^1\text{H-NMR}$ (500 MHz, CDCl_3) δ 7.74 (d, $J = 1.8$ Hz, 1H, ArH), 6.89 (d, $J = 1.9$ Hz, 1H, ArH), 6.76 (s, 2H, ArH).

$^{13}\text{C-NMR}$ (125 MHz CDCl_3), 181.4, 179.9 (C=O), 141.1, 138.1 (C, C aromatic), 137.6, 133.5, 126.1(CH, C-aromatic).

Synthesis of 5-((3-(trifluoromethyl) phenyl) amino) benzo[b]thiophene-4,7-dione (108)



The benzo[b]thiophene-4,7-dione (1.0 eq) was stirred with cerium trichloride heptahydrate (1.2 eq) in EtOH at room temperature. After 15 minutes, the appropriate aniline (2 eq) was added, and the reaction was stirred for 12 h. The resulting mixture was concentrated in vacuum, and the residue was partitioned between satd. aq. NH₄Cl and AcOEt. The combined organic layers were washed with HCl 6N and dried over anhydrous magnesium sulfate, filtered and concentrated. The crude product was purified using silica gel column chromatography, Biotage Isolera One system, Cartridge: ZIP KP 30g, using nHexane/EtOAc as eluent to afford the title compound as mixture of two region-isomer (80:20).

Yellow solid

T.L.C system: n-hexane-EtOAc 8:2 v/v, R_f: 0.37

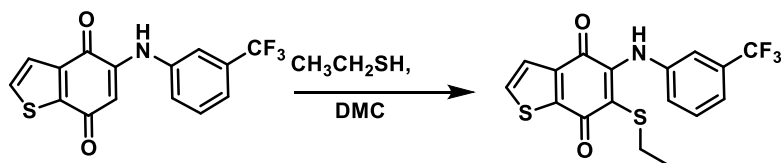
Yield: 67%

Purity: 100%

UPLC-MS method C: 1.95 MS (ESI)⁺: 324.0[M+H]⁺, 1.99 MS (ESI)⁺: 324.0[M+H]⁺,

¹H-NMR (500 MHz, CDCl₃) δ 7.71 (dd, *J* = 6.5, 5.0 Hz, 2H, ArH), 7.57 (dd, *J* = 5.0, 2.6 Hz, 3H, ArH), 7.55 – 7.46 (m, 2H, ArH), 7.46 – 7.35 (m, 3H, ArH), 7.25 – 7.22 (m, 2H, ArH), 7.15 (dt, *J* = 7.6, 2.1 Hz, 3H, ArH), 6.16 (s, 1H, ArH), 6.09 (s, 1H, ArH).

Synthesis of 6-(ethylthio)-5-((3-(trifluoromethyl) phenyl) amino) benzo[b]thiophene-4,7-dione (109)



To a solution of 2-chloro-3-((3-(trifluoromethyl) phenyl) amino) naphthalene-1,4-dione in DCM ethanethiol and DIPEA were added, and the reaction was stirred at room temperature. The resulting solution was washed with HCl 1N and NaHCO₃. The combined organic layers was dried over anhydrous magnesium sulfate, filtered and concentrated. The crude product was purified using silica gel column chromatography, Biotage Isolera One system, Cartridge: ZIP KP 30g, using nHexane/EtOAc EtOAc as eluent to afford the title compound.

Purple solid

T.L.C system: n-hexane-EtOAc 8:2 v/v, Rf: 0.37

Yield: 86%

Purity:92%

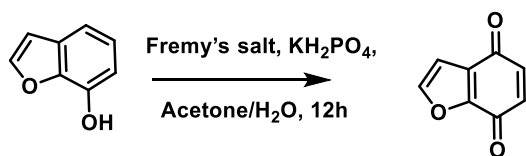
UPLC-MS method C: 2.46 MS (ESI)+: 384.0[M+H]⁺,

¹H NMR (500 MHz, CDCl₃) δ 7.80 – 7.69 (m, 1H, ArH), 7.61 (dd, *J* = 8.3, 5.0 Hz, 1H, ArH), 7.55 (d, *J* = 5.0 Hz, 1H, ArH), 7.50 – 7.43 (m, 1H, ArH), 7.42 (d, *J* = 7.7 Hz, 1H, ArH), 7.19 (d, *J* = 8.0 Hz, 1H, ArH), 2.72 – 2.57 (m, 2H, CH₂), 1.08 (td, *J* = 7.4, 3.6 Hz, 3H, CH₃).

¹³C NMR (126 MHz, CDCl₃) δ 176.6, 176.1 (C=O), 144.6, 139.0 (C, C-aromatic), 135.1, 132.1, 128.9, 127.4, 125.5, 125.4, 121.2, 119.2 (CH, C-aromatic), 116.6, 28.3(CH₂), 14.4 (CH₃).

¹⁹F NMR (471 MHz, CDCl₃) δ -62.14.

Synthesis of benzofuran-4,7-dione (111)



To a solution of benzofuran-7-ol in Acetone, a solution of Fremy's salt in a 0.1 M of aqueous dipotassium phosphate was added, and the mixture was stirred for 12h. The mixture was concentrated in vacuum and extracted with DCM 3 times. The combined organic layers were dried over anhydrous magnesium sulfate, filtered and concentrated. The crude product was purified using silica gel column chromatography, Biotage Isolera One system, Cartridge: ZIP KP 30g, using nHexane/EtOAc as eluent to afford the title compound

Yellow solid

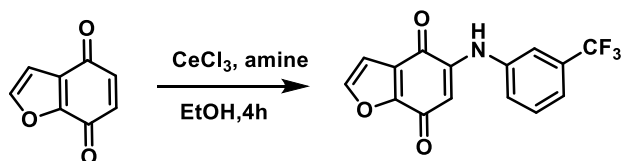
T.L.C system: n-hexane-EtOAc 8:2 v/v, Rf: 0.28

Yield: 45%

Purity: 100 %

$^1\text{H NMR}$ (500 MHz, CDCl_3) δ 7.63 (d, $J = 5.0$ Hz, 1H, ArH), 7.49 (d, $J = 5.0$ Hz, 1H, ArH), 6.80 (d, $J = 10.2$ Hz, 1H, ArH), 6.73 (d, $J = 10.2$ Hz, 1H, ArH).

Synthesis of 5-((3-(trifluoromethyl) phenyl) amino) benzofuran-4,7-dione (112)



The benzofuran-4,7-dione (1.0 eq) was stirred with cerium trichloride heptahydrate (1.2 eq) in EtOH at room temperature. After 15 minutes, the appropriate aniline (2 eq) was added, and the reaction was stirred for 12 h. The resulting mixture was concentrated in vacuum, and the residue was partitioned between satd. aq. NH₄Cl and AcOEt. The combined organic layers were washed with HCl 6N and dried over anhydrous magnesium sulfate, filtered and concentrated. The crude product was purified using silica gel column chromatography, Biotage Isolera One system, Cartridge: ZIP KP 30g, using nHexane/EtOAc as eluent to afford the final compound as mixture of two regioisomer (98:2)

Red solid

T.L.C system: n-hexane-EtOAc 8:2 v/v, R_f: 0.28

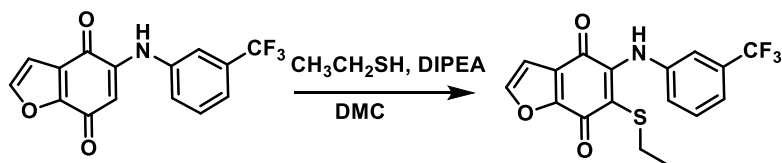
Yield: 58%

Purity: 98 %

UPLC-MS method C: 2.17 MS (ESI)⁺: 308.0[M+H]⁺, 2.22 MS (ESI)⁺: 308.0[M+H]⁺,

¹H NMR (500 MHz, CDCl₃) δ 7.73 (s, 1H, ArH), 7.67 (d, *J* = 1.9 Hz, 1H, ArH), 7.46 (dt, *J* = 16.0, 7.9 Hz, 2H, ArH), 7.20 (d, *J* = 7.8 Hz, 1H, ArH), 6.86 (d, *J* = 1.9 Hz, 1H, ArH), 2.64 (q, *J* = 7.4 Hz, 2H, CH₂), 1.08 (t, *J* = 7.4 Hz, 2H, CH₃).

Synthesis of 6-(ethylthio)-5-((3-(trifluoromethyl) phenyl) amino) benzofuran-4,7-dione (113)



To a solution of 5-((3-(trifluoromethyl) phenyl) amino) benzofuran-4,7-dione in DCM ethanethiol and DIPEA were added and the reaction was stirred at room temperature. The resulting solution was washed with HCl 1N and NaHCO₃. The combined organic layers were dried over anhydrous magnesium sulfate, filtered and concentrated. The crude product was purified using silica gel column chromatography, Biotage Isolera One system, Cartridge: ZIP KP 30g, using nHexane/EtOAc as eluent to afford the title compound

Purple solid

T.L.C system: n-hexane-EtOAc 8:2 v/v, R_f: 0.28

Yield: 86%

Purity: 88 %

UPLC-MS method B: Rt: 2.709, MS (ESI)-: 332.1-334.1[M-H]-

¹H NMR (500 MHz, CDCl₃) δ 7.83 – 7.70 (m, 1H, ArH), 7.61 (dd, *J* = 8.3, 5.0 Hz, 1H, ArH), 7.55 (d, *J* = 5.0 Hz, 1H, ArH), 7.47 (d, *J* = 7.8 Hz, 1H, ArH), 7.19 (d, *J* = 7.9 Hz, 1H, ArH), 2.65 (dq, *J* = 9.5, 7.4 Hz, 2H, CH₂), 1.08 (td, *J* = 7.4, 3.6 Hz, 3H, CH₃).

References

1. Picard, M., Taivassalo, T., Gouspillou, G., Hepple, R. T. Mitochondria: isolation, structure and function. *J. Physiol.* **589**, 4413–4421 (2011). doi: 10.1113/jphysiol.2011.212712.
2. Gray, M. W. Lynn Margulis and the endosymbiont hypothesis: 50 years later. *Mol. Biol. Cell* **28**, 1285–1287 (2017). doi: 10.1091/mbc.E16-07-0509.
3. Chinnery, P. F., Hudson, G. Mitochondrial genetics. *Br. Med. Bull.* **106**, 135–159 (2013). doi: 10.1093/bmb/ldt017
4. Friedman, J. R., Nunnari, J. Mitochondrial form and function. *Nature* **505**, 335–343 (2014). doi: 10.1038/nature12985.
5. Copyright © 2005 Pearson Education, Inc. publishing as Benjamin Cummings Chapter 6: A Tour of the Cell.
6. Youle, R. J., van der Bliek, A. M. Mitochondrial fission, fusion, and stress. *Science*. **337**, 1062–1065 (2012). doi: 10.1126/science.1219855.
7. Chen, H., Chan, D. C. Mitochondrial dynamics-fusion, fission, movement, and mitophagy-in neurodegenerative diseases. *Hum. Mol. Genet.* **18**, 169–176 (2009). doi: 10.1093/hmg/ddp326.
8. Guo, R., Gu, J., Zong, S., Wu, M., Yang, M. Structure and mechanism of mitochondrial electron transport chain. *Biomed. J.* **41**, 9–20 (2018). doi: 10.1016/j.bj.2017.12.001
9. Akram, M. Citric Acid Cycle and Role of its Intermediates in Metabolism. *Cell Biochem. Biophys.* **68**, 475–478 (2014). doi: 10.1007/s12013-013-9750-1.
10. Rich, P. R., Maréchal, A. The mitochondrial respiratory chain. *Essays Biochem.* **47**, 1–23 (2010). doi: 10.1042/bse0470001.
11. Sarewicz, M., Osyczka, A. Electronic connection between the quinone and cytochrome C redox pools and its role in regulation of mitochondrial electron transport and redox signaling. *Physiol. Rev.* **95**, 219–43 (2015). doi: 10.1152/physrev.00006.2014.
12. Hackenbrock, C. R., Chazotte, B., Gupte, S. S. The random collision model and a critical assessment of diffusion and collision in mitochondrial electron transport. *J. Bioenerg. Biomembr.* **18**, 331–368 (1986).
13. Milenkovic, D., Blaza, J. N., Larsson, N. G., Hirst, J. The Enigma of the Respiratory Chain Supercomplex. *Cell Metab.* **25**, 765–776 (2017). doi: 10.1016/j.cmet.2017.03.009.
14. Vinogradov, A. D. Catalytic properties of the mitochondrial NADH-ubiquinone oxidoreductase (Complex I) and the pseudo-reversible active/inactive enzyme transition. *Biochim. Biophys. Acta - Bioenerg.* **1364**, 169–185 (1998). doi: 10.1016/s0005-2728(98)00026-7
15. Wittig, I., Schägger, H. Supramolecular organization of ATP synthase and respiratory chain in mitochondrial membranes. *Biochim. Biophys. Acta - Bioenerg.* **1787**, 672–680 (2009). doi: 10.1016/j.bbabi.2008.12.016
16. Cruciat, C. M., Brunner, S., Baumann, F., Neupert, W., Stuart, R. A. The cytochrome

- bcl and cytochrome c oxidase complexes associate to form a single supracomplex in yeast mitochondria. *J. Biol. Chem.* **275**, 18093–18098 (2000). doi: 10.1074/jbc.M001901200
17. Guo, R., Zong, S., Wu, M., Gu, J., Yang, M. Architecture of Human Mitochondrial Respiratory Megacomplex I2III2IV2. *Cell* **170**, 1247–1257.e12 (2017). doi: 10.1016/j.cell.2017.07.050.
 18. Taylor, R. W., Turnbull, D. M. Mitochondrial DNA mutations in human disease. *Nat. Rev. Genet.* **6**, 389–402 (2005). doi:10.1038/nrg1606
 19. Stewart, J. B., Chinnery, P. F. The dynamics of mitochondrial DNA heteroplasmy: Implications for human health and disease. *Nat. Rev. Genet.* **16**, 530–542 (2015). doi: 10.1038/nrg3966.
 20. Kirkinetzos, I. G., Moraes, C. T. Reactive oxygen species and mitochondrial diseases. *Semin. Cell Dev. Biol.* **12**, 449–457 (2001). doi:10.1006/scdb.2001.0282
 21. Kivisild, T. Maternal ancestry and population history from whole mitochondrial genomes. *Investig. Genet.* **6**, 3 (2015). doi: 10.1186/s13323-015-0022-2
 22. Luo, S., Valencia C. A., Zhanf J., lee N., Slone J., Gui B., Wang A., Zhuo L., Brown J., Chen Y., Hwu W., Fan P., Wong., Stwal P., Huang T., Biparental Inheritance of Mitochondrial DNA in Humans. *Proc. Natl. Acad. Sci.* **115**, 201810946 (2018). doi: 10.1073/pnas.1810946115
 23. Murphy, M. P. How mitochondria produce reactive oxygen species. *Biochem. J.* **417**, 1–13 (2009). doi: 10.1042/BJ20081386.
 24. Ray, P., Huang, B., Tsuji, Y. Reactive oxygen species (ROS) homeostasis and redox regulation in cellular signaling. *Cell Signal* **24**, 981–990 (2012). doi: 10.1016/j.cellsig.2012.01.008
 25. Wang, Y., Branicky, R., Noë, A., Hekimi, S. Superoxide dismutases: Dual roles in controlling ROS damage and regulating ROS signaling. *J. Cell Biol.* **217**, 1915–1928 (2018). doi: 10.1083/jcb.201708007.
 26. Chamulitrat, W., Mason, R. P. Lipid peroxy radical intermediates in the peroxidation of polyunsaturated fatty acids by lipoxygenase. Direct electron spin resonance investigations. *J. Biol. Chem.* **264**, 20968–20973 (1989).
 27. Lenaz G, Bovina C, Formiggini G, Parenti Castelli G. Mitochondria, oxidative stress, and antioxidant defences. *Acta Biochim Pol.* **46** 1-21 (1999)
 28. DiMauro, S. Mitochondrial diseases. *Biochim. Biophys. Acta - Bioenerg.* **1658**, 80–88 (2004). doi:10.1016/j.bbabi.2004.03.014
 29. Bhat, A. H., Dar K. B., Aness S., Zagar M. A., Masood A., Sofi M. A., Ganie S. A., Oxidative stress, mitochondrial dysfunction and neurodegenerative diseases; a mechanistic insight. *Biomed. Pharmacother.* **74**, 101–110 (2015). doi: 10.1016/j.biopha.2015.07.025.
 30. Schon, E., Manfredi, G. Neuronal degeneration and mitochondrial dysfunction. *J. Clin. Invest.* **111**, 303–312 (2003). doi: 10.1172/JCI200317741
 31. Mariana G. Rosca and Charles L. Hoppel Mitochondrial dysfunction in heart failure

Heart Fail Rev. **5** 18 (2012) doi: 10.1007/s10741-012-9340-0

32. Yu-Wai-Man, P., Griffiths, P. G., Chinnery, P. F. Mitochondrial optic neuropathies - Disease mechanisms and therapeutic strategies. *Prog. Retin. Eye Res.* **30**, 81–114 (2011). doi: 10.1016/j.preteyeres.2010.11.002
33. Viscomi, C., Bottani, E., Zeviani, M. Emerging concepts in the therapy of mitochondrial disease. *BBA - Bioenerg.* **1847**, 544–557 (2015). doi: 10.1016/j.bbabi.2015.03.001.
34. Osborne, N. N., Del Olmo-Aguado, S. Maintenance of retinal ganglion cell mitochondrial functions as a neuroprotective strategy in glaucoma. *Curr. Opin. Pharmacol.* **13**, 16–22 (2013). doi: 10.1016/j.coph.2012.09.002
35. Carelli, V. La Morgia C., Valentino M. L., Barboni P., Ross-Cisneros F., Sadun A., Retinal ganglion cell neurodegeneration in mitochondrial inherited disorders. *Biochim. Biophys. Acta - Bioenerg.* **17**, 518–528 (2009). doi: 10.1016/j.bbabi.2009.02.024
36. Y Kushnareva, Y Seong, A Y Andreyev, T Kuwana, W B Kiosses, M Votruba, and D D Newmeyer Mitochondrial dysfunction in an Opa1^{Q285STOP} mouse model of dominant optic atrophy results from Opa1 haploinsufficiency *Cell Death Dis.* **7** 2309 (2016) doi: 10.1038/cddis.2016.160
37. Man, P. Y. Man, P. Y., Griffiths P. G., Brown D. T., Howell N., Turnbull D., MChinnery P. F., The epidemiology of Leber hereditary optic neuropathy in the North East of England. *Am.J Hum.Genet.* **72**, 333–339 (2003). doi:10.1086/346066
38. Dalton, M. R. An Overview of Leber 's Hereditary Optic Neuropathy. *The Kabod I.* **2** (2015)
39. Lodi R, Tonon C, Valentino ML, Iotti S, Clementi V, Malucelli E, Barboni P, Longanesi L, Schimpf S., Wissinger B, Baruzzi A, Barbiroli B, Carelli, V. Deficit of in vivo mitochondrial ATP production in OPA1-related dominant optic atrophy *Ann Neurol* **5**, 719-23 2004. doi:10.1002/ana.20278
40. Piotrowska, A., Korwin, M., Bartnik, E., Tońska, K. Leber hereditary optic neuropathy - Historical report in comparison with the current knowledge. *Gene* **555**, 41–49 (2015). doi:10.1016/j.gene.2014.09.048
41. Esposti, M. D., Carelli V., Ghelli A., Ratta M., Crimi M., Sangiorgi S., Montagna P., Lenaz G., Lugaresi E., Cortelli P., Functional alterations of the mitochondrially encoded ND4 subunit associated with Leber's hereditary optic neuropathy. *FEBS Lett.* **352**, 375–379 (1994). doi:10.1016/0014-5793(94)00971-6
42. Yu-Wai-Man, P., Soiferman, D., Moore, D. G., Burté, F., Saada, A. Evaluating the therapeutic potential of idebenone and related quinone analogues in Leber hereditary optic neuropathy. *Mitochondrion* **1–7** (2017) doi: 10.1016/j.mito.2017.01.004
43. Kirches, E. LHON: Mitochondrial Mutations and More. *Curr. Genomics* **12**, 44–54 (2011). doi: 10.2174/138920211794520150
44. Zhou, Z. J., McCall, M. A. Retinal ganglion cells in model organisms: Development, function and disease. *J. Physiol.* **586**, 4343–4345 (2008). doi: 10.1113/jphysiol.2008.160838.
45. Nikoskelainen, E. K., Marttila R.J., Huoponen K., Juvonen V., Lammine T., Sonniinen P., Savontaus M. L., Leber's 'plus': Neurological abnormalities in patients with Leber's

- hereditary optic neuropathy. *J. Neurol. Neurosurg. Psychiatry* **59**, 160–164 (1995). doi: 10.1136/jnnp.59.2.160
46. Rai, P. K., Russell, O. M., Lightowers, R. N., Turnbull, D. M. Potential compounds for the treatment of mitochondrial disease. 1–14 (2015). doi: 10.1093/bmb/ldv046
 47. Hurko, O. Drug Development for Rare Mitochondrial Disorders. *Neurotherapeutics* **10**, 286–306 (2013). doi: 10.1007/s13311-013-0179-4.
 48. Enns, G. M. Treatment of mitochondrial disorders: antioxidants and beyond. *J. Child Neurol.* **29**, 1235–40 (2014). doi: 10.1177/0883073814538509.
 49. Khan, N. A., Govindaraj, P., Meena, A. K., Thangaraj, K. Mitochondrial disorders : Challenges in diagnosis & treatment. *Indian J Med Res* **141**, 13–26 (2015).
 50. Sharma, S., Black, S. M. Carnitine homeostasis, mitochondrial function and cardiovascular disease. *Drug Discov. Today Dis. Mech.* **6**, e31–e39 (2009). doi: 10.1016/j.ddmec.2009.02.001
 51. Barshop, B. A., Naviaux R. K., McGowan K. A., Levine F., Nyhan W.L., Loupis-Geller A., Hass R.H., Chronic treatment of mitochondrial disease patients with dichloroacetate. *Mol. Genet. Metab.* **83**, 138–149 (2004). doi:10.1016/j.ymgme.2004.06.009
 52. Komen, J. C., Thorburn, D. R. Turn up the power - Pharmacological activation of mitochondrial biogenesis in mouse models. *Br. J. Pharmacol.* **171**, 1818–1836 (2014). doi: 10.1111/bph.12413
 53. Wang, Y., Hekimi, S. Understanding Ubiquinone. *Trends Cell Biol.* **26**, 367–378 (2016). doi: 10.1016/j.tcb.2015.12.007.
 54. Frei, B., Kim, M. C., Ames, B. N. Ubiquinol-10 is an effective lipid-soluble antioxidant at physiological concentrations. *Proc. Natl. Acad. Sci. U. S. A.* **87**, 4879–83 (1990). doi:10.1073/pnas.87.12.4879
 55. Gueven, N., Woolley, K., Smith, J. Border between natural product and drug: Comparison of the related benzoquinones idebenone and coenzyme Q10. *Redox Biol.* **4C**, 289–295 (2015). doi: 10.1016/j.redox.2015.01.009
 56. Kanabus, M., Heales, S. J., Rahman, S. Development of pharmacological strategies for mitochondrial disorders. *Br. J. Pharmacol.* **171**, 1798–1817 (2014). doi: 10.1111/bph.12456.
 57. Schiff, M., Rustin, P. Idebenone in Friedreich ataxia and Leber’s hereditary optic neuropathy: close mechanisms, similar therapy?: Table 1. *Brain* aww085 (2016). doi:10.1093/brain/aww085
 58. Klopstock, T. Yu-Wai-Man P, Dimitriadis K, Rouleau J, Heck S, Bailie M, Atawan A, Chattopadhyay S, Schubert M, Garip A, Kernt M, Petraki D, Rummey C, Leinonen M, Metz G, Griffiths PG, Meier T, Chinnery . A randomized placebo-controlled trial of idebenone in Leber’s hereditary optic neuropathy. *Brain* **134**, 2677–2686 (2011). doi: 10.1093/brain/awr170.
 59. Koopman W.J., Beyrath J, Fung C. W., Koene S, Rodenburg R. J., Willems P.H., Smeitink J.A., Mitochondrial disorders in children : toward development of small-molecule treatment strategies. **8**, 1–17 (2016). doi: 10.15252/emmm.201506131

60. Weyer, G., Erzigkeit, H., Hadler, D., Kubicki, S. Efficacy and safety of idebenone in the long-term treatment of Alzheimer's disease: A double blind, placebo controlled multicentre study. *Hum. Psychopharmacol. Clin. Exp.* **11**, 53–65 (1996).
61. Esposti MD, Ngo A, Ghelli A, Benelli B, Carelli V, McLennan H, Linnane AW. The interaction of Q analogs, particularly hydroxydecyl benzoquinone (idebenone), with the respiratory complexes of heart mitochondria. *Arch. Biochem. Biophys.* **330**, 395–400 (1996). doi:10.1006/abbi.1996.0267
62. Jaber, S., Polster, B. M. Idebenone and neuroprotection: antioxidant, pro-oxidant, or electron carrier? *J. Bioenerg. Biomembr.* **47**, 111–8 (2015). doi: 10.1007/s10863-014-9571-y
63. King, M. S., Sharpley, M. S., Hirst, J. Reduction of hydrophilic ubiquinones by the flavin in mitochondrial NADH:ubiquinone oxidoreductase (Complex I) and production of reactive oxygen species. *Biochemistry* **48**, 2053–62 (2009). doi: 10.1021/bi802282h.
64. Haefeli RH, Erb M, Gemperli AC, Robay D, Courdier Fruh I, Anklin C, Dallmann R, Gueven N. NQO1-dependent redox cycling of idebenone: Effects on cellular redox potential and energy levels. *PLoS One* **6**, (2011). doi: 10.1371/journal.pone.0017963.
65. Colucci, M. a, Moody, C. J., Couch, G. D. Natural and synthetic quinones and their reduction by the quinone reductase enzyme NQO1: from synthetic organic chemistry to compounds with anticancer potential. *Org. Biomol. Chem.* **6**, 637–656 (2008). doi: 10.1039/b715270a
66. Stringer JL, Gaikwad A, Gonzales BN, Long DJ Jr, Marks LM, Jaiswal AK. Presence and Induction of the Enzyme NAD(P)H: Quinone Oxidoreductase 1 in the Central Nervous System. *J. Comp. Neurol.* **471**, 289–297 (2004). doi:10.1002/cne.20048
67. Nguyen, T., Nioi, P., Pickett, C. B. The Nrf2-antioxidant response element signaling pathway and its activation by oxidative stress. *J. Biol. Chem.* **284**, 13291–13295 (2009). doi: 10.1074/jbc.R900010200.
68. Raxone, N. Raxone idebenone. **44**, Assessment Report (EMA/480039/2015)
69. Smith, T. G., Seto, S., Ganne, P. & Votruba, M. A randomized, placebo-controlled trial of the benzoquinone idebenone in a mouse model of OPA1-related dominant optic atrophy reveals a limited therapeutic effect on retinal ganglion cell dendropathy and visual function. *Neuroscience* **319**, 92–106 (2016). doi: 10.1016/j.neuroscience.2016.01.042.
70. Giorgio V, Petronilli V, Ghelli A, Carelli V, Rugolo M, Lenaz G, Bernardi P. The effects of idebenone on mitochondrial bioenergetics. *Biochim. Biophys. Acta - Bioenerg.* **1817**, 363–369 (2012). doi: 10.1016/j.bbabi.2011.10.012.
71. Seo Y, Park J, Kim M, Lee HK, Kim JH, Jeong JH, Namkung W. Inhibition of ANO1/TMEM16A chloride channel by idebenone and its cytotoxicity to cancer cell lines. *PLoS One* **10**, 7–9 (2015). doi: 10.1371/journal.pone.0133656
72. Bodmer, M., Vankan, P., Dreier, M., Kutz, K. W., Drewe, J. Pharmacokinetics and metabolism of idebenone in healthy male subjects. *Eur. J. Clin. Pharmacol.* **65**, 493–501 (2009). doi: 10.1007/s00228-008-0596-1
73. Heitz F.D., Erb M., Anklin C., Robay D., Pernet V., Gueven N. Idebenone Protects against Retinal Damage and Loss of Vision in a Mouse Model of Leber's Hereditary

- Optic Neuropathy. *PLoS One* **7**, (2012). doi: 10.1371/journal.pone.0045182.
74. Guy J., Feuer W.J., Davis J.L., Porciatti V., Gonzalez P.J., Koilkonda R.D., Yuan H., Hauswirth W.W., Lam B.L. Gene Therapy for Leber Hereditary Optic Neuropathy: Low- and Medium-Dose Visual Results. *Ophthalmology* **124**, 1621–1634 (2017). doi: 10.1016/j.ophtha.2017.05.016.
 75. Koilkonda R., Yu H., Talla V., Porciatti V., Feuer W.J., Hauswirth W.W., Chiodo V., Erger K.E., Boye S.L., Lewin A.S., Conlon T.J., Renner L., Neuringer M., Detrisac C., Guy J. LHON gene therapy vector prevents visual loss and optic neuropathy induced by G11778A mutant mitochondrial DNA: Biodistribution and toxicology profile. *Investig. Ophthalmol. Vis. Sci.* **55**, 7739–7753 (2014). doi: 10.1167/iovs.14-15388.
 76. Yang S, Ma SQ, Wan X, He H, Pei H, Zhao MJ, Chen C, Wang DW, Dong XY, Yuan JJ, Li B. Long-term outcomes of gene therapy for the treatment of Leber’s hereditary optic neuropathy. *EBioMedicine* **10**, 258–268 (2016). doi: 10.1016/j.ebiom.2016.07.002.
 77. GenSight Biologics reports positive 72-week data from REVERSE Phase III clinical trial of GS010 for the treatment of Leber Hereditary Optic Neuropathy (LHON). **010**, 37–39 (2018).
 78. Colella, P., Ronzitti, G. & Mingozzi, F. Emerging Issues in AAV-Mediated In Vivo Gene Therapy. *Mol. Ther. - Methods Clin. Dev.* **8**, 87–104 (2018).
 79. Kaemmerer, W. F. How will the field of gene therapy survive its success? *Bioeng. Transl. Med.* **3**, 166–177 (2018).
 80. Morrison, C. \$1-million price tag set for Glybera gene therapy. *Nat. Biotechnol.* **33**, 217–218 (2015)
 81. Liao, C., Sitzmann, M., Pugliese, A., Nicklaus, M. C. Software and resources for computational medicinal chemistry. *Future Med. Chem.* **3**, 1057–1085 (2011). doi: 10.4155/fmc.11.63.
 82. Song, C. M., Lim, S. J., Tong, J. C. Recent advances in computer-aided drug design. *Brief. Bioinform.* **10**, 579–591 (2009). doi: 10.1093/bib/bbp023
 83. Xia D., Esser L., Tang W.K., Zhou F., Zhou Y., Yu L., Yu C.A. Structural analysis of cytochrome bc1 complexes: Implications to the mechanism of function. *Biochim. Biophys. Acta - Bioenerg.* **1827**, 1278–1294 (2013). doi: 10.1016/j.bbabbio.2012.11.008
 84. Barragan, A. M., Crofts, A. R., Schulten, K. Identification of Ubiquinol Binding Motifs at the Q. (2015). doi: 10.1021/jp510022w
 85. Esser L, Quinn B, Li Y.F., Zhang M., Elberry M., Yu L., Yu C.A., Xia D. Crystallographic studies of quinol oxidation site inhibitors: A modified classification of inhibitors for the cytochrome bc1 complex. *J. Mol. Biol.* **341**, 281–302 (2004). doi:10.1016/j.jmb.2004.05.065
 86. Gao X, Wen X, Esser L, Quinn B, Yu L, Yu CA, Xia D. Structural Basis for the Quinone Reduction in thebc1Complex: A Comparative Analysis of Crystal Structures of Mitochondrial Cytochromebc1with Bound Substrate and Inhibitors at the QiSite. *Biochemistry* **42**, 9067–9080 (2003). doi:10.1021/bi0341814
 87. Gangwal, R. P., Dhoke, G. V., Damre, M. V., Khandelwal, K. & Sangamwar, A. T.

- Structure-Based Virtual Screening and Molecular Dynamic Simulation Studies to Identify Novel Cytochrome bc1 Inhibitors as Antimalarial Agents. *J. Comput. Med.* **2013**, 1–9 (2013). doi: 10.1155/2013/637901
88. Faig M, Bianchet MA, Talalay P, Chen S, Winski S, Ross D, Amzel LM. Structures of recombinant human and mouse NAD (P) H : quinone oxidoreductases : Species comparison and structural changes with substrate binding and release. **97**, (2000). doi:10.1073/pnas.050585797
 89. Faig M, Bianchet MA, Winski S, Hargreaves R, Moody CJ, Hudnott AR, Ross D, Amzel LM. Structure-Based Development of Anticancer Drugs : Complexes of NAD (P) H : Quinone Oxidoreductase 1 with Chemotherapeutic Quinones. **9**, 659–667 (2001).doi : 10.1016/S0969-2126(01)00636-0
 90. Winski S.L., Faig M., Bianchet M.A., Siegel D., Swann E., Fung K., Duncan M.W., Moody C.J., Amzel L.M., Ross D. Characterization of a mechanism-based inhibitor of NAD(P)H:Quinone oxidoreductase 1 by biochemical, x-ray crystallographic, and mass spectrometric approaches. *Biochemistry* **40**, 15135–15142 (2001). doi: 10.1021/bi011324i
 91. Asher, G., Dym, O., Tsvetkov, P., Adler, J., Shaul, Y. The crystal structure of NAD(P)H quinone oxidoreductase 1 in complex with its potent inhibitor dicoumarol. *Biochemistry* **45**, 6372–6378 (2006). doi:10.1021/bi0600087
 92. Meunier, B., Fisher, N., Ransac, S., Mazat, J. P., Brasseur, G. Respiratory complex III dysfunction in humans and the use of yeast as a model organism to study mitochondrial myopathy and associated diseases. *Biochim. Biophys. Acta - Bioenerg.* **1827**, 1346–1361 (2013). doi: 10.1016/j.bbabi.2012.11.015.
 93. Crofts, A. R. The Q-cycle - A personal perspective. *Photosynth. Res.* **80**, 223–243 (2004). doi: 10.1007/s11120-010-9537-9
 94. Bordoli L, Kiefer F, Arnold K, Benkert P, Battey J, Schwede T. Protein structure homology modeling using SWISS-MODEL workspace. *Nat. Protoc.* **4**, 1–13 (2009). doi: 10.1038/nprot.2008.197.
 95. Bairoch, A., Apweiler, R. The SWISS-PROT protein sequence database and its supplement TrEMBL in 2000. *Nucleic Acids Res.* **28**, 45–48 (2000). doi:10.1093/nar/28.1.45
 96. De Vitry, C., Ouyang, Y., Finazzi, G., Wollman, F. A., Kallas, T. The chloroplast rieske iron-sulfur protein. At the crossroad of electron transport and signal transduction. *J. Biol. Chem.* **279**, 44621–44627 (2004). doi:10.1074/jbc.M406955200
 97. Sliwoski, G., Kothiwale, S., Meiler, J., Lowe, E. W. Computational methods in drug discovery. *Pharmacol. Rev.* **66**, 334–95 (2014). doi: 10.1124/pr.112.007336.
 98. Molecular Operating Environment (MOE), 2013.08; Chemical Computing Group ULC, 1010 Sherbooke St. West, Suite #910, Montreal, QC, Canada, H3A 2R7, 2019 <http://www.chemcomp.com>
 99. Erb M., Hoffmann-Enger B., Deppe H., Soeberdt M., Haefeli R.H., Rummey C., Feurer A., Gueven N. Features of idebenone and related short-chain quinones that rescue ATP levels under conditions of impaired mitochondrial complex I. *PLoS One* **7**, (2012). doi: 10.1371/journal.pone.0036153.

100. Schrödinger, LLC, New York, NY, 2018 <https://www.schrodinger.com/>
101. Mahajan, A., Gill, N. S., Arora, R. a Review on Molecular Docking. *Int J Recent Adv Pharm Res* **4**, 1–7 (2014).
102. Monks T.J, Hanzlik R., Cohen M.G.,Graham G. Quinone Chemistry and Toxicity'. *Toxicology and Applied Pharmacology* **16**, 2–16 (1992).
103. Mortensen, A. Carotenoids and other pigments as natural colorants. *Pure Appl. Chem* **78**, 1477–1491 (2006). doi: 10.1351/pac200678081477
104. Yang, B. Burkhardt L., H., Krishnamoorthy S., Murali A., Prakash G. K. S., Narayanan S.R. High-Performance Aqueous Organic Flow Battery with Quinone-Based Redox Couples at Both Electrodes. *Journal of The Electrochemical Society* **163**, 1442–1449 (2016). doi: 10.1149/2.1371607jes
105. Verweij, J., Pinedo, H. M. Mitomycin C: mechanism of action, usefulness and limitations. *Anticancer. Drugs* **1**, 5–13 (1990).
106. Kumagai, Y., Shinkai, Y., Miura, T., Cho, A. K. The chemical biology of naphthoquinones and its environmental implications. *Annu. Rev. Pharmacol. Toxicol.* **52**, 221–47 (2012). doi: 10.1146/annurev-pharmtox-010611-134517
107. Papageorgiou, V. P., Assimopoulou, A. N., Couladouros, E. A., Hepworth, D., Nicolaou, K. C. The chemistry and biology of alkannin, shikonin, and related naphthazarin natural products. *Angew. Chemie - Int. Ed.* **38**, 270–300 (1999). doi: 10.1002/(SICI)1521-3773(19990201)38:3<270::AID-ANIE270>3.0.CO;2-0.
108. Hargreaves, I. P. Coenzyme Q10 as a therapy for mitochondrial disease. *Int. J. Biochem. Cell Biol.* **49**, 105–111 (2014). doi: 10.1016/j.biocel.2014.01.020.
109. Wellington, K. W. Understanding cancer and the anticancer activities of naphthoquinones – a review. *RSC Adv.* **5**, 20309–20338 (2015). DOI: 10.1039/c4ra13547d
110. Klotz, L. O., Hou, X., Jacob, C. 1,4-naphthoquinones: From oxidative damage to cellular and inter-cellular signaling. *Molecules* **19**, 14902–14918 (2014). doi: 10.3390/molecules190914902.
111. Tobias Johnsson Wass, J. R., Ahlberg, E., Panas, I., Schiffrin, D. J. Quantum chemical modeling of the reduction of quinones. *J. Phys. Chem. A* **110**, 2005–2020 (2006). doi:10.1021/jp055414z
112. Harrison, N. M. An Introduction to Density Functional Theory. *Technology* **2**, 1–26 (1995). doi: /10.1119/1.19375
113. Peverati, R., Truhlar, D. G. Quest for a universal density functional: the accuracy of density functionals across a broad spectrum of databases in chemistry and physics. *Philos. Trans. A. Math. Phys. Eng. Sci.* **372**, 20120476 (2014). doi: 10.1098/rsta.2012.0476
114. Marenich, A. V, Ho, J., Coote, M. L., Cramer, C. J. & Truhlar, D. G. Computational electrochemistry: prediction of liquid-phase reduction potentials. *Phys. Chem. Chem. Phys.* **16**, 15068–106 (2014). doi: 10.1039/c4cp01572j
115. Méndez-hernández, D. D., Tarakeshwar, P., Gust, D., Moore, T., Moore, A. L. Simple

- and accurate correlation of experimental redox potentials and DFT-calculated HOMO / LUMO energies of polycyclic aromatic hydrocarbons. *Journal of Molecular Modeling*, **7** 2845–2848 (2013). doi: 10.1007/s00894-012-1694-7
116. Namazian, M., Almodarresieh, H. A., Noorbala, M. R. & Zare, H. R. DFT calculation of electrode potentials for substituted quinones in aqueous solution. *Chem. Phys. Lett.* **396**, 424–428 (2004). doi: 10.1016/j.cplett.2004.08.089
 117. Riahi, S., Eynollahi, S., Ganjali, M. R. Calculation of standard electrode potential and study of solvent effect on electronic parameters of anthraquinone-1- carboxylic acid. *Int. J. Electrochem. Sci.* **4**, 1128–1137 (2009).
 118. Gaussian 98 (Gaussian, Inc., Pittsburgh, PA, 1998) <http://www.gaussian.com/>
 119. Borges R.S., Carneiro A.S., Barros T.G., Barros C.A., Neto A.M., da Silva A.B. Understanding the cytotoxicity or cytoprotective effects of biological and synthetic quinone derivatives by redox mechanism. *J. Mol. Model.* **20**, 2541 (2014). doi: 10.1007/s00894-014-2541-9
 120. da Silva, A. J. M. *et al.* Antitumoral, Antileishmanial and Antimalarial Activity of Pentacyclic 1,4-Naphthoquinone Derivatives. *J. Braz. Chem. Soc.* **20**, 176–182 (2009).doi: 10.1590/S0103-50532009000100026
 121. Janeczko, M., Demchuk, O. M., Strzelecka, D., Kubiński, K., Masłyk, M. New family of antimicrobial agents derived from 1,4-naphthoquinone. *Eur. J. Med. Chem.* **124**, 1019 (2016). doi: 10.1016/j.ejmech.2016.10.034
 122. Ferreira M.P., Cardoso M.F., da Silva F.C., Ferreira V.F., Lima E.S., Souza J.V. Antifungal activity of synthetic naphthoquinones against dermatophytes and opportunistic fungi: Preliminary mechanism-of-action tests. *Ann. Clin. Microbiol. Antimicrob.* **13**, 1–6 (2014). doi: 10.1186/1476-0711-13-26
 123. Ahn J.H., Cho S.Y., Ha J.D., Chu S.Y., Jung S.H., Jung Y.S., Baek J.Y., Choi I.K., Shin E.Y., Kang S.K., Kim S.S., Cheon H.G., Yang S.D., Choi J.K. Synthesis and PTP1B inhibition of 1,2-naphthoquinone derivatives as potent anti-diabetic agents. *Bioorganic Med. Chem. Lett.* **12**, 1941–1946 (2002). doi: 10.1016/S0960-894X(02)00331-1
 124. Chan T.S, Teng S, Wilson J.X., Galati G., Khan S., O'Brien P.J. Coenzyme Q cytoprotective mechanisms for mitochondrial complex I cytopathies involves NAD(P)H: Quinone oxidoreductase 1(NQO1). *Free Radic. Res.* **36**, 421–427 (2002).doi: 10.1080/10715760290021270
 125. Spinazzi, M., Casarin, A., Pertegato, V., Salviati, L., Angelini, C. Assessment of mitochondrial respiratory chain enzymatic activities on tissues and cultured cells. *TL - 7. Nat. Protoc.* **7** VN-re, 1235–1246 (2012). doi: 10.1038/nprot.2012.058.
 126. Nelson, E. E., Guyer, A. E. DCPIP (2,6-dichlorophenolindophenol) as a genotype-directed redox chemotherapeutic targeting NQO1*2 breast carcinoma. *Free Radic Res* **45**, 276–292 (2011). doi: 10.3109/10715762.2010.526766
 127. James, A. M., Cochemé, H. M., Smith, R. A. J., Murphy, M. P. Interactions of mitochondria-targeted and untargeted ubiquinones with the mitochondrial respiratory chain and reactive oxygen species: Implications for the use of exogenous ubiquinones as therapies and experimental tools. *J. Biol. Chem.* **280**, 21295–21312 (2005). doi:10.1074/jbc.M501527200

128. Levin, L. A., Gordon, L. K. Retinal ganglion cell disorders: Types and treatments. *Prog. Retin. Eye Res.* **21**, 465–484 (2002).doi: 10.1016/S1350-9462(02)00012-5
129. Zhang X.M., Li Liu D.T., Chiang S.W., Choy K.W., Pang C.P., Lam D.S., Yam G.H. Immunopanning purification and long-term culture of human retinal ganglion cells. *Mol. Vis.* **16**, 2867–2872 (2010).
130. Winzeler, A. & Wang, J. T. Purification and Culture of Retinal Ganglion Cells. *Cold Spring Harb. Protoc.* **8**, 614–617 (2013). doi: 10.1101/pdb.top070961.
131. Wood, J. P. M., Chidlow, G., Tran, T., Crowston, J. G. & Casson, R. J. A comparison of differentiation protocols for RGC-5 cells. *Investig. Ophthalmol. Vis. Sci.* **51**, 3774–3783 (2010). doi: 10.1167/iovs.09-4305
132. Krishnamoorthy, R. R., Clark, A. F., Daudt, D., Vishwanatha, J. K., Yorio, T. A forensic path to RGC-5 cell line identification: Lessons learned. *Investig. Ophthalmol. Vis. Sci.* **54**, 5712–5719 (2013). doi: 10.1167/iovs.13-12085.
133. Hall, A. E. International Cell Line Authentication Committee ICLAC . org Case Study : RGC-5 is not rat retinal ganglion ICLAC Case Study : RGC-5 “ New manuscripts containing data derived from RGC-5 cells will be editorially rejected without review .” ICLAC Case Study. 6–7 (2015). doi: 10.1016/j.exer.2013.10.012
134. Van Bergen N.J., Wood J.P., Chidlow G., Trounce I.A., Casson R.J., Ju W.K., Weinreb R.N., Crowston J.G. Recharacterization of the RGC-5 retinal ganglion cell line. *Investig. Ophthalmol. Vis. Sci.* **50**, 4267–4272 (2009). doi: 10.1167/iovs.09-3484
135. Agarwal, N. RGC-5 cells. *Investig. Ophthalmol. Vis. Sci.* **54**, 7884 (2013). doi: 10.1167/iovs.13-13292
136. Costantini, S., Di Bernardo, G., Cammarota, M., Castello, G. & Colonna, G. Gene expression signature of human HepG2 cell line. *Gene* **518**, 335–345 (2013). doi: 10.1016/j.gene.2012.
137. Kovalevich, J., Langford, D. Neuronal Cell Culture. *Methods Mol. Biol. - Neuronal Cell Cult. Methods Protoc.* **1078**, 9–21 (2013). doi: 10.1007/978-1-62703-640-5_2
138. <https://www.lgcstandards-atcc.org/>.
139. Jia, Z., Zhu, H., Misra, H. P., Li, Y. Potent induction of total cellular GSH and NQO1 as well as mitochondrial GSH by 3H-1,2-dithiole-3-thione in SH-SY5Y neuroblastoma cells and primary human neurons: Protection against neurocytotoxicity elicited by dopamine, 6-hydroxydopamine, 4-hydroxy-2-no. *Brain Res.* **1197**, 159–169 (2008). doi: 10.1016/j.brainres.2007.12.04
140. Das, J. The role of mitochondrial respiration in physiological and evolutionary adaptation. *Bioessays.* **9** 890–901 (2006). doi:10.1002/bies.20463
141. Brand, M. D., Nicholls, D. G. Assessing mitochondrial dysfunction in cells. *Biochem. J.* **435**, 297–312 (2011). doi: 10.1042/BJ20110162
142. Tan, A. S., Berridge, M. V. Evidence for NAD(P)H:quinone oxidoreductase 1 (NQO1)-mediated quinone-dependent redox cycling via plasma membrane electron transport: A sensitive cellular assay for NQO1. *Free Radic. Biol. Med.* **48**, 421–429 (2010). doi: 10.1016/j.freeradbiomed.2009.11.016.

143. Halim, A.B. Do we have a satisfactory cell viability assay? Review of the currently commercially-available assays. *Curr. Drug Discov. Technol.* **15**, (2018). doi: 10.2174/1570163815666180925095433
144. Tai, K.-K., Pham, L., Truong, D. D. Idebenone induces apoptotic cell death in the human dopaminergic neuroblastoma SHSY-5Y cells. *Neurotox. Res.* **20**, 321–8 (2011). doi: 10.1007/s12640-011-9245-z
145. Molecular Probes by Life Technologies. CellROX[®] Oxidative Stress Reagents. 1–6 (2012).
146. Kelts, J. L., Cali, J. J., Duellman, S. J., Shultz, J. Altered cytotoxicity of ROS-inducing compounds by sodium pyruvate in cell culture medium depends on the location of ROS generation. *Springerplus* **4**, (2015). doi: 10.1186/s40064-015-1063-y.
147. Criddle D.N., Gillies S, Baumgartner-Wilson H.K., Jaffar M, Chinje E.C., Passmore S, Chvanov M., Barrow S., Gerasimenko O.V., Tepikin A.V., Sutton R., Petersen O.H. Menadione-induced reactive oxygen species generation via redox cycling promotes apoptosis of murine pancreatic acinar cells. *J. Biol. Chem.* **281**, 40485–40492 (2006). doi:10.1074/jbc.M607704200
148. Callies, O., Hernández Daranas, A. Application of isothermal titration calorimetry as a tool to study natural product interactions. *Nat. Prod. Rep.* **33**, 881–904 (2016). doi: 10.1039/c5np00094g.
149. Vos, M., Verstreken, P., Klein, C. Stimulation of electron transport as potential novel therapy in Parkinson's disease with mitochondrial dysfunction. *Biochem. Soc. Trans.* **43**, 275–9 (2015). doi: 10.1042/BST20140325
150. Wang, J., Li, S., Yang, T., Yang, J. Single-step synthesis of idebenone from Coenzyme Q0 via free-radical alkylation under silver catalysis. *Tetrahedron* **70**, 9029–9032 (2014).doi: 10.1016/j.tet.2014.10.017
151. Duncton, M. A. J. Minisci reactions: Versatile CH-functionalizations for medicinal chemists. *Medchemcomm* **2**, 1135 (2011). doi: 10.1039/C1MD00134E
152. Delarmelina, M., Greco, S. J., Carneiro, J. W. d. M. Single step mechanism for nucleophilic substitution of 2,3-dichloro naphthoquinone using nitrogen, oxygen and sulfur nucleophiles: A DFT approach. *Tetrahedron* **73**, 4363–4370 (2017). doi: 10.1016/j.tet.2017.05.095
153. Ruiz-Castillo, P., Buchwald, S. L. Applications of Palladium-Catalyzed C-N Cross-Coupling Reactions. *Chem. Rev.* **116**, 12564–12649 (2016). doi:10.1021/acs.chemrev.6b00512
154. Xiao, L. W. *et al.* [1,1'-Bis(Diphenylphosphino)Ferrocene]Dichloropalladium/1, 1'-Bis(Diphenylphosphino)Ferrocene Catalyzed Synthesis of 2,3-Diamino-1,4-Naphthoquinones. *Synthesis (Stuttg)*. 989–998 (2007). doi: 10.1002/chin.200732096
155. Stavber, S. Recent Advances in the Application of Selectfluor/TMF-TEDA-BF₄ as a Versatile Mediator or Catalyst in Organic Synthesis *Stojan. Molecules* **16**, 6432–6464 (2011). doi: 10.3390/molecules16086432
156. Li, C., Zhang, K., Xu, X. H. & Qing, F. L. Copper-mediated oxidative trifluoromethylthiolation of quinones. *Tetrahedron Lett.* **56**, 6273–6275 (2015).doi: 10.1016/j.tetlet.2015.09.117

157. Hu, Y., Stumpfe, D., Bajorath, J. Recent Advances in Scaffold Hopping. *J. Med. Chem.* **60**, 1238–1246 (2017).doi: 10.1021/acs.jmedchem.6b01437
158. Keyari, C. M. Kearns K. A., Dunca N. S, Eickholt E. A., Abbott G., Beall D. H., Diaz P., Synthesis of New Quinolinequinone Derivatives and Preliminary Exploration of their Cytotoxic Properties. *J. Med. Chem.* **56**, 3806–3819 (2013). doi: 10.1021/jm301689x
159. Mulchin B.J., Newton C.G., Baty J.W., Grasso C.H., Martin W.J., Walton M.C., Dangerfield E.M., Plunkett C.H., Berridge M.V., Harper J.L., Timmer M.S., Stocker B.L. The anti-cancer, anti-inflammatory and tuberculostatic activities of a series of 6,7-substituted-5,8-quinolinequinones. *Bioorganic Med. Chem.* **18**, 3238–3251 (2010). doi: 10.1016/j.bmc.2010.03.021
160. Hussain, H., Specht, S., Sarite, S. R., Hoerauf, A. & Krohn, K. New quinoline-5,8-dione and hydroxynaphthoquinone derivatives inhibit a chloroquine resistant Plasmodium falciparum strain. *Eur. J. Med. Chem.* **54**, 936–942 (2012). doi: 10.1016/j.ejmech.2012.06.046.
161. Jiang Z, Liu N, Dong G, Jiang Y, Liu Y, He X, Huang Y, He S, Chen W, Li Z, Yao J, Miao Z, Zhang W, Sheng C. Scaffold hopping of sampangine: Discovery of potent antifungal lead compound against Aspergillus fumigatus and Cryptococcus neoformans. *Bioorganic Med. Chem. Lett.* **24**, 4090–4094 (2014). doi: 10.1016/j.ejmech.2017.10.043.
162. Orzeł, A. Podsiadły R., Podemska K., Strzelczyk R. Dyes based on the 6,7-dichloro-5,8-quinolinedione skeleton as new type II photoinitiators for radical polymerisation. *Color. Technol.* **130**, 185–190 (2014). doi: 10.1111/cote.12083
163. Landelle, G., Panossian, A., Leroux, F. R. ChemInform Abstract: Trifluoromethyl Ethers and Thioethers as Tools for Medicinal Chemistry and Drug Discovery. *ChemInform* **45**, no-no (2014). doi: 10.1002/chin.201441240
164. Lii C.K., Liu K.L, Cheng Y. P. Lin A. H., CGen H. W. Tsai C. W., Sulforaphane and a -Lipoic Acid Upregulate the Expression of the π Class of Glutathione S -Transferase through c-Jun and. *J. Nutr.* 885–892 (2010). doi: 10.1016/j.semancer.2015.02.007
165. Jia, Z., Hallur, S., Zhu, H., Li, Y. & Misra, H. P. Potent upregulation of glutathione and NAD(P)H:quinone oxidoreductase 1 by alpha-lipoic acid in human neuroblastoma SH-SY5Y cells: Protection against neurotoxicant-elicited cytotoxicity. *Neurochem. Res.* **33**, 790–800 (2008). doi:10.1007/s11064-007-9496-5
166. Sridhar, J., Liu, J., Foroozesh, M., Stevens, C. L. K. Inhibition of cytochrome P450 enzymes by quinones and anthraquinones. *Chem. Res. Toxicol.* **25**, 357–365 (2012). doi: 10.1021/tx2004163.
- 167 Prakash, K., Jieun, R., Hyeongmin, K., Iksoo, K., Jeong, T. K., Hyunil K., Jae M., Choa G., Yunb L., Pharmaceutical particle technologies: An approach to improve drug solubility, dissolution and bioavailability *Asian J. Pharm.* **9**, 304–316 (2014) doi: 10.1016/j.ajps.2014.05.005
168. Abdelkader, H., G. Alany, R. Controlled and Continuous Release Ocular Drug Delivery Systems: Pros and Cons. *Curr. Drug Deliv.* **9**, 421–430 (2012). doi: 10.2174/156720112801323125
169. Madeira, V. M. C. *Overview of mitochondrial bioenergetics. Methods in Molecular*

Biology **810**, (2012). doi: 10.1007/978-1-61779-382-0_1.

170. Riss T.L., Moravec R. A., Niles A. L., Duellman S., Benink H. A., Worzella T. J., Minor L. Cell Viability Assays. *Assay Guid. Man.* **114**, 785–796 (2013).